

https://dspace.org/

The effects of indigenous South African plant extracts (cotyledon c. orbiculata and tulbaghia. violacea) on triple negative breast cancer cells

Alaouna, Mohammed

2024
University of the Witwatersrand, Johannesburg
https://hdl.handle.net/10539/43301
Alaouna, Mohammed. (2024). The effects of indigenous South African plant extracts (cotyledon c. orbiculata and tulbaghia. violacea) on triple negative breast cancer cells [PhD thesis, University of the Witwatersrand, Johannesburg]. WireDSpace.

Downloaded from a DSpace repository. https://dspace.org/

THE EFFECTS OF INDIGENOUS SOUTH AFRICAN PLANT EXTRACTS (*COTYLEDON C. ORBICULATA* AND *TULBAGHIA. VIOLACEA*) ON TRIPLE NEGATIVE BREAST CANCER CELLS.



Mohammed Alaouna

A dissertation submitted to the Faculty of Health Sciences, University of the Witwatersrand, in fulfilment of the requirements for the degree of Doctor of Philosophy (Internal Medicine).

Johannesburg, 2024

DECLARATION

I declare that this dissertation is my own, unaided work. It is being submitted for the degree of Doctor of Philosophy in Internal Medicine at the University of the Witwatersrand, Johannesburg. It has not been submitted before for any degree or examination at any other university.

Please see Appendix D for Turnitin report and Appendix E for ethics waiver.

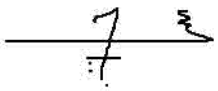

24 May 2024

Abstract:

This dissertation explored the potential therapeutic applications of water and methanol extracts of *C. orbiculata* and *Tulbaghia violacea*, indigenous to Southern Africa, targeting triple-negative breast cancer (TNBC). TNBC, a significant subset of breast cancer cases, is notably challenging because of the absence of key hormone receptors, often leading to less favourable patient outcomes and a high relapse rate within five years. The research approach was both thorough and meticulous, utilising two cell lines: one representing normal breast tissue and the other representing TNBC. Extensive cytotoxicity assays were conducted to determine the IC_{50} values for TNBC cells, which is critical for understanding how plant extracts affect cellular activities such as migration, invasion, adhesion, cell cycle regulation, and apoptosis induction. Additionally, the antioxidant properties of these extracts were examined, which showed significant effects, especially in the aqueous extract of *Tulbaghia violacea*, on TNBC cellular dynamics.

This study employed a comprehensive array of analytical techniques, including Fourier transform infrared spectroscopy (FTIR), gas chromatography-mass spectrometry (GC-MS), and nuclear magnetic resonance (NMR) spectroscopy, to identify the specific molecular constituents of these extracts. Computational docking studies have focused on the interactions between these molecules and the anti-apoptotic protein, COX2. Whole transcriptome sequencing of RNA from both TNBC and normal breast cells treated with *T. violacea* extract provided valuable insights into the affected signaling pathways. An antibody array assay further elucidated protein changes in the receptor tyrosine kinase (RTK) pathway. The half-maximal inhibitory concentration (IC_{50}) values were determined for the *aqueous and methanol extracts of T. violacea* at 400 µg/mL and 820 µg/mL, respectively, and for *C. orbiculata at* 830 µg/mL and 700 µg/mL, respectively. Exposure to *the water-soluble extract of T. violacea* resulted in a marked increase in apoptosis in TNBC cells, with approximately 82% undergoing programmed cell death, compared to 32% in normal breast cells. Chemical profiling identified a range of compounds, including 36 distinct

compounds identified through GC-MS and 61 identified through NMR, many of which bear structural similarities to known anti-cancer agents. Notably, five compounds demonstrated a high affinity forbinding to COX2, with d-glycero-d-galacto-heptose achieving an impressive docking score, surpassing several established COX2 inhibitors.

This study highlights the therapeutic potential of *T. violacea* compounds and lays the groundwork for further exploration of their mechanisms of action and potential applications in cancer treatment. This emphasises the importance of investigating natural plant extracts as a source for the development of new and effective treatments for TNBC, which is an area of urgent need in oncology.

ACKNOWLEDGEMENTS

I am deeply grateful to Allah for His countless blessings and unwavering guidance throughout my PhD journey.

Special thanks are due to my supervisor, Professor Zodwa Dlamini, for her exceptional dedication to my research. Professor Dlamini's efforts in securing and extending funding were critical, ensuring the continuity of my work amidst various challenges. Her commitment to the completion of this thesis, along with her expert guidance, has been an indispensable source of support throughout this journey.

I am equally thankful for the guidance of Dr. Rodney Hull, whose expertise in research methodology has been invaluable. Dr. Rodney has been instrumental in guiding me through each step of the research process, encompassing meticulous lab work, data analysis, and the nuances of academic writing. His profound understanding of research dynamics and his skill in imparting this knowledge have significantly shaped the direction and quality of my work.

I express my gratitude to Dr. Clement Penny for his significant contribution by allowing me to use the Internal Medicine Oncology Lab at Wits University.

My deepest appreciation goes to my parents for their unconditional love, relentless encouragement, and faith in my capabilities. Their sacrifices and steadfast support have been a constant source of inspiration.

To my beloved wife, my sincere thanks for being my pillar of strength, understanding my commitment to this journey, and providing unwavering support and encouragement. Your firm belief in me has been invaluable.

I am blessed with wonderful children, whose love, understanding, and patience have been a constant motivation. Your smiles and laughter have brought joy and inspiration during the most challenging times.

My gratitude also extends to the members of the Internal Medicine Lab group for their collaboration, support, and stimulating discussions. Their collective expertise has greatly

enriched my research experience.

Finally, I am thankful to all my friends, colleagues, and mentors who have supported me in various capacities during my PhD journey. Your encouragement, constructive feedback, and camaraderie have been pivotal in my academic and personal growth.

I am humbled and thankful to everyone who has contributed to my PhD thesis. This achievement would not have been possible without your support.

RESEARCH OUTPUT

1.1 Publications in peer-reviewed/refereed journals

1. **Alaouna M**, Penny C, Hull R, Molefi T, Chauke-Malinga N, Khanyile R, Makgoka M, Bida M, Dlamini Z. Overcoming the Challenges of Phytochemicals in Triple Negative Breast Cancer Therapy: The Path Forward. Plants (Basel). 2023 Jun 16;12(12):2350. doi: 10.3390/plants12122350. PMID: 37375975; PMCID: PMC10301029
2. Hull, R., Marima, R., **Alaouna, M.**, Demetriou, D., Reis, R.M., Molefi, T. and Dlamini, Z., (2022). **Viral Encoded miRNAs in Tumourigenesis: Theranostic Opportunities in Precision Oncology**. *Microorganisms*, *10*(7), p.1448
3. Dlamini, Z., Hull, R., Mbatha, S. Z., **Alaouna, M.**, Qiao, Y-L. Yu, H., and Chatziioannou A. (2021). **Prognostic alternative splicing signatures in esophageal carcinoma**. *Cancer management and research.* 13. 4509-4527
4. Dlamini, Z., Alaouna, M., Mbatha, S., Bhayat, A., Mabongo, M., Chatziioannou, A., Hull, R. (2021). Genetic Drivers of Head and Neck Squamous Cell Carcinoma: Aberrant Splicing Events, Mutational Burden, HPV Infection and Future Targets. *Genes*, 12, doi:10.3390/genes12030422.
5. Dlamini, Z., Alaouna, M., Cholo, M.C., Hull, R. (2020). Is targeting dysregulation in apoptosis splice variants in Mycobacterium tuberculosis (MTB) host interactions and splicing factors resulting in immune evasion by MTB strategies a possibility? *Tuberculosis* (Edinburgh, Scotland), 124, 101964, doi: 10.1016/j.tube.2020.101964
6. **Alaouna, M.,** Hull, R.**,** Penny, C., Dlamini, Z. (2019)**. Esophageal cancer genetics in South Africa.** *Clin Exp Gastroenterol*., 12:157-177.

1.2 Published Conference Abstracts

1. Zodwa Dlamini, Clement Penny and Rodney Hull (2022). Identification of anti-neoplastic compounds on a triple negative breast cancer cell line from *T. violacea* , *Cancer Res* 82 (12_Supplement): 4060.
2. Dlamini, Z., Alouna, M. Hull, R and Penny, C. (2021). The effects of extracts of the indigenous South African plant, *Tulbaghia* violacea , on triple negative breast cancer cells, Cancer Research, *Cancer Research* 81 (13 Supplement), 2843-2843
3. ALAOUNA, M., PENNY, C., ULLL, R. & DLAMINI, Z. 2023. The molecular composition of a water-soluble extract from the leaves of the indigenous Southern African plant *Tulbaghia violacea* that displays anti-cancer activity against a triple negative breast cancer cell line. Cancer

Research, 83, 3831-3831

4. DLAMINI, Z., HULL, R., ALOUNA, M. & PENNY, C. 2023. Changes in the transcriptome of a triple negative breast cancer cell line following treatment with a water-soluble extract from the leaves of the indigenous Southern African plant *Tulbaghia* violacea. Cancer Research, 83, 3820-3820.
5. HULL, R., DLAMINI, Z., PENNY, C. & ALAOUNA, M. 2023.The anticancer activity of a water-soluble extract from the leaves of the indigenous Southern African plant *Tulbaghia* violacea against a triple negative breast cancer cell line. Cancer Research, 83, 3830-3830.

1.3 Publications in progress

1. Alaouna, M., et al., Tapping into the Potential of the South African Plant, Tulbagh-ia violacea, for Triple Negative Breast Cancer (TNBC) Treatment. Plants, 2024.(Submitted)
2. Alaouna, M., et al., Exploring Tulbaghia violacea South African Plant Extract as a Therapeutic Approach for Tripple Negative Breast Cancer (TNBC) Metastasis. Plants, 2024.(Submitted)

2.

Table of Contents

Abstract:..... v
ACKNOWLEDGEMENTS vii
RESEARCH OUTPUT ix
1.1 Publications in peer-reviewed/refereed journals ix
1.2 Published Conference Abstracts ix
1.3 Publications in progress x
Table of Contents xi
List of Figures xvi
List of Tables xxi
List of Abbreviation xxii
Chapter 1 Introduction 1
1.4 Triple negative breast cancer (TNBC) 6
1.5 Emerging Breast Cancer Subtypes and Genetic Alterations: Implications for Survival Outcomes and Therapeutic Significance 7
1.6 Epidemiology and Risk Factors for TNBC 9
1,6.1 Socio-economic Status 10
1,6.2 Mutations in BRCA 11
1,6.3 Mutations in other genes are also involved in TNBC pathogenesis. 13
1,6.4 Additional Risk Factors: Obesity, Parity, and Breast-feeding 13
1.7 Therapeutic Options 14
1,7.1 Chemotherapy 14
1,7.2 Salts of Platinum 15
1,7.3 Targeted Agents 15
1,7.4 Anti-Angiogenic Agents 15
1,7.5 Bevacizumab 16
1,7.6 Sunitinib and Sorafenib 16
1,7.7 Poly (ADP-ribose) Polymerase (PARP) Inhibitors 16
1,7.8 EGFR Inhibitors 16
1.8 Phytochemicals: Anti-cancer plant compounds 17
1,8.1 Cell cycle arrest 20
1,8.2 Phytochemicals as antioxidants: cancer prevention. 21

1,8.3 Redox Regulation of Cell Proliferation and Survival 22
1,8.4 Phytocides as regulators of miRNAs 29
1,8.5 Phytochemical targeting angiogenesis 30
1,8.6 Phytochemicals targeting the Wnt signaling pathway 36
1,8.7 Phytochemical targeting of the RTK signaling pathway 37
1.9 Cotyledon orbiculata (Crassulaceae) 41
1.10 Tulbaghia violacea 42
Chapter 2 Methods and Materials 45
2.1 Methods 47
2,1.1 Cell culture 47
2,1.2 Thawing of cells 48
2,1.3 Cell cryopreservation 48
2,1.4 Cell count determination 49
2,1.5 Determination of changes in the cell morphology caused by treatment with various extracts 49
2,1.6 Determination of the IC50 value for the crude extracts 51
2,1.7 Treatment of cells with purified fractions: Bioassays and cytotoxicity assays 51
2,1.8 Real-Time Cell Analysis (RTCA) by XCelligence 53
2.2 Determining the effects of Active plant extracts on TNBC cells 55
2,2.1 Analysis of the effect of active plant extracts on cellular apoptosis 55
2,2.2 Antioxidant assay 61
2,2.3 Detection of the molecular components present in the crude extracts 62
2,2.4 Gas chromatography (GC) in conjunction with mass spectroscopy (MS) analysis 63
2,2.5 NMR Spectroscopy 64
2.3 Computational modelling of the interaction between COX -2 and the components of the *T. violacea* water-soluble extract. 65
2.4 Effects of the extracts on protein expression. 67
2,4.1 Protein Extraction Protocol. 67
2,4.2 Quantification methods 68
2,4.3 Bradford assay 68
2,4.4 Qubit assay 70
2,4.5 SDS-PAGE Analysis 70
2,4.6 Proteome Profiler Arrays 72

2.5 The effect of active purified fractions on miRNA transcription and gene expression 73
2.6 Next generation sequencing 74
2.7 Statistical Analysis 74
Chapter 3 Results 76
3.1 Introduction 76
3,1.1 The cytotoxic effects of *T. violacea* and *C. orbiculata leaf* extract on normal and TNBC cancer cell lines 77
3.2 Determination of the IC50 values for each of the crude extracts on MDA MB 231 cells 77
3.3 Determination of the IC50 through Real Time Cell Analysis 77
3.4 Determination of the IC50 through the use of alamar blue cytotoxicity assays 85
3.5 Pro-apoptotic and anti-proliferative activities of *T. violacea* water soluble extracts 90
3.6 Morphological changes following treatment with plant extracts 91
3.7 Apoptosis assay 101
3.8 Cell cycle assay 103
3.9 Measuring the effect, the active plant extract had on cell invasion and migration 106
3.10 Migration assays 106
3.11 Scratch assay for migration analysis 107
3.12 Migration assay using RTCA cell invasion and migration assay plates 113
3.13 Cell invasion assays 114
3.14 Boyden dye-based assay 114
3.15 3.4.2.2.Invasion assay using RTCA cell invasion and migration assay plates 116
3.16 Cell adhesion assays 117
3.17 Determination of Antioxidant Activity Using the 2,2-Diphenyl-1-picrylhydrazyl (DPPH) Radical Scavenging Method 119
3.18 Determination of the molecular composition of the *T. violacea* water soluble extract 122
3.19 FITR to examine the biological materials. 122
3.20 Gas Chromatography mass spectrophotometry 125
3.21 NMR Spectroscopy 129
3.22 Proteomic analysis of the RTK pathway 162
3.23 Whole transcriptome analysis of treated and untreated TNBC and normal breast cells 197
Chapter 4 Discussion 212
4.1 Background 212
4.2 Determining the IC50 values 214

4.3 Morphological studies on normal and TNBC cancer cell lines treated leaf extracts from *T. violacea* 216
4.4 The water-soluble crude extract of *T. violacea* induced apoptosis in TNBC cells. 217
4.5 *T. violacea* crude water-soluble extracts altered the cell cycle of TNBC and normal breast cancer cells. 218
4.1.1 Summary 221
4.2 Effect of *T. violacea* water-soluble leaf extract on the metastatic potential of MDA-MB231 cells. 222
4,5.1 Background 222
4.2.1 The *water-soluble crude extract of T. violacea* inhibited the migration of TNBC cells. 223
4.2.2 Effect of *T. violacea* crude water-soluble extract on the adhesion of TNBC cells. 224
4.2.3 Effect of *T. violacea* crude extract on TNBC cell invasion. 225
4.2.4 The effect of *T. violacea* crude extracts on cell migration in triple-negative breast 226
4.2.5 Summary 227
4.4 Determination of the molecular composition of the *T. violacea* water soluble extract 229
4.4.1 4 H-Pyran-4-one, 2,3-dihydro-3,5-dihydroxy-6-methyl (DDMP) 230
4.4.2 1,2,4-Triazine-3,5(2H,4H)-dione (6-azauracil) 232
4.4.3 Benzaldehyde, 4-(1-methylethyl)-(cuminaldehyde) 234
4.4.4 Vanillin 235
4.4.5 Oxime-, methoxy-phenyl 238
4.4.6 Pyrrolidine 239
4.4.7 Schizandrin 239
4.4.8 Taurolidine 242
4.4.9 Alpha-Pinene 245
4.6 RTK pathway analysis following treatment of cells with T. violacea crude water-soluble extract 246
4.4.10 Transcriptome analysis 248
4.4.11 The transcriptome and increased levels of apoptosis 249
4.4.12 The transcriptome and S phase checkpoint activation 250
Chapter 5 Conclusion 251
Chapter 6 Appendices 255
6.1 Appendices A 255

6.2 Appendix B 263
6,2.1 Ethics waiver 263
References 265

List of Figures

Figure 1.1 The estimated global cancer incidence and age-standardised incidence rates by continent in 2020 were based on the GLOBOCAN data. 3
Figure 1.2 Estimated global incidence of new cancer cases in females in 2020. 4
Figure 1.3 It is the most prevalent and deadly cancer in South Africa. 5
Figure 1.4 Treatment strategies for breast cancer. 5
Figure 1.5 General classes of targeted therapeutics used in the treatment of triple-negative breast cancer (TNBC). 7
Figure 1.6 Frequency of different molecular subtypes of triple-negative breast cancer (TNBC). 8
Figure 1.7 Structural features and protein interaction domains of BRCA1 and BRCA2. 12
Figure 1.8 The roles of phytochemicals in cancer therapy 19
Figure 1.9 Hallmarks of Cancer 20
Figure 1.10 Schematic representation of oncogenic signals, ROS generation, and the role of phytochemicals in cancer. 24
Figure 1.11 Intrinsic and extrinsic apoptotic pathways. 27
Figure 1.12 Mechanisms involved in blood vessel development. 32
Figure 1.13 GnRH signaling pathway regulates LH and FSH production 34
Figure 1.14 Signal transduction pathway of the ErbB receptor. 39
Figure 2.1 Depiction of the calculation of morphological features 51
Figure 2.2 The layout of the 96-well plate was used to determine IC50 in the alamar blue assay 53
Figure 2.3 Layout of the excelligence e plate for the determination of the IC50. 54
Figure 2.4 Cell invasion and migration plate setup. 59
Figure 2.5 Scratch Assay. 60
Figure 2.6 The target cyclooxygenase-2 (COX-2) enzyme. 66
Figure 2.7 The structure of the anticancer bioactive compounds identified from *T. violacea* 67
Figure 3.1 shows a cell number titration curve used to determine the optimal seeding density for MDA-MB-231 cells using the xCELLigence Real-Time Cell Analysis (RTCA) system. 79
Figure 3.2 shows the determination of the IC50 81
Figure 3.3 shows the determination of the IC50 82
Figure 3.4 shows the determination of the IC50 84

Figure 3.5 shows the determination of the IC50 85
Figure 3.6 Figure 3.6 shows the determination of the IC50 (half-maximal inhibitory concentration) value for the water extract of *T. violacea* against the MDA-MB231 triple-negative breast cancer cell line using an Alamar blue cytotoxicity assay. 87
Figure 3.7 depicts the determination of the IC50 (half-maximal inhibitory concentration) value for the methanol extract of *T. violacea* against the MDA-MB231 triple-negative breast cancer cell line using an Alamar blue cytotoxicity assay. 87
Figure 3.8 depicts the determination of the IC50 value for the C. orbiculata water extract against MDA-MB-231 triple negative breast cancer cells using an Alamar blue cytotoxicity assay. 88
Figure 3.9 depicts the determination of the IC50 value for the C. orbiculata methanol extract against the MDA-MB-231 triple negative breast cancer cell line using the Alamar blue cytotoxicity assay. 89
Figure 3.10 depicts a series of microscopic images illustrating the morphological changes observed in MDA-MB-231 triple-negative breast cancer cells after treatment 94
Figure 3.11 depicts the morphological changes observed in MDA-MB-231 triple-negative breast cancer cells 95
Figure 3.12 depicts a series of microscopic images showing the morphological changes in MDA-MB-231 triple-negative breast cancer 96
Figure 3.13 depicts various morphological characteristics of untreated MDA-MB-231 cells over a 72-hour period. 97
Figure 3.14 depicts the morphological changes observed in MDA-MB-231 cells 98
Figure 3.15 depicts the morphological changes observed in untreated MCF10A cells over a 72-hour period. 99
Figure 3.16 depicts the morphological changes observed in MCF10A cells at various time points after treatment with the water-soluble extract of *T. violacea*. 100
Figure 3.17 depicts the flow cytometry analysis of apoptosis in MCF10A and MDA-MB-231 cells treated with the *T. violacea* water-soluble extract 102
Figure 3.18 depicts the results of an Annexin V apoptosis assay performed on triple-negative breast cancer (TNBC) cells and normal breast cells after treatment with varying concentrations of the *T. violacea* water-soluble extract 103
Figure 3.19 depicts the results of a cell cycle analysis performed on both triple-negative

breast cancer (TNBC) and normal breast cell lines using flow cytometry. 105
Figure 3.20 depicts the results of a scratch assay performed to evaluate the impact of different plant extracts on the migration of MDA-MB-231 triple-negative breast cancer cells..... 109
Figure 3.21 depicts the changes in the area of a scratch created in a monolayer of MDA-MB231 cells following treatment with various plant extracts. 110
Figure 3.22 depicts the assessment of the effects of various extracts on the migration of triple-negative breast cancer (TNBC) cells using a scratch assay. 111
Figure 3.23 depicts the results of a scratch assay performed on MCF-10A cells, which are normal breast cells. 112
Figure 3.24 depicts the results of a scratch assay performed on MCF-10A cells, which are normal breast cells. 112
Figure 3.25 Figure 3.25 depicts the results of an RTCA cell migration assay examining the effect of the *T. violacea* water-soluble crude extract on MDA-MB231 triple-negative breast cancer cells. 113
Figure 3.26 presents a bar graph depicting the results of a cell invasion assay that measured the ability of MDA-MB-231 triple-negative breast cancer cells and MCF-10A normal breast cells 116
Figure 3.27 depicts the results of an invasion assay examining the effect of the water-soluble extract of *T. violacea* on the invasive ability of MDA-MB-231 triple-negative breast cancer cells. 117
Figure 3.28 a bar graph depicting the cell adhesion levels of different cell lines to the Geltrex™ matrix. 119
Figure 3.29 depicts the antioxidant activity of various plant extracts, including the *T. violacea* water-soluble extract, *T. violacea* methanol-soluble extract, C. orbiculata water-soluble extract, and C. orbiculata methanol-soluble extract, as determined 121
Figure 3.30 shows the Fourier-transform infrared (FTIR) spectra of the water-soluble and methanol-soluble extracts from *C. orbiculata*. 124
Figure 3.31 shows the Fourier-transform infrared (FTIR) spectra of the water-soluble and methanol-soluble extracts from Tulbaghia violacea. 124
Figure 3.32 shows the mass charge spectrum for the water-soluble extract of *T. violacea*. 126
Figure 3.33 shows the nuclear magnetic resonance (NMR) spectrum of the water-soluble extract from the plant *T. violacea*. 130

Figure 3.34 depicts the molecular docking of various bioactive anticancer compounds identified from Tulbaghia violacea extracts with the cyclooxygenase-2 (COX-2) protein 157
Figure 3.35 depicts the molecular docking analysis of various compounds identified in the crude extracts of *Tulbaghia violacea* with the cyclooxygenase-2 (COX-2) protein. 161
Figure 3.36 shows the results of a protein profiler array, which allows for the detection and semi-quantitative analysis of the relative levels of phosphorylation of 43 receptor tyrosine kinases (RTKs) and two2 additional proteins. 163
Figure 3.37 Fold changes in the expression of the different tyrosine kinases. 166
Figure 3.38 presents a series of volcano plots representing the differential gene expression analysis between various cell lines and treatment conditions 198
Figure 3.39 39 illustrates the expression changes shared between treated and untreated normal breast and triple-negative breast cancer (TNBC) cell lines. (A) The Venn diagram showingshows the overlap of genes whose expression changed after treatment ofin TNBC..... 200
Figure 3.40 4039 illustrates the expression changes shared between treated and untreated normal breast and triple-negative breast cancer (TNBC) cell lines 202
Figure 3.41 presents a heatmap visualisationvisualization of the functional enrichment analysis performed using the DAVID online tool 205
Figure 3.42 depicts the mRNA expression levels of pro-apoptotic and anti-apoptotic genes in normal breast cells and triple-negative breast cancer (TNBC) cells,..... 208
Figure 3.43 The figure depicts the mRNA levels of various cell cycle genes involved in S phase progression or arrest, as determined by next-generation sequencing 210
Figure 4.1depicts the extrinsic (blue box) and intrinsic (orange box) pathways of apoptosis, a form of programmed cell death 213
Figure 4.2 2depicts a circular diagram illustrating the different phases of the cell cycle..... 219
Figure 5.1 Signaling Pathway Network Regulating Cellular Processes, ... 253
Figure 6.1 4H-Pyran-4-one, 2,3-dihydro-3,5-dihydroxy-6-methyl- T. violacea aqueous compound NMR spectrum. 255
Figure 6.2 1,2,4-Triazine-3,5(2H,4H)-dione T. violacea aqueous compound NMR spectrum 256
Figure 6.3 1,2,4-Triazine-3,5(2H,4H)-dione T. violacea aqueous compound NMR spectrum 257
Figure 6.4 1,2,4-Triazine-3,5(2H,4H)-dione T. violacea aqueous compound..... 257
Figure 6.5 Vanillin T. violacea aqueous compound NMR spectrum..... 258
Figure 6.6 Oxime-and methoxy-phenyl T. violacea aqueous compound NMR spectra. 259

Figure 6.7 Figure 5.7. Pyrrolidine T. violacea aqueous compound NMR spectrum. 259
Figure 6.8 Schizandrin T. violacea aqueous compound NMR spectrum.....260
Figure 6.9. Alpha-Pinene *T. violacea* aqueous compound NMR spectrum.....261
Figure 6.10 Taurolidine T. violacea aqueous compound NMR spectrum. 261

List of Tables

Table 2.1 List of materials used in this study 45
Table 2.2 Cell lines details and origins 46
Table 2.3 Concentrations of extract used in the antioxidant assay 62
Table 2.4 Standards for the Bradford assay 69
Table 2.5 Stacking and separating gel solutions 71
Table 3.1 Final IC50 values adopted for the rest of this study 89
Table 3.2 GC MS spectral of some compounds identified in the MS analysis of the methanol soluble fraction of *T. violacea* 126
Table 3.3 Examples of compounds detected by NMR analysis of the crude water-soluble *T. violacea* extract. 131
Table 3.4 Compounds with known anti-cancer activity. 132
Table 3.5 Compounds with known medical applications. 140
Table 3.6 Molecular docking score for the anticancer bioactive compounds of *T. violacea* water crude extract with COX-2 protein 158
Table 3.7 Function protein interactions and the result of exposure to the water-soluble *T. violacea* 166
Table 5.1 List of Proteins in the Signaling Pathway Network 254
Table 6.1 Examples of compounds detected by NMR analysis of the crude water-soluble T. 262

List of Abbreviation

2,2-Diphenyl-1-picrylhydrazyl (DPPH) 108

4 H-Pyran-4-one, 2,3-dihydro-3,5-dihydroxy-6-methyl (DDMP) 184

5-fluorouracil (5FU) 45

6-Azauracil (6AU) 186

6-mercaptopurine (6MP) 186

6-thioguanine (6-TG) 186

Alamar Blue (AB) 47

cell index (CI) 48

colorectal cancers (CRC) 37

cyclin-dependent kinase (CDK) 193

cyclin-dependent kinase 2 (CDK2) 176

cyclin-dependent kinases (CDKs) 52

cytosine arabinoside (ARA-C) 186

death receptors (DRs) 23

differential interference contrast (DIC) 96

dimethyl sulfoxide (DMSO) 43

disease-free survival (DFS) 6

double strand break (DSB) 189

endothelial progenitor cells (EPCs) 28

epidermal growth factor
(EGF) 28
epithelial-to-mesenchymal transitions
(EMTs) 34
extracellular matrix
(ECM) 28
extracellular signal-regulated kinase
(ERK) 31
focal adhesion kinase
(FAK) 31
follicle-stimulating hormone
(FSH) 31
Food and Drug Administration
(FDA) 190
Fourier transform infrared
(FTR) 57
Fourier transform infrared spectroscopy
(FITR) iii
Free inductive decay
(FID) 59
G protein-coupled receptor
(GPCR) 31
gas chromatography-mass spectrometry
(GC-MS) iii
GnRH-associated peptide
(GAP) 32
gonadotropin-releasing hormone
(GnRH) 31
guanosine monophosphate
(GMP) 187
hormone replacement the
(HRT) 4
human epidermal grov .tor 2 receptors
(HER2) iii
interleukin-1
(IL-1) 196
Jun N-terminal kinase
(JNK) 31
L-3,4-dihydroxyphenylalanine
(L-DOPA) 187
luteinizing hormone
(LH) 31
mass spectrometry
(MS) 58

matrix metalloprotease 9
(MMP9) 29
metastatic breast cancer
(MBC) 4
methoxy-phenyl oxime
(MPO) 191
mitogen-activated protein kinase
(MAPK) 31
multidrug resistance protein 1
(MRP1) 191
National Cancer Database
(NCDB) 10
Non-homologous DNA end-joining
(NHEJ) 189
nuclear magnetic resonance
(NMR) iii
oestrogen receptor
(ER) 6
pathological complete response
(pCR) 14
phosphatidylserine
(PS) 51
phosphoinositide-dependent kinase-1
(PDK-1) 37
Poly (ADP-ribose) Polymerase
(PARP) 15
potassium bromide
(KBr) 57
progression-free survival
(PFS) 16
proteins in the receptor tyrosine kinase
(RTK) iii
reactive nitrogen species
(RNS) 182
reactive oxygen species
(ROS) 19
Real-Time Cell Analysis
(RTCA) 48
second mitochondrial activator of caspases/direct IAP-binding protein with low pI
(Smac/DIABLO) 23
signal transducer and transcription
(STAT) 19
smooth muscle cells

(FGF) 32
follicle-stimulating hormone
(FSH) 35
Food and Drug Administration
(FDA) 223
Fourier transform infrared
FTIR 70
Fourier transform infrared spectroscopy
(FITR) iii
Free inductive decay
(FID) 72
G protein-coupled receptor
(GPCR) 35
gas chromatography-mass spectrometry
(GC-MS) iii
gonadotropin-releasing hormone
(GnRH) 36
guanosine monophosphate
(GMP) 219
hormone replacement therapy
(HRT) 4
human epidermal growth factor receptor 2
(HER2) 10
Human Phospho-Receptor Tyrosine Kinase
(RTK) 80
hydro-3,5-dihydroxy-6-methyl-
(DDMI) 139
L-3,4-dihydroxyphenylalanine
(L-DOPA) 219
LDL receptor protein
(LRP) 39
liquid chromatography mass spectrometry
(LC-MS) 213
luteinizing hormone
(LH) 35
mass spectrometry
(MS) 213
matrix metalloprotease
(MMP) 33
metastatic breast cancer
(MBC) 16
mitogen-activated protein kinase
(MAPK) 36
multidrug resistance protein 1
(MRP1) 225
Mycobacterium tuberculosis
(MTB) vii
National Cancer Database
(NCDB) 10
next-generation sequencing
(NGS) 48
normalized cell index

3-phosphoinositide-dependent kinase
(PDK) 44
4 H-Pyran-4-one, 2,3-dihydro-3,5-dihydroxy-6-methyl-
(DDMP) 214
5-fluorouracil
(5FU) 218
6-azauracil
(6AU) 219
(6AZU) 218
azauracil
(AZU) 218
basal-like subtypes
(BL1 and BL2) 7
cell index
(CI) 61
colorectal cancer
(CRC) 220
cyclin-dependent kinase 2
(CDK2) 202
Cyclins and cyclin-dependent kinases
(CDKs) 66, 115
Cyclooxygenase 2 protein
(COX-2) 74
death receptors
(DRs) 26
differential interference contrast
(DIC) 118
dimethyl sulfoxide
(DMSO) 54
Diphenyl-1-picrylhydrazyl
(DPPH) 131
Direct Inhibitor of Apoptosis-Binding protein
(DIABLO) 26
disease-free survival
(DFS) 14
double strand break
(DSB) 221
endothelial progenitor cells
(EPCs) 33
epithelial-to-mesenchymal transitions
(EMTs) 40
extracellular matrix
(ECM) 67
extracellular signal-regulated kinase
(ERK) 36
factor-kappaB
(NF-kB) 148
fibroblast growth factor
(FGF) 32
fibroblast growth factor (bFGF

(NCI) 62

nuclear magnetic resonance

(NMR) iii

oestrogen receptor

(ER) 6

pathological complete response

(pCR) 14

phosphatidylserine

(PS) 64

poly (ADP-ribose) polymerase

(PARP) 217

poly-ADP ribose polymerase

(PARP) 16

potassium bromide

(KBr) 71

propidium iodide

(PI) 111

reactive nitrogen species

(RNS) 211

reactive oxygen species

(ROS) 21

real-time cell analysis

(RTCA) 100

Real-Time Cell Analysis

(RTCA) 62

Second mitochondria-derived activator of caspase

(Smac) 26

signal transducer and transcription

(STAT) 21

smooth muscle cells

(SMCs) 32

systemic inflammatory response syndrome

(SIRS) 228

trinitrobenzene sulfonic acid

(TNBS) 223

Triple Negative Breast Cancer

(TNBC) iii

tumour necrosis factor

(TNF) 230

tyrosine kinase inhibitors

(TKIs) 16, 35

untranslated region

(UTR) 30

X chromosome-linked inhibitor of apoptosis protein

(XIAP) 27

(SMCs) 28

Sonic Hedgehog

(SHH) 180

Src homology 3

(SH3) 35

systemic inflammatory response syndrome

(SIRS) 194

Triple Negative Breast Cancer

(TNBC) iii

tumour necrosis factor

(TNF) 196

tyrosine kinase inhibitors

(TKIs) 15

uridine monophosphate

(UMP) 187

X chromosome-linked inhibitor of apoptosis protein

(XIAP) 24

Chapter 1 Introduction

Cancer claimed the lives of 9.6 million people throughout the world in 2018 [5]. Breast cancer is a major health concern worldwide, with over 2.1 million new cases and 63000 deaths recorded in 2018 [6]. Breast cancer in women is the most frequent cancer in the world, accounting for 2.26 million cases in 2020. Breast cancer causes an estimated 458,000 fatalities per year, emphasising the seriousness of this disease worldwide [7]. Breast cancer burden is affected by numerous variables including population growth, age, high fasting plasma glucose, high body mass index, and socioeconomic development index (SDI) quintiles [8]. Breast cancer contributes significantly to the overall mortality in women, emphasising the need for continued research, prevention, and treatment efforts to mitigate its burden [9]. Furthermore, protein consumption has been linked to breast cancer incidence and death, highlighting the possible influence of dietary variables on the breast cancer burden [10]. Understanding the empowering experiences of breast cancer survivors is also critical for alleviating the burden of breast cancer and improving patient outcomes [6]. These findings underscore the urgent need for comprehensive strategies to address the global burden of breast cancer, including public health interventions, early detection, and personalised risk assessment. The most frequent malignancies in the United States are breast, lung, prostate, colorectal, and melanoma cancers [11]. Although Asia has the highest number of cancer cases, the island nations of Oceania, Australia, New Zealand, Polynesia, and Micronesia have the highest age-standardised rates. Breast cancer is the most commonly diagnosed and deadly malignancy in women worldwide (Figure 1.2 A). Lung and cervical uterine cancers are the third and fourth most common cancers, respectively, and kill a proportionately higher number of patients. Breast cancer accounts for more than 25% of all cancer cases in women and 15% of all cancer-related deaths in females [6]. While only 5–10% of cancers are hereditary, 90–95% arise from environmental and lifestyle factors. Inherited breast cancer often involves mutations in BRCA1 and BRCA2. However, not all individuals with these mutations develop breast cancer, highlighting the importance of genetic and environmental interactions [12]. Metastatic breast cancer is often fatal with just a 23 percent five-year survival rate. Breast cancer often metastasizes to organs such as bones, liver, or lungs [8] (Figure 1.2B).

Breast cancer is the most frequent cancer among women in South Africa and ranks second in terms of cancer-related mortality, trailing only in cervical and uterine cancers (Figure 1.3). One out of Every 29 women in South Africa are expected to be diagnosed with breast cancer. In 2014, the age-standardised incidence rate was 32 years per 100,000 women [13]. Breast cancer is divided into two types: hormone-sensitive and hormone-insensitive cancers. The goal of this study was to investigate hormone-refractory and triple-negative breast cancers.

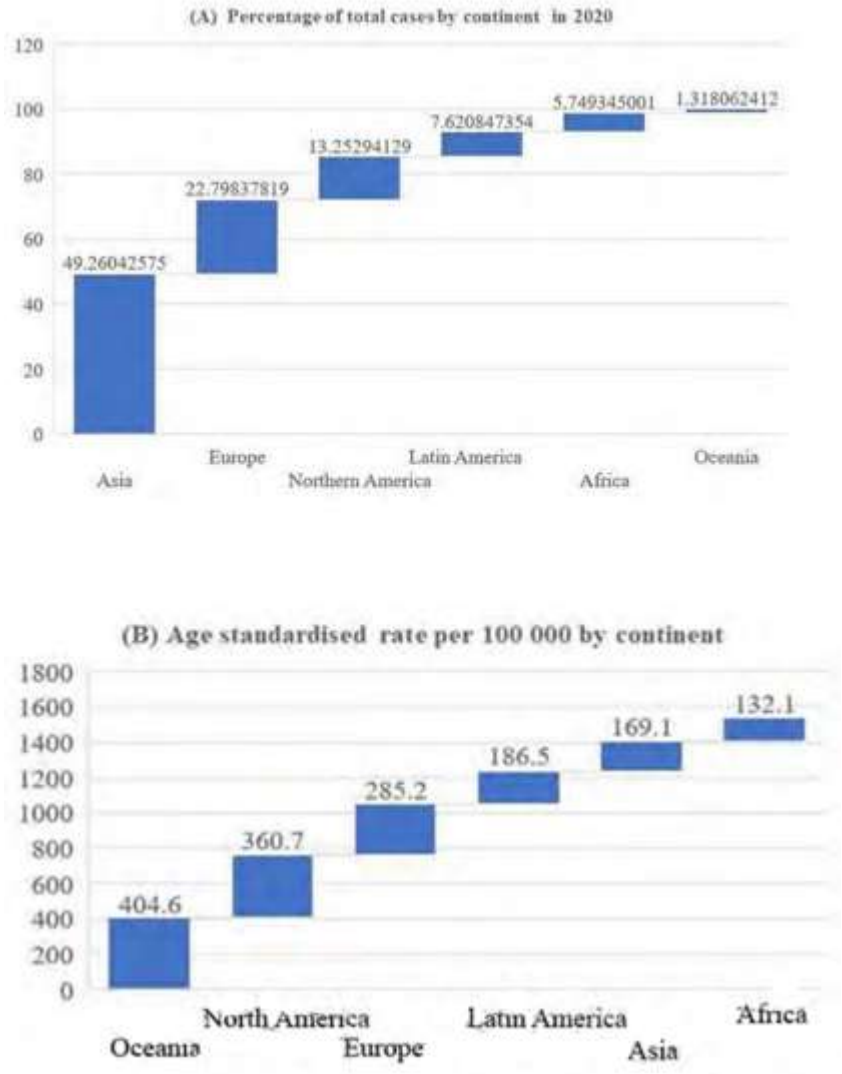

Figure 1.1 The estimated global cancer incidence and age-standardised incidence rates by continent in 2020 were based on the GLOBOCAN data. (A) Pie chart showing the estimated percentage of new cancer cases diagnosed in 2020 for each continent. Asia had the highest percentage at 49.3% of global cancer cases, followed by Europe at 22.8%, North America at 12.8%, Latin America and the Caribbean at 7.3%, Africa at 6.1%, and Oceania at 1.3%.(B) The bar graph displays the age-standardised cancer incidence rate per 100,000 people for each continent in 2020. Australia and New Zealand (Oceania) had the highest age-standardized incidence rate at 532.5 cases per 100,000 people. North America had the second highest rate at 368.7 per 100,000 people. Europe ranked third at 319.6 per 100,000 people. Latin America and the Caribbean have incidence rate of 189.6 per 100,000. Asia and Africa had the lowest age-standardised incidence rates at 152.3 and 129.3 per 100,000, respectively.

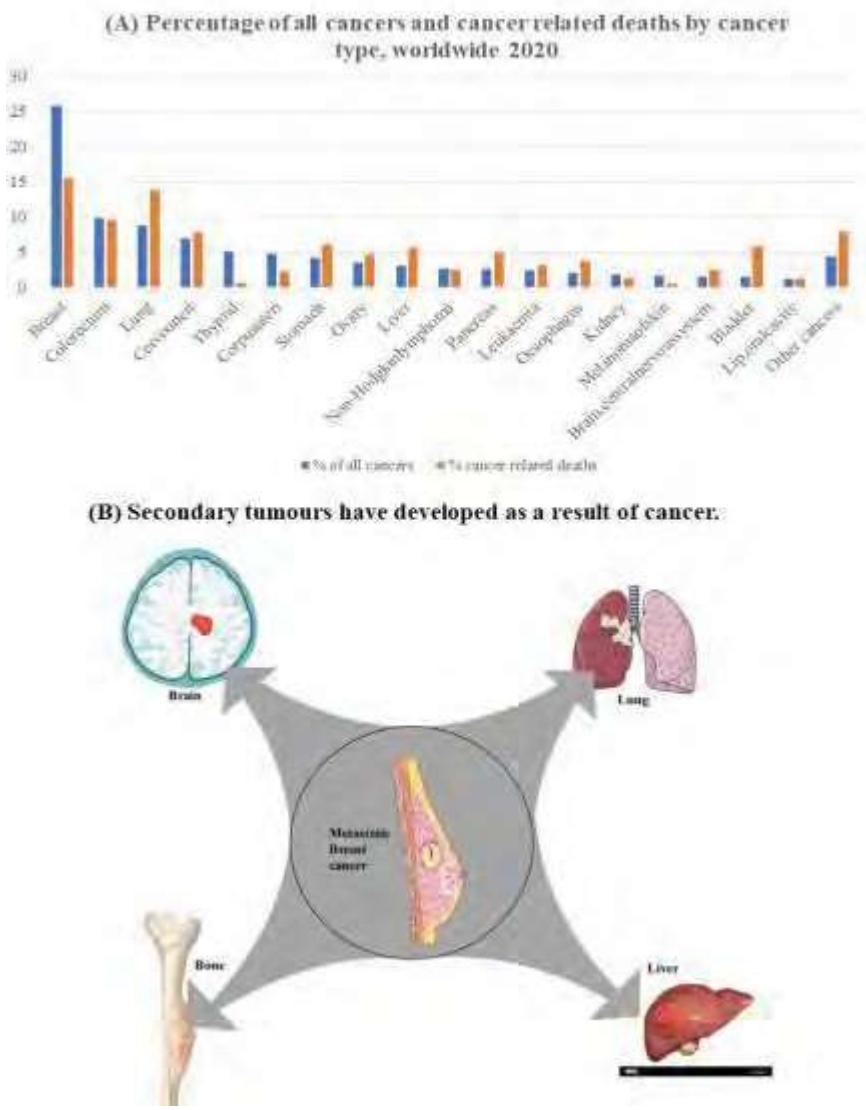

Figure 1.2 Estimated global incidence of new cancer cases in females in 2020. The bar graph presents the number of new cancer cases diagnosed in females worldwide in 2020 for the top 10 cancer sites based on the GLOBOCAN 2020 data. Breast cancer had the highest incidence (2.26 million cases, 24.5% of all cancers in women), followed by colorectal (0.57 million, 9.4%), lung (0.54 million, 8.4%), cervical (0.60 million, 6.5%), and thyroid (0.43 million, 5.1%) cancers. Corpus uteri, stomach, ovarian, liver, and non-Hodgkin lymphoma were the 6th to 10th most common sites, with incidences ranging from 0.23 to 0.42 million cases. The data represent estimates of new primary cancer cases, and not secondary tumours, resulting from metastasis. This figure highlights the substantial global burden of cancer in women and the key cancer sites for prevention and control.

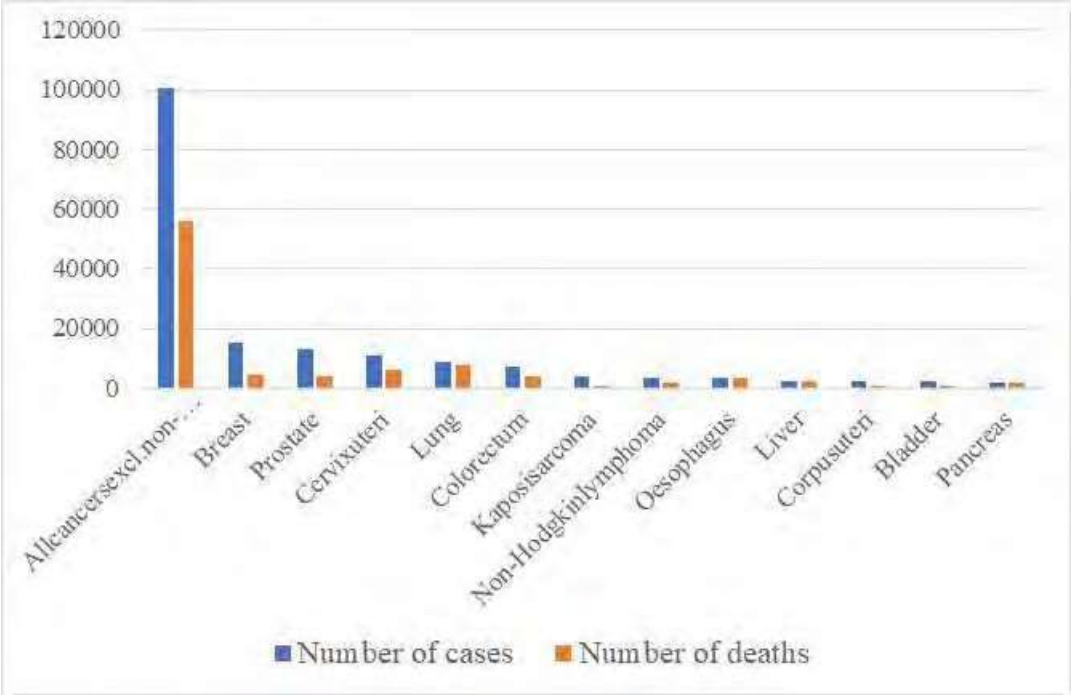

Figure 1.3 It is the most prevalent and deadly cancer in South Africa. The bar graph shows the top 10 most frequently diagnosed cancers and the top 10 causes of cancer-related deaths in South Africa, based on the 2022 National Cancer Registry data. Prostate, breast, cervical, colorectal, and lung cancers are the most commonly diagnosed cancers, whereas lung, colorectal, breast, cervical, and prostate cancers are the leading causes of cancer-related mortality. The data highlight the significant burden of cancers that are common globally and more frequently in developing countries such as South Africa.

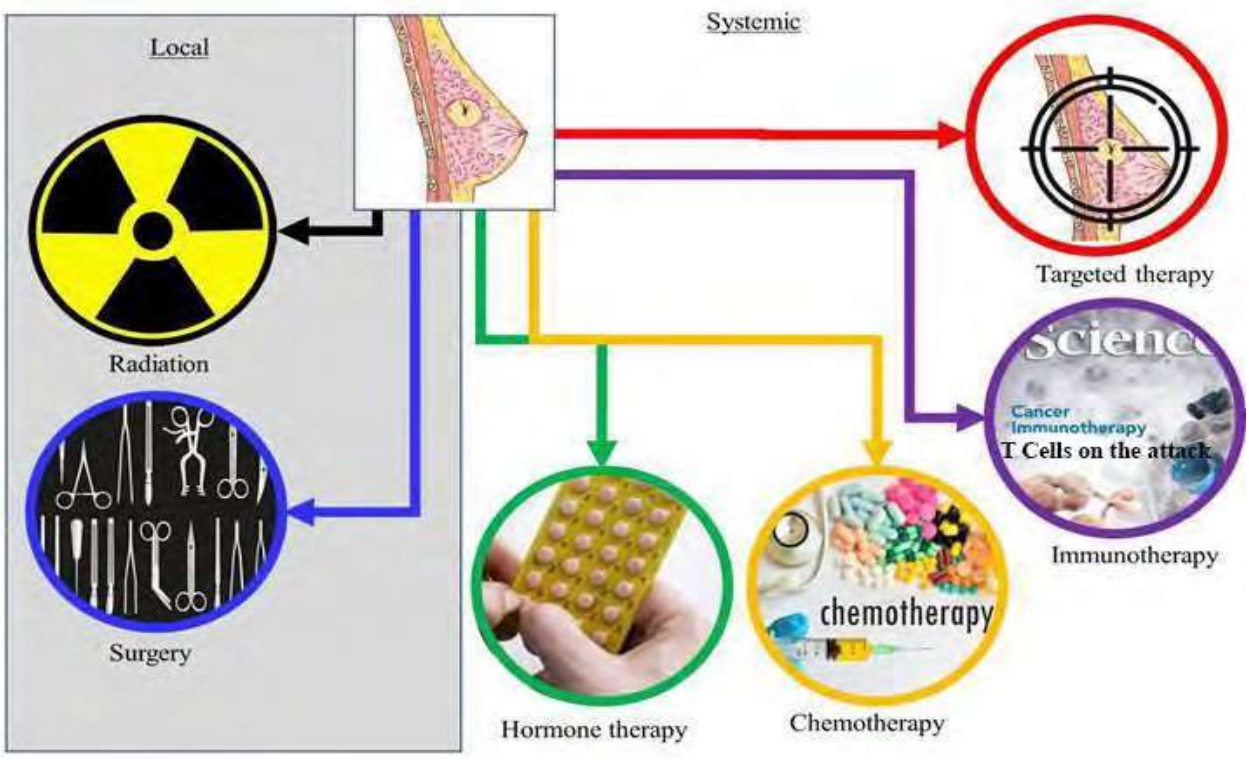

Figure 1.4 Treatment strategies for breast cancer. The diagram illustrates the main treatment options for breast cancer, based on the extent of the disease. Surgery (lumpectomy or mastectomy) and radiation therapy are the primary treatments for localised tumours confined to the breast. Systemic therapies are necessary if

cancer spreads to other parts of the body (metastasised). These include chemotherapy, hormone therapy, targeted therapy, and immunotherapy, which can be administered alone or in combination to control tumour growth and improve survival outcomes in patients with metastatic breast cancer.

1.4 Triple negative breast cancer (TNBC)

Triple-negative breast cancer (TNBC) is a highly aggressive subtype of breast cancer prone to metastasis. Abnormal cellular mutations that produce TNBC account for a tenth–a twentieth of all breast cancer cases (Li et al., 2014). In TNBC, mutations lead to downregulation of hormone receptors in breast cancer cells, such as progesterone, oestrogen, and HER2 receptors (Carey et al., 2007). Due to the absence of these receptors, there is currently no effective treatment for this condition. The recent surge in the number of TNBC patients and their high recurrence rates have resulted in poor survival (Shin et al., 2015). Dent et al. conducted their research. Research including 1,601 patients with breast cancer was performed to assess the likelihood of TNBC recurrence three years after therapy.
Of these, 180 (11.2%) were diagnosed with TNBC. These individuals had a greater risk of distant recurrence during the first three years and a higher death rate within the first five years after diagnosis [14]. TNBC has an earlier age of onset [15] and is more common in black populations than in other ethnicities [16].

Advances in understanding the molecular and genetic variety of TNBC have the potential to help identify cutting-edge biomarkers for detection, classification, and prognosis as well as new therapeutic targets. These biomarkers may encompass genetic mutations, epigenetic markers, and distinctive gene expression patterns, covering areas such as proteomics, transcriptomics, miRNAs, and other noncoding RNAs. TNBC is characterised by a wide array of irregular gene, miRNA, and lncRNA expression profiles [17].

A matched-control study revealed that breast tumours harbouring p53 mutations predominantly lack oestrogen receptors (ER) and exhibit reduced distant disease-free survival (DFS) [18]. Despite having a lower overall risk of breast cancer than Caucasian women, African-American women die from the disease at a higher rate [19]. These individuals are often diagnosed at a younger age and frequently have tumours with minimal oestrogen, progesterone, and HER-2/neu expression [20]. The higher incidence of BRCA-1 mutation-related breast cancer risk factors in African Americans indicates a genetic

propensity to develop high-risk breast cancer subtypes [21]. Certain BRCA mutations, known as founder mutations, have been found to occur more frequently in specific ancestry groups, such as the Ashkenazi Jewish community, than in others [22] (Figure 1.5).

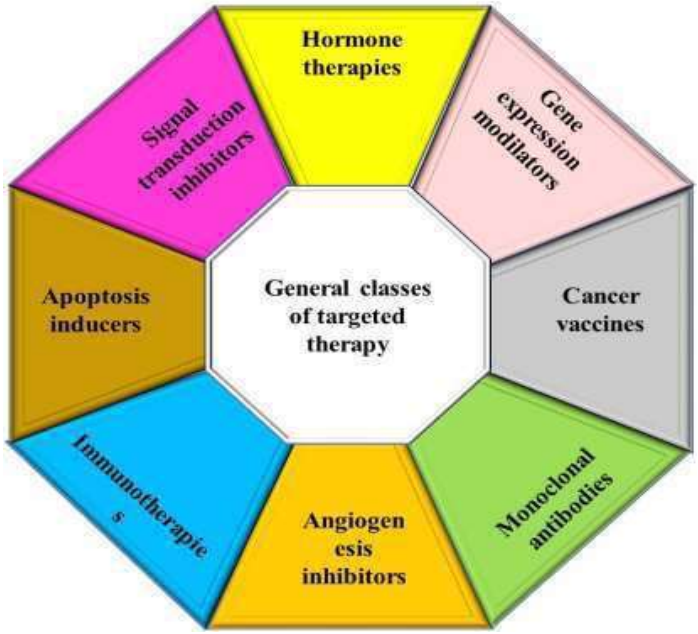

Figure 1.5 General classes of targeted therapeutics used in the treatment of triple-negative breast cancer (TNBC). The diagram illustrates the main categories of targeted therapies being developed and utilised for TNBC. These include inhibitors of signaling pathways commonly activated in TNBC, such as PI3K/AKT/mTOR and EGFR, antibody-drug conjugates that deliver cytotoxic agents directly to tumour cells, PARP inhibitors that exploit defective DNA repair in BRCA-mutated cancers, and immunotherapies that enhance antitumour immune responses. By precisely targeting molecular features or vulnerabilities more prevalent in TNBC cells compared to normal tissues, these approaches aim to provide more effective and selective treatment options for this aggressive breast cancer subtype

1.5 Emerging Breast Cancer Subtypes and Genetic Alterations: Implications for Survival Outcomes and Therapeutic Significance

Gene expression profiling of breast cancer has identified various biological subgroups associated with survival outcomes. Consequently, contemporary breast cancer categorisation systems have emerged [23]. TNBCs are classified into many "intrinsic" subgroups based on their molecular characteristics. Two basal-like subtypes (BL1 and BL2), a mesenchymal subtype, an immunomodulatory subtype, luminal androgen receptor (LAR) subtype, and mesenchymal stem-like subtype. Notably, claudin-deficient mesenchymal stem-like subtype

is clinically relevant. Tumours that display HER2-enrichment are also considered to be therapeutically significant subtypes [24].

Rare claudin-low subtypes are almost always triple-negative breast tumours with little to no luminal differentiation markers (approximately 80% lower). They also exhibit high levels of EMT indicators, increased immune response gene expression, and malignant stem cell characteristics [25].

In triple-negative breast cancer, the most common initial genetic aberration is observed in TP53, with mutations present in approximately 80–85% of cases [26]. Numerous recurrent gene alterations have been documented, indicating that TNBCs exhibit molecular heterogeneity [27]. These hereditary defects included enhanced MYC expression (seen in 40% of patients), MCL1 modulation (seen in 20% of patients), RB1 mutation or failure (seen in 20% of patients), sporadic mutations in BRCA1 or 2 (seen in 15-20% of patients), mutation or deletion of PTEN (seen in 10% of patients), amplification of CCNE1 (seen in 9% of patients), mutation of USH2A (seen in 9% of patients), mutation of PIK3CA (seen in 8% of patients), FGFR2 amplification (seen in 4% of patients), and mutation (seen in 2% of patients) (Figure 1.6).

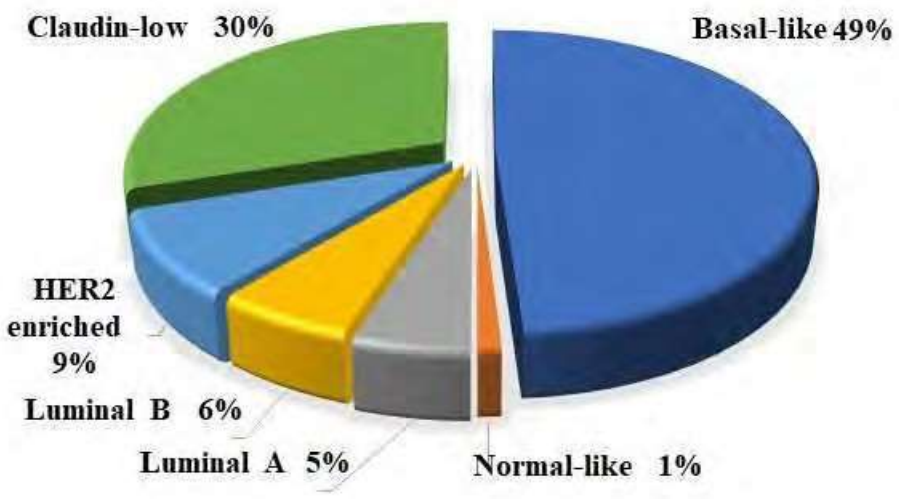

Figure 1.6 Frequency of different molecular subtypes of triple-negative breast cancer (TNBC). The pie chart shows the distribution of TNBC tumours into distinct molecular subtypes based on gene expression profiling. The majority of TNBCs fall into basal-like (70-80%) and claudin-low (20-30%) subtypes, which are characterised by high expression of proliferation-related genes and low expression of luminal differentiation markers. A small proportion of TNBCs is classified as luminal A, luminal B, HER2-enriched, or normal-like,

highlighting the molecular heterogeneity within this breast cancer subtype. Identifying the specific molecular subtypes of TNBC can provide prognostic information and guide the selection of targeted therapies.

1.6 Epidemiology and Risk Factors for TNBC

A survey also indicated that breast cancer has become the most frequently diagnosed cancer among women in sub-Saharan African nations, with the incidence rates almost doubling over the preceding two decades [28]. Breast cancer affects more than 60% of the population in the less developed parts of Eastern Turkey, but only 46% in India and 32% in sub-Saharan Africa [29]. Given that TNBC subtypes account for 15–20 percent of all breast cancers, the global case count is approximately 170,000 out of the 1 million cases of breast cancer identified each year globally [30, 31]. Several risk factors have been linked to an increased chance of developing this illness, which is discussed in further detail in the following sections.ge, ethnicity, race.

There are many risk factors for triple-negative breast cancer, such as age, race, and ethnicity [32-34]. TNBC is more prevalent in younger individuals and treatment often begins at approximately 39 years of age [35]. Furthermore, women with TNBC have their first child at a later age than women without TNBC [36]; African-Americans and premenopausal women are more prone to basal-like TNBC tumours than others. Basal-like breast cancer affects 26% of African-American individuals compared to 16% of non-African groups [37].

Within South Africa's ethnically varied population, the probability of developing breast cancer varies among the ethnic groups. Black women face a lifetime risk of 1 in 53, while white women have a risk of 1 in 15, coloured women a risk of 1 in 21, and Indian women a risk of 1 in 20 [38, 39]. Breast cancer is becoming increasingly common in South African women [40]. Due to increased life expectancy and urbanisation, established risk factors for breast cancer are becoming more prevalent [41]. Breast cancer patients in South Africa now have a high death rate due to lack of access to medical centres in remote regions, lack of information, poor healthcare facilities, and screening limitations [42]. These epidemiological statistics have been confirmed by various studies. For example, a study in Johannesburg, South Africa examined the biological features of patients with breast cancer. Black women diagnosed with breast cancer in Johannesburg were much younger than those of other races. Premenopausal black women account for 34% of all diagnosed breast cancer cases,

compared to 10% in Caucasian women, 23% in women, and 15% in Indian women [43]. These results are comparable to those of a recent study on patients with breast cancer of different ethnicities in the United States [44].

Income and education level were revealed to be substantially related to patients' age at diagnosis and menopausal status independent of race [45]. Hormone receptor activation is another factor that influences prognosis and regeneration. Black and coloured women were more likely to have oestrogenic and progesterone receptor-negative malignancies than white women were. Furthermore, black women have a higher frequency of tumours with enhanced HER2 levels than Caucasian women do [45]. It has been observed that individuals of African heritage tend to show similar patterns of breast cancer incidence irrespective of geographical location. The average age at diagnosis was 44.8 years in a study comprising 507 women with breast cancer from Nigeria and Senegal, with the majority diagnosed with TNBC [46].

1,6.1 Socio-economic Status

As the socioeconomic status of patients with breast cancer improves, the incidence of all forms of breast cancer decreases noticeably [47]. The US National Cancer Database (NCDB) has conducted substantial data-driven research on 260,577 breast cancer cases reported in a community cancer hospital registry. This study aimed to monitor and determine the prevalence of the TNBC subtypes. The findings highlighted that, among smaller groups, patients with TNBC exhibited differences linked to their socioeconomic status [48].

In this study, socioeconomic status was determined based on patients' residential areas and their health insurance coverage. The findings revealed that non-Hispanic black women and Hispanic women had an 84% and 17% higher likelihood, respectively, of developing TNBC than their Caucasian counterparts. This was validated by examining the expression of HER2 in the different demographic groups. Asian/Pacific Islanders were 1.45 times more likely than white women to be diagnosed with a HER2-overexpressing subtype, whereas black women were 1.84 times more likely to have TNBC tumours that were oestrogen receptor-positive but HER2-negative. The race-related overall risk of developing TNBC was found to be similar across all socioeconomic groups [49]. The study also found that within the same racial group, individuals from lower socioeconomic backgrounds had a higher propensity to develop

TNBC subtypes. Compared to the general population, they have a 1.14-fold greater chance of being diagnosed with TNBC [49]. Given that the incidence patterns of TNBC along racial or ethnic lines persist even after accounting for socioeconomic factors, ethnicity may have a more significant influence on the occurrence of TNBC than was previously understood.

1,6.2 Mutations in BRCA

Genetic factors account for 5-10% of all new breast cancer diagnoses [50]. In 40- 60% of women, mutations in the BRCA1 and BRCA2 genes are linked with an elevated lifetime risk of breast cancer [51]. BRCA1 and BRCA2 mutations are relatively common, occurring in approximately 1 in 400 to 1 in 800 individuals carrying a harmful mutation in either gene [52]. Studies have shown that 50–70% of breast cancers linked to BRCA1 mutations are triple-negative [53]. Approximately 16% of the tumours with BRCA2 mutations are triple-negative. A meta-analysis of 12 studies including approximately 2533 women showed that those with TNBC were almost five and a half times more likely to have a BRCA1 mutation than those with non-TNBC [54]. Patients with TNBC and BRCA1 mutations exhibit increased tumour frequency and severity [55]. Among individuals aged over 60 years, the prevalence of cancers attributed to BRCA1 mutations diminishes by an average of 3.5–7.7 percent. Premenopausal women with BRCA1 mutations who develop TNBC have a higher BMI and are more likely to develop TNBC [56].

A patient's history affects the likelihood of developing breast cancer because of BRCA1 and BRCA2 mutations. A study of TNBC cases based on race and ethnicity found significant mutation rate in BRCA 1 and 2. For example, a BRCA mutation was found in 50% of Jewish Ashkenazi females [57], but only 22.2 percent of white females, and approximately 20.4 percent of African American females [58]. The three most common mutations in Ashkenazi Jews were identified as BRCA1185delAG, BRCA15382insC, and BRCA2-6174delT (Struewing et al., 1997) (Figure 1.7). In Jewish Ashkenazi women diagnosed with breast cancer, a BRCA1 mutation was found in 10% of cases. In contrast, across all ethnicities, only 2% of breast cancer patients test positive for BRCA2 mutations [59].

In a major clinical investigation involving over 507 African women from Nigeria and

Senegal, researchers discovered that TNBC, defined by the lack of all three hormone receptors, was the most common hormone receptor status observed. The most prevalent subtypes detected were ER-positive, progesterone, and HER2 negative [60]. Although this may help explain why poorer nations have a worse prognosis, it is unclear why there are such a wide range of molecular subtypes. A study of 400 patients with breast cancer in Nigeria found that 7.1 percent had BRCA1 mutations, and 3.9 percent had BRCA2 mutations [61]. In a report of 29 percent of African American patients with TNBC, a significant proportion had a genetic mutation, including BRCA1 or BRCA2 [62].

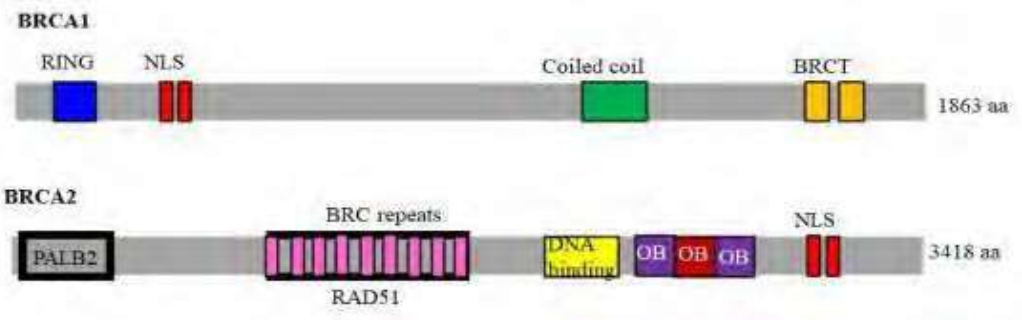

Figure 1.7 Structural features and protein interaction domains of BRCA1 and BRCA2. Schematic diagrams depicting the key functional domains and regions of BRCA1 and BRCA2 proteins involved in interactions with other proteins. BRCA1 contains an N-terminal RING domain that confers E3 ubiquitin ligase activity, a central region with multiple protein-binding sites, and two C-terminal BRCT domains that mediate its interaction with phosphorylated proteins. BRCA2 has an N-terminal region that binds to PALB2, eight centrally located BRC repeats that interact with RAD51, and a C-terminal region that is involved in DNA binding and interaction with additional proteins. These structural features and interaction domains are critical for the tumor suppressor functions of BRCA1 and BRCA2 in DNA repair, cell cycle regulation, and maintenance of genomic stability [63].

BRCA1 has a nuclear localisation sequence and a RING domain at its amino-terminus that interacts with the BRCA1-associated RING domain protein 1 (BARD1) (NLS).

The BRCA1 protein's C-terminal region has a coiled-coil domain that interacts with BRCA2's partner and localiser (PALB2), which is necessary for the formation of the BRCA1-CtIP complex. This complex is necessary for ataxia-telangiectasia, Rad3-related (ATR) protein activation, and acceleration of homologous recombination (HR) [64]. In BRCA1's central region, the Serine Cluster Domain (SCD) is phosphorylated by ATM kinase, which plays a pivotal role in activating G2/M and S-phase checkpoints [65]. BRCA2 interacts with PALB2 at its N-terminus (amino acids 21-39)[66]. BRCA2 contains eight BRC repeats that connect to the RAD51 [67]. The DNA-binding domain consists of three oligonucleotide-binding

(OB) folds and a helical domain (H) (T). The BRCA2 C-terminus is defined by a nuclear localisation signal (NLS) and a phosphorylation site for cyclin-dependent kinase (CDK) at serine 3291 [68]. These modifications allow BRCA2 to bind to both single- and double-stranded DNA and improve its interaction with RAD51, which is required for DNA repair [69].

1,6.3 Mutations in other genes are also involved in TNBC pathogenesis.

Many retrospective studies have been conducted to identify the most prevalent genetic variants in TNBC patients . Pathogenic mutations in BRCA1 and BRCA2 were found in Pathogenic mutations in BRCA1 and BRCA2 were found in a previous study, where it was reported that 71.93% of the patients had BRCA1 mutations, and 14.03% had BRCA2 mutations [70]. Furthermore, 2.2% of patients with TNBC have mutations in other genes involved in homologous recombination DNA repair. A study on triple-negative breast cancer (TNBC) found that a fraction of patients have mutations in genes involved in homologous recombination DNA repair, such as RAD51D, RAD50, and RAD51C [71].

The incidence of breast cancer increases two-to fourfold when genes with a high penetrance rate are present [72]. A recent clinical study of 289 Afro-American women with breast cancer revealed a broad, heterogeneous spread of mutations, with 22% of these patients having pathogenic germline mutations. This resulted in the identification of 57 distinct mutations in 65 patients. Furthermore, almost 80% of the mutants appear to be BRCA1 or BRCA2, with the remainder bearing PALB2, CHEK2, BARD1, ATM, PTEN, and TP53 alterations [73].

1,6.4 Additional Risk Factors: Obesity, Parity, and Breast-feeding

TNBC risk factors vary from those associated with other forms of breast cancer. Decreased lifelong sensitivity to testosterone, long periods of breastfeeding, and young age when giving birth to their first child generally provide protection against hormone-positive breast cancer. Conversely, longer breastfeeding duration has been linked to a lower prevalence of TNBC [74]. Kwan and associates presented the findings of a prospective breast cancer survival study, indicating that premenopausal women with TNBC are more prone to being overweight

[75].

1.7 Therapeutic Options

TNBC differs from other breast cancer subtypes owing to its biochemical variability. Distinctive clinicopathological traits, unique risk factors, aggressive clinical course, different recurrence patterns, absence of traditional therapy, and poor overall prognosis. It continues to pose significant clinical challenges with numerous unresolved issues in the treatment of TNBC patients. Present research endeavours are concentrated on acquiring a more profound comprehension of the biology driving this
tumour subtypes with the aim of identifying more effective treatment methods for this particularly challenging patient group.

1,7.1 Chemotherapy

Non-specific cytotoxic chemotherapy is the standard treatment for TNBC in both neoadjuvant and metastatic stages. Treatment for this patient group is difficult for both the patient and the oncologist because the tumours are resistant to endocrine therapies and anti-HER2 medications. The absence of specific prognostic indicators or evidence of a therapeutic response in TNBC makes it challenging to identify patients with more aggressive disease who may not respond to existing treatments. This has an impact on tailoring treatment strategies based on the likelihood of response to specific drugs.

Several clinical studies have shown that multi-agent chemotherapy regimens are successful for the neoadjuvant treatment of TNBC [76]. Despite their poor prognosis, TNBC tumours are particularly chemosensitive, albeit for a shorter duration than that of other breast cancers. In various trials, polychemotherapy, particularly regimens that include taxanes, has been proven to be effective for TNBC. This technique has shown favourable outcomes in numerous facets of the disease, including a decreased chance of recurrence and improvements in disease-free survival (DFS) and overall survival (OS) [77]. An ongoing argument exists as to whether one regimen is better than another.

1,7.2 Salts of Platinum

Platinum-containing drugs have been the focus of extensive research for the treatment of research. Platinum compounds, which inhibit DNA activity by generating interstrand DNA cross-links, may be particularly useful in the treatment of some breast cancers. DNA integrity, genomic stability, homologous recombination, and double-strand DNA repair are dependent on BRCA1. In preclinical studies, cancer cells lacking this gene were shown to be more susceptible to DNA-damaging treatments, including alkylators and radiation [78]. TNBC is commonly associated with diminished BRCA function and compromised DNA damage repair, potentially increasing its sensitivity to DNA damaging agents.

Recent findings have highlighted the antitumour activity of platinum-based treatments in BRCA1- related breast cancers. Among women with identified BRCA mutations, preoperative chemotherapy impacted the rates of pathological complete response (pCR). Remarkably, treatment with cisplatin alone resulted in a pCR rate of 83%. Among the 18 patients treated with cisplatin, a clinical response, categorised as either partial or complete, was observed in 8 cases [79]. Although platinum-based drugs have shown potential efficacy, they are infrequently used in preoperative or adjuvant treatment protocols except in clinical trials.

1,7.3 Targeted Agents

The FDA has not officially approved any targeted medication for the treatment of triple-negative breast cancer (TNBC). The development of these drugs in this scenario is problematic owing to the lack of standards for testing a large variety of potential targets that vary across institutions. This diversity causes problems in identifying the appropriate participants for clinical studies [80].

1,7.4 Anti-Angiogenic Agents

The FDA has not officially approved targeted medications for the treatment of patients with TNBC. This is particularly true for triple-negative populations, which have higher VEGF expression and higher rates of angiogenesis [81].

1,7.5 Bevacizumab

Bevacizumab, a VEGF-targeting monoclonal antibody, has been approved for the treatment of certain forms of colon, lung, kidney, and brain cancer [82]. In November 2011, the FDA cancelled the accelerated clearance of bevacizumab for the treatment of metastatic HER2-negative breast cancer. However, a recent study has examined the effectiveness of this antibody in treating TNBC [83].

1,7.6 Sunitinib and Sorafenib

In experimental breast cancer models, the pharmacological tyrosine kinase inhibitors (TKIs) sunitinib and sorafenib have demonstrated antiangiogenic properties and have been used as anticancer agents. For MBC, these drugs have been found to be ineffective when alone administered [84].

1,7.7 Poly (ADP-ribose) Polymerase (PARP) Inhibitors

Various overlapping repair systems are in place to safeguard the integrity of genomic DNA when confronted with single- and double-strand damage. The base excision repair mechanisms of PARP-1 and PARP-2 are required for single-stranded DNA repair. BRCA performs two functions, homologous recombination and DNA double-strand repair. Cancers exhibiting a "BRCA1-like" phenotype, characterised by compromised DNA repair capabilities, may be more vulnerable to therapy with PARP inhibitors. These suppressors interfere with single-stranded DNA restoration, resulting in less accurate DNA repair mechanisms [85]. Several studies have investigated the efficacy and safety of PARP inhibitors, both as independent therapies and in conjunction with chemotherapeutic agents such as cisplatin, carboplatin, or temozolomide. This study is based on preclinical research suggesting that tumours with BRCA1 mutations are more vulnerable to DNA-damaging drugs and PARP inhibition [86].

1,7.8 EGFR Inhibitors

EGFR (HER1) is overexpressed in approximately 60–70% of patients with basal-like breast cancer (BLBC) and triple-negative breast cancer (TNBC) [87]. In preclinical models of breast cancer, erlotinib, a tyrosine kinase inhibitor that suppresses EGFR phosphorylation, and cetuximab, a monoclonal antibody targeting EGFR, showed minimal effectiveness as sole therapies [88]. However, EGFR inhibition has been shown to have antitumour efficacy when combined with chemotherapy [89]. Clinical trials combining EGFR-targeted medications with chemotherapy have yielded inconsistent results in the management of advanced-stage breast cancer.

1.7.8.1 Cetuximab

Cetuximab has been tested in conjunction with various chemotherapy protocols for metastatic cancer. The combination of cetuximab and carboplatin had an 18% response rate and 27% treatment advantage rate. Despite these results, the majority of participants in this study died within two months of being diagnosed, demonstrating aggressive TNBC aggressiveness [90]. As previously documented, cetuximab monotherapy is ineffective following irinotecan and carboplatin treatments [83]. Progression-free survival (PFS) appears to improve when cetuximab and cisplatin are used simultaneously [91].

1.7.8.2 Erlotinib/Gefitinib

TKIs targeting EGFR are now being explored for the treatment of TNBC, and they have shown antitumor activity when combined with chemotherapy [92]. Further studies are needed to determine the relevance of small-molecule EGFR inhibitors in the treatment, particularly when coupled with chemotherapy.

1.8 Phytochemicals: Anti-cancer plant compounds

Plants contain non-nutritive bioactive substances known as phytochemicals (Phyto). Phytochemicals are a diverse group of organic chemicals [93]. Recently, phytochemicals isolated from green plants that have been used for medicinal purposes have become the focus of research for new cancer-preventative and cancer-therapeutic compounds [94]. A wide range of plants have been proven to be valuable sources of phytochemicals with therapeutic

capabilities. The molecules isolated from these plants have laid the foundation for the synthesis of chemical compounds. As a result, medicinal flora continues to be a vital source for the identification of new therapeutic compounds [95, 96]. Phytochemicals found in vegetables, fruits, and herbs have the potential to treat cancer and infections, and promote healing. Many plant products contain thousands of phytochemicals, which have been identified and categorised [97]. Numerous chemicals have been shown to exhibit anticancer activity, causing little or no damage to healthy cells [98]. Surprisingly, plants are the source of 47 percent of the FDA-approved cancer treatments [95]. This new source of potential anticancer agents is important, as the effectiveness of current therapies is jeopardised by drug resistance. Many of the current therapies already in use are based on compounds isolated from plants; however, the effectiveness of these and other chemotherapies is limited because of their substantial toxicity to ordinary, healthy, and non-targeted tissues. It is hoped that further investigations will identify new cancer therapeutic agents as well as cancer-preventive agents. Some of the recently synthesised anti-cancer compounds based on compounds isolated from plants include vinblastine and vincristine. These two anticancer drugs are derived from medicinal herbs such as comfrey [95]. There is a wide range of phytochemicals that can help prevent or cure cancer because of the variety of chemicals. Plants have evolved to play various reproductive, protective, and developmental roles. Given the incidence of cancer in humans, it is vital to investigate the function of phytochemicals in cancer prevention and therapy [99] (Figure 1.8).

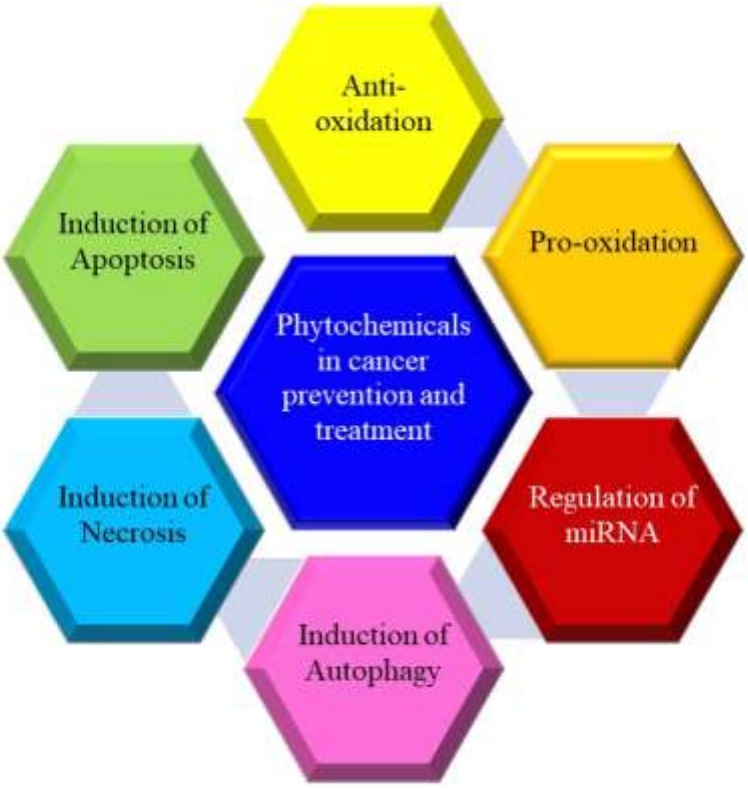

Figure 1.8 The roles of phytochemicals in cancer therapy. Phytochemicals contribute to cancer prevention and treatment by affecting cancer cells through various mechanisms. These include protecting cells from oxidative damage to prevent DNA harm, inducing cell death via reactive oxygen species (ROS), triggering apoptosis, necrosis, and autophagy, or modulating gene expression through miRNA regulation.

Phytochemicals contribute to cancer prevention and treatment by affecting cancer cells through various mechanisms. These include protecting cells from oxidative damage to prevent DNA damage; inducing cell death via reactive oxygen species (ROS); triggering apoptosis, necrosis, and autophagy; and modulating gene expression through miRNA regulation.

Whole or raw plant extracts (more than 120,000 extracts from 6,000 species) have been widely examined over the last several decades [100]. plants have been demonstrated to have anti-cancer or anti-tumor properties [101]. Although numerous plant extracts have been investigated as anticancer agents in clinical trials, only a few have investigated the biochemical or molecular pathways involved in cancer or tumour development and regulation. Plant-derived chemicals have demonstrated activity through various mechanisms, aligning with established hallmarks of cancer (Figure 1. 1). These include cell cycle inhibitors, antagonists of mitogenic signaling (growth and proliferation), inhibitors of

metastasis, and modulators of immune system receptors (Mans et al., 2000). Anti-cancer compounds have been isolated from diverse plant families, notably, *Fabaceae, Asteraceae, Zingiberaceae, Euphorbiaceae, Meliaceae, Solanaceae, Moraceae,* and *Liliaceae.*

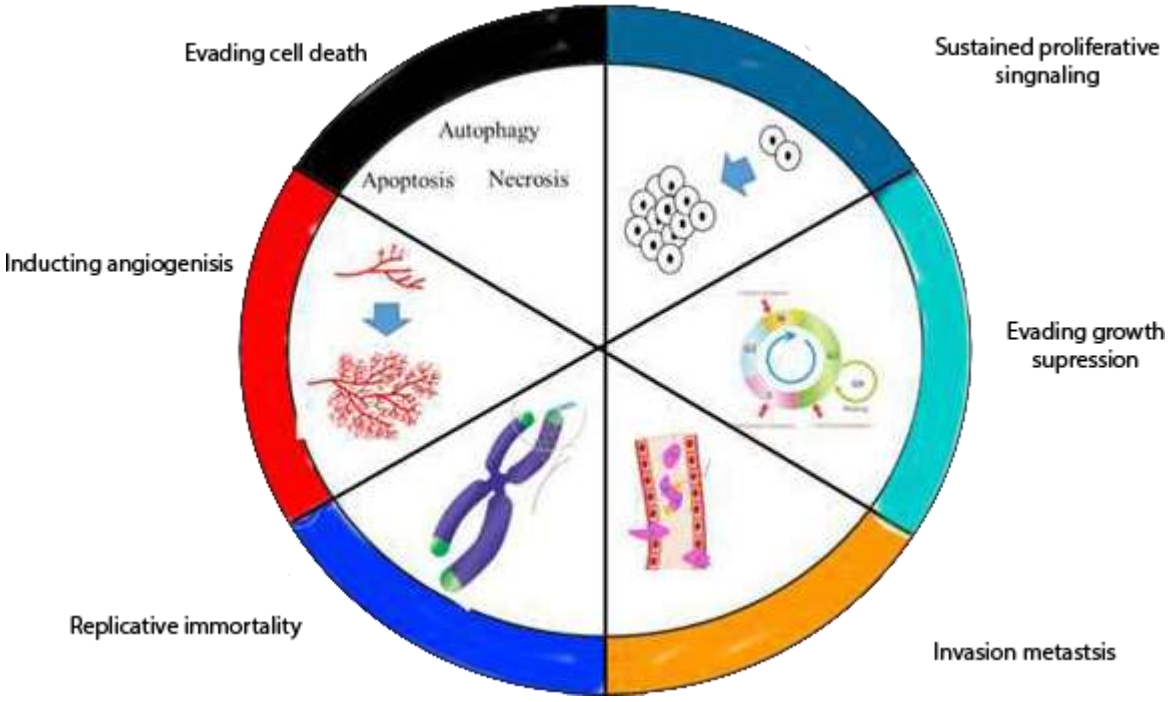

Figure 1.9 Hallmarks of Cancer The diagram illustrates six essential alterations in cell physiology that collectively dictate malignant growth: sustaining proliferative signaling, evading growth suppressors, resisting cell death, enabling replicative immortality, inducing angiogenesis, and activating invasion and metastasis. These hallmarks are promoted by genome instability and inflammation and are further supported by reprogramming cellular energetics and evading immune destruction. Cancer cells acquire these capabilities through various mechanisms such as producing their own growth signals, bypassing the negative regulation of cell proliferation, evading apoptosis, maintaining telomere length, stimulating blood vessel formation, and activating invasion and metastasis. Together, these hallmarks enable cancer cells to survive, proliferate, and spread, leading to the development and progression of malignant tumours [102].

1,8.1 Cell cycle arrest

Plant-derived chemicals have been found to disrupt various cellular signaling pathways that cause cell cycle arrest and cell death (Keren et al., 2010). These include the p53 pathway,

nuclear factor-kappa-controlled β-controlled pathways (Nfk-B), signaling pathways linked to nuclear factor 2, growth pathway inhibitors, signal transducer and transcription (STAT) activator pathways, and Wnt/-catenin pathways.

1,8.2 Phytochemicals as antioxidants: cancer prevention.

Oxidative stress occurs when the creation of reactive oxygen species (ROS) exceeds the body's antioxidative systems' defensive capabilities, interrupting biological processes. This imbalance can arise from excessive endogenous ROS generation, exposure to external oxidative stressors, or reduced antioxidant capacity owing to disruptions in antioxidant production and distribution (Ray et al., 2012). ROS, a group of molecules that originates from oxygen metabolism, are present in all aerobic organisms. These compounds are produced by several enzymes including the mitochondrial respiratory chain, cytochrome P450 system, NAD(P)H oxidoreductases, and xanthine oxidase (Reijnders, 1975). Additionally, external factors such as inflammatory triggers, consumption of oxidising agents, and radiation exposure significantly contribute to the development of oxidative stress.

ROS are commonly regarded as detrimental owing to their high reactivity, causing cellular damage and contributing to the pathophysiology of a variety of diseases, such as neurological disorders, inflammatory conditions, accelerated aging, and cancer. It is important to understand the vital functions of ROS in normal cellular processes. They are involved in maintaining the redox balance of regulatory molecules, aiding signal transmission, controlling enzyme functions, and supervising cell cycle and proliferation (Park and Park, 2021).

ROS are formed when one or more electrons are missing from the outer orbit of an unpaired radical molecule (or atom), making them unstable and reactive. It must steal electrons from neighbouring molecules to maintain their stability. This free radical is generated by degradation of the original target molecule, which ultimately damages other molecules or cellular components (Mukherji and Singh, 1984). Excessive free radicals may injure human cells in a variety of ways, the most serious of which is DNA damage, which can lead to cancer and other disorders (Dreher and Junod, 1996).

1,8.3 Redox Regulation of Cell Proliferation and Survival

ROS, which have been revealed to be secondary transmitters in numerous signaling pathways, particularly those involved in cell growth, are critical for maintaining cellular homeostasis. A slight increase in ROS levels, such as superoxide and hydrogen peroxide, has been shown to boost proliferation in various cell types, which may contribute to the initiation of carcinogenesis (Brown et al., 1999). These effects are likely increased by a shift in redox-sensitive sites on key transcription factors, protein kinases, and phosphatases, which are crucial for regulating the cell cycle (Besse-Patin and Estall, 2014). Such alterations may affect biological activity or interactions with other proteins. Furthermore, activating essential redox-regulated survival pathways may indirectly boost cell proliferation by increasing antioxidative stress mechanisms.

1.8.3.1 Transcription Factors

ROS can affect the function of numerous important transcription factors involved in cell cycle control. This is performed mostly by oxidative alterations of certain amino acids in their DNA-binding motifs, or by changes in the phosphorylation status produced by redox reactions. Thiol-rich cysteine residues in the zinc-finger motifs of the DNA-binding domains of numerous transcription factors are highly vulnerable to oxidative alterations. ‘

The consequences of these redox shifts on transcription factors differ; they may either amplify or reduce transcriptional activity, depending on the specific transcription factor (Brigelius-Flohé and Flohé, 2011).

1.8.3.2 Targeting ROS

In response to specific oncogenic signals, cells experience increased ROS production, partly due to metabolic activities linked to unchecked cell growth and proliferation. This sustained oxidative stress can deplete cellular antioxidants, leading to a redox imbalance. Increased intracellular ROS levels can aid the initiation and progression of cancer. The genetic instability caused by ROS-induced DNA damage can make these cells more susceptible to

additional oxidative harm from external ROS-generating agents. This susceptibility provides a possible molecular basis for developing novel treatment techniques focused on selective eradication of these cancer cells (Bay, 2023). Genetic instability resulting from ROS-mediated DNA damage could render cells more susceptible to additional oxidative damage from external ROS sources. This heightened vulnerability offers a biochemical rationale for developing novel therapeutic approaches that target and preferentially eliminate cancer cells that are prone to oxidative stress (Bay, 2023; Ellermann et al., 2017).

Specific phytochemicals function as natural antioxidants, effectively neutralising free-radical damage and lowering the likelihood of cancer initiation in humans (Rohman et al., 2006). Plant-based antioxidants include a diverse range of compounds including flavonoids, polyphenols, tocopherols, and terpenoids (Dimitrios, 2006). Many plant-derived phytochemicals such as terpenoids, phenolic acids, and alkaloids are known to have anticancer effects. These effects are shown by their impact on ROS signaling pathways (Chirumbolo et al., 2018). This conclusion is consistent with the antioxidative and ROS-eliminating characteristics of several phytochemicals, which have been shown to induce apoptosis via ROS generation. A well-known example is xanthohumol, a well-studied phytochemical. Xanthohumol, a prenylated flavonoid discovered in the female flowers of the hops plant (Humulus lupulus L.), is gaining popularity for its potential use in a variety of applications, particularly as a chemopreventive and antineoplastic agent. Its involvement in scavenging ROS assists in avoiding DNA damage and destroying carcinogens, partially by boosting the production of phase II cytoprotective enzymes (Albensi et al., 2019). Xanthohumol is also known for its unique anticancer effects, which include blocking DNA synthesis, boosting apoptosis, and preventing cancer cell invasion. (Albensi and Biology 2019).

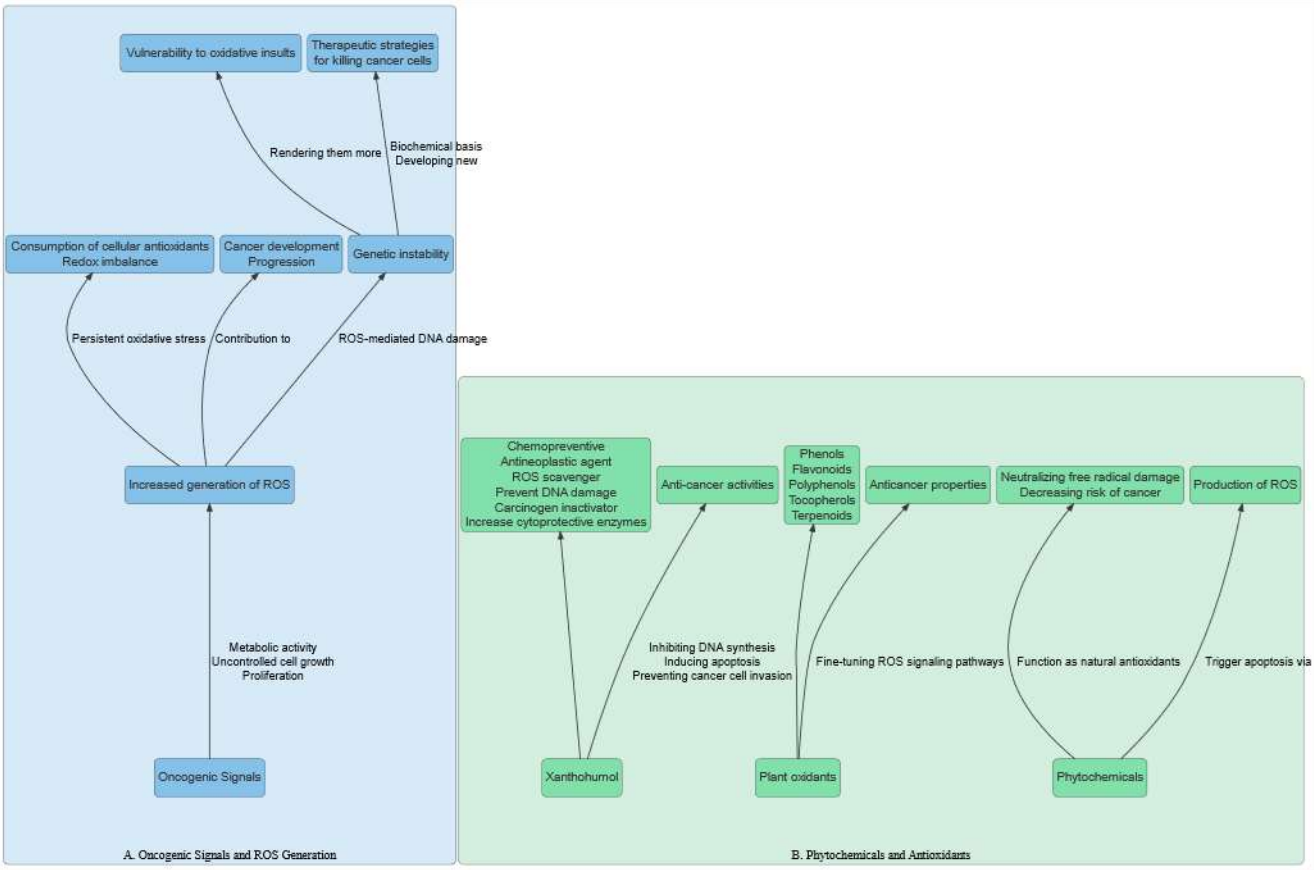

Figure 1.10 Schematic representation of oncogenic signals, ROS generation, and the role of phytochemicals in cancer. This diagram illustrates how oncogenic signals, such as aberrant activation of growth factor receptors and oncogenes, can lead to increased generation of reactive oxygen species (ROS) in cancer cells. Elevated ROS levels contribute to oxidative stress, DNA damage, and genetic instability, which further promotes cancer progression. However, phytochemicals, including phenols, flavonoids, and terpenoids, can exert anticancer effects by modulating ROS signaling pathways. These compounds act as antioxidants, scavenge free radicals, and reduce the oxidative damage. Moreover, phytochemicals can induce apoptosis in cancer cells by triggering ROS-mediated cell death pathways, such as the activation of caspases and release of cytochrome c from the mitochondria. By targeting multiple oncogenic pathways and regulating ROS homeostasis, phytochemicals have demonstrated promising potential as chemopreventive and therapeutic agents for cancer management.

A common method through which phytochemicals aid in cancer therapy is to induce or modulate autophagy and apoptosis. The pathways involved in these processes are complex and require a brief overview before potential targeting can be explored. In mammalian cells, apoptosis occurs via two distinct molecular routes. The intrinsic or mitochondrial route originates internally and is based on the release of pro-apoptotic proteins from mitochondria. This route is primarily activated by cancer treatment and radiation, offering benefits to cancer cells by bypassing intrinsic apoptotic signals. External protein death ligands bind to pro-apoptotic death receptors, which activate the extrinsic apoptotic pathway (DRs). Both routes lead to the activation of caspases, a set of specialised proteases, which then initiate a sequence of events. These events encompass "blebbing" of the plasma membrane, cellular

contraction, condensation of chromatin, and fragmentation of internucleosomal DNA, which are all characteristic signs of apoptosis.

1.8.3.3 The intrinsic apoptosis pathway

The intrinsic apoptotic pathway is initiated when the mitochondrial outer membrane ruptures, allowing apoptotic components to enter the cell. These include cytochrome C and Smac/DIABLO, also known as the second mitochondrial activator of caspases and a direct inhibitor of apoptosis-binding protein (MOMP). MOMP is controlled by internal cellular stress detectors that alter connections within the Bcl-2 protein family (Birkinshaw and Czabotar, 2017) (figure 1.10). The Bcl-2 family is divided into three groups, BH1-4, according to the number and arrangement of Bcl-2 homology domains. In response to diverse cellular stresses, the BH3-only proapoptotic proteins get activated. They activate MOMP by boosting the formation of oligomers of pro-apoptotic proteins Bax and Bak on the mitochondrial outer membrane (mitochondrial outer membrane permeabilisation). Other multi-BH domain proteins, including Bcl-2, Bcl-XL, and Mcl-1, prevent MOMP formation by neutralising proapoptotic family members. The production of apoptogenic substances by the mitochondria produces a cascade of cellular changes that may lead to irreversible cell death (Deledda et al., 2022). Cytochrome C is necessary for the formation of the cytosolic apoptosome complex, which includes the adaptor proteins Apaf-1 and caspase 9. When this complex is formed, caspase-9 is activated, causing further processing and activation of the effector caspases. Furthermore, the release of Smac/DIABLO improves its interaction with X-chromosome-linked inhibitor of apoptosis protein (XIAP). XIAP binds to caspase-3, caspase-7, and caspase-9 via its IAP repeat domain, which acts as a key regulatory point to prevent premature caspase activation. However, the interaction between Smac/DIABLO and XIAP inhibits XIAP activity, bypassing this regulatory step and enabling apoptosis (LaCasse et al. 2009). Cancer-related alterations, such as the loss of proapoptotic proteins p53 and Bax or increased expression of anti-apoptotic components, such as Bcl-2 and Mcl-1, disrupt intrinsic apoptosis signaling, making it more difficult to effectively eradicate mutant cells.

1.8.3.4 The extrinsic apoptosis pathway

Extrinsic apoptosis occurs when signals from external death ligands activate the cellular apoptotic machinery via proper death receptors (DRs) (Romero, 2017) (Figure 1.10). TNF, FasL, and TRAIL are TNF family death ligands produced largely by immune cells including T cells, NK cells, NKT cells, macrophages, and dendritic cells. Although all death ligands can induce apoptosis under specific circumstances, TRAIL has emerged as one of the most intriguing therapeutic targets. TRAIL exclusively triggers apoptosis in cancer cells, whereas normal and non-transformed cells remain untouched. Furthermore, unlike FasL or TNF, increased activation of TRAIL death receptors does not cause considerable damage in vivo [103]. Consequently, a significant portion of the research on the therapeutic exploitation of the extrinsic apoptotic pathway in cancer therapy has focused on TRAIL death receptors, employing TRAIL or TRAIL agonist antibodies (Figure 1. 2).

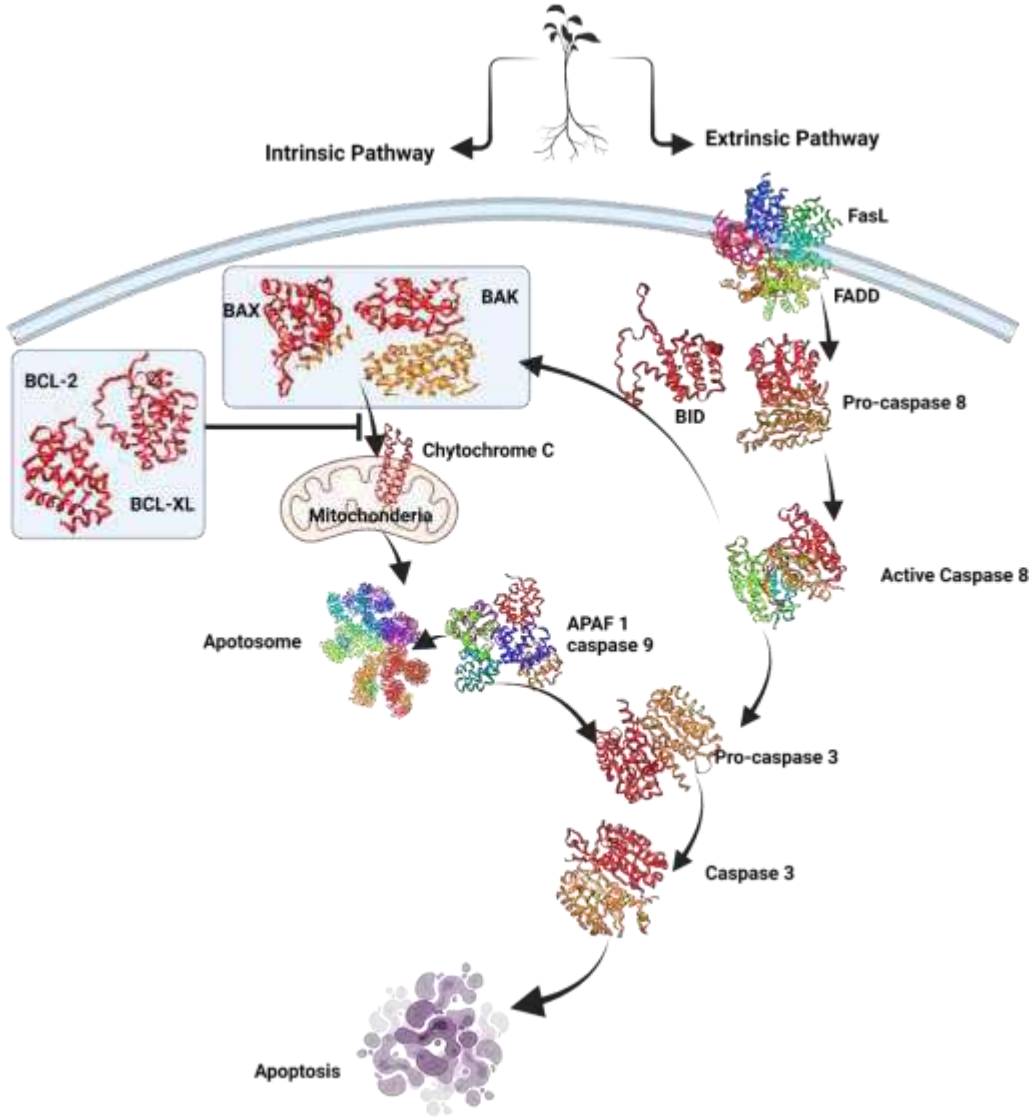

Figure 1.11 Intrinsic and extrinsic apoptotic pathways. The diagram illustrates the two main pathways that lead to programmed cell death (apoptosis) in mammalian cells. The extrinsic pathway is initiated by the binding of death ligands such as FasL or TRAIL to their corresponding cell surface receptors. This interaction triggers the formation of the death-inducing signaling complex (DISC) and the activation of caspase-8, which in turn cleaves and activates downstream effector caspases, such as caspase-3 and caspase-7, resulting in apoptosis. The intrinsic pathway, also known as the mitochondrial pathway, is triggered by various cellular stresses such as DNA damage or oxidative stress. These stimuli cause changes in the mitochondrial membrane permeability, leading to the release of cytochrome c into the cytosol. Cytochrome c binds to Apaf-1 and procaspase-9 to form an apoptosome complex that activates caspase-9. Active caspase-9 cleaves and activates effector caspases, which ultimately leads to apoptosis. The intrinsic and extrinsic pathways converge at the

level of effector caspase activation, and both pathways are tightly regulated by pro- and anti-apoptotic proteins such as members of the Bcl-2 family. Targeting apoptosis Bcl-2 and Bax production is important in breast cancer cell death because they enhance cytochrome c release and activate the caspase cascade. Bcl-2 and Bax production is important in breast cancer cell death because they enhance cytochrome c release and activate the caspase cascade. This is particularly evident in response to the phytochemical Pyranocycloartobiloxanthone A [104]. Scutellarin, a phenolic phytochemical, is known for its ability to activate the p53 pathway, thereby facilitating apoptosis [105]. Scutellarin inhibits Bcl-2, thereby promoting the pro-apoptotic protein p53. This activation enhances Bax protein synthesis and caspase-3-dependent cell death in human colon cancer cells. Scutellarin inhibits Bcl-2, thereby promoting the pro-apoptotic protein p53. Bcl-2 and Bax production is important in breast cancer cell death because they enhance cytochrome c release and trigger the caspase cascade. Bcl-2 and Bax production is important in breast cancer cell death because they enhance cytochrome c release and trigger the caspase cascade [105]. Capsaicin, a well-known phytochemical, has been shown to cause apoptosis in various cancer cells by activating the p53 pathway [106]. Many phytochemicals have been shown to aid cancer treatment by lowering NF-kB activity, which increases cancer cell death [107]. NF-kB expression is usually high in cancer cells because it regulates both antiapoptotic and apoptotic genes [107, 108]. Alkaloids and flavonoids have been shown to kill cancer cells by blocking the NF-kB signaling pathway. Xanthohumol is one such phytochemical with a broad variety of uses [109], Magnolol [108] Morusin [110], urosolic acid [111], Corilagin [112]. Alkaloids and flavonoids may trigger apoptosis in cancer cells by inhibiting the NF-kB signaling pathway. These plant compounds trigger apoptosis through a mitochondria-dependent pathway. (Figure 1.10). Phytochemicals may cause cancer cells to create ROS, which alter the mitochondrial membrane potential and release a number of damaging substances, including cytochrome c. Following its release, cytochrome C, in collaboration with Apaf- 1 and caspase 9, forms the apoptosome, which subsequently activates the executor, caspase 3, initiating apoptosis [113]. Phytochemicals induce extrinsic apoptosis by upregulating the expression of death ligands such as FasL, TNF-α, and TRAIL. These ligands cause apoptosis by attaching to death receptors (DRs) such as FAS and TNFR, which activate caspase-8. Caspase-8 transforms Bid into tBid, which together with the increased amounts of BAX and BAK proteins in the mitochondria, activates the intrinsic apoptotic pathway,

leading to caspase activation.

1,8.4 Phytocides as regulators of miRNAs

MicroRNAs (miRNAs) are noncoding RNA molecules with unique nucleotide sequences. They influence post-translational gene expression [114]. This is accomplished by targeting specific messenger RNA (mRNA) molecules through this sequence. Mature miRNAs typically attach to the 3' untranslated region (UTR) of their corresponding messenger RNA (mRNA) genes, resulting in RNA disintegration or translation inhibition [115]. Furthermore, miRNAs can adhere to the 5' untranslated segment (5'UTR) and coding region of their target genes [116]. In conclusion, miRNAs modulate mRNA transcription and processes, such as growth, differentiation, apoptosis, cell cycle control, metabolism, viral replication, aging, immune responses, and carcinogenesis. Through these mechanisms, miRNAs are estimated to regulate approximately one-third of the human genes [117]. To date, over 1500 human miRNAs have been identified using sequencing and microarray technologies in conjunction with bioinformatics analyses of multiple miRNA databases [118]. In summary, miRNAs function mechanically by silencing or activating genes and can act as tumour suppressors or oncogenes in various types of cancers [119]. Partial complementarity increases the translation barrier, whereas complete complementarity promotes mRNA breakdown [120].

The production of miRNAs is affected by several factors, including impairments in the transcription machinery, changes in epigenetic mechanisms and miRNA biosynthesis, and mutations or alterations in DNA copy number. Given that gene expression profiles in cancer cells differ significantly from those in normal tissues, it stands to reason that mRNA transcription levels are similarly altered in cancer. Furthermore, it is well known that miRNA transcription is altered in cancer cells [121]. Numerous studies have shown that phytochemicals can control miRNA expression via methods other than transcriptional regulation. Resveratrol is a phytoalexin derived from grapes, which has been used for the treatment of cancer and other ailments for many years. Notably, resveratrol has been shown to dysregulate two miRNAs in oestrogen-responsive breast cancer cells, specifically miR-542-3p (whose levels decreased following resveratrol treatment) and miR-122-5p (whose levels increased following resveratrol treatment), both of which cause cell death by

apoptosis. In contrast, treatment with resveratrol has been proven to enhances miR-122-5p in triple-negative breast cancer cells [122]. Although numerous phytochemicals have undergone clinical trials for cancer treatment, scientists still encounter significant challenges associated with the limited bioavailability and effectiveness of dietary plant components [123, 124]. Phytochemicals hold potential as cancer-regulatory agents, and the understanding of miRNA activity, along with their gene-targeting mechanisms, presents a promising avenue for developing future therapies to treat this disease.

1,8.5 Phytochemical targeting angiogenesis

Similar to normal tissues, tumour tissues cannot grow or spread locally or systemically without angiogenic support. Blood vessels are crucial because they supply the necessary oxygen and nutrients for tumour growth [125]. During angiogenesis, endothelial cells proliferate and migrate in response to external cues to form the vessel walls. This process involves several phases, including initiating activity in the endothelial cell layer of a pre-existing capillary, releasing metalloproteinases to break down the protein-dense extracellular matrix (ECM), penetrating the matrix, and dividing. Endothelial cells undergo these phases to develop new vascular networks, supporting the expansion of nearby tissues, including tumours [126].

Normal cells maintain homeostasis by balancing the stimulation and inhibition of chemical signals and blood vessels develop only when necessary. The development and spread of cancers require angiogenic assistance. Cancer cells produce proangiogenic substances that stimulate the formation of new blood vessels. Furthermore, normal cells near tumour cells may contribute to angiogenesis by producing signaling molecules [125]. Compounds that hinder the development of new blood vessels include angiostatin, endostatin, interferons, interleukin 1 and 12, tissue inhibitors of metalloproteinases, and retinoic acid [127]. Natural angiogenesis inhibitors include angiogenin, epidermal growth factor (EGF), oestrogen, and fibroblast growth factor. Compounds that prevent the formation of new blood vessels include angiostatin, endostatin, interferons, interleukins 1 and 12, tissue inhibitors of metalloproteinases, and retinoic acid.

Vascular Endothelial Growth Factor (VEGF) and basic fibroblast growth factor (bFGF, often called FGF2) are essential regulators of tumour angiogenesis [128]. Unique microRNA (miRNA) expression profiles specific to angiogenesis have been discovered [129]. These miRNAs can potentially function as pro- or anti-angiogenic agents [130].

Anatomically, blood arteries consist of an inner endothelial cell lining and an exterior layer of basement membrane, followed by mural support cells such as pericytes and vascular smooth muscle cells (SMCs). Vasculogenesis is the process of developing new blood vessels from progenitor cells, whereas sprouting angiogenesis involves the generation of new vascular entities from preexisting arteries. Vascular co-option, intussusception, and vasculogenic mimicry are other methods for producing new blood vessels. Endothelial progenitor cells (EPCs) in bone marrow play an important role in the initiation and progression of postnatal neovascularization during vasculogenesis [131]. Endothelial progenitor cells (EPCs) express CD34, CD31, VEGFR-2, and Tie-2 during vasculogenesis. In contrast, tumour cells generate proangiogenic chemicals, including VEGF and cytokines, such as stromal-derived factor-1, which promote the proliferation and differentiation of bone marrow-derived dendritic cells. Proangiogenic signals from tumours activate matrix metalloprotease 9. (MMP9). MMP enzymes are crucial in angiogenesis and metastasis because they break down the extracellular matrix (ECM), enabling cellular mobility and tissue penetration while boosting tumour development and dispersion [132].

Once activated, MMP9 facilitates proteolytic transformation of the membrane-tethered KIT ligand into a soluble functional form. This activated form of Kit ligand then increases hematopoietic cell and endothelial progenitor cell motility (EPCs) Once activated, MMP9 promotes the proteolytic transformation of the membrane-tethered Kit ligand to its soluble, functional form. This activated Kit ligand increases haematopoietic and endothelial progenitor cell motility (EPCs) [133]. Endothelial progenitor cells (EPCs) may attach to angiogenic sprouts and integrate into the endothelial layer of the blood vessels. In this context, adhesion molecules such as P-Selectin, E-selectin, and integrins play an essential role in boosting EPC attachment to vessel walls. Endothelial progenitor cells (EPCs) may connect to angiogenic sprouts and form the endothelial layer of the blood vessels. In this context, adhesion molecules such as P-selectin, E-selectin, and integrins play crucial roles in

boosting the attachment of EPCs to vessel walls [134]. VEGF predominantly stimulates endothelial cell differentiation [135].

The process of sprouting angiogenesis begins with the instability of endothelial cells, which leads to an endothelial-to-mesenchymal shift. These changes improve the migratory, invasive, and proliferative properties. The surrounding extracellular matrix (ECM) and basement membrane are then disintegrated by activated proteases such as matrix metalloproteinases (MMPs). This breakdown enables guided cell migration and proliferation. Polarisation of these moving endothelial cells eventually results in the creation of a vascular lumen [136]. Following these events, there is a reversal in the process, with cells transitioning from a proliferative phase to a quiescent state [137]. The key signaling pathways involved in activating angiogenesis morphogenetic processes are VEGF (Vascular Endothelial Growth Factor) and Notch [138].

Proangiogenic signals cause a variety of alterations in sprouting endothelial cells, including enhanced invasive and motile activity, protease activation, changes in cell-cell contacts, and apical-basal polarity inversion. The endothelial cells responsible for sprouting, which are located near the tip of the angiogenic sprout, are referred to as "tip cells." When stimulated by VEGF, these tip cells actively project extended filopodia, detecting and directing the development of the growing artery towards
locations with increased VEGF concentrations in the arterial bed (Figure 1.12).

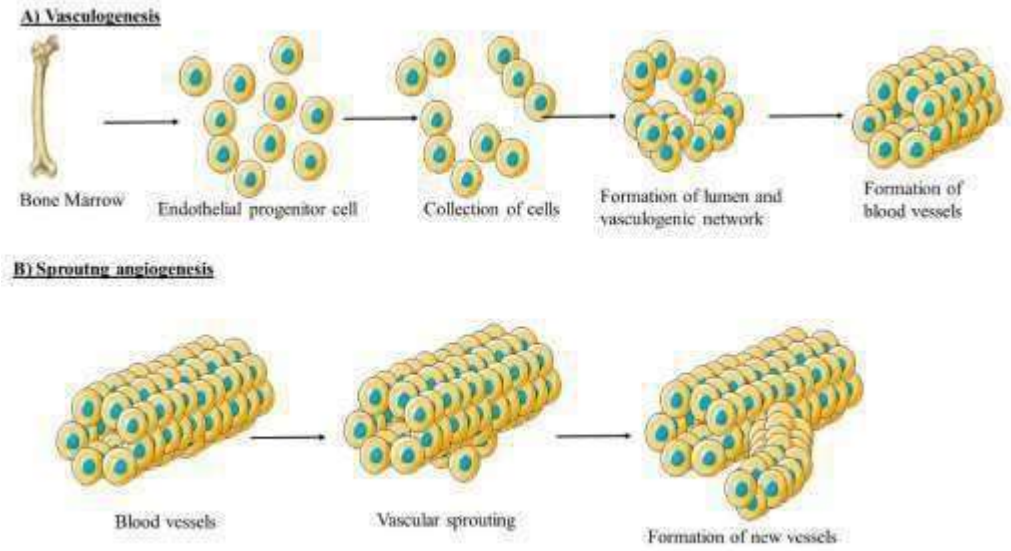

Figure 1.12 Mechanisms involved in blood vessel development. This diagram illustrates the various

processes through which new blood vessels can form in both normal tissues and tumours. In normal tissues, angiogenesis occurs through the recruitment and differentiation of bone marrow-derived endothelial progenitor cells (EPCs) into mature endothelial cells, which subsequently form capillaries. Angiogenesis involves the migration and proliferation of endothelial cells from parent vessels to form new capillary sprouts. Intussusceptive microvascular growth is a process in which existing blood vessels split and remodel to form new capillary networks. In tumours, an additional mechanism called vasculogenic mimicry can occur, in which tumour cells form vessel-like structures to provide blood supply for the growing tumour s. Understanding the diverse mechanisms of blood vessel formation is crucial for developing targeted therapies that can inhibit tumour angiogenesis and limit cancer progression**.**

Angiogenesis inhibitors may either prevent the creation of new blood vessels or assist in the removal of existing vessels once an inflammatory reaction subsides. Pharmaceutical angiogenesis inhibitors include anti-VEGF antibodies and anti-cancer tyrosine kinase inhibitors (TKIs), which suppress angiogenesis growth factor receptor activity and function. Nonetheless, cancer cells may use various angiogenic pathways, which seem redundant, to acquire resistance to specific therapies by progressively relying on signaling pathways unaffected by intervention. Suppression or lack ofangiogenesis may lead to treatment resistance. For example, hypoxic tumour cells in the middle of in situ spheroid carcinoma cannot be differentiated. This situation may serve as a survival strategy when such cells are exposed to therapeutic treatments, such as radiation or chemotherapeutic drugs, which only damage DNA during the division phase.

ytochemicals targeting the Gonadotrophin releasing hormone pathway

Gonadotropin-releasing hormone (GnRH) is the main regulator of the reproductive system. This neurohormone is produced and released by a dedicated collection of neurones found in the septal-preoptic-hypothalamic region of the brain [139]. Capillaries may arise in normal tissues through several mechanisms including (a) recruitment and differentiation of bone marrow-derived endothelial progenitor cells (EPCs) into endothelial cells, (b) sprouting angiogenesis, and (c) intussusceptive microvascular growth (Figure 1. 4) [140].

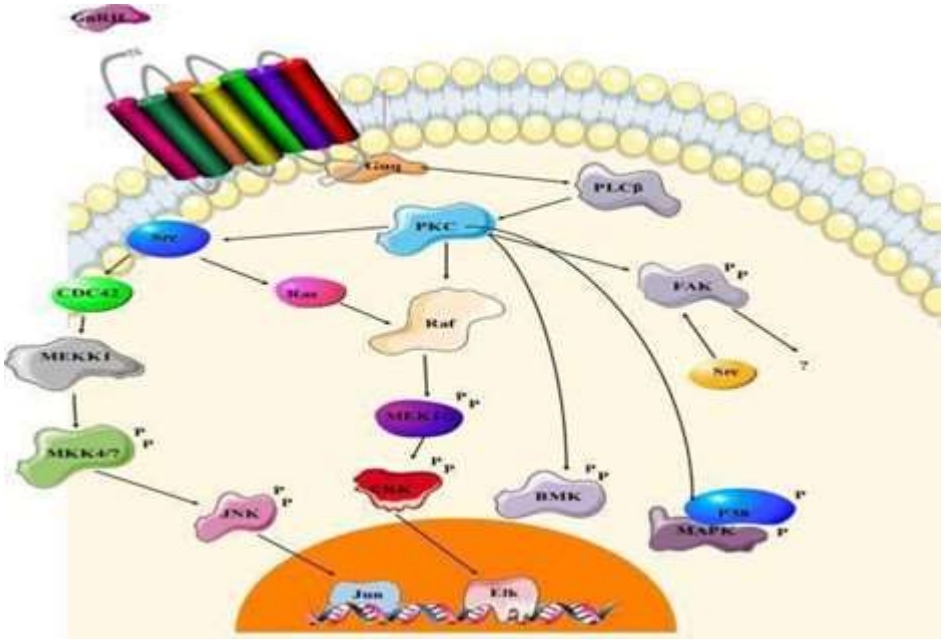

Figure 1.13 GnRH signaling pathway regulates LH and FSH production The diagram illustrates the complex signaling cascade initiated by gonadotropin-releasing hormone (GnRH) in the anterior pituitary gland, leading to the production of luteinizing hormone (LH) and follicle-stimulating hormone (FSH). GnRH binds to its G protein-coupled receptor (GnRH-R) on gonadotrope cells, triggering the dissociation of G proteins and activation of multiple downstream signaling pathways. These include mobilisation of intracellular calcium, calcium influx, and activation of protein kinase C (PKC). This signaling cascade ultimately results in the synthesis and release of the common alpha subunit and distinct beta subunits of LH and FSH. This intricate GnRH signaling pathway plays a crucial role in regulating the production and secretion of these gonadotropins, which are essential for reproductive function and control of gonadal activity.

The human gonadotropin-releasing hormone (GnRH) gene has a single gene copy on chromosome 8p11.2-p21, and is composed of four exons separated by three introns [141, 142]. The gonadotropin-releasing hormone (GnRH) gene encodes a pre-prohormone with a 23-amino acid signal peptide. The signal peptide varied from a GnRH decapeptide to two serine residues. Following the decapeptide, a GKR sequence is required for signaling amidation at the carboxy terminus as well as for enzymatic precursor cleavage. This area is followed by a 56-amino acid peptide called the GnRH-associated peptide (GAP) [141, 143].

GnRH activity in extra-pituitary cells can exert a suppressive effect on cell proliferation, indicating that its signaling pathways may diverge from those associated with mitogenic or stress-inducing G protein-coupled receptors (GPCRs). When stimulated by gonadotropin-releasing hormone (GnRH), T3-1 cells activate all four subfamilies of mitogen-activated protein kinases (MAPK), including ERK, JNK, p38MAPK, and BMK [144]. Among these subfamilies, Jun N-terminal kinases (JNKs) demonstrate the most significant activation,

showing a twenty-fold enhancement [145]. GnRH receptor (GnRHR) stimulation significantly increases ERK1 and ERK2 activity in GnRHR-expressing cell lines [146, 147].

GnRH (Gonadotropin-releasing hormone) is produced in the hypophysial portal circulation and eventually reaches the anterior pituitary gland. It boosts the production and release of two gonadotropins that control gonadal sex hormone development [148]. Gonadotropin-releasing hormone (GnRH) binds to the GnRH receptor (GnRH-R), a member of the seven-transmembrane G protein-coupled receptor (GPCR) family, with high affinity [149]. GnRHs (gonadotropin- releasing hormones) interact with their corresponding heptahelical receptors, a distinctive aspect of their engagement [150]. When GnRHs bind to their heptahelical receptors, the Gq or G11 proteins are activated. This activation then increases phosphoinositide turnover, resulting in the successive activation of enzymes, including PLC (phospholipase C), PLD (phospholipase D), and PLA2 (phospholipase A2). This activation also causes the mobilisation and influx of calcium ions (Ca2 +), as well as the translocation and activation of protein kinase C (PKC) [151, 152]. This sequence of events culminates in the production of arachidonic acid and generation of bioactive lipoxygenase products. Ultimately, these biochemical processes lead to the synthesis and release of gonadotropin [153]. GnRH receptors (GnRH-R) in the pituitary gland function as molecular targets for GnRH agonists and antagonists. These compounds represent the most widely utilised pharmacological therapies for hormone-dependent malignancies, including prostate, breast, and ovarian cancer. GnRH receptors (GnRH-Rs) are expressed in various cancerous tissues. Stimulating these receptors with GnRH agonists has been consistently linked to anticancer effects, including antiproliferative and antimetastatic actions [143, 154]. Activation of the GnRH receptor (GnRH-R) results in diverse biological outcomes, likely because of the different intracellular signaling pathways associated with this receptor in various tissues. In gonadotropes, activation engages the Gq/phospholipase C pathway. In contrast, the predominant pathway in cancer cells is the Gi/cAMP pathway [155, 156].

GnRH receptor (GnRH-R) has emerged as a viable target for new molecular-targeted therapies for cancers that exhibit these receptors. This category includes diverse treatments, such as GnRH agonists and antagonists, conjugates of GnRH agonists with cytotoxic agents (such as doxorubicin) or nutraceuticals (such as curcumin), and nanoparticles engineered to

target GnRH-R for the delivery of anticancer agents.

1,8.6 Phytochemicals targeting the Wnt signaling pathway.

The Wnt protein family is essential for regulating cell fate and maintaining homeostasis during various developmental phases [157]. In humans, the Wnt gene family is comprised of 19 glycoproteins, each with a high degree of cysteine richness and preservation [158]. The word 'Wnt' is obtained from the combination of two genes: 'Wingless (Wg),' which was the first Wnt gene discovered in Drosophila via genetic screening aimed at uncovering genes that modify embryonic patterning; and 'Wnt,' which is derived from the combination of two genes [159] and 'Int-1', a mouse proto-oncogene discovered for its role in triggering breast tumour formation. Subsequently, int-1 was identified as a member of the Wnt protein family [160].

Wnt proteins are classified by the physiological response they cause when they connect with the Frizzled (Fzd) membrane receptor. Wnt proteins that generate a -catenin-dependent transcriptional response are referred to as "canonical," whereas those that cause alternative responses are known as "non-canonical." In contrast to the canonical Wnt pathway, the non-canonical Wnt pathway incorporates a greater spectrum of cytoplasmic signaling components, making it more complicated and poorly understood [161].

The Wnt/-catenin signaling pathway is triggered when particular Wnt isoforms bind to their respective Frizzled receptors in conjunction with an LDL receptor protein family co-receptor, either LRP5 or LRP6 [162]. When Wnt binds to Fzd, it draws a key cytoplasmic regulatory complex to the membrane, which is stabilized by the tumour suppressor proteins Axin and APC. GSK-3, a serine/threonine kinase, aggressively phosphorylates β-catenin in the absence of Wnt signaling, indicating its destruction by the proteasome. Wnt signaling, on the other hand, inactivates GSK-3, enabling -catenin to accumulate and interact with the T-cell factor/lymphoid enhancer factor (Tcf/Lef) family of DNA-binding proteins. As Axin proteins are essential for the anchoring of both GSK3 and -β-catenin, they play a dual role in regulating the activation and repression of the Wnt/β-catenin pathway [163].

Transcriptional regulatory mechanisms play a vital role in modifying Wnt pathway responses. TLE/Gro, ICAT, Chibby, Sox9, and the CtBP/APC factor are proteins that control the interaction of

Catenin and Tcf/Lef Interactions such as those between TCF and TLE/Gro, provide TCF/LEF molecules with repressive function [164]. The occurrence of multiple isoforms of each protein, resulting from alternative splicing processes, adds to the functional heterogeneity of Tcf/Lef proteins [165]. Direct interactions between β-catenin and cyclic AMP-responsive element-binding protein (CREB)-binding protein (CBP)/p300 have been identified in vertebrates [166].In vertebrate systems, interactions between catenin and the CREB-binding protein (CBP)/p300 are required for transcriptional target activation[167]. The Wnt/-catenin signaling system is dual in nature, tightly controlling both cellular proliferation and differentiation [168]. The change from- catenin/CBP to -catenin/p300 interaction may signal a crucial cellular transition point. CBP and β-catenin interact to drive transcriptional pathways essential for stem/progenitor cell survival and proliferation [169].

Recently, the Wnt/Tcf signaling pathway and its target genes HOXB9 and Lef1 were identified as essential mediators of chemotactic invasion and colony formation in a lung cancer model [170]. Wnt signaling promotes epithelial-to-mesenchymal transition by decreasing the activity of the GSK3-mediated degradation complex, Wnt signaling promotes epithelial-to-mesenchymal transitions (EMTs). This suppression leads to elevated nuclear concentrations of β-catenin, thereby activating the transcription factors associated with EMT [171]. Wnt-mediated responses are likely to function in conjunction with other cell fate determination systems to promote epithelial-to-mesenchymal transition (EMT) in cancer [172].

1,8.7 Phytochemical targeting of the RTK signaling pathway

Growth factors bind to tyrosine kinase receptors on the cell surface. When a growth factor binds to a receptor, it activates the kinase domain, resulting in tyrosine phosphorylation and subsequent intracellular signaling cascades [173]. The most extensively studied receptor growth (RTK) family is the EGF receptor tyrosine kinase family, often known as the ErbB receptor family. These receptors interact with a wide range of growth factors including EGF,

and their functions in development, physiology, and cancer have been thoroughly investigated. ErbB receptors engage in various signal transduction pathways including the RAS/ERK, PI3K/AKT, and JAK/STAT pathways [174]. Additionally, ErbB receptors can translocate to the nucleus and initiate transcriptional processes [175].

ErbB receptors are typically activated by autocrine or paracrine ligand production. This activation triggers the dimerisation and activation of tyrosine kinase domains, which are accomplished by the trans-tyrosine phosphorylation of both the kinase domains and C-terminal tails. For example, co-receptors phosphorylate six tyrosine residues at ErbB3's C-terminus. This characteristic allows ErbB3 to signal in the absence of a functional kinase domain. Phosphorylated tyrosine residues act as docking sites for SH2 domain-containing signaling molecules. Adaptor proteins with an SH2 domain, including Grb2, Nck, and Shc, bind to the phosphorylated ErbB receptors. Furthermore, these adaptor proteins connect with other proteins via tyrosine phosphorylation of their own residues, which is regulated by ErbB receptors, or via domains, such as the Src homology 3 (SH3) domain, which binds to the proline-rich regions of other proteins. These linkages activate transcription factors and initiate a kinase cascade, causing biological consequences including cell proliferation and survival. ErbB receptors activate three main kinase cascades: RAS/ERK, PI3K/AKT, and JAK/STAT [176].

The EGF receptor family includes four different receptors: ErbB1 (also known as EGFR or HER1), ErbB2 (HER2/neu), ErbB3 (HER3), and ErbB4 (HER4) (HER4). These receptors exhibit evolutionary conservation and functional redundancy, both of which are necessary for effective signaling pathways [177]. Except for ErbB2, all members of the EGF receptor family have both ligand-binding and intracellular tyrosine kinase domains. ErbB3 is remarkable for its nonfunctional tyrosine kinase domain, which lacks catalytic activity. This indicates that ErbB3 primarily functions as a co-receptor in collaboration with other ErbB receptors [178] (Figure 1. 5).

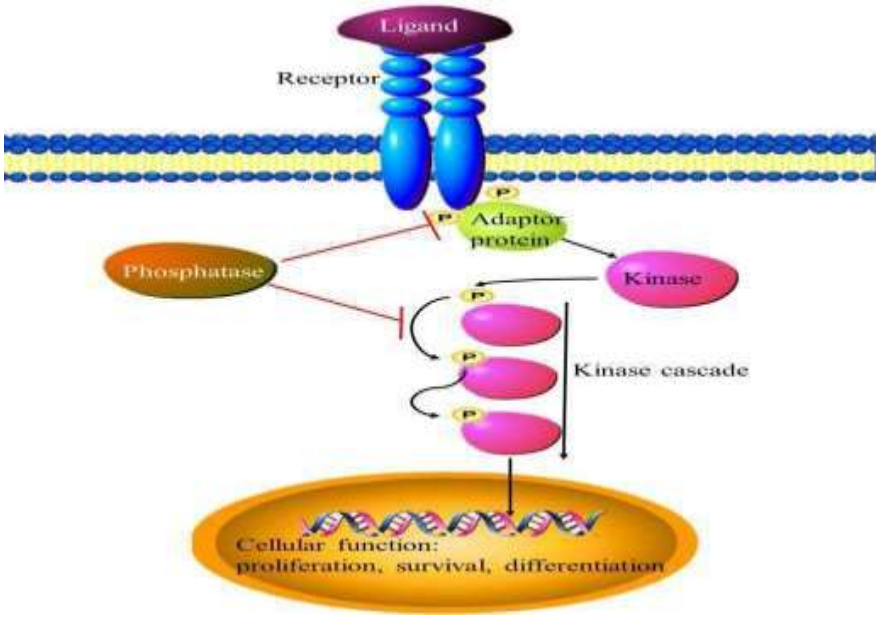

Figure 1.14 Signal transduction pathway of the ErbB receptor. The diagram illustrates the core components of the ErbB receptor-signaling pathway. Binding of a ligand to the extracellular domain of the ErbB receptor triggers activation of an adapter protein. The activated adapter protein then initiates a kinase cascade that involves the sequential phosphorylation and activation of multiple kinases. This kinase cascade ultimately regulates various cellular functions, including proliferation, survival, and differentiation. This pathway highlights the critical role of the ErbB receptor in transmitting extracellular signals to the cell interior and modulating the key cellular processes implicated in cancer development and progression.

ErbB receptors bind to a ligand, and upon binding, ErbB receptors undergo dimerisation and autophosphorylation of tyrosine residues on their C-terminal tails. This activates adaptor proteins that connect to receptors, triggering the phosphorylation and activation of kinases. Cascading events triggered by activation of the EGF receptor family lead to vital cellular processes, including proliferation, survival, and differentiation. Within this framework, phosphatases, enzymes that dephosphorylate proteins can exert a negative influence on these signaling pathways, whereas transforming growth factor-beta (TGF-β) exemplifies the complexities inherent in any strategy aimed at modifying cancer signaling pathways. This complexity underscores the challenges of targeting these pathways for therapeutic purposes [179]. TGF- exists in three isoforms, each of which binds to the TGF- receptor, a tetrameric complex comprising two type-I and two type-II transmembrane serine-threonine kinases. The Smad transcription factor family, including Smad4 (DPC4), a tumour suppressor typically missing in pancreatic and colorectal malignancies (CRC) as well as familial juvenile polyposis, regulates both positive and negative TGF-β signaling. TGF is involved in a range of biological processes, including proliferation, differentiation, development, wound healing, and formation of the extracellular matrix (ECM). Epithelial-to-mesenchymal

transition (EMT) and metastasis are essential for cancer treatment. TGF- typically inhibits the proliferation of normal epithelial and haematopoietic cells, as well as early stage carcinomas, but this inhibitory effect is often reduced in mid-stage malignancies. TGF- promotes the invasion and metastasis of advanced-stage tumours. TGF- is involved in a range of biological processes, including proliferation, differentiation, development, wound healing, and the formation of the extracellular matrix (ECM). Epithelial-to-mesenchymal transition (EMT) and metastasis are essential for cancer treatment. TGF- generally controls the proliferation of normal epithelial and haematopoietic cells, as well as early stage carcinomas, but this suppressive effect often decreases in mid-stage malignancies. TGF- may accelerate invasion and metastasis in advanced-stage tumours [180, 181]. TGF-β, which is released by certain aggressive tumours, stimulates tumour cell proliferation after epithelial-to-mesenchymal transition (EMT) and inhibits immune effector cells. In the field of signaling molecules, substantial studies have been conducted on reactive oxygen species (ROS) as promoters of cell growth and survival, specifically their effects on certain transcription factors. However, it is critical to remember that many proteins involved in essential signal transduction pathways play important roles in these processes. Upstream signaling pathways mediated by these non-transcriptionally active proteins typically lead to the activation of transcription factors. This highlights the importance of a variety of essential signaling molecules in redox regulation [182].

PI3K, a lipid kinase, is required for several cellular signaling pathways, including those involved in cell proliferation, motility, and survival. When activated, PI3K produces PIP3, which draws Akt to the cell membrane. Akt is activated in the membrane by 3-phosphoinositide-dependent kinase-1 phosphorylation (PDK-1). PTEN functions as a negative regulator of this pathway by dephosphorylating PIP3, which in turn inhibits Akt activation. Furthermore, ROS (reactive oxygen species) are known to affect the control of Akt activity, bringing a new dimension to the management of this pathway [183].

MAPKs (Mitogen-Activated Protein Kinases), a class of highly conserved serine/threonine kinases, are critical regulators of many physiological activities. These functions include cell growth, energy metabolism, gene expression regulation, and programmed cell death. The MAPK signaling cascade is differentiated by the successive activation of several kinases via phosphorylation. The various kinases involved in each step of the cascade define the precise

targets that are affected, thereby controlling cellular responses [184]. The complexities of MAPK signaling pathways make it challenging to correctly predict the impact of certain stimuli. ROS (reactive oxygen species)-induced MAPK pathway activation is well known, notably, the phosphorylation and subsequent activation of p38 and ERK1/2 MAPKs in response to oxidative stress. These phosphorylation processes appear to be dependent on redox reactions, as demonstrated by their suppression by antioxidants. Furthermore, differences in MAPK activity caused by different redox states have been linked to alterations in the cellular proliferation rates. This suggests that ROS may play a role in promoting cell proliferation via MAPK activation, highlighting the complex link between redox conditions and cellular signaling mechanisms [185].

Initially recognised as oncogenes in cancer cells, the Ras family of membrane-associated GTPases comprises three primary variants that exhibit substantial sequence similarity: H-Ras, N-Ras, and K-Ras. Although a significant portion of research is centred on their involvement in oncogenesis, Ras proteins are also crucial in normal cellular operations. They are crucial for directing the cell cycle during the transition from G1 to S phase. This dual functionality highlights the intricacy and significance of Ras proteins in standard cellular processes and cancer development [186]. Oxidative agents typically increase Ras activity leading to increased cell proliferation. In contrast, antioxidants usually reduce both of these interconnected phenomena. This dynamic underscore the significant role of oxidative states in controlling cellular functions through the modulation of pivotal signaling molecules such as Ras [187]. Given the role of the MAPK pathway as a crucial downstream effector of Ras, it is reasonable to infer that both processes are mechanistically linked. Ras-induced variations in proliferation indices may be due to the concomitant changes in MAPK activity. Further investigation of this theory is critical, particularly given the prevalence of mutations that result in persistent Ras activation in human cancer. Understanding this relationship may provide significant insights into tumourigenesis and prospective treatment targets.

1.9 Cotyledon orbiculata (Crassulaceae)

Cotyledon orbiculata, a small shrub characterised by succulent leaves, is a member of the Crassulaceae family [188-190]. This plant is traditionally used for medicinal purposes in

Southern Africa, where it is indigenous. Leaves are commonly used in local remedies for the treatment of corns and warts [190] to ease dental and ear pain, diminish inflammation, and assist in the control of epilepsy. Commonly, sap drawn from leaves is heated to prepare it for therapeutic applications [191, 192]. Research has shown that extracts from *Cotyledon orbiculata* possess antimicrobial, anti-inflammatory, and antioxidant properties, making it a valuable resource for medicinal applications [190]. Given the role of the MAPK pathway as a downstream effector of Ras, it is reasonable to hypothesise that both processes are mechanistically linked. Ras-induced changes in proliferation indices might be a consequence of simultaneous changes in MAPK activity. Further investigation of this concept is critical, particularly considering the prevalence of mutations that cause Ras to remain activated in human cancers. Understanding this relationship may provide valuable insights into tumourigenesis and prospective treatment targets [189]. Phytochemical studies have shown that *C. orbiculata leaves* possess bufadienolide glycosides, namely *orbicusides* A, B, and C. These compounds are recognised for their toxicity to sheep and goats, causing a disease known as krimpsiekte poisoning [193]. The toxic compound present in *C. orbiculata* is recognised for its ability to suppress the central nervous system and possesses characteristics similar to those of a local anaesthetic [191]. *C. orbiculata* is abundant in phytochemicals, such as saponins, tannins, reducing sugars, and triterpene steroids [188].

Studies of extracts from C*otyledon orbiculata* have demonstrated their anticancer splicing effects on VEGF165, a growth factor crucial for angiogenesis. These extracts also influenced alternative splicing of Axl and BclX genes. ELISA using antibodies targeting VEGF165 splice variants revealed that the extract from *C. orbiculata* prompted a splicing shift from angiogenesis-promoting VEGF165 to its anti-angiogenic variant, VEGF165b [194].

1.10 Tulbaghia violacea

Tulbaghia comprises approximately 63 species, most of which are characterised by rhizomes (Govaerts and Simpson, 2015). *C. orbiculata* is used in traditional medicinal practices to treat various conditions, such as oesophageal cancer, asthma, tuberculosis, coughs, digestive problems, and colds [188, 190]. *T. violacea* is known as Isihaqa by Zulus [195] as well as a snake repellent [196]. Moreover, studies have indicated that excessive consumption of *T. violacea* can lead to adverse effects, such as gastroenteritis, gastrointestinal pain, and

inflammation [191, 192]. A common secondary metabolite discovered in *T. violacea* phytochemicals is steroid saponin [197]. These saponins have been shown to aid in the inhibition of platelet aggregation and blood coagulation. *T. violacea* has been reported *to be* responsible for its in vitro fibrinolytic activity [198]. The garlic-like scent of *T. violacea* is attributed to sulfur compounds, which are released when its tissues or organs, such as leaves and rhizomes, are damaged or wounded. This results in an alliaceous odour [199]. This is a distinctive characteristic of this species. 1,4-tetrathiazol-2,7-dioxide and 2,4,5,7-tetrathiazo-2-dioxide are examples of such compounds [200]. *The aqueous extract of T. violacea* contains a variety of free sugars including glucose, fructose, sucrose, arabinose, rhamnose, xylose, and glycosides [200]. Kaempferol and quercetin are two flavonoids present in *T. violacea* [200]. CHO, MCF7, and HeLa cells undergo apoptosis after exposure to a 50:50 aqueous:methanol extract of *T. violacea;* however, H157 and MG63 cells do not undergo apoptosis [201]. Caspase-3 activation and DNA fragmentation are associated with apoptosis. Following purification of this pro-apoptotic extract, a novel component was identified. *In vitro* studies have shown that methyl-D-glucopyranoside can induce apoptosis in cervical cancer cells [202, 203].

T. violacea leaves and bulbs have been shown to suppress the growth of various cancer cell lines including MCF-7, WHCO3, HT29, and HeLa [204, 205].

According to the phytochemistry of *T. violacea*, its bioactivity may be linked to substances such as allylsulfur, phenolic glycosides, or free glycosides. *Tulbaghia* species emit a garlic-like odour when their leaves or rhizomes are injured. *Tulbaghia*'s characteristic scent is produced by S-(methylthiomethyl) cysteine-4-oxide, a cysteine-derived amino acid found in the cytoplasm. When Tulbaghia tissue is disrupted, a C-S lyase enzyme present in the cell vacuoles interacts with marasmin. This interaction causes marasmin to break down into the thiosulfinate marasmicin (2,4,5,7-tetrathiaoctan-4-oxide, 2), a process similar to the conversion of alliin to allicin in garlic [196, 206].

1.5 Rationale for Targeting COX-2 in Molecular Docking Studies

Targeting Cyclooxygenase-2 (COX-2) in molecular docking research is a strategic strategy because of its crucial involvement in inflammation and cancer progression. COX-2 is

commonly elevated in many types of malignancies, such as triple-negative breast cancer (TNBC), and its increased levels are linked to worse prognosis and a higher likelihood of metastasis [207]. COX-2 selective inhibitors can trigger apoptosis and decrease inflammation in cancer cells, indicating their potential as targets for developing anticancer drugs [208].

Compounds derived from medicinal plants such as Tulbaghia violacea have been shown to inhibit COX-2 and have anticancer properties, providing more evidence for investigating COX-2 in molecular docking research [209]. Research indicates that *T. violacea* extracts may have anticancer properties by influencing COX-2 activity [210]. Compounds from natural sources have been studied for their ability to inhibit COX-2, using molecular docking. Research has shown promising results in terms of affinity and selectivity for the COX-2 active site [211-213].

To investigate the interaction between bioactive compounds from *T. violacea* and the COX-2 enzyme, molecular docking methods can be used to analyse the binding modalities and possible inhibitory effects of these compounds [214]. Previous studies have used molecular docking to identify chemicals that strongly bind to the COX-2 active site, thereby providing an understanding of the structural characteristics required for COX-2 inhibition [215-217]. The choice of COX-2 as a target for molecular docking investigations is justified because of its known involvement in cancer progression, its increased presence in TNBC, the blocking actions of natural substances, and the possible connection between *T. violacea* extract and COX-2 suppression. Molecular docking studies are useful for examining how bioactive molecules interact with COX-2, and can help in developing new therapeutic treatments for inflammation and cancer.

Chapter 2 Methods and Materials

Table 2.1 List of materials used in this study

Cell culture media		
CF-10A media	Leibovitz's MEDIUM 171 10% foetal calf serum 1% Penicillin/Streptomycin	HYCLONE® #SV30160.03 Bio Whittaker® Lonza #17-602E
MDA-MB-231	Leibovitz's L-15 Medium 10% foetal calf serum 1% Penicillin/Streptomycin	HYCLONE® #SV30160.03 Biowhittaker® Lonza #17-602E
Cell viability assay		
Trypan Blue stain	1:1 mixture with 1xPBS	Sigma
Counting slides	dual room	Bio-Rad # 145-001
Protein extraction		
Lysis buffer SDS Protein inhibitor cocktail	Each Tablet contains AEBSF•HCl, Aprotinin, Leupeptin, Pepstatin Sodium Fluoride, Sodium Orthovanadate, Sodium Pyrophosphate	Sigma #P4417-100TAB
SDS-PAGE		
Acrylamide/bis-acrylamide solution	Acrylamide 29.2 g Bis-acrylamide 0.8 g	
Gel casting buffers	1.5 M Tris-HCl, pH 8.8 (to prepare resolving gel): 18.15 g of Tris base Adjust pH to 8.8 using 6N HCl. Make up the final volume to 100 mL	
Gel casting buffers	0.5 M Tris-HCl, pH 6.8 (to prepare stacking gel): 6 g of Tris base. Adjust pH to 6.8 using 6N HCl. Make up the final volume to 100 mL	
Loading buffer	Bromophenol blue 0.004% 2-mercaptoethanol 10% Glycerol 20% SDS 4% Tris-HCl 0.125 M Tris-HCl 25 mM Glycine 200 mM SDS 0.1% (w/v)	
10%SDS 10% Ammonium persulphate TEMED		

For more detailed information about the cell lines, please refer to Appendix A. Additionally, the ethics

waiver for the use of these cell lines is included in Appendix E.

Table 2.2 Cell lines details and origins

	MCF-10A	MDA-MB-231
Ethnicity	Caucasian	
Morphology	Basal epithelium	Basal
Age	36	43
Hormone sensitivity	Normal	TNBC
Tissue	Breast; mammary gland;	Mammary gland, breast; metastatic site derived: pleural effusion
Culture media	Mammary Epithelial Cell Basal Media supplemented with MEGM media kit and 100 ng/ml cholera toxin	Leibovitz's L-15 medium

waiver for the use of these cell lines is included in Appendix E.

2.1 Methods

2.1.1 Preparation of plant extracts

Plant extracts of *T. violacea* and *C. orbiculata* were produced using aqueous extraction of water-soluble components and methanol-based extraction of nonwater-soluble components. Both plants were sourced from a local nursery (Tulip Garden Center, Johannesburg, South Korea). The plant species was confirmed by the staff at the C. E. Moss herbarium at the University of the Witwatersrand. The leaves of both plant species were collected, rinsed with water, and, to ensure successful extraction, cut into smaller sections and dried for 120 hours in a well-ventilated oven at 40 ^{o}C. Once dried, the plant material was finely ground and passed through an 850-micron sieve. This process aids the penetration of the solvent into the cellular structure of the plant to dissolve secondary metabolites. To extract water-soluble compounds, the dry powder was dissolved in one liter of boiling water and allowed to cool for 24 h. Subsequently, the solution was filtered to obtain an aqueous extract. The filtrate was freeze-dried to yield the dried aqueous plant extract, which was stored for 72 h.Compounds that were insoluble in water were extracted by dissolving the dried powder in 250 mL pure methanol. This mixture was then filtered to remove particles that were not soluble in methanol. The filtrate was placed in a Soxhlet extractor for 72 h, after which the crude methanol extract was evaporated completely. The resulting powder was freeze-dried to ensure its formation of a dry powder.

New solutions were prepared daily throughout the experiment using both the aqueous and methanolic raw extracts. For the aqueous extract, the required volume of dried extract was dispersed in an adequate amount of physiological saline, deionised water, or a cell culture medium. A designated quantity of the methanol extract was mixed with a minimal volume of dimethyl sulfoxide (DMSO) in physiological saline, deionised water, or culture medium. In each case, the final DMSO concentration did not exceed 0.5 percent.

2,1.1 Cell culture

MCF-10A and MDA-MB-231 cell lines were used in this study, as shown in Table 2. These cell lines

were propagated in tissue culture flasks with medium supplemented with penicillin/streptomycin (10000 IU/ml) and 10% foetal calf serum (FCS), and incubated at 37 °C in a ThermoForm Series II incubator devoid of CO2. Cell passaging was performed every three days or when the cells reached 70% confluence. The medium was aspirated, and the cells were washed with PBS at this stage of confluence. One millilitre of trypsin-EDTA was used to remove the adherent cells, followed by a 5-minute incubation. The action of trypsin was stopped by adding 1 ml of FBS-containing medium. The supernatant was removed after 5 min of centrifugation at 1300 rpm, and the cell sediment was reconstituted in fresh medium. Reconstructed cells were transferred to new tissue culture flasks for further incubation.

2,1.2 Thawing of cells

Cells maintained at cryogenic temperatures were removed from a -80 °C freezer and thawed gradually on ice. After defrosting, the cells were transferred to a 15-ml centrifuge tube and spun for 5 min at 800 rpm. The supernatant was removed after centrifugation and the cell sediment was resuspended in 5 ml of medium containing 1% penicillin/streptomycin and 10% foetal calf serum (FCS). This resuspended mixture was then transferred to a cell culture flask and incubated in a CO2-free atmosphere at 37 °C. Following good cell adhesion, the medium was replaced with a solution containing 10% foetal FCS. Cell growth was evaluated over a 5-hour period.

2,1.3 Cell cryopreservation

Adhering cells were trypsinised and the resulting cell suspension was centrifuged at 800 rpm for 5 min. The collected cell sediment was reconstituted under appropriate conditions, containing 1% penicillin/streptomycin, 20% foetal calf serum (FCS), and 10% dimethyl sulfoxide (DMSO). One millilitre of this mixture was portioned into a labelled cryovial and stored overnight at -20 °C. It was then moved to a -80 °C freezer for further preservation.

2,1.4 Cell count determination

A Countess™-3 Automated Cell Counter was used for cell counting. The device is a fully automated cell counter and assay platform that uses cutting-edge optics and image analysis algorithms to analyse trypan blue-stained samples in suspension. It has a simple user interface and the ability to save data and generate reports that can be transferred to a PC using a USB drive. The cells were mixed 1:1 with trypan blue solution (Sigma #T8154) and loaded into a quartz haemocytometer, which was then inserted into the instrument. Both sites of the haemocytometer were loaded and counts were performed in duplicate for each sample.

2,1.5 Determination of changes in the cell morphology caused by treatment with various extracts

The analysis of cell morphology can be used to determine the physiological state of cells; therefore, morphology can be used as a qualitative and quantitative measure in various biological assays. Various parameters can be automatically determined from microscopic images using analysis software. These include the shape, area, perimeter, circularity, roundness, and solidity. The shape analysis was dependent on the shape factor (S). It is a dimensionless quantity obtained by measuring the diameter, perimeter, area, and other parameters of a selected cell [218]. The shape factor (S) is given by

$$S = \frac{4\pi A}{p^2}$$

Where,

A = the area of the cell P = the cell perimeter

MDA-MB231 and MCF-10A cells were exposed to all four extracts, and microscopic images were captured at 0, 24, 48, and 72 h. As a positive control within the experiment, the cells were administered 5-fluorouracil (5FU). The captured images were then annotated using the public-domain Java image-processing program, ImageJ. The perimeter measurements were plotted against the area of the cell.

These plots were used to assess the cell shrinkage and membrane blebbing. The cell circularity, roundness, and solidity were measured.

The roundness of a cell is a measure of its area-to-perimeter ratio. Simply put, if two concentric circles are placed over an object with different diameters, a round object falls between the two circles. The difference between the diameters of the circles was dependent on the tolerance level. This was calculated using the following equation:

$$\text{Roundness} = \frac{(4\pi)\ \text{area}}{(\text{convex perimeter})^2}$$

Round objects have a result of 1; the lower the value, the less round the object [118, 219]. Generally, cells undergoing apoptosis become less round and more irregular in shape [220, 221]. The circularity of a cell measures the proximity of its mass centre to the centre of a theoretical circle encompassing the cell. This measurement is calculated by

Circularity = Radius_circumscribing / Radius_inscribing

In three dimensions, this can also be used to describe sphericity; once again, the closer it is to 1, the more circular [222].

The density of a cell is measured by its solidity, which is the ratio of the area of an item to the area of the convex hull of an object. The convex hull of an object is defined as the smallest convex form that contains an item (Figure 2.1).

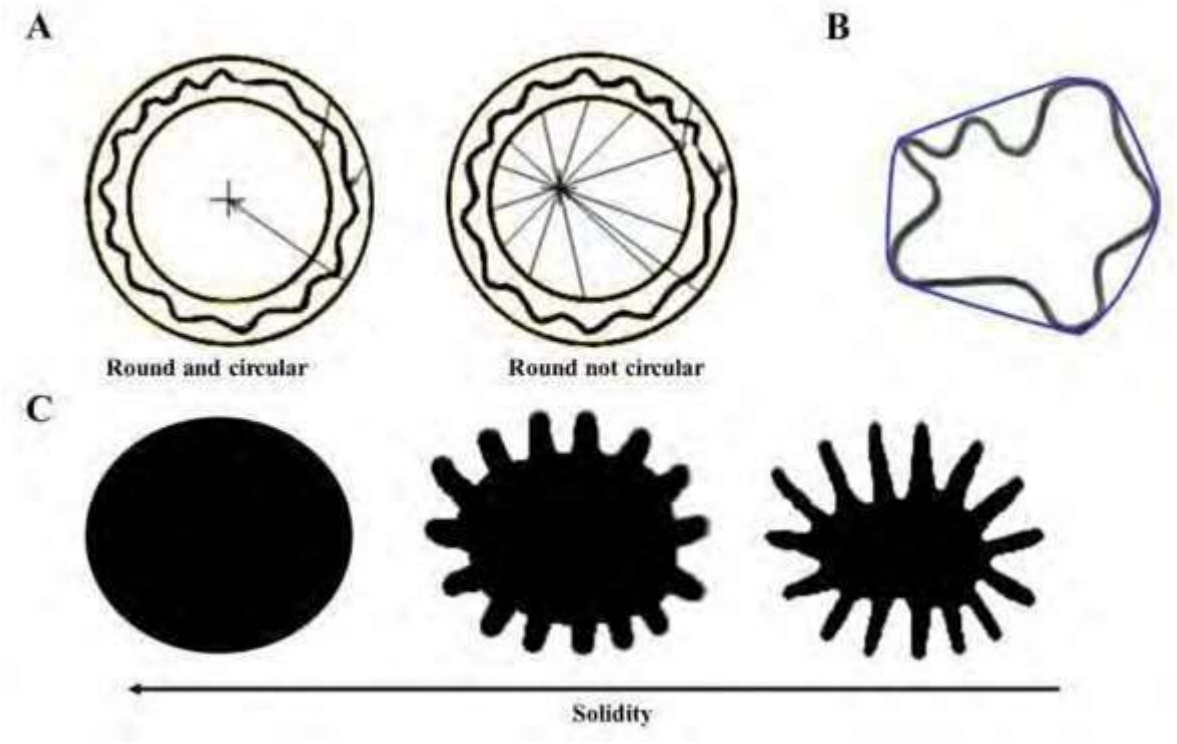

Figure 2.1 Depiction of the calculation of morphological features The figure illustrates the key morphological features used in the quantitative analysis, including the roundness, circularity, convex hull, and solidity. Panel A shows examples of shapes that are round, circular, and round, but not circular, highlighting the distinction between these two geometric properties. Panel B depicts the concept of a convex hull, which is the smallest convex polygon enclosing a given shape. Panel C shows varying degrees of solidity, which is a measure of the compactness or density of an object relative to its convex hull area. These morphological features are essential for characterising and quantifying the shape, size, and texture of objects or regions of interest in image analysis applications across various domains including biology, materials science, and computer vision.

2,1.6 Determination of the IC_{50} value for the crude extracts

2,1.7 Treatment of cells with purified fractions: Bioassays and cytotoxicity assays.

Under normal conditions, the cells were grown in 24-well plates and allowed to multiply overnight. Subsequently, the original medium was replaced with serum-free medium for 24 h to induce serum deprivation. This step was designed to reduce cell division and synchronise the cell cycle during the G0 phase. Following fasting, the cells were exposed to varying amounts of crude plant extract. The plant extract stock solution was made by combining the crude extract with 10% Foetal Bovine Serum in sterile tissue culture medium (FBS). Extracts that were soluble in methanol were diluted in tissue culture medium with dimethyl sulfoxide (DMSO) to produce a final concentration of 2%. Under

serum-free culture conditions, the stock solution was diluted to the desired concentration. Finally, the cells were exposed to the diluted extract for 24 h in fresh culture medium supplemented with 10% FBS. Cell viability was determined using Alamar Blue (AB).

Alamar Blue, also known as resazurin, is a water-soluble dye used to assess cell viability. Its solubility in the culture medium, non-toxicity to cells, and its ability to permeate cell membranes make it a suitable indicator. Alamar Blue has been demonstrated to act as an intermediary electron acceptor in the electron transport chain without interfering with the normal electron flow [223]. Alamar Blue can be reduced by NADPH, FADH, FMNH, NADH, and cytochrome. When electrons are added to AB, its colour changes from oxidised nonfluorescent blue (resazurin) to diluted fluorescent pink (resorufin). Oxidised state transition can be used to determine cell viability. This is accomplished through quantitative measurements, such as calorimetric or fluorometric tests with detectable colour changes, indicating the presence or absence of viable cells because only viable cells oxidise AB. For spectrophotometric absorbance measurements, wavelengths of 570, 600, 540, and 630 nm were used.

Alamar Blue tests were used to determine the IC50 values of plant extracts and their activity against the Triple-Negative Breast Cancer (TNBC) cell line. The cells were grown in 96-well plates using a previously described method. Cell counting was performed to determine the number of cells seeded in a multiwell plate. The cells were serum-starved for 24 h after overnight growth to synchronise the cell cycle.

Cultured cells were treated with different concentrations of the plant extracts (100, 200, 300, 400, 500, and 600 ug/ml). Each concentration was tested in triplicate for each of the four extracts, with a 0.2% DMSO control acting as a control for the methanol extracts dissolved in DMSO (Figure 2.2). The concentration of DMSO was the same as that of the most concentrated methanol extract. Untreated control cells were grown in regular tissue culture media. Cells incubated with 5-fluorouracil (5FU) functioned as a positive control. Cells were allowed to multiply for 48 h after treatment. The medium was then replaced with fresh media infused with a 10%
concentration of Alamar Blue and the cells were cultured for another 4 h. After 4 h, the cells in the

96-well plate were treated with a solution containing 10% Alamar Blue and incubated again. Absorbance of the plates was measured using a Spectromax ABS+ plate reader (Molecular Devices). The percentage of live cells was determined based on the decrease in AB, which was proportional to the dye intensity, using the formula A590nm - (A600nm - A690nm).

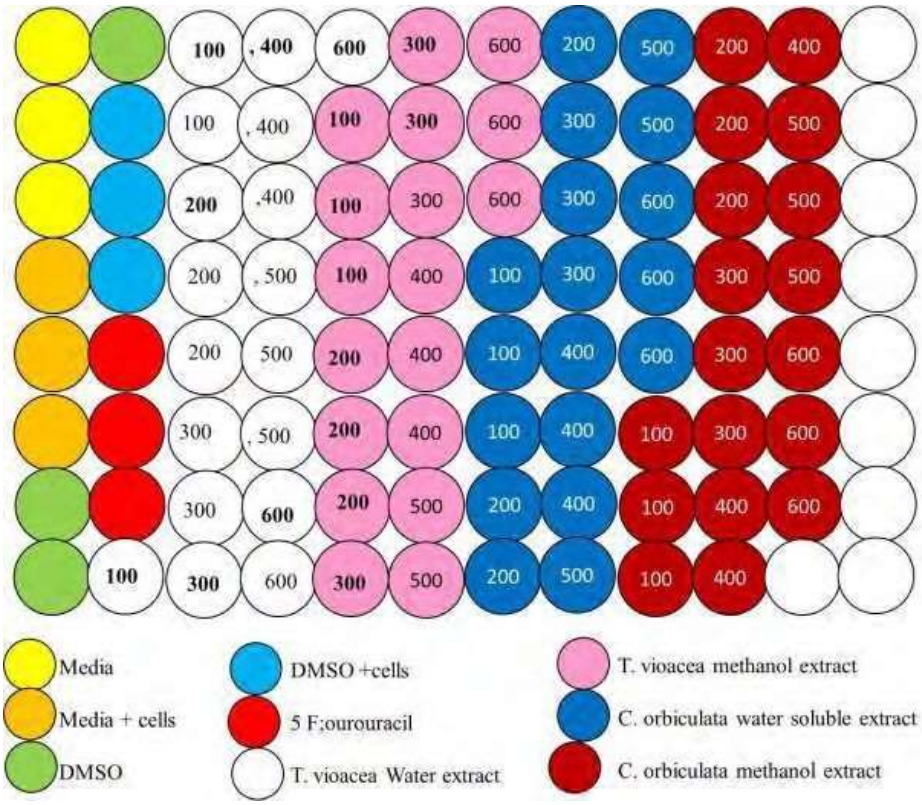

Figure 2.2 The layout of the 96-well plate was used to determine IC50 in the alamar blue assay The figure depicts the arrangement of different treatments and controls within a 96-well plate for the alamar blue assay to evaluate the half-maximal inhibitory concentrations (IC50) of various compounds. The plate was divided into quadrants, with each well containing a numerical value that represented the concentration or amount of treatment. The treatments included media control, DMSO vehicle control, DMSO with cells, *T. violacea* methanol and water extracts, C. orbiculata methanol and water-soluble extracts, and the chemotherapeutic drug 5-Fluorouracil as a positive control. The layout allows for testing multiple concentrations of each treatment in replicates, enabling the determination of dose-response curves and IC50 values for cytotoxicity or growth inhibition in cell-based assays.

2,1.8 Real-Time Cell Analysis (RTCA) by XCelligence

The XCelligence system is a real-time cell analyser that monitors cell attachments by measuring electrical impedance in real time. As cells proliferate and expand across the surface of the plate, their impedance is represented by cell index (CI) values. CI counts the number of live cells that interact with the electrodes on the E-plate over time. The CI value was zero if no cells were present on the electrode.

As the number of cell attachments increases, so do the CI values, and variations in cell adhesion and viability produce changes in the CI. CI values accurately depict the number of cells and their biological conditions. The normalised cell index (NCIti) was calculated by dividing the cell index (CIti) at each time point by the normalised time index (CIti) (CIti = CIti/CIti).

The xCelligence RTCA system was employed to measure the impact of various concentrations of plant extracts on the two cell lines in real-time. In addition, the IC_{50} was established using the XCelligence system by plotting the CI against the concentration of the extracts. The concentrations of the plant extracts were varied, and the cells and controls were seeded in E16 × Celligence plates. Initial titration curves were obtained to determine the appropriate number of cells to be added to each well of an E16 plate. This involved adding various numbers of cells to the e-16 plate, running the RTCA plate for 24 h, and monitoring CI. The selected cell number was based on the speed of cell growth and the time taken for cells to start dying off due to overcrowding. The recommended number of MDA-MB-231 cells to seed per well of the XCelligence e-plate for the RTCA experiments was 4000 cells/well, which corresponds to a cell density of 20,000 cells/mL

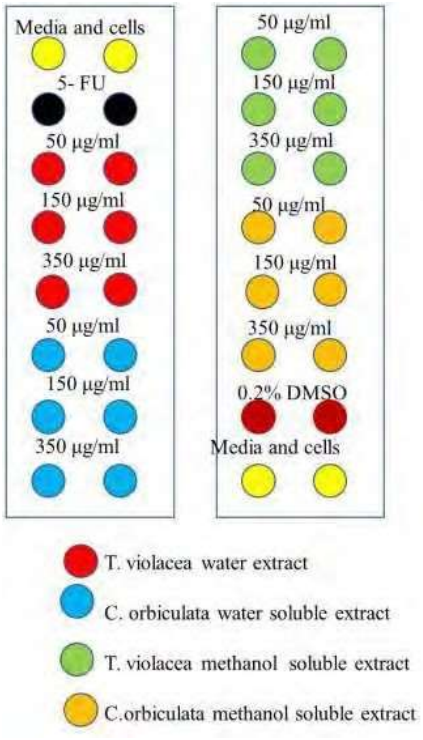

Figure 2.3 Layout of the excelligence e plate for the determination of the IC50. The appropriate number of cells

was subsequently dispensed into all wells of the electronic plate (e-plate). Varying concentrations of the four plant extracts (0, 50, 150, and 350 ug/ml) were used to treat cells. In addition, a vehicle control for the methanol extract was added to both wells. This involved the addition of media at a concentration of 0.2% DMSO. In this study, 5-fluorouracil (5FU) was used as a positive control at concentrations of 25 and 100 µM. For untreated cells, the control setup consisted of the addition of only full medium to these cells. The cells were grown on an e-16 plate and monitored by the RTCA device for 24 h before treatment. The extracts, DMSO, or the drug were added to each well at a final volume of 200 µL of medium per well (Figure 2.3). After treating the cells with varied doses of plant extract, a kinetic record of the cells was established, which offers important information about the cell's biological status, including cell viability. Cell impedance data were used to generate a plot of cell viability versus the logarithmic value of compound concentration. Using this plot, the IC_{50} value for each crude extract was calculated using the RTCA software.

Figure 2.3 depicts the layout of the E16 × CELLigence plate used to determine the half-maximal inhibitory concentration (IC50) of the four plant extracts in MDA-MB-231 triple-negative breast cancer cells. The plates were divided into sections, with different concentrations of each extract applied to the wells. Specifically, concentrations of 0, 50, 150, and 350 µg/mL were tested for the *T. violacea water extract, T. violacea methanol* extract, *C. orbiculata* water extract, and *C. orbiculata* methanol extract. Additionally, two wells contained 0.2% DMSO as a vehicle control of 0.2% DMSO to account for the solvent used in the methanol extracts. The chemotherapeutic drug 5-fluorouracil (5-FU) was used as a positive control at concentrations of 25 and 100 µM. Finally, two wells with untreated cells served as negative controls. This layout allowed for simultaneous evaluation of the cytotoxic effects of various extract concentrations on MDA-MB-231 cells using the real-time monitoring capabilities of the xCELLigence system.

2.2 Determining the effects of Active plant extracts on TNBC cells

2,2.1 Analysis of the effect of active plant extracts on cellular apoptosis

Flow cytometry was used to assess the apoptotic effects of the active plant extracts, which commonly exhibit anticancer effects by inducing cell death in targeted cells. The Muse™ Annexin V and Dead Cell Kit (Merck, MCH100105) was used for the study, which assesses cells in several states: alive, in early or late apoptosis, and dead. Cells were stained with annexin V or 7-aminoactinomycin D (7-AAD) using this kit.

During apoptosis, phosphatidylserine (PS) is externalised on the cell surface. Annexin V, a calcium-dependent phospholipid-binding protein, binds to PS and functions as a fluorescent marker to detect apoptotic cells. 7-AAD is a fluorescent compound that binds DNA with high affinity, but cannot

penetrate live or healthy cells. It stains dead cells or those in late-stage apoptosis, where the membrane integrity is compromised, allowing the dye to enter.

Using these strains, four distinct cell populations were identified and quantified using a Guava Muse flow cytometer, providing a detailed analysis of the apoptotic effects of the plant extracts. These are:

1) Annexin V (-) and 7-Aminoactinomycin D (-) – Healthy live cells
2) Annexin V (+) and 7-Aminoactinomycin D (-)- Early-stage apoptosis
3) Annexin V (+) and 7-Aminoactinomycin D (+) – Late-stage apoptosis
4) Annexin V (-) and 7-Aminoactinomycin D (+) – Dead cells

Five unique cell populations were individually propagated in distinct flasks. One flask was designated as the untreated control, whereas the other served as a positive control for cellular death. The remaining three flasks were exposed to varying concentrations of *T. violacea* water extract: one at the IC_{50} concentration, another at a concentration marginally below the IC_{50}, and the final one at a concentration exceeding the IC_{50}.

The cultured cells were serum-starved for 24 h, followed by treatment with the respective compounds for 48 h. The plant extracts were dissolved in normal culture medium. Both the untreated control and the positive control were left untreated. The positive control cells were separated after 48 h, spun down, and the cell pellet was placed in hot water to kill cells. All pellets were resuspended in 1 percent FBS in 1X Assay Buffer HSC after the other cell samples were detached (CatLog No. 4700-1325). In a 1:1 ratio, the cell suspension, annexin V, and dead cell reagent were combined (100 µL each). This cell mixture was incubated for 20 min before analysing the Annexin V and dead cell programs on the Muse instrument. The analysis was calibrated using a positive control, consisting of heat-killed cells. The percentages of live, early apoptotic, and combined late apoptotic and dead cells in each cell population were documented. These data are represented in a bar graph illustrating the percentage of cells in each category for each cell population. This experiment was repeated three times for three technical replicates, and the experiment was repeated three times for three biological replicates.

2.2.1.1 Analysis of the effects of active plant extracts on cell cycle progression

The effect of active plant extracts on the cell cycle progression of treated cells was evaluated using flow cytometry and propidium iodide (PI) labelling. PI is a DNA-binding stain that attaches to DNA in a manner that is directly proportional to its concentration. Consequently, the fluorescence intensity emitted by the stained cells corresponded to the DNA quantity, thereby indicating the cell cycle stage. When cells divide, they undergo four stages as described below. The first phase, also known as the resting phase, consists of gap 0 (G0) or the senescent stage, in which the cell has stopped dividing. This is followed by the Gap 1 (G1) stage, during which the cells grow in size. The second phase, also known as the synthesis (S) phase, is where the DNA replication occurs. Gap2 (G2) is the third phase, which occurs during DNA synthesis and mitosis. At this stage, the cells continue to develop. The concluding phase, known as mitosis (M), is characterised by the termination of cellular growth and subdivision into two daughter cells. The cell cycle is directed by cyclins and cyclin-dependent kinases (CDKs) that regulate cell progression at each stage. Consequently, the DNA content of the cells was indicative of cell cycle stage. Cells in the S-phase had more DNA than those in the G1 phase, and G2 cells appeared twice as bright as G1 cells.

The cells were exposed to three different concentrations of *Tulbaghia violacea* water-soluble extract: a concentration below the IC_{50}, an IC_{50} concentration, and one above the IC_{50}. Comparing the cell cycle profiles across these three concentrations enabled me to gain a more comprehensive understanding of how *T. violacea* extract influences cell cycle progression and whether these effects are dose dependent. This approach provided more detailed information than simply testing a single concentration, even if it was the IC50. The cells were collected and preserved in ice-cold 100% ethanol after a 48-hour treatment period. To remove the RNA, the fixed cells were rehydrated and treated with RNase at 37°C. This step is vital because propidium iodide (PI) can attach to RNA, similar to DNA, which could influence the precision of fluorescence measurements. After RNase treatment, the cells were stained with 1 mg/ml propidium iodide (PI) and incubated at 4°C overnight in the dark to ensure precise DNA content measurement. This staining process is critical for an accurate assessment. Finally, the stained cells were analysed using the cell cycle analysis program on a Muse flow cytometer. This step was essential to determine

the effect of the extract on cell cycle progression.

2.2.1.2 Measuring the effect, the active plant extract had on cell invasion and migration

Cell invasion and migration tests were performed to evaluate the effect of the active plant extract on cancer cell migration and invasion, particularly its capacity to enter the extracellular matrix (ECM). This assay utilised the RTCA xCELLigence system, which employs a CIM e16 plate. The assay was complemented by a synthetic ECM, specifically Geltrex™ (Invitrogen), to closely mimic the natural environment and assess the ability of cells to migrate through and invade the ECM under the influence of the plant extract.

The E16 CIM plate was divided into two, with 8 wells being used for the migration assay and 8 wells being used for the invasion assay (4). For the invasion assay using the xCELLigence system, an upper section of the CIM plate was prepared by adding 50 µL of undiluted Geltrex to each well designated for invasion. In the lower chamber, 100 µL of medium with FBS was added to all but four wells, which received medium without serum. Consistent with previous methodologies, 5000 cells at a density of 25000 cells/ml, were seeded into each well of the upper chamber.

The water-soluble *T. violacea* extract was injected into the migration and invasion portions of the plate to obtain a final concentration of 200 µg/ml in three wells in each area. Once the CIM plate was assembled, it was placed in the xCELLigence system. Cell index (CI) readings were subsequently taken every 15 min over a 72-hour period. This ongoing surveillance facilitated real-time observations of cell migration and invasion, providing essential insights into the effects of *T. violacea* extracts on these cellular activities.

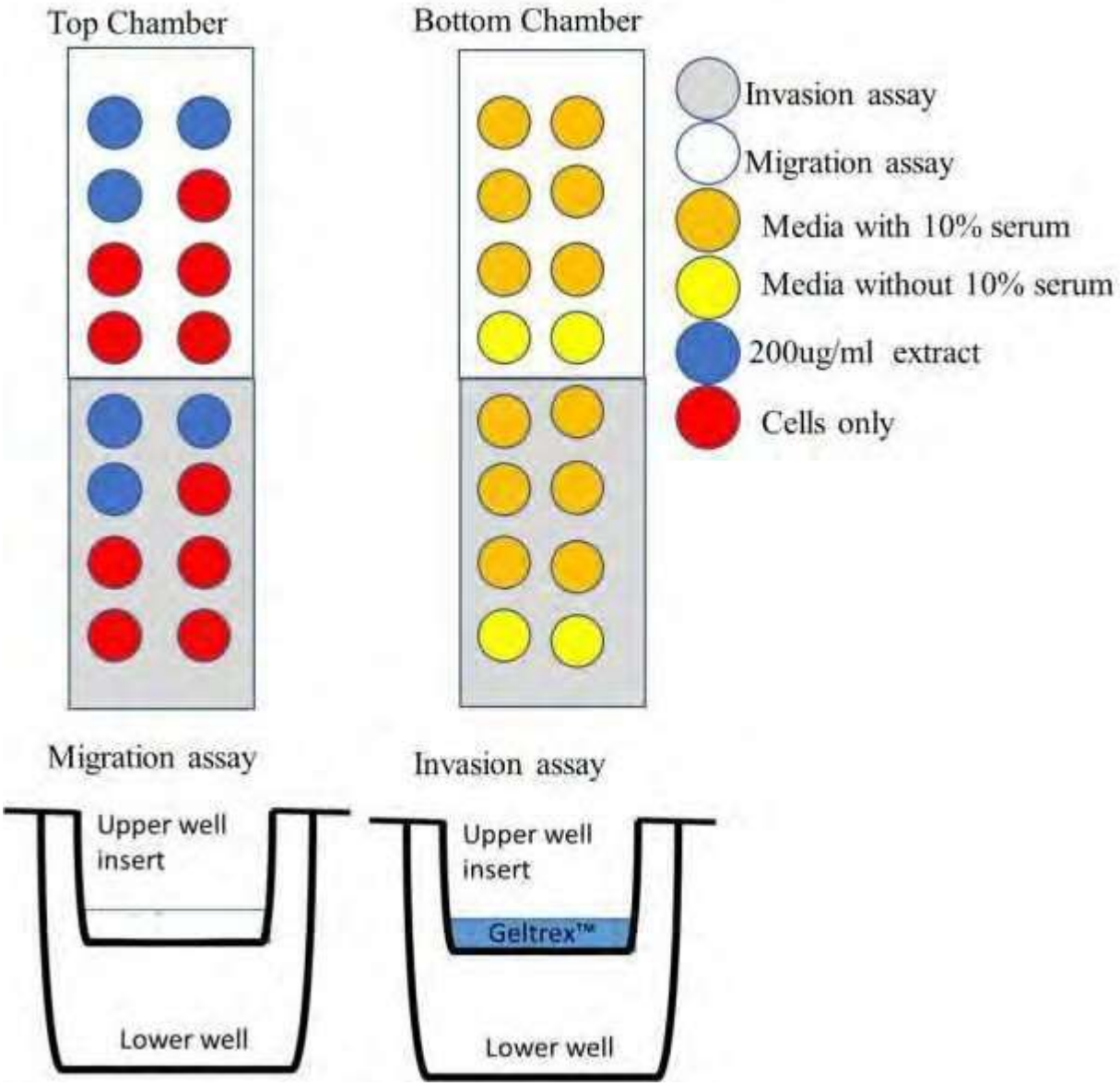

Figure 2.4 Cell invasion and migration plate setup. This diagram illustrates the experimental setup for cell invasion and migration assays using the xCELLigence system and a CIM e16 plate. The plate was divided into two sections: the " top and " bottom chambers " bottom chambers. The Top Chamber contained 12 circular wells arranged in three rows, with differently coloured circles representing various experimental conditions or treatments tested for cell invasion and migration. The Bottom Chamber also shows 12 circular wells arranged in three rows, with different coloured circles indicating additional experimental conditions. The legend at the bottom provides details on the specific components and conditions being tested, including "Invasion assay", "Migration assay", "Media with 10% serum", "Media without 10% serum", " 200 µg/ml extract", and "Cells only". Additionally, the diagram includes schematic representations of the "Upper well insert" and "Lower well" for both the invasion and migration assays, with the "Geltrex" label indicating the use of a basement membrane extract in the invasion assay.

2.2.1.3 Scratch assay for migration analysis

Cells were grown on a plate to form a confluent monolayer. A cell-free zone was established by inscribing a line through the monolayer using a pipette tip (Figure 2.5). The cells were then treated with two different doses of the *water-soluble T. violacea* extract: one slightly below the IC_{50} (200 µg/ml) and another above the IC_{50} (300 µg/ml). 5-Fluorouracil (5FU) was used as a positive control, and a set of cells was left untreated for comparison.

Cell migration and proliferation were monitored under a microscope for 48 hours. Measurements of the gap width were taken every 2 h during the initial 6 h, and then at 24 and 48 h. Gap closure, indicative of cell migration and proliferation, was quantified by measuring changes in gap width. The gathered data were charted over time to examine the effects of the extracts on cells. The mean width of the gap was computed and the pace of gap closure was meticulously recorded. This information was then used to calculate the migration rate after treatment with the plant extracts compared with the control group.

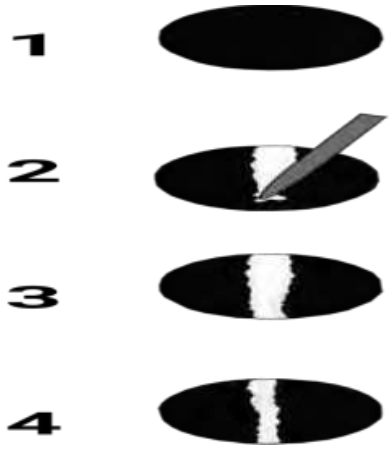

Figure 2.5 Scratch Assay. This figure illustrates the key steps involved in the scratch assay, a common experimental technique used to study cell migration in vitro. A confluent cell monolayer is shown in panel (1). A "wound" or cell-free area is then created in the monolayer by dragging a pipette tip across the cell surface, as depicted in panel (2). The initial boundary of this cleared area is shown in panel (3) to mark the starting point of cell migration. Panel (4) shows the cells migrating inward over time to occupy and close the void space created by the scratch, representing the migratory process being studied. This assay allows for the quantitative analysis of cell migration by measuring the rate of gap closure caused by cell motility.

2.2.1.4 Measuring the effect of active plant extracts on Cell Adhesion.

A test was performed using Geltrex™ (Invitrogen), a synthetic ECM analogue, to investigate the influence of the water-soluble extract on the adhesion characteristics of MDA-MB231 and MCF-10A cells to the extracellular matrix (ECM). The procedure involved applying 250 l of undiluted Geltrex™ solution to the surface of 12-well plates, followed by 30 min of solidification at 37 °C. After solidification, the wells were washed for 30 min with blocking solution containing 0.5 percent bovine serum albumin (BSA) in DMEM F12.

Cells were treated with the water-soluble extract at a concentration of 500 µg/mL, as previously described. After a 24-hour treatment period, the cells were washed, reconstituted in serum-free medium, and added to the wells at a uniform concentration of 1×10^5 cells/ml. The cells were treated for 2 h to promote cell adhesion. Following incubation, the adherent cells were washed and fixed for 10 min at room temperature. After another wash, cells were stained with crystal violet for 10 min.

The dye was then extracted from the stained cells using an SDS solution. The absorbance readings were recorded at 550 nm. Control wells devoid of cells were used to establish the reference points. The absorbance levels served as an indicator of the number of cells that adhered to the ECM analogue, thus quantifying the adhesive effect of the water-soluble extract on these cell lines.

2,2.2 Antioxidant assay

The 2,2-diphenyl-1-picrylhydrazyl (DPPH) test was used to evaluate the antioxidant activity of the plant extracts. The colour of this compound changes depending on its oxidation state. DDPH is purple in the stable radical form, whereas the yellow form occurs following electron scavenging. This colour change can be monitored spectrophotometrically and can be used as an indication of the antioxidant activity of a compound that can react with DDPH. The assay was performed according to Blios' method [224]. A standard DPPH solution was prepared by dissolving the DPPH powder in methanol to a final concentration of 500 µM/mL. The extract concentrations were determined based on the IC_{50} values. These concentrations are presented in Table 2.3. A 96-well plate was prepared with a methanol-only blank, a negative control of DDPH

solution, and then various concentrations of extracts in triplicate with the DPPH solution were added to the extracts. The solution was incubated for 30 min in the dark.

The absorbance of the wells was measured at 515 nm using a plate reader to determine the degree of radical neutralisation. The following activity was calculated using the percentage of DPPH scavenging activity:

A515 of tested compound - blank
100% - A515 initial DPPH methanol solution – blank X 100

The concentration required to neutralise 50% of DPPH (EC50) was determined by plotting a graph of the natural logarithm of the percentage of DPPH remaining against the concentration of the sample. If the sample failed to neutralise 50% of the DPPH at a concentration of 500 µg/mL, it was eliminated as a poor antioxidant.

Table 2.3 Concentrations of extract used in the antioxidant assay[ZD1][ZD2]

	Concentration of test compound (µg/mL)				
T. violacea water soluble extract	33	133	200	266	333
T. violacea methanol soluble extract	66	266	400	533	633
C. orbiculate water soluble extract	*40*	*7125*	*200*	*250*	*300*
C. orbiculate methanol soluble extract	33	133	200	266	333
Quercitin	100	200	300	400	

2,2.3 Detection of the molecular components present in the crude extracts

2.1.1.1 Fourier transform infrared (FTR) spectroscopy was used to examine the biological materials.

FTIR spectroscopy for non-destructive biological material investigation is a rapidly growing field of study. FTIR relies on molecular bonds with changing electrical dipole moments caused by atomic displacement and natural vibrations. By scanning at multiple wavelengths and combining and analysing the composite spectra, FTIR spectroscopy can identify the types of molecules present in a mixture of compounds. The fingerprint region (600–1,450 cm-^{1}), along with the amide I and amide II (amide I/II) regions (1,500–1,700 cm^{-1}), are often the most critical spectral areas for the characterisation of biological materials. Stretching vibrations associated with S-H, C-H, N-H, and O-H belongs to the higher-wave region (2,550–3,500 cm1), whereas the bending and carbon skeleton fingerprint vibrations belong to the lower-wave region. The powdered solid samples were ground with IR-transparent potassium bromide (KBr) and compressed to form pellets. The pellet was subsequently placed in an FTIR spectrophotometre (Thermo Scientific Nicolet iS20 FTIR spectrometer) for analysis.

2,2.4 Gas chromatography (GC) in conjunction with mass spectroscopy (MS) analysis

GC analysis was performed on the aqueous extract of *T. violacea* to identify the chemical constituents of the crude extract. GC coupled with mass spectroscopy is the method of choice for identifying compounds in complex plant extracts. The retention durations of the peaks identified in the chromatogram were compared to those of the reference compounds under identical conditions to identify the peaks. Quantitative analyses were performed during this procedure. Positive peak identification was accomplished by determining the molar mass of the substance and obtaining information about its molecular structure using mass spectroscopy [225].

GC-MS analysis of bioactive chemicals from *Tulbaghia* leaf water extracts was carried out on an Agilent Technologies GC system outfitted with the GC-7890A/MS-5975C model (Agilent Technologies, Santa Clara, CA, USA) and stationary phase columns (30 m length, 250 µm diameter, 0.25 µm film thickness) for analysis. An electron ionisation system with high-energy electrons (70 eV) was used for GC-MS spectroscopy detection. Helium gas with a purity of 99.995% was used as the carrier gas at a rate of 1 mL/min. The temperature protocol began with a 3 °C/min increase from

50 to 150 °C, which was maintained for approximately 10 min. Subsequently, the temperature was increased to 300 °C at the rate of 10 °C/min. One microlitre of the prepared 1% extract, diluted in suitable solvents, was injected for analysis. The relative quantity of chemical components in each *T. violacea* extract was quantified as a percentage based on the peak area observed in the chromatogram.

2,2.5 NMR Spectroscopy

In addition to providing information on the structure of a molecule, NMR spectroscopy can be used to detect the content and purity of a sample. NMR is a non-destructive technology compared to Heat analysis and mass spectrometry (MS). Proton NMR (1H NMR) is one of the most frequently used NMR methods. The structure of a molecule can be deduced by observing how the protons in the molecule interact with their surroundings. As a result, NMR spectra can be used to monitor the course of chemical reactions such as those involving synthesis.

Because of the spin property of nuclei with odd masses or atomic numbers, NMR can be used to identify elements such as hydrogen (1H), carbon, and 13C. A magnetic field may be applied to the nuclei, which align themselves in one of two ways: with or against the applied magnetic field. The low- and high-energy states exhibit distinct energy levels. Electromagnetic radiation can trigger a transition from a low-energy to a high-energy state. Free inductive decay (FID) occurs when radiation is stopped and the nuclei relax. Peaks in the NMR spectra were obtained by transforming the FID into a Fourier transform. Different elements have different frequencies, which result in different chemical shifts. NMR spectra can reveal the number of protons represented by a peak, the coupling constant (J-coupling), and the splitting pattern of a peak (often referred to as "neighbours"). Because 1H NMR analyses 1H nuclei, it is imperative to use deuterated solvents. Otherwise, the solvent signal obscured the signal of interest.

The NMR tube was cleaned and approximately 10 mg of the starting material was added. A nonmagnetic nucleus, deuterium, does not give rise to NMR signals when dissolved in a nonmagnetic solvent such as deuterium oxide (D2O). The ideal solvent height for a good spectrum is between 4.5

and 5 centimeters. All substances were dissolved before the samples were shaken gently. NMR tubes were carefully inserted into the spinner. To ensure that all samples were exposed to a uniform magnetic field, the spinner was turned after it was placed in the magnet. To eliminate fingerprints and grimes, 2-propanol and laboratory tissues were used to wipe the exterior of the NMR tube. If the NMR tube is not inserted sufficiently far, the rotor might harm the instrument; hence, it is accompanied by a sample depth gauge. The samples were placed in a different manner on the NMR spectrometer. An autosampler-equipped Varian 600 MHz spectrometer was used. After the NMR test was completed, the spectra were analysed and peaks were assigned.

The NMR spectrum was interpreted using an appropriate application to analyze the spectrum (MestReNova). NMR shifts may be correlated with distinct peaks. To get a sense of the environment in which the protons are present, and examine the chemical changes. The total number of protons was calculated by adding all the peaks. The number of neighbours is represented by the splitting of the proton peaks. The J-coupling method was used to determine the strength of the proton interactions.

2.3 Computational modelling of the interaction between COX -2 and the components of the *T. violacea* water-soluble extract.

Molecular docking is used to determine the optimal alignment of a ligand in relation to a protein. Bioactive constituents of *T. violacea*, identified via GC-MS and NMR analyses, were selected for docking experiments with cyclooxygenase 2 protein (COX-2), which is known for its role in modulating apoptosis and inflammation. Figure 2.5 depicts the three-dimensional X-ray crystallographic structure of COX-2 acquired from the Protein Data Bank (PDB ID: 1PXX).

For the molecular docking assessment (depicted in Figure 2.6), Schrodinger software suite 2020 and PyMol molecular graphics system 2.4. The target protein COX-2 and selected bioactive compounds from *T. violacea* were prepared in accordance with the established protein and ligand preparation guidelines. Throughout the docking procedure, various configurations of the ligand were generated and a final refinement of the ligand position was performed. The docking score for each tested

bioactive molecule, indicative of the effectiveness of its interaction with the target protein, was computed for the most favourable pose.

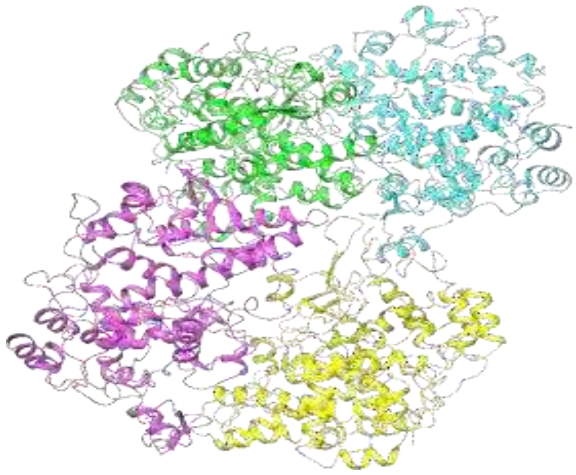

Figure 2.6 The target cyclooxygenase-2 (COX-2) enzyme. This figure depicts the three-dimensional structure of the COX-2 enzyme obtained from the Protein Data Bank (www.rcsb.org, PDB ID: 1PXX). COX-2 is a key enzyme involved in the inflammatory response and a common target for anti-inflammatory drugs. The ribbon diagram shows the overall tertiary structure of the enzyme, with α-helices represented in purple and β-sheets in yellow. This molecular model of COX-2 was used for computational docking studies to analyse the binding interactions between the enzyme and bioactive compounds identified in *T. violacea* extracts. Understanding these interactions is crucial to evaluate the potential anti-inflammatory and anticancer effects of plant extracts.

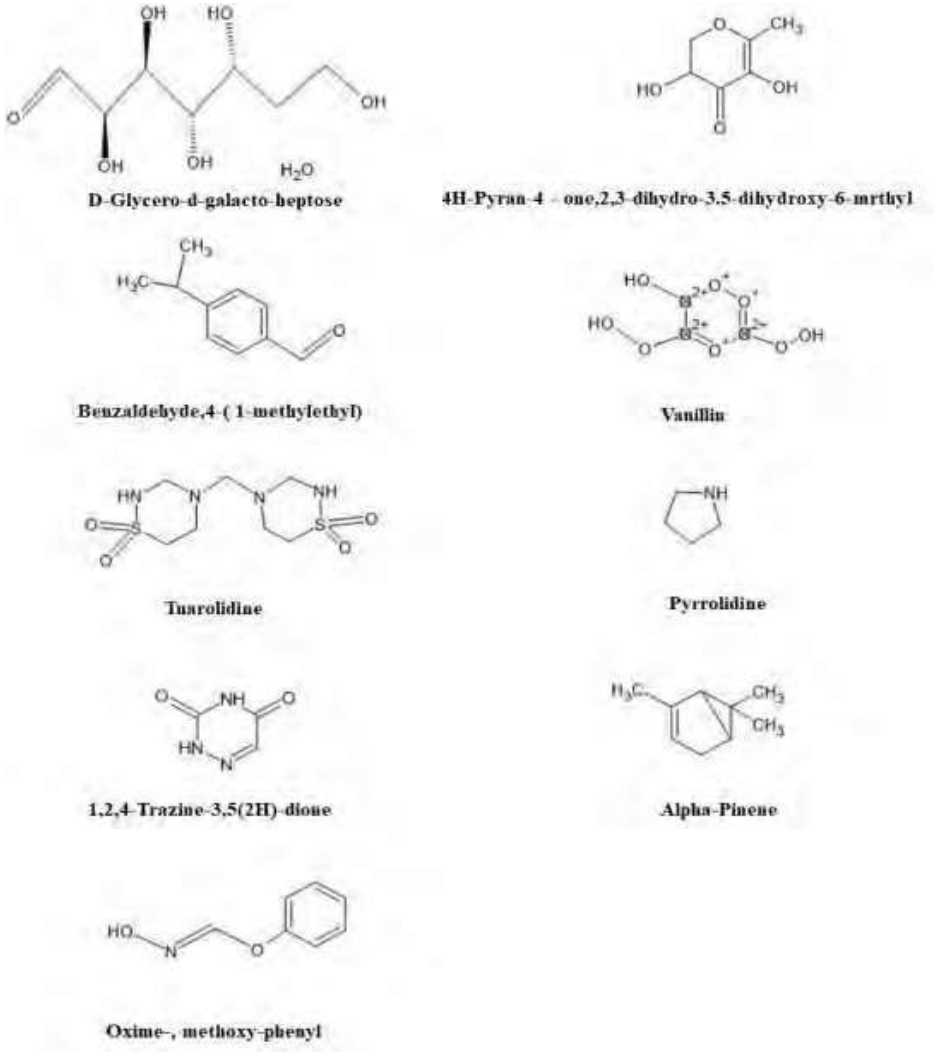

Figure 2.7 The structure of the anticancer bioactive compounds identified from *T. violacea* The structure of the anticancer bioactive compounds identified from *T. violacea* was used for molecular docking analysis, which depicts the chemical structures of various bioactive compounds identified from *T. violacea* through analytical techniques such as gas chromatography-mass spectrometry (GC-MS) and nuclear magnetic resonance (NMR) spectroscopy. These compounds were subsequently utilised for in silico molecular docking studies to evaluate their potential interactions and binding affinities with target proteins implicated in cancer pathways, such as cyclooxygenase-2 (COX-2). The specific compounds included D-Glycero-d-galacto-heptose, 4H-Pyran-4-one,2,3-dihydro-3,5-dihydroxy-6-methyl-, benzaldehyde,4-(1-methylethyl)-, Vanillin, Thioridine, Pyridoline, 1,2,4-Triazine-3,5(2H)-dione, Alpha-Pinene, and Oxime-, and methoxy-phenyl-. Chemical structures were obtained from the PubChem database (www.pubchem.ncbi.nlm.nih.gov), a public repository of chemical information maintained by the National Institutes of Health (NIH).

2.4 Effects of the extracts on protein expression.

2,4.1 Protein Extraction Protocol.

MCF-10A and MDA-MB-231 cells were grown in culture dishes containing standard media. One

flask was subjected to the IC_{50} concentration of the water-soluble extract (200 µg/ml), whereas the other was left untreated as a control. The medium was removed after treatment and the cells were rinsed with ice-cold PBS. A cold plastic cell scraper was used to gently separate the cells. The medium was removed after treatment and the cells were rinsed with ice-cold PBS. A cool plastic cell scraper was used to gently separate the cells.

The scraped material was centrifuged at 2000 g for 5-7 minutes at 4 °C and the supernatant was discarded. The cell pellet was rinsed with ice-cold PBS before lysis using ice-cold lysis buffer containing protease inhibitors. The material was sonicated using 10 pulses from an MSE ultrasonic disintegrator for efficient cell lysis (Soniprep 150 analogue).

The material was sonicated and incubated in microfuge tubes for 30 min to achieve complete cell lysis. This was followed by 20-minute centrifugation at 16000 g at 4 °C. The supernatant, which included the cell lysate, was carefully transferred to a separate tube and placed on ice for further analysis, and the pellet was discarded. The material was sonicated and incubated in microfuge tubes for 30 min to achieve complete lysis. This was followed by 20-minute centrifugation at 16000 g at 4 °C. The supernatant, which included the cell lysate, was carefully transferred to a separate tube and placed on ice for further analysis, while the pellet was discarded.

2,4.2 Quantification methods

Because all downstream analyses are dependent on accurate and repeatable quantification of crude protein extracts, quantification of crude protein isolates is an important step in the proteomics workflow. In this study, multiple protein quantification methods were used. Two standard solutions of bovine serum albumin at concentrations of 1 mg/mL and 2 mg/mL were prepared and assessed over a three-day period using the techniques described below.

2,4.3 Bradford assay

The Bradford assay, developed in 1976, is based on the interaction between the Coomassie Brilliant

Blue G250 dye and proteins. Under acidic conditions, binding of this dye to proteins causes a colour change from brown to red. A spectrophotometre was used to quantify the change to blue light at a wavelength of 595 nm. There is a direct correlation between the intensity of the blue colour and the amount of protein present, allowing for the quantification of the protein concentration in a sample. The assay is also moderately resistant to salts and chaotropic agents but is affected by many common sample buffer detergents, such as CHAPS and SDS.

To prepare the standards for the assay, a standard Bovine Serum Albumin (BSA) solution (Bio-Rad) with an initial concentration of 2 mg/mL was used. This stock solution (2 mg/mL) was further diluted 1:1 to obtain a 1 mg/mL stock solution. Six standards with known concentrations were prepared using 1 mg/mL stock solution, encompassing the anticipated concentration range of the samples. The standards used in this study ranged from 100 to 1 mg/ml, as outlined in Table 2.4.

Table 2.4 Standards for the Bradford assay

	BSA stock	PBS buffer
0ug/ul (reference/blank)	0ul	100ul
100ug/ml	10ul	90ul
200ug/ml	20ul	80ul
500ug/ml	50ul	50ul
750ug/ml	75ul	25ul
1mg/ml	100ul	0ul

Equal amounts of Bradford reagent, protein samples, and buffers (mixed at a 1:1 ratio) were combined and allowed to rest for 10 min at room temperature. Absorbance was measured at 595 nm for both the reference standards and test samples using a Nanodrop spectrophotometre. The spectrophotometer's software generated a standard curve,
which was used to calculate the protein concentrations in the samples by comparing their absorbance values with the curve.

2,4.4 Qubit assay

The Fluorescent Qubit® Protein Assay Kit (Thermo Fisher Scientific, Waltham, Massachusetts, USA) was used as an alternative technique for protein quantification. This procedure was performed according to the manufacturer's instructions. To prepare the Qubit® working solution, the Qubit® protein reagent was mixed with Qubit® protein buffer at a 1:200 ratio. To construct the standard curve, 10 µL of the Qubit® standards included in the kit was mixed with 190 µL of the working solution. The tubes were vortexed for 3 seconds and incubated at room temperature for 15 minutes. The samples were then placed into 500-µl tubes, and their fluorescence was measured using a Qubit® 2.0 Fluorometer (ThermoFisher Scientific, Waltham, Massachusetts, USA) employing the standard protein program. A standard curve was obtained from the Qubit® fluorimeter readings. The samples were processed similarly, with 10 µL of the sample combined with 190 µL of the working solution and incubated for 15 min before fluorescence measurement on the Qubit® fluorimeter. A standard curve was used to calculate the sample concentration, which was then modified to account for a 20-fold dilution factor.

2,4.5 SDS-PAGE Analysis

The integrity of the extracted proteins was confirmed by sodium dodecyl sulfate-polyacrylamide gel electrophoresis (SDS-PAGE). The internal surfaces of the gel plates were cleaned with ethanol and, in some cases, nitric acid, to ensure that there was no grease or dirt on the plates. The plates were assembled using a gel-casting cassette. The separation and stacking gels were prepared as shown in table below. (Table 2.5).

Table 2.5 Stacking and separating gel solutions

	12 percent separating gel	6% separating gel
Tris-cl buffer at pH 6.8		2.52
pH8.8 tris-HCl 1.875M		
Water	6.7ml	5.32ml
30% Acrylamide (stock)	8ml	2ml
10%SDS	0.2 ml	0.1ml
Persulfate of ammonium (10 percent)	0.1ml	50ul
TEMED	10ul	5ul
Total volume	20 ml	10ml

The separating gel was dispensed between the glass plates inside the casting cassette. This cassette was then positioned on a flat surface and deionised water was gently added to the gel to ensure evenness. Once the gel solidified, water on top of the separating gel was drained. Following the protocol outlined in Table 2.4, the stacking gel was concocted and applied to the cured resolving gel. A 10-well comb was used to allow the gel to solidify. After gelation, the comb was extracted, the gel was retrieved from the cassette, and a gel apparatus was set up. The electrophoresis buffer, which included Tris-glycine SDS, was added to both the upper and lower reservoirs.

2.5 µg of protein was combined with 5 µl of 5x loading buffer and heated at 95-100 °C for 5 min to unfold the proteins before being immediately frozen on ice. These preparations were carefully loaded onto an SDS-PAGE gel and electrophoresis was performed at 180 volts for approximately 40 min. A protein ladder for the molecular weight reference was placed in the first well. After electrophoresis, the gel was carefully removed and the stacking portion was detached from the resolving section. The corners of the gel were trimmed for orientation. The gel was fixed in a solution of methanol and acetic acid on a soft rocking platform for 4–8 h. It was then immersed in Coomassie blue stain and gently shaken for at least 2 h at ambient temperature. destaining, the gels were captured using a gel

documentation system and preserved in 20% glycerol water solution.

2,4.6 Proteome Profiler Arrays

To investigate cellular responses to environmental changes, it is crucial to analyse the phosphorylation patterns of kinases and proteins. The Human Phospho-RTK Array offers a rapid, sensitive, and cost-effective approach for detecting the relative phosphorylation levels of 43 kinase phosphorylation sites and two total proteins.

Proteome profiler array analysis was performed using three biological replicates for each condition (treated MCF-10A, untreated MCF-10A, treated MDA-MB-231, and untreated MDA-MB-231). The signal intensity for each protein was quantified using the Bio-Rad analysis software, and the mean signal intensity across the three replicates was calculated for each protein in each condition. To determine statistically significant differences in protein expression between the treated and untreated groups, a two-tailed unpaired Student's t-test was performed for each protein, comparing the mean signal intensities of the treated and untreated samples. Statistical significance was set at $P < 0.05$. Initially, Array Buffer 1 (2.0 mL) was added to each well as a blocking buffer. The membranes, labelled with numbers facing up, were incubated for 1 h on an oscillating platform shaker.

For each sample, up to 300 µg dilution was performed to reach a final volume of 2 mL using Array Buffer 1. After the blocking step, the buffer was removed and replaced with diluted samples. This step was followed by an overnight incubation with agitation. The next day, each membrane was washed triple 10-minute wash with 1X wash buffer in individual plastic containers. The multi-well dish was cleaned and dried for future use.

For detection, the anti-phospho-tyrosine-HRP antibody was diluted in 1X Array Buffer 2 according to the manufacturer’s instructions. After washing, the membranes were returned to a multi-well dish and 2 mL of attenuated detection buffer was added to each specimen. Subsequently, they were incubated for 2 h in antibody recognition solution at ambient temperature on an oscillating platform.

Next, each membrane was washed thrice in 1X Wash Buffer for ten minutes. A chemi reagent, that is, a mixture of chemi reagents A and B (2 ml each), was prepared. The post-wash membranes were positioned on the lower sheet of the plastic sleeve, and 1 ml of the mixed reagent was applied to each membrane. The plastic sleeve was then sealed and excess reagents and air bubbles were removed.

The membranes were then covered with a clinging film, ensuring smoothness, and placed in a film cassette shielded from light. They underwent examination using the ChemiDoc™ MP imaging system (Bio-Rad 170-8280), with photographs documented over a 10-minute period at intervals of 150 s. Signal identification was achieved by overlaying the array image with a transparency overlay aligned with the reference spots. The density (pixels per mm^2) was assessed using Bio-Rad analysis software to compare expression variations between treated and untreated cells as well as between malignant and normal cells. This density was equal to the protein expression level, and a plot of protein expression changes was created.

2.5 The effect of active purified fractions on miRNA transcription and gene expression

2.5.1.1 mRNA extraction.

Total RNA was isolated using the RNeasy Mini Kit (QIAGEN ID 74004). Cells grown in a tissue culture flask under normal conditions were treated for 48 h with 200 µg water-soluble *T. violacea* extract. Following treatment, the cells were collected and counted. The formed cell sediment was resuspended in the RLT buffer and transferred to a microcentrifuge tube. The kit was set up to process up to 1×10^7 cells per extraction or spin column.

To homogenise the cells, they were vigorously agitated in the RLT buffer. Subsequently, ethanol was added to the lysate to facilitate adherence of RNA to the RNeasy membrane. The mixture was passed through an RNeasy Mini Spin column. The column was placed in a collecting tube and centrifuged at 12000 x g for 1 min. The filtrate was discarded, and the column was cleaned using a cleaning buffer. This spin-and-discard operation was performed twice to ensure complete washing.

Following the last washing step, ethanol was introduced into the column and centrifuged to facilitate the passage. The column was subsequently left to air-dry before being transferred to a fresh collection tube. Subsequently, an elution buffer was added to the spin column, which was then spun at 12,000 × g for 1 min to aid in RNA elution. The collected eluate, which included pure RNA, was stored at -80 °C for later use.

2.6 Next generation sequencing

NGS was performed using Inqaba Biotec. RNA fragments were analysed using a bioanalyzer. A sequencing library was prepared using a MiSeq RNA-0 rRNA reduction library kit (Illumina). DNA sequencing was conducted using the NextSeq 300 system, employing paired-end sequencing technology. This process was performed at a sequencing depth of 10 million bases, and spanned 300 cycles. This resulted in high-quality sequence data suitable for further analysis. Following sequencing, the raw sequencing data were analysed using the Galaxy platform (Galaxy Europe (galaxyproject.eu)) with a pipeline consisting of the following tools: Trimmomatic was used to trim the reads, and FastQC was used to generate the quality control reports. HiSAT2 was used to align the reads. Differential gene expression was analysed using the Limma package (limma-voom). The HG38 Huab genome was used as the reference genome, and reference mapping was performed using Bowtie 2. Vocano plots were created using GraphPad Prism and PANTHER was used for gene ontology analysis. Pathway analysis was performed using PANTHER, Ingenuity Pathway Analysis, and Reactome.

2.7 Statistical Analysis

All experiments were performed in triplicate, with three technical replicates per biological replicate unless otherwise stated. Data are presented as mean ± standard deviation (SD). Statistical analyses were conducted using the GraphPad Prism 9 software (GraphPad Software, San Diego, CA, USA).

For comparisons between two groups, unpaired two-tailed Student's t-test was used. When comparing three or more groups, one-way analysis of variance (ANOVA) was performed, followed by Tukey's post hoc test for multiple pairwise comparisons.

To determine IC50 values, non-linear regression analysis was conducted using the log(inhibitor) vs.

response-variable slope (four parameters) function in GraphPad Prism. This analysis generated a sigmoidal dose-response curve by plotting the logarithm of the inhibitor concentration against the response (cell viability).

For all statistical tests, a p-value less than 0.05 was considered statistically significant. The following notation was used to indicate the level of significance: * $p < 0.05$, ** $p < 0.01$, *** $p < 0.001$, and **** $p < 0.0001$.

Chapter 3 Results

3.1 Introduction

In traditional Southern African medicine, water infusions of *T. violacea* (wild garlic) and the succulent shrub *C. orbiculata* have been used to treat various ailments including cancer. Many previous studies using these two plants have indicated that they may have verifiable effects on tumour cells. Most drugs currently used to treat cancer are phytochemical derivatives. Many of these studies began with the examination of raw extracts derived from plants, which are commonly used in traditional herbal medicine. Once these extracts were confirmed to have anticancer activity, they were purified to identify their active compounds. Synthetic derivatives of these compounds can then be created with lower toxicity and better solubility, which can be used in clinical trials. The first step was to scientifically validate the anticancer activity of the plant extracts.

This involves the ropriate preparation of plant extracts. For example, although prior research has indicated the potential anti-cancer properties of *T. violacea* extracts, these studies predominantly utilised organic solvent extraction techniques, which differ from the traditional practice of preparing water-based infusions of the plant. Once an extract is prepared, it must be tested to establish whether it is cytotoxic to cancer cells. This initial step prevents further effort from being wasted on extracts that show no activity. Ideally, these extracts should have little or no cytotoxicity in normal cells. This suggests that the extract is likely to target cancer-related pathways. It is crucial to identify the specific pathways affected by these extracts by testing their ability to target cancer-associated processes. This encompasses resistance to apoptosis and increased proliferation, migration, and invasion abilities, along with the ability to bypass the cell cycle checkpoints. Finally, it was important to identify the molecules and compounds present in the extracts. This will allow for these individual compounds to be tested in the future.

The plant samples, sourced from a nursery specializing in African native plants, were initially transported to the CE Moss Herbarium at the University of the Witwatersrand's School of Animal,

Plant and environmental science. At this location, our specimens were conclusively identified as *T. violacea* and C. orbiculata.

3,1.1 The cytotoxic effects of *T. violacea* and *C. orbiculata leaf* extract on normal and TNBC cancer cell lines

Despite the traditional medicinal use of *T. violacea* and *C. orbiculata* for the treatment of various ailments, including cancer, there have been limited scientific investigations to substantiate these applications. This study focused on preparing water-soluble and methanol-soluble extracts from the leaves of both plants to test their efficacy in killing cancer cells, particularly triple-negative breast cancer cells. This also involved establishing IC_{50} values for these crude extracts, which would allow the use of relevant concentrations in further tests of the anticancer properties of these extracts.

3.2 Determination of the IC_{50} values for each of the crude extracts on MDA MB 231 cells

It is critical to identify the exact concentrations of a chemical that should be employed in a specific model in any study that analyzes the biological activity of an agent. To determine the anticancer potential of these plant extracts, it is crucial to determine the concentration at which these compounds are lethal to cells representing both cancerous and normal tissues. This would allow further experiments to be performed, where the cells were treated with concentrations slightly below the IC_{50} value, thereby eliciting an effect without causing cell death at such a level as to obscure any observations on the nature of the cells' reaction to treatment with these compounds.

3.3 Determination of the IC_{50} through Real Time Cell Analysis

Real-time and continuous monitoring enables label-free evaluation of cell proliferation, viability, and cytotoxicity, exposing the physiological state of the cells, while avoiding the costly chemicals used in traditional cell analysis. The dynamic management of cell status by the xCELLigence system during the course of an experiment provides constant information regarding cell growth, morphological changes, and cell death. Additionally, the xCELLigence system can produce time-dependent

physiological IC_{50} values, which are more revealing than the single EC_{50} endpoints used in traditional toxicity testing.

To conduct these assays, it is essential to initially observe the growth and proliferation of the cell line under standard growth conditions and with varying quantities of initial cells. Determining the lethal concentration of plant extracts is essential for accurately seeding the correct number of cells in plates for experiments. The aim of these experiments was to examine the effects of the plant extracts on cellular growth and proliferation. Furthermore, these data are essential for evaluating the cytotoxic effects of the extracts and determining their IC_{50} values. This is because seeding plates with too many cells results in a rapid increase in CI values, followed by a sharp decrease as nutrients and space become exhausted. This leads to a very short time at which the effects of the extract can be observed. There were too few cells, and the CI remained too low to observe the beneficial effects of the extracts on the cells. Figure 3.1 shows the results of the cell titration assay. It can be clearly seen that the best concentration for seeding the plates was 20000 cells/ml or 4000 cells per well on the e-plate. Regardless of the initial seeding density, the MDA-MB-231 cells exhibited rapid growth in the first 5 h after seeding. Depending on the number of cells used to seed the plate, they reached a plateau and remained constant number of cells. The highest concentration of cells (40000 cells/ml) grew rapidly past a CI of 1, making it unsuitable for growth-related experiments (Figure 3.1).

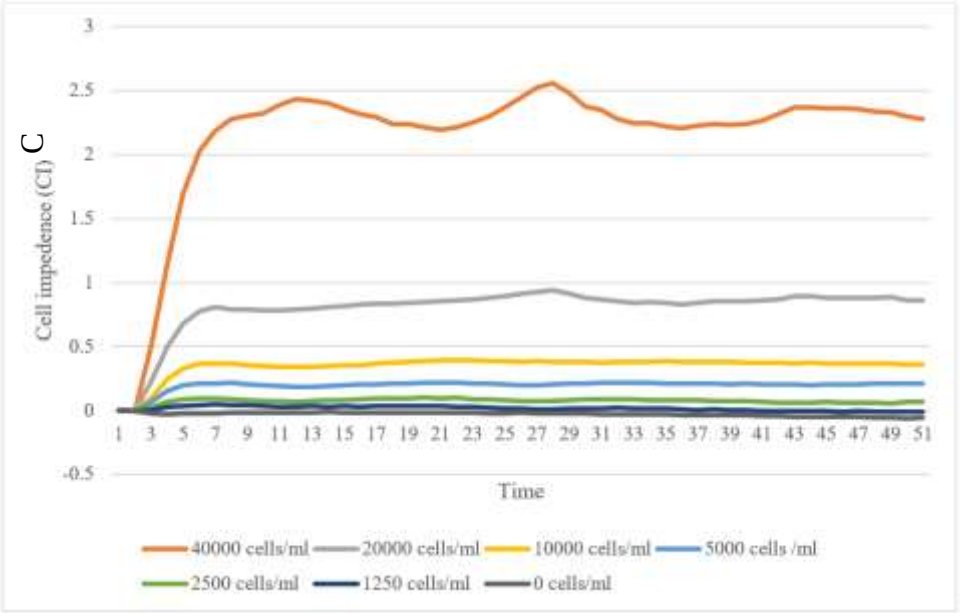

Figure 3.1 shows a cell number titration curve used to determine the optimal seeding density for MDA-MB-231 cells using the xCELLigence Real-Time Cell Analysis (RTCA) system. shows a cell number titration curve used to determine the optimal seeding density for MDA-MB-231 cells using the xCELLigence Real-Time Cell Analysis (RTCA) system. The graph plots cell impedance, which correlates with cell number and viability, over time for different initial seeding densities ranging from 0 to 40,000 cells/mL. The curves demonstrate that seeding too few cells (≤2,500 cells/mL) results in low impedance values, making it difficult to observe the proliferation effects. In contrast, seeding too many cells (40,000 cells/mL) leads to rapid growth, followed by a sharp decline owing to overcrowding and depletion of nutrients. Based on this titration, an initial seeding density of 20,000 cells/mL (4,000 cells per well) was chosen as the optimal, exhibiting a robust proliferation pattern suitable for monitoring the effects of the test compounds on cell growth using the RTCA system.

T. violacea and *C. orbicula* raw extracts were tested for cytotoxicity in both triple-negative breast cancer (TNBC) cell lines (MDA-MB 231) and a normal breast cell line (MCF10A) at various dilutions. Observations were documented for 72 h after treatment. IC_{50} values, denoting the concentration required to reduce cell growth by 50%, were calculated using GraphPad Prism software (GraphPad Software, San Diego, CA, USA). The results are presented in Table 3.1. The chemotherapeutic drug 5-FU was used as the positive control. The experiment found that *Water-soluble T. violacea* 1EAF extracts were more cytotoxic than the methanol-derived extracts. This agent is believed to initiate caspase-6 activation and induce cancer cell death. 5-FU also generates mitochondrial ROS in the p53-dependent signaling pathway [226, 227]. 5-FU may cause changes in cell cycle regulation, resulting in changes in the G1 cyclin expression [228, 229]. Because of its propensity to trigger apoptosis in various methods, it has been used as a cancer therapeutic agent. Because of its propensity to trigger apoptosis in various methods, it has been used as a cancer

therapeutic agent [230].

Figure 3.2A illustrates the growth curve of MDA-MN 231 cells following treatment with varying concentrations of the water-soluble *T. violacea* extract. This figure also includes the growth curve for cells treated with the positive control, which was 25 µM of the chemotherapy drug 5FU, as well as a growth control that only contained media for comparison. The intermediate concentration of the extract was observed to have effects similar to the positive 5FU control. The highest extract concentration completely prevented cell growth and proliferation after a small initial increase. It then appears to rapidly kill the cells. The logarithmic concentration function was plotted using these data (Figure 3.2B). The IC50 value of the *water-soluble extract of T. violacea* was determined to be 395 µg/mL using this method.

Figure 3.3A illustrates the growth curve of MDA-MN 231 cells subjected with different concentrations of the methanol-soluble *T. violacea* extract. This figure also includes the growth curve for cells treated with 25µM µM 5FU as a positive control, and a growth control comprising DMSO vehicle control and media. DMSO had an initial inhibitory effect on cell growth. The cells appeared to recover after 24 h of treatment. The lowest and intermediate concentrations of the extract had similar effects on cells, both of which were much lower than the effect observed after treatment with 5FU. Figure 3.3A presents the growth patterns of MDA-MN 231 cells following treatment with varying concentrations of methanol-soluble *T. violacea* extract. Additionally, the figure shows comparative growth curves for cells treated with 25µM 5FU as a positive control, along with a growth control that included a DMSO vehicle control mixed with media. This figure also emphasises the initial growth-inhibitory effect of DMSO on the cells, which was utilised in the analysis.

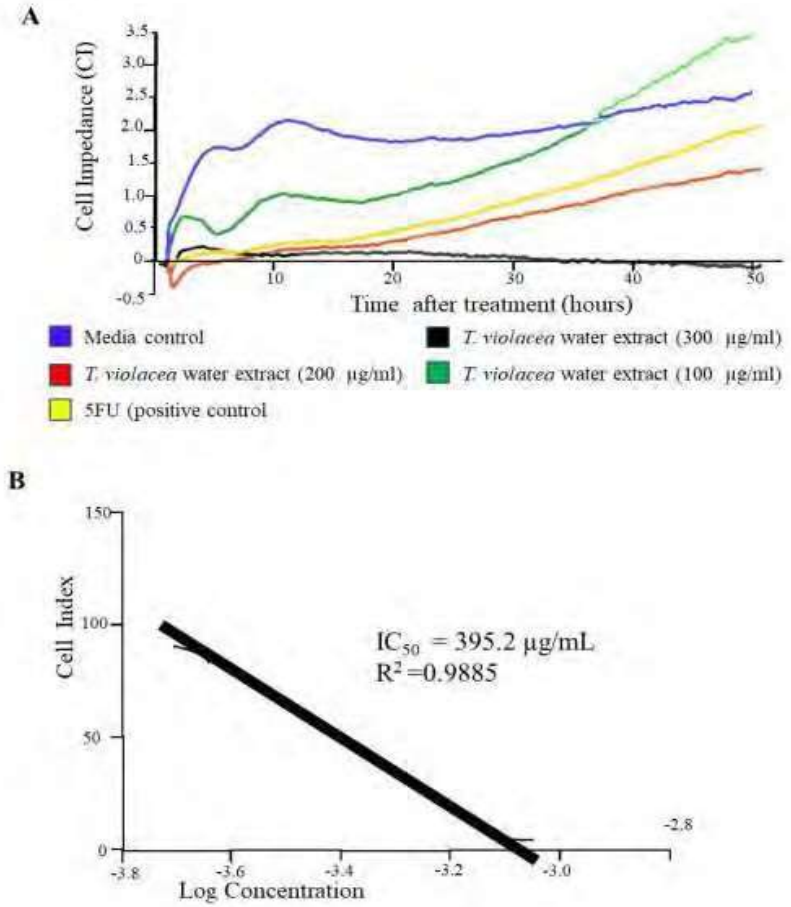

Figure 3.2 shows the determination of the IC50 (half-maximal inhibitory concentration) of the water-soluble extract of *Tulbaghia violacea* on the triple-negative breast cancer MDA-MB-231 cell line using the real-time cell analysis (RTCA) assay. Panel A displays the growth curves of MDA-MB-231 cells treated with various concentrations of the *T. violacea* water extract over time. The growth curves included a media-only control to represent untreated cell growth as well as a positive control treated with the chemotherapeutic drug 5-fluorouracil (5FU) at a sub-lethal concentration. Panel B illustrates how RTCA software determines the IC50 value by plotting the cell index (CI), which correlates with cell viability, as a function of the logarithm of the extract concentration. The media controls were used to represent 100% cell viability. By fitting a dose-response curve to these data, the IC50 concentration that inhibits 50% of the cell growth can be calculated.

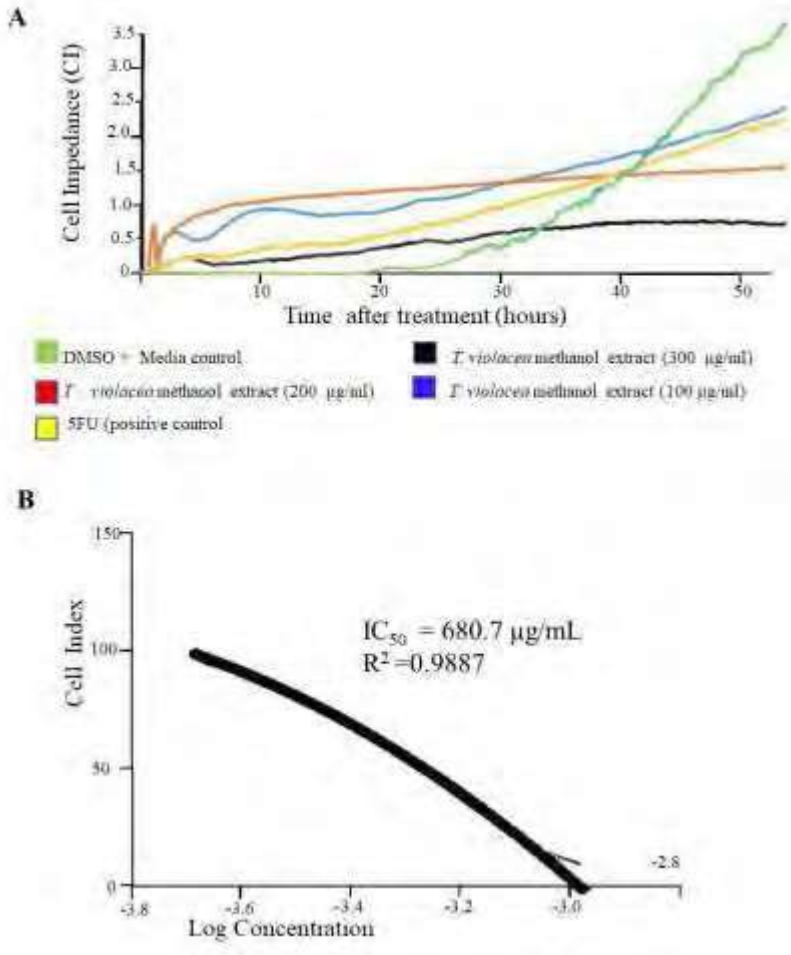

Figure 3.3 shows the determination of the IC50 (half-maximal inhibitory concentration) for the methanol-soluble extract of *Tulbaghia violacea* on the triple-negative breast cancer MDA-MB-231 cell line using the real-time cell analysis (RTCA) assay. Panel A displays the growth curves of MDA-MB-231 cells treated with various concentrations of the *T. violacea* methanol extract over time. The growth curves included a DMSO-only control to represent the vehicle used to solubilise the extract as well as a positive control treated with the chemotherapeutic drug 5-fluorouracil (5FU) at a sub-lethal concentration. Panel B illustrates how the RTCA software determines the IC50 value by plotting the cell index (CI), which correlates with cell viability, as a function of the logarithm of the extract concentration. A DMSO control was used to represent 100% cell viability. By fitting a dose-response curve to this data, the IC50 concentration that inhibits 50% of cell growth can be calculated.

Figure 3.4A Figure 3.4A depicts the growth curve of MDA-MB 231 cells treated with various doses of the water-soluble *C. orbiculata* extract. 3.4A depicts the growth curve of MDA-MB 231 cells treated with various doses of the water-soluble *C. orbiculata* extract. Additionally, this figure includes the growth curve for cells subjected to the positive control, 25µM 5FU, as well as a growth control composed only of media. The medium and lower concentrations of the extract had a lesser influence on cell proliferation than the positive control. The highest concentration had the most significant

effect on the cell growth. Nonetheless, the extract appeared to lack strong cytotoxic effects. A decline in cell number, noticeable at 50 h post-treatment, was evident in all groups. These data were used to construct a logarithmic concentration curve (Figure 3.4B). Based on these observations of cell growth, the IC_{50} value for the *C. orbiculate* water-soluble extract was determined to be 680 µg/ml.

The growth curve of MDA-MB 231 cells treated with varied concentrations of the methanol-soluble *C. orbiculata* extract is shown in Figure 3.5A. The figure also includes the growth curve for cells exposed to the positive control, 25µM 5FU, and a growth control featuring media with Dimethyl Sulfoxide (DMSO) as a vehicle control. In this experiment, as shown in Figure 3.5A, the DMSO control demonstrated an effect similar to that observed in the experiment illustrated in Figure 3.3, namely, a marked suppression of cell growth followed by recuperation followed by swift proliferation around 20 h post-treatment. This DMSO effect seems potent enough to obscure any milder effects exerted by the *C. orbiculata* extract, as the higher concentration appears to exert a reduced inhibitory influence on cell growth, especially in the initial phases after treatment. This was further substantiated by the logarithmic concentration plot (Figure 3.5B), which indicated a linear correlation between cell viability and extract concentration. The exceedingly high Value of Linear Extrapolation (VLE) calculated for IC_{50} appears to validate the absence of any significant cytotoxic effect.

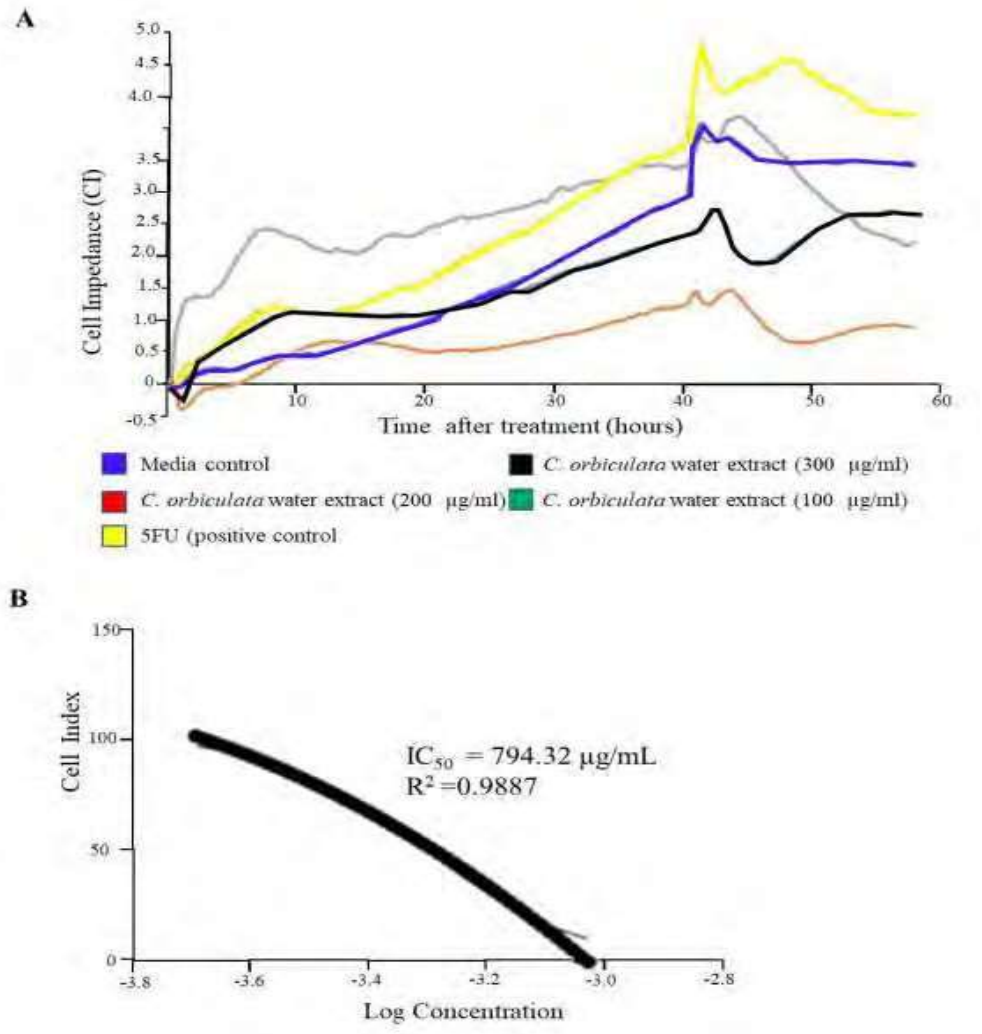

Figure 3.4 shows the determination of the IC50 (half-maximal inhibitory concentration) of the water-soluble extract of Crassula orbiculata on the triple-negative breast cancer MDA-MB-231 cell line using the real-time cell analysis (RTCA) assay. Panel A displays the growth curves over time for various concentrations of the C. orbiculata water extract (200, 300, and 100 µg/mL), as well as a media control and positive control treated with the chemotherapeutic drug 5-fluorouracil (5FU) at a sub-lethal concentration. The y-axis represents the cell index, which correlates with cell viability and proliferation, whereas the x-axis shows the time after treatment in hours. Panel B illustrates how the RTCA software calculates the IC50 value by plotting the cell index (CI), a measure of cell viability, against the logarithm of the extract concentration. The media control is used to represent 100% cell viability. By fitting a dose-response curve to these data, the concentration of the extract required to inhibit 50% of cell growth (IC50) was determined.

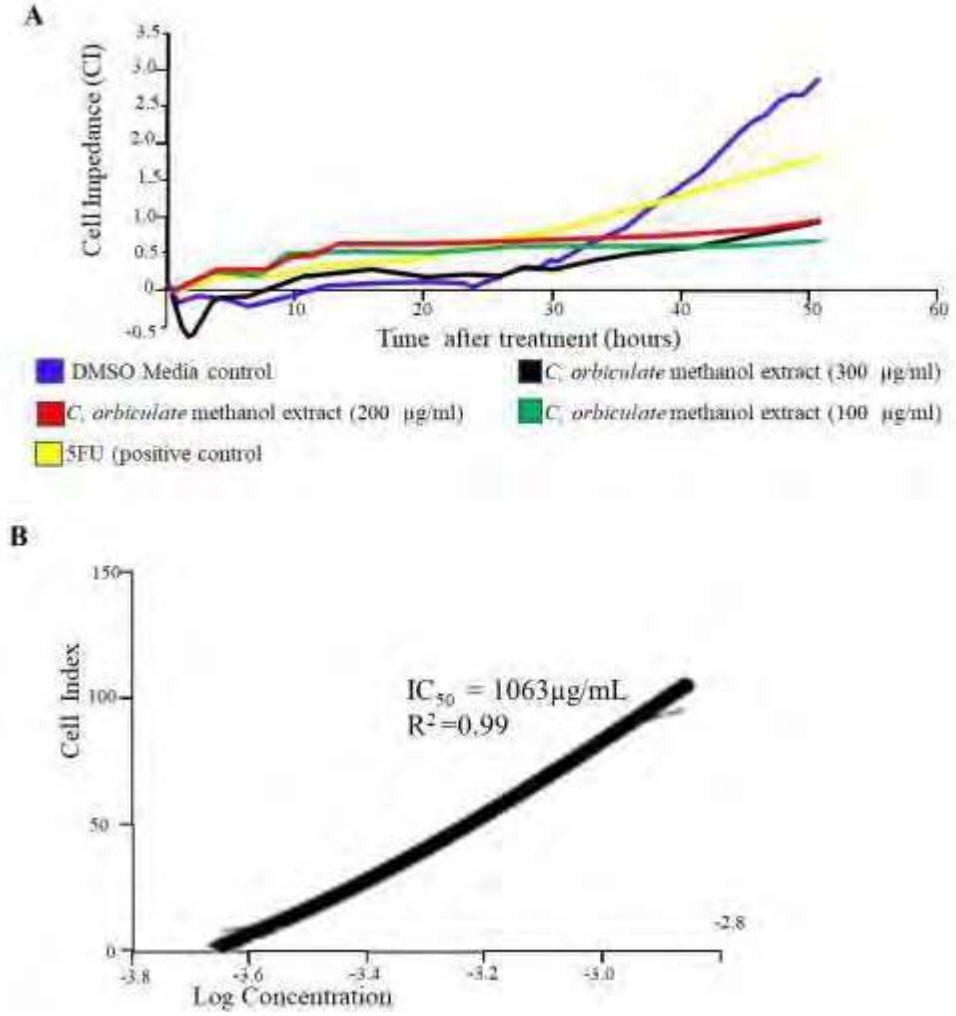

Figure 3.5 shows the determination of the IC50 (half-maximal inhibitory concentration) for the methanol-soluble extract of *C. orbiculata* in the triple-negative breast cancer MDA-MB-231 cell line using the real-time cell analysis (RTCA) assay. Panel A displays the growth curves over time for MDA-MB-231 cells treated with various concentrations of the *C. orbiculata* methanol extract (300 µg/mL and 100 µg/mL), as well as a media control and a positive control treated with the chemotherapeutic drug 5-fluorouracil (5FU) at a sub-lethal level. The y-axis represents the cell index, which correlates with cell viability and proliferation, while the x-axis shows the time after treatment in hours. Panel B illustrates how RTCA software determines the IC50 value by plotting the cell index (CI), a measure of cell viability, against the logarithm of the extract concentration. The media control is used to represent 100% cell viability. By fitting a dose-response curve to this data, the IC50 concentration that inhibits 50% of cell growth can be calculated.

3.4 Determination of the IC_{50} through the use of alamar blue cytotoxicity assays

The reduction in alamar blue, an indicator of metabolic cell function, was measured using fluorescence and calorimetry in drug sensitivity assays. The Alamar Blue assay kit is ideal for this purpose because it is simple, reproducible, and economical. Figures 3.6–3.9 show the results obtained

for the Alamar blue cytotoxicity assays conducted with each of the extracts. To achieve this, cells were initially exposed to various concentrations of the extract, followed by treatment with Alamar Blue for a duration of two hours. Living cells can reduce the dye through metabolic reactions, leading to changes in colour and fluorescence of the dye. These changes were measured using a plate reader, and the percentage of viable cells was calculated by comparing them to an untreated control.

As shown in Figure 3.6, the IC_{50} value for the *water-soluble extract of T. violacea* was 350 g/ml, and the linear relationship between concentration and viability was represented by an R-squared value of 0/9572. This *T. violacea* water extract extracted from leaves had the greatest cytotoxicity against TNBC cancer cell lines, much stronger than the activity observed in the *T. violacea* methanol extract (820 µg/ml) (Figure 3.7). This extract demonstrated a linear relationship between concentration and viability, implying that despite its poor activity, it still had a concentration-dependent effect on cell viability.

The IC50 value of the *C. orbiculata* water extract was determined to be 880 µg/ml, as shown in Figure 3.8. This value is notably higher than the IC_{50} for the *methanol extract of C. orbiculata (530 µg/mL*), as indicated in Figure 3.9. The linear relationship between concentration and cell viability was not as definite for either of these extracts, with both R squared values being less than 0.95.

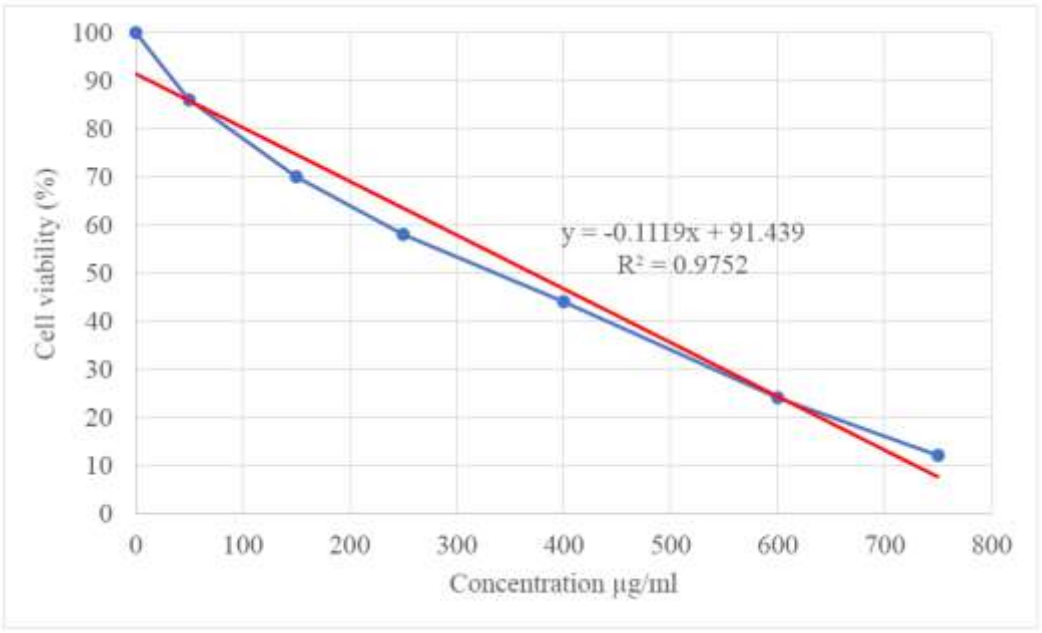

Figure 3.6 Figure 3.6 shows the determination of the IC50 (half-maximal inhibitory concentration) value for the water extract of *T. violacea* against the MDA-MB231 triple-negative breast cancer cell line using an Alamar blue cytotoxicity assay. The graph plots the percentage of viable cells remaining after treatment with varying concentrations of the extract. The x-axis represents the concentration of the extract in µg/ml, while the y-axis shows the percentage of cell viability compared to an untreated control. The data points are fitted with a linear regression line. The IC50 value, which is the concentration required to reduce cell viability by 50%, can be determined from the intersection point of the regression line with 50% viability on the y-axis. As indicated on the graph, the IC50 value for the *T. violacea* water extract against MDA-MB231 cells is approximately 350 µg/ml, where only 50% of the cells remain viable after treatment.

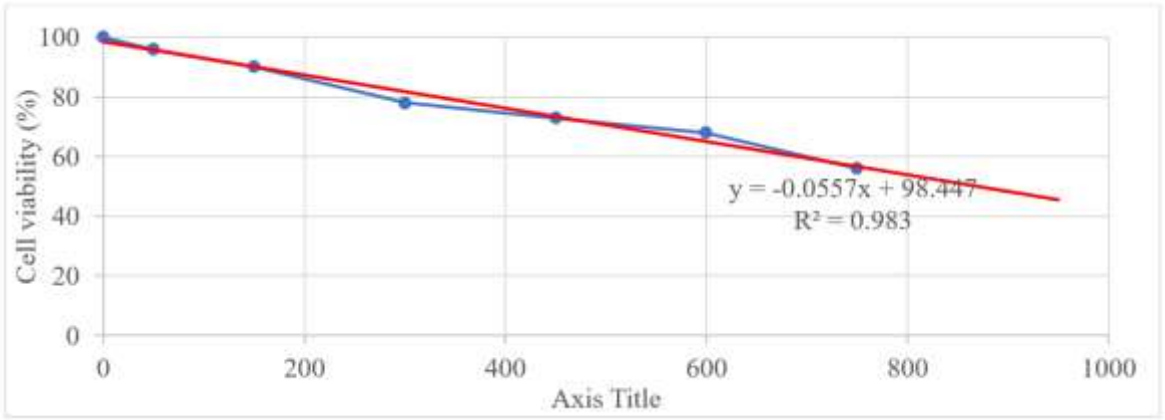

Figure 3.7 depicts the determination of the IC50 (half-maximal inhibitory concentration) value for the methanol extract of *T. violacea* against the MDA-MB231 triple-negative breast cancer cell line using an Alamar blue cytotoxicity assay. The graph plots the percentage of viable cells remaining after treatment with varying concentrations of the methanol extract on the y-axis. The x-axis represents the concentration of the methanol extract in µg/ml. The data points are fitted with a linear regression line. The IC50 value, which is the concentration required to reduce cell viability by 50%, can be determined from the point where the regression line intersects 50% viability on the y-axis. As indicated on the graph, the methanol extract exhibits cytotoxic effects only at relatively high concentrations. Therefore, the trend

line needs to be extended to accurately pinpoint the IC50 value, which is calculated to be 880 µg/ml based on the linear regression analysis.

(half-maximal inhibitory concentration) value for the water extract of *T. violacea* against the MDA-MB231 triple-negative breast cancer cell line using an Alamar blue cytotoxicity assay. The graph shows the percentage of viable cells remaining after treatment with varying concentrations of the extract. The x-axis represents the concentration of the extract in µg/ml, while the y-axis shows the percentage of cell viability compared with the untreated control. Data points were fitted using a linear regression line. The IC50 value, which is the concentration required to reduce cell viability by 50%, was determined from the intersection point of the regression line with the 50% viability on the y-axis. As indicated in the graph, the IC50 value for the *T. violacea* water extract against MDA-MB231 cells was approximately 350 µg/ml, and only 50% of the cells remained viable after treatment.

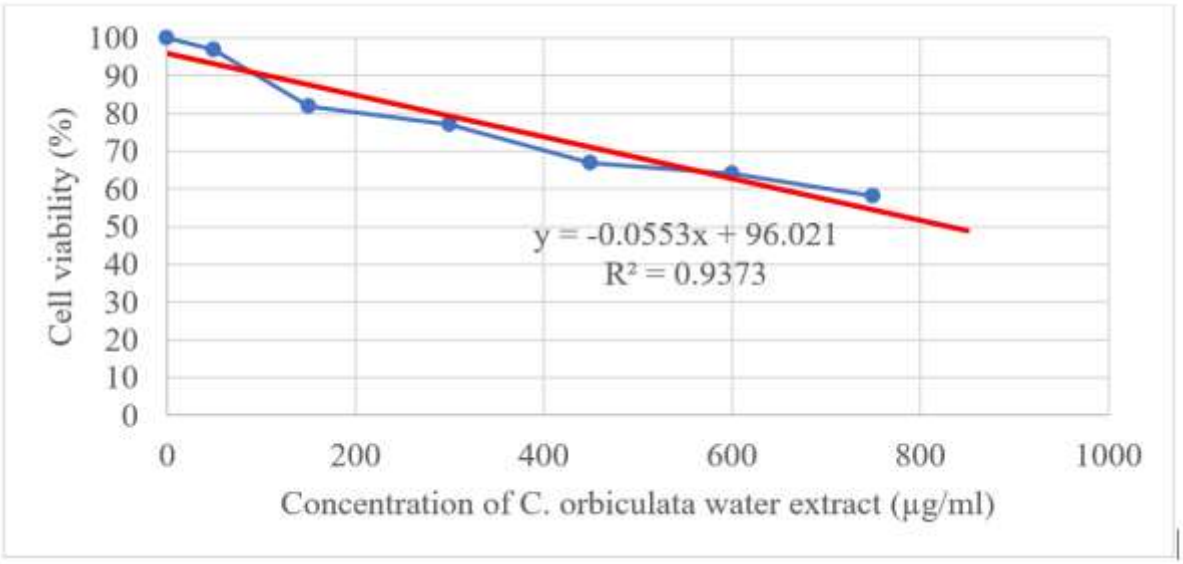

Figure 3.8 depicts the determination of the IC50 value for the C. orbiculata water extract against MDA-MB-231 triple negative breast cancer cells using an Alamar blue cytotoxicity assay. The graph shows the percentage of viable cells remaining after treatment with varying concentrations of the extract. The x-axis represents the concentration of the C. orbiculata water extract in µg/ml, while the y-axis displays the percentage of cell viability. The data points are fitted with a linear trend line, and the equation of the line is provided. At lower concentrations, the extract exhibits minimal cytotoxic effects on the cells. However, as the concentration increases, a reduction in cell viability is observed. To determine the IC50, which is the concentration required to inhibit 50% of cell growth, the trend line is extrapolated. The IC50 value for this extract is calculated to be 820 µg/ml from the point where the trend line intersects 50% cell viability on the y-axis.

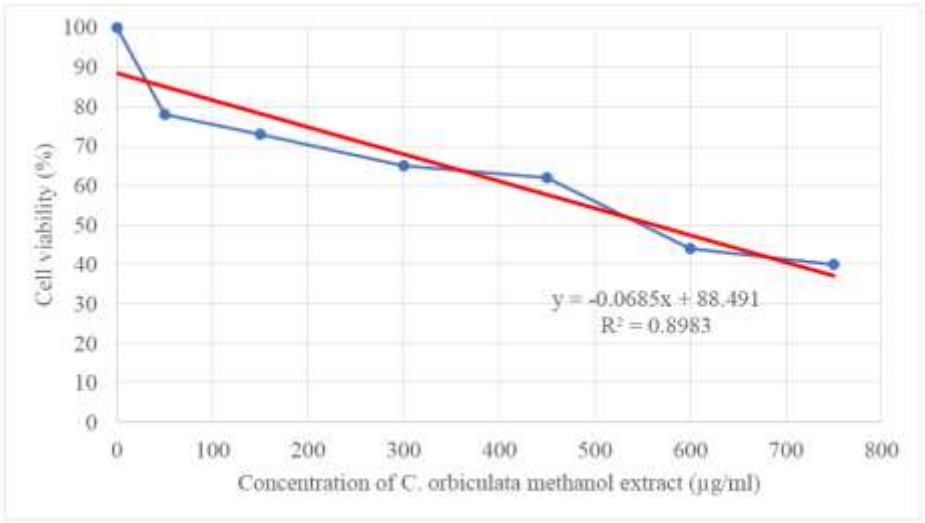

Figure 3.9 depicts the determination of the IC50 value for the C. orbiculata methanol extract against the MDA-MB-231 triple negative breast cancer cell line using the Alamar blue cytotoxicity assay. The graph shows the percentage of viable cells remaining after treatment with varying concentrations of the methanol extract along the x-axis (µg/ml). The y-axis represents the percentage of cell viability. The data points are fitted with a linear trend line, and the equation of the line is provided. As the concentration of the methanol extract increases, there is a decrease in cell viability, indicating a dose-dependent cytotoxic effect. To calculate the IC50, which is the concentration required to inhibit 50% of cell growth, the trend line is extrapolated. The IC50 value for the C. orbiculata methanol extract is determined to be 530 µg/ml from the point where the trend line intersects the 50% cell viability level on the y-axis.

Table 3.1 Final IC50 values adopted for the rest of this study

Sample	IC_{50} by RTCA µg/mL	IC_{50} by Alamar blue µg/mL	Adopted IC_{50} µg/mL
T. violacea water soluble extract	395.2	350	400
T. violacea methanol soluble extract	820.7	820	820
C. orbiculata water extract	794.3	880	830
C. orbiculata methanol extract	1063	530	700

Table 3.1 summarizes the IC_{50} values determined using both methods and provides the final values used in future experiments and the actual concentrations used to treat the cells. These four compounds were tested in MDA-MB-231 and MCF10A cells. The concentrations selected for these tests corresponded closely with the IC_{50} values derived from the Alamar Blue assay and RTCA system. In

both the resazurin/Alamar Blue cell viability tests and the xCELLigence RTCA system, the IC50 values of the *T. violacea* water-soluble extract and methanol-soluble extract were found to be similar. However, this consistency was not observed for *the methanol extracts of C. orbiculata* and *C. orbiculata, for which* the IC_{50} values exhibited significant discrepancies. Owing to the high IC_{50} values determined for the other extracts and the difficulties associated with the methanol-soluble extracts, the majority of further experiments focused solely on the *T. violacea* water-soluble extract.

3.5 Pro-apoptotic and anti-proliferative activities of *T. violacea* water soluble extracts

Scientists coined the term "apoptosis" to define a particular form of cellular demise marked by distinct morphological alterations.

These changes include cellular constriction, the assumption of an irregular shape due to membrane blebbing, formation of membrane-bound apoptotic bodies, and ultimate disintegration of intracellular components, which are then phagocytosed by adjacent cells. The cornerstone for characterising apoptosis-inducing stimuli and guiding research into the biochemistry and signal transduction of apoptosis is the morphological alterations linked to apoptosis. The activation of an intracellular signal transduction system that leads to these morphological changes and apoptosis involves two separate pathways: intrinsic and extrinsic.

Previous research has shown that *T. violacea* and *C. orbiculata* extracts can induce apoptosis in cultured cells, particularly in cell lines originating from human cancer tissues. Notably, leaf extracts of

T. violacea, as opposed to bulb extracts, has been observed to inhibit tumour development by triggering apoptosis. This phenomenon is linked to the production of reactive oxygen species (ROS) and activation of caspase-3 (Saibu et al., 2015). Annexin-V tests confirmed the induction of apoptosis, and the cleavage of poly (ADP-ribose) polymerases (PARP) suggested that the growth-inhibitory effects were connected to the beginning of apoptosis. Furthermore, Lyantagaye [202] presented data supporting the pro-apoptotic activities of *T. violacea extracts*, indicating that *T. violacea* extracts have pro-apoptotic activities [202].

Following the anticancer activity revealed in the cytotoxicity experiments, additional research was performed to investigate the possible proapoptotic activity of these plant extracts. The effect of the crude extract on the selected cell lines was evaluated using morphological evaluation and flow cytometry analysis to quantify cell death (using the annexin apoptosis test) and cell cycle progression by evaluating DNA levels. Following the anticancer activity revealed in the cytotoxicity experiments, additional research was done to investigate the possible pro-apoptotic activity of these plant extracts. The effect of the crude extract on the selected cell lines was evaluated using morphological evaluation as well as flow cytometry analysis to quantify cell death (using the annexin apoptosis test) and cell cycle progression by evaluating DNA levels. These assessments were conducted using a Muse™ flow cytometer and compatible kits.

3.6 Morphological changes following treatment with plant extracts

The remarkable consistency of morphological changes in various circumstances involving naturally occurring or chemically induced cell death reflects the similarity of biochemical events during apoptosis. Approximately 50 years ago, this morphological regularity of dying cells was discovered, leading to the unifying concept of apoptosis. Since then, many studies have focused on intracellular signaling in the apoptotic process as well as the molecular background that controls the initiation of morphological changes [231]. Historically, morphological alterations and the disappearance of cells have served as the primary indicators of cell death. Numerous early morphological investigations have revealed substantial differences in cell death both *in vivo* and *in vitro* [232].

In 1972, Kerr et al. used morphological evidence to develop a unifying concept. This concept relates to a specific type of cell death that serves as a mechanism for removing unnecessary cells during embryonic development, regular turnover of cells in proliferating tissues, and various pathological conditions [233]. The cells were then exposed to various crude extracts for 72 h. Following the treatment period, the effect of the crude extract on cell shape was evaluated in both MDA-MB 231 and MCF10A cell lines. Morphological changes in MDA-MB 231 cells were compared to negative

controls (untreated cells) Following the treatment period, and the influence of the crude extract on cell shape was evaluated in both MDA-MB 231 and MCF10A cell lines. The morphological changes in MDA-MB 231 cells were compared to those in negative controls (untreated cells), whereas the changes in MCF10A cells were evaluated against positive controls (cells treated with 25 µM 5FU). These comparisons were conducted after a 72-hour treatment using concentrations equivalent to the IC_{50} values of each specific plant extract.

Figure 3.10 depicts the morphological evaluation of MDA-MB-231 cells after treatment with all four extracts at their respective IC_{50} concentrations. Notably, while both cell types, MDA-MB-231 and MCF10A, exhibited morphological changes when treated with 25 µM 5FU, alterations in cell morphology were more subtle when exposed to the crude extracts. To conduct a more preciseEvaluation of any morphological variations and images of both MCF10A and MDA- MB231 cells treated with *T. violacea* water-soluble extract over a 72-hour period. The captured images were subsequently analysed using ImageJ software, which determined both the cell area and perimeter length of the cells within the images. Both cell shrinkage and blebbing are characteristics of apoptosis, and shrinkage results in a decrease in cell area, whereas blebbing increases the perimeter length of a cell. Figure 3.11 shows the result of plotting the area against the perimeter size of the MDA-MB231 cells following treatment with the *T. violacea* water-soluble extract at 0, 24, 48, and 72 h. The 0 h treatment served as the untreated control and showed that the size and shape of these cells were naturally varied, with very few large cells. At 24 hours after treatment, many smaller cells underwent cell shrinkage; however, at the same time, the perimeter of many cells increased, which may indicate membrane blebbing. This situation was maintained for 48 h after treatment. At 72 h, many more cells showed signs of contraction with reduced cell perimeter size, and there were more smaller cells, which implies that many of the cells were undergoing cell shrinkage. It is also important to note that there were far fewer cells at this stage.

Figure 3.12 shows the result of plotting the area against the perimeter size of the MCF-10A cells following treatment with the *T. violacea* water-soluble extract at 0, 24, 48, and 72 h. Cellular morphology appears to remain relatively consistent after treatment, with notable variability in both cell size and shape. This trend continued up to the 72-hour point, at which time there was a noticeable

increase in the population of small cells showing signs of cell shrinkage. In this example, unlike in the triple-negative breast cancer (TNBC) cell line, there was no significant decrease in the total cell count following therapy.

In the case of untreated TNBC cells, there was only a slight decline in the cell count over time, as depicted in Figure 3.11 A and B. This trend followed an initial increase in cell numbers after 24 h. However, as expected, a reduction in cell count occurred due to the depletion of available space and nutrients. There was very little change in the circularity, roundness, or solidity of untreated TNBC cells over 72 h (Figure 3.11C–D). The scenario differed when TNBC cells were exposed to *T. violacea* water-soluble extract at the IC_{50} value. As treatment with the water-soluble *T. violacea* extract progressed, a marked reduction in cell number was observed, primarily attributable to the increased occurrence of apoptosis (Figure 3.12 A). Concurrently, there was a decrease in cell roundness, circularity, and solidity, all of which were indicative of changes in cell morphology associated with apoptosis (Figure 3.12 B-D).

It appears that in both cases, with and without treatment with *T. violacea* water-soluble extract at the IC_{50} concentration, there was indeed a slight decrease in the cell count over the 72-hour period, as previously mentioned. This pattern occurred after an initial rise at 24 h in both untreated (Figure 3.15A) and treated (Figure 3.16A) cells. However, this initial increase was considerably less pronounced in the treated cells.

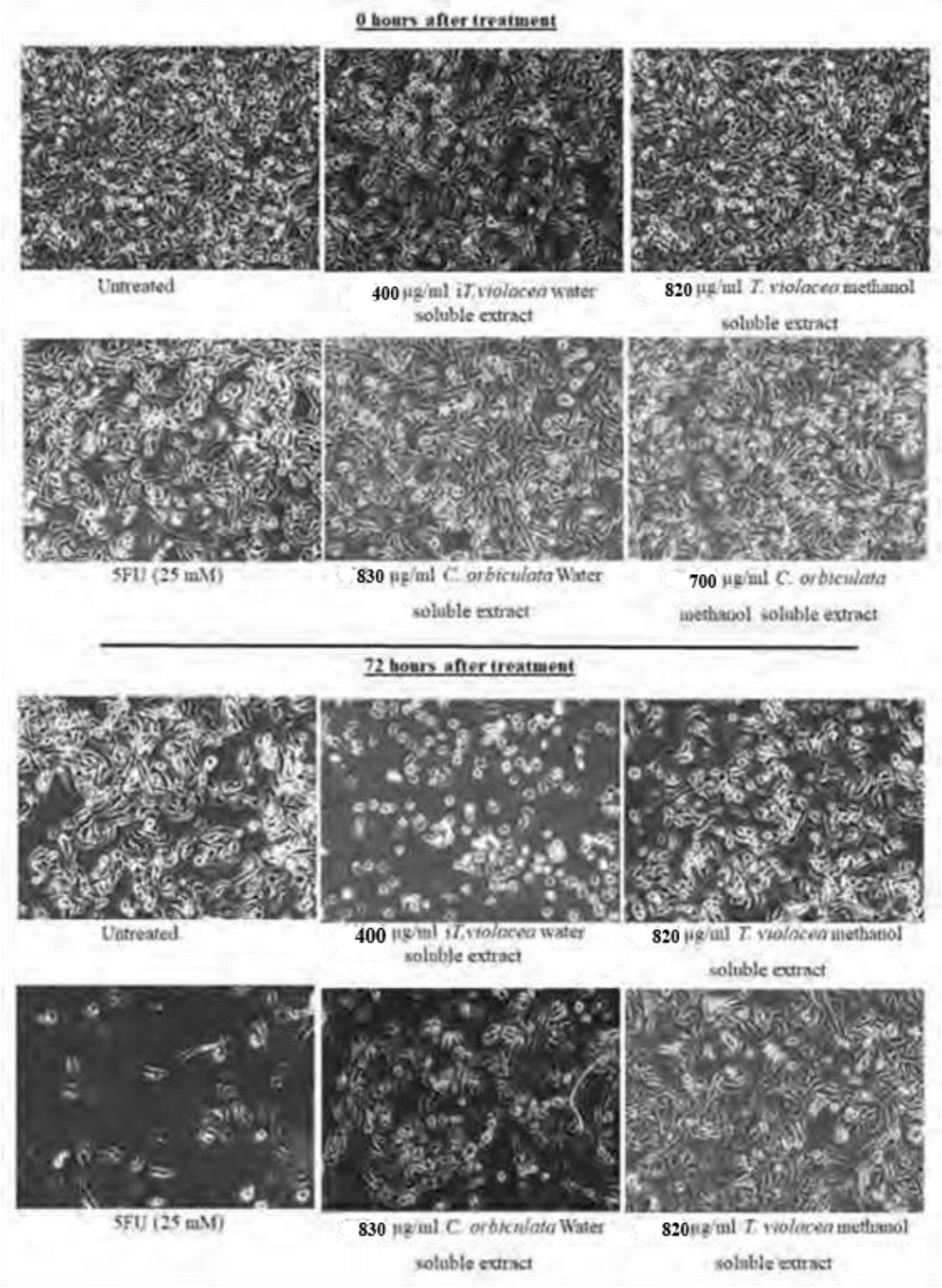

Figure 3.10 depicts a series of microscopic images illustrating the morphological changes observed in MDA-MB-231 triple-negative breast cancer cells after treatment with various plant extracts over time. The top panel (A) shows the cells at 0 h, immediately after treatment, while the bottom panel (B) displays the cells at 72 h post-treatment. The different columns represent cells treated with the following conditions: untreated control, 400 µg/ml *T. violacea* water-soluble extract, 820 µg/ml *T. violacea* methanol-soluble extract, 25 µM 5-fluorouracil (5FU) as a positive control, 830

µg/ml *C. orbiculata* water-soluble extract, and 700 µg/ml *C. orbiculata* methanol-soluble extract. Images were captured using a Nikon light microscope equipped with a Leica digital camera at 20x magnification. The figure legend notes that these experiments were performed in triplicate to ensure reproducibility and consistency of the observed morphological changes.

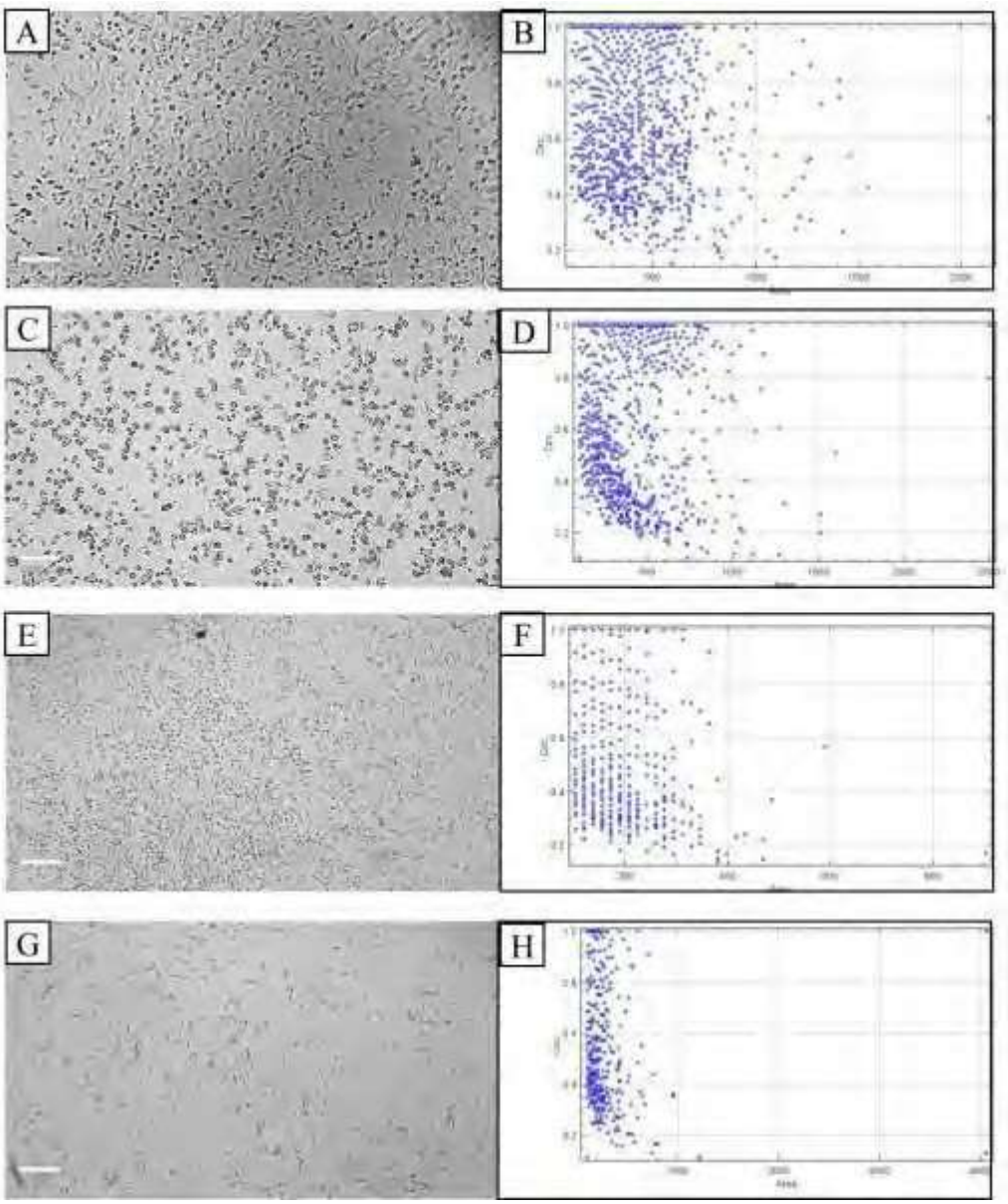

Figure 3.11 depicts the morphological changes observed in MDA-MB-231 triple-negative breast cancer cells following treatment with the water-soluble extract of *Tulbaghia violacea* over a 72-hour period. Images are arranged in rows, with each row representing a specific time point after treatment: 0 h (A, B), 24 h (C, D), 48 h (E, F), and 72 h (G, H). The left column (A, C, E, G) shows bright-field microscopic images of the cells, whereas the right column (B, D, F, H) displays fluorescence microscopy images, likely stained with a fluorescent dye to highlight specific cellular features or structures. This arrangement allowed for the visualisation and comparison of cellular morphological changes induced by *T. violacea* extract over the course of 72 h. The time-lapse images enabled the observation of potential alterations in cell shape, size, membrane integrity, and overall viability in response to plant extract treatment.

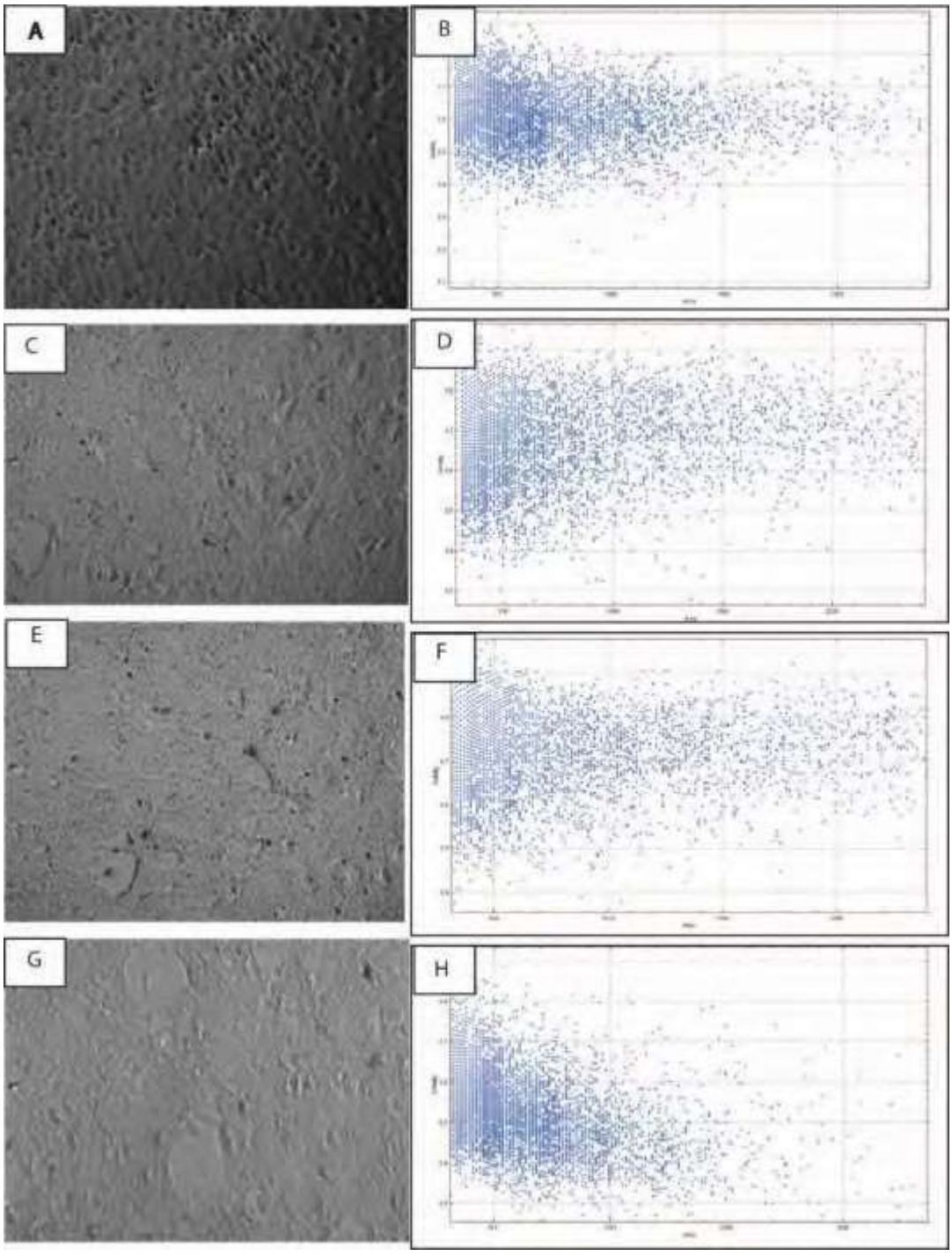

Figure 3.12 depicts a series of microscopic images showing the morphological changes in MDA-MB-231 triple-negative breast cancer cells over time when treated with *T. violacea* water extract. The images were arranged in a grid, with each panel representing a different time point after treatment: 0 h (A, B), 24 h (C, D), 48 h (E, F), and 72 h (G, H). The left column (A, C, E, G) shows bright-field microscopic images, whereas the right column (B, D, F, H) displays fluorescence microscopy images, likely stained to highlight specific cellular features or structures. This arrangement allows for the visualisation and comparison of cellular morphological alterations induced by *T. violacea* water extract

over a 72-hour treatment period. Time-lapse images enabled the observation of potential changes in cell shape, size, membrane integrity, and overall viability in response to the plant extract treatment.

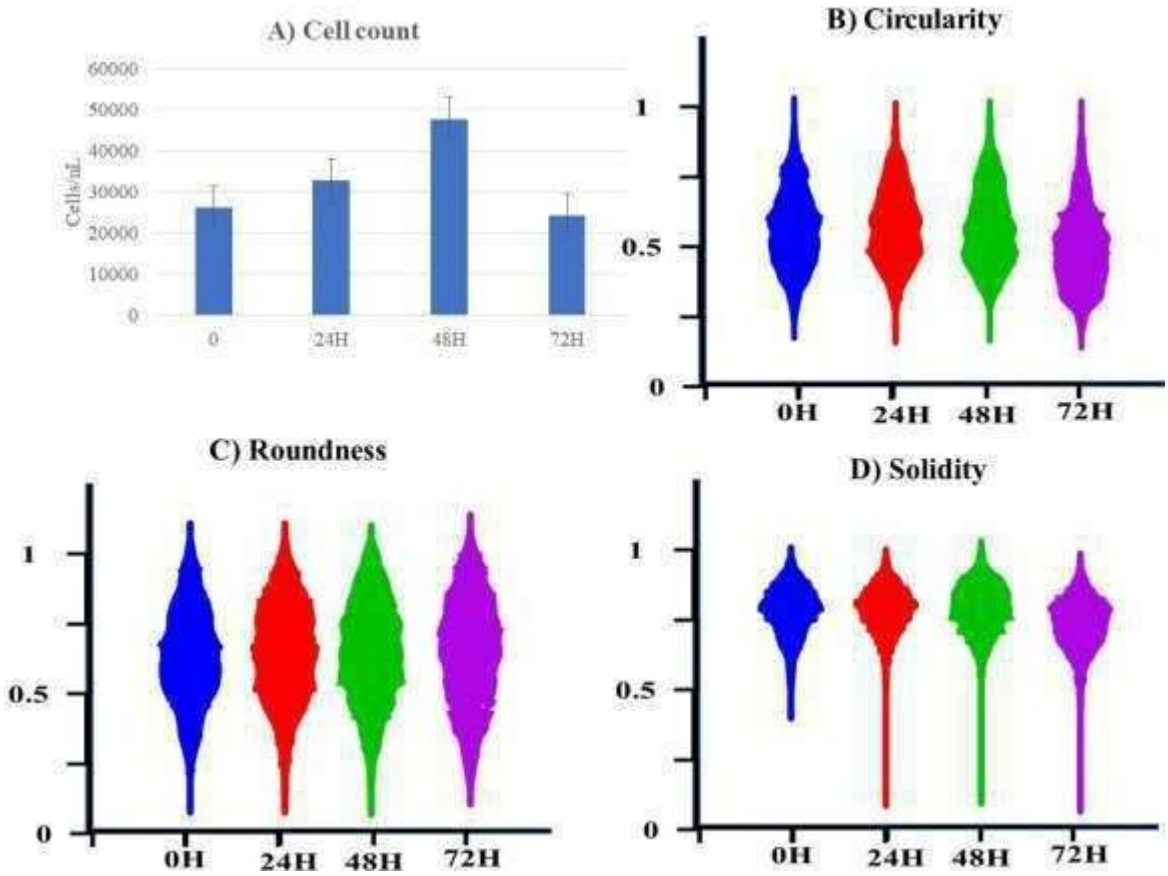

Figure 3.13 depicts various morphological characteristics of untreated MDA-MB-231 cells over a 72-hour period. A) The cell count increases over time as cells proliferate for 72 h when cell death increases due to nutrient depletion. B) Cell circularity remained constant until 48 h, after which it decreased as apoptosis increased, causing membrane blebbing. C) The roundness of the cells did not change significantly throughout 72 h. D) There was no substantial change in cell solidity during the initial 24 h. Solidity remained unaltered for the next 24 h but showed a slight decrease between 48 and 72 h.

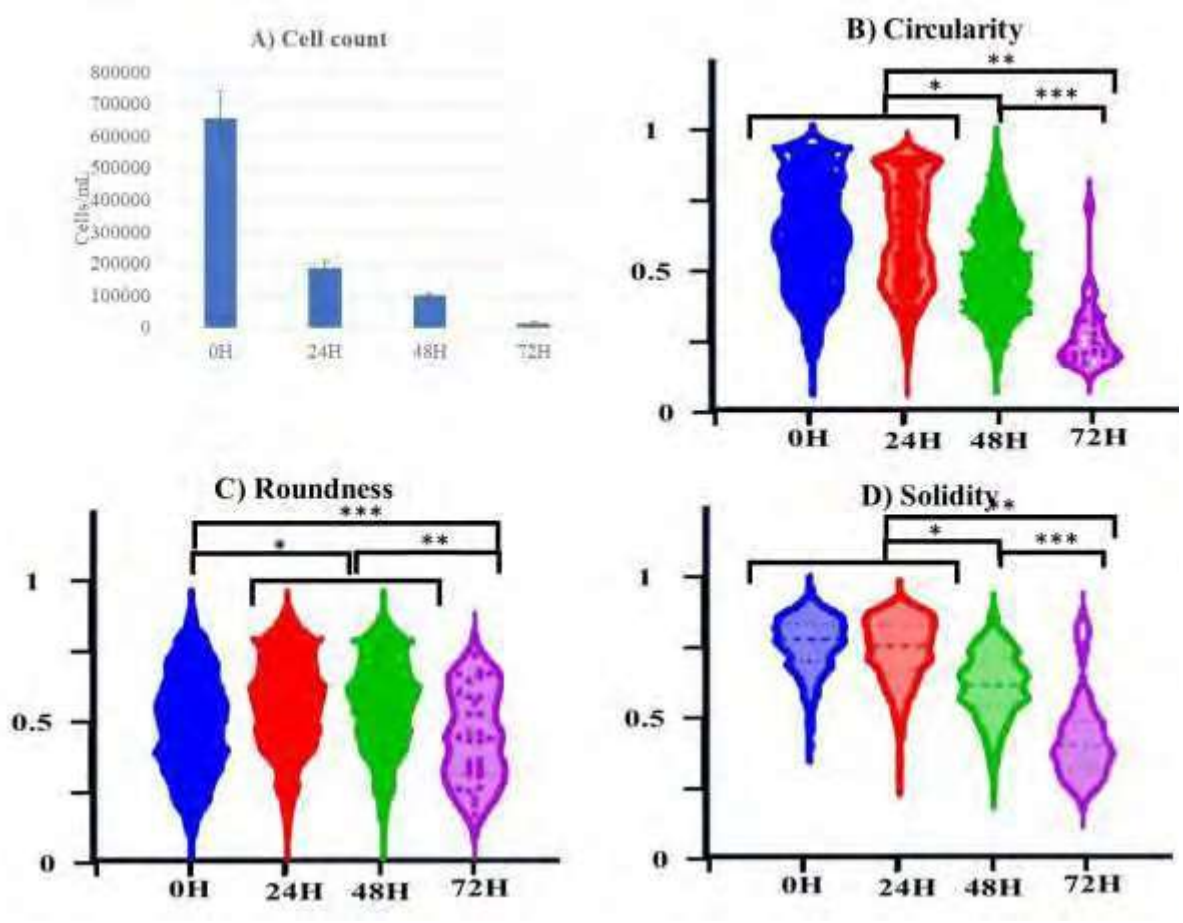

Figure 3.14 depicts the morphological changes observed in MDA-MB-231 cells at various time points after treatment with the *water-soluble extract of T. violacea*. A) Over time, there was a noticeable reduction in cell number due to increased cell death. B) The circularity of the cells changed during treatment, with a significant increase at 48 h compared to 0 and 24 h, and a further pronounced increase at 72 h. C) Cell roundness showed a significant decrease within the first 24 h of treatment, but remained unchanged at 34 and 48 h before decreasing substantially again at 72 h. D) Regarding cell solidity, there was no significant change during the first 24 h, but a marked decrease was observed between 48 and 72 h.There was no significant change in cell solidity within the first 24 h of treatment. However, a significant change in solidity occurred over the subsequent 24 h (* $p = 0.001$), and there was a notable decrease in solidity between the 48 and 72-hour intervals (** $p = 0.0001$).

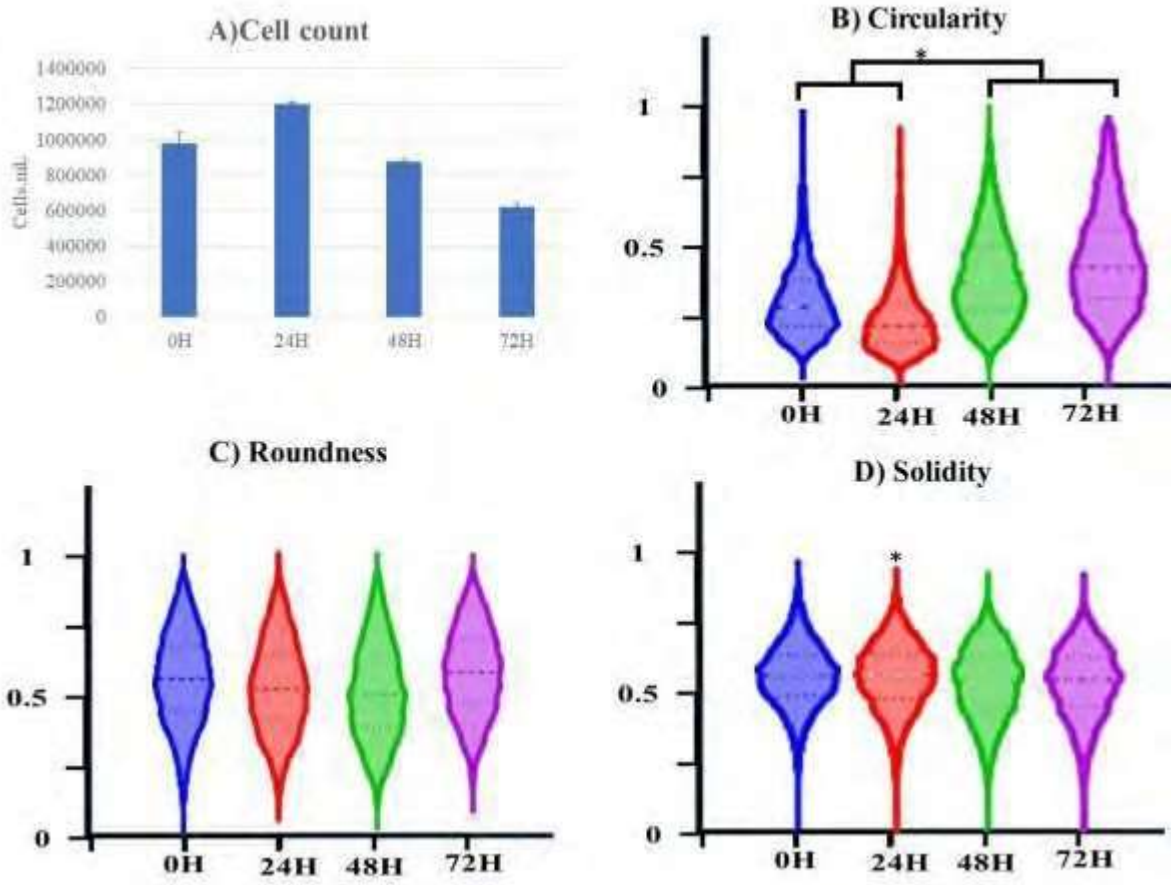

Figure 3.15 depicts the morphological changes observed in untreated MCF10A cells over a 72-hour period. A) The cell count initially increased but then decreased over time. B) Cell circularity remained relatively stable for the first 24 h but showed a significant increase at the 48-hour time point. C) Cell roundness did not change significantly throughout the 72-hour observation period. D) Similarly, the cell solidity did not exhibit any notable changes within the first 24 h.

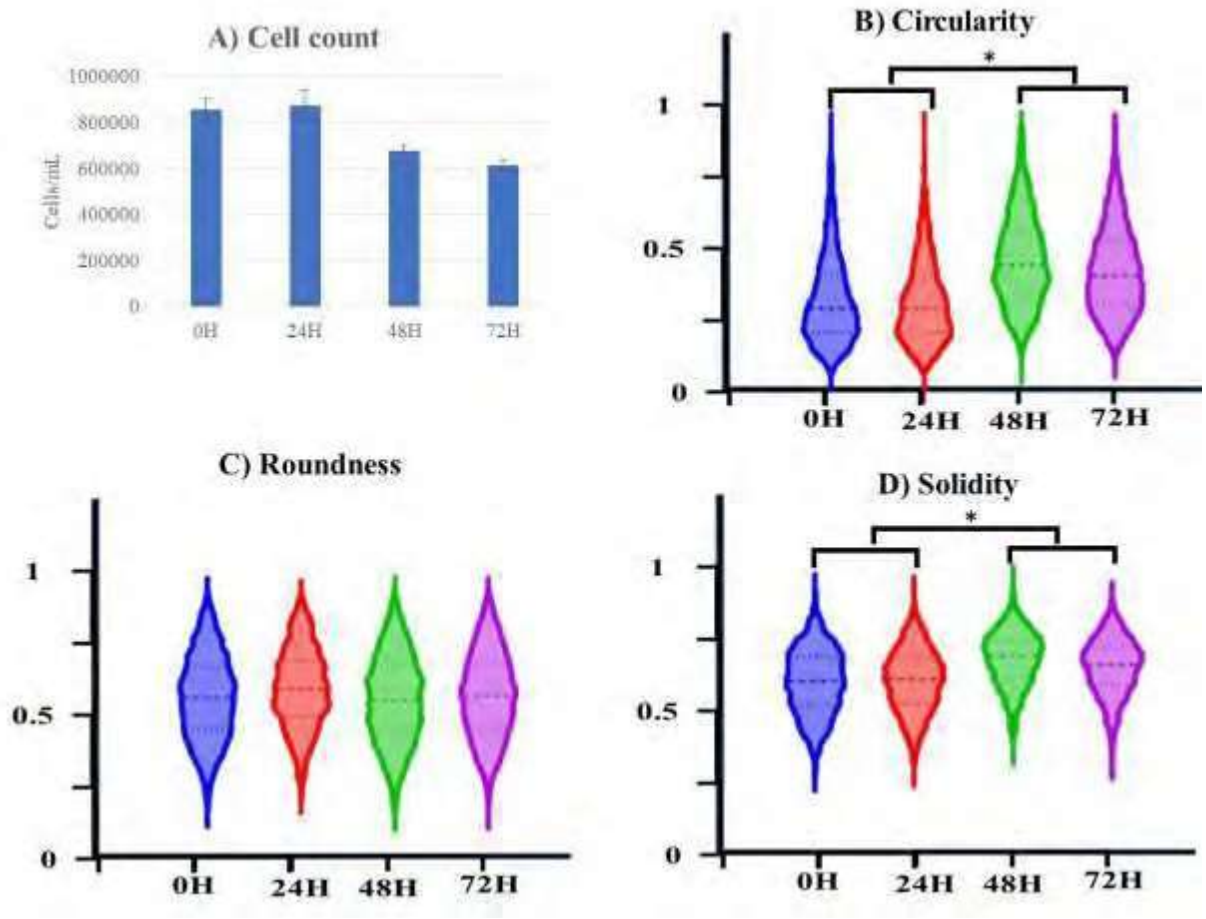

Figure 3.16 depicts the morphological changes observed in MCF10A cells at various time points after treatment with the water-soluble extract of *T. violacea*. Over time, there was a slight decrease in cell count. Notably, cell circularity increased significantly 48 h post-treatment. However, cell roundness remained relatively unchanged throughout the 72-hour period. Interestingly, a marked increase in cell solidity was evident 48 h after extract exposure, indicating potential morphological alterations induced by the treatment.

An increase in circularity was observed after 48 h in both the treated and untreated cells (Figures 3.16 B and 3.16 B). There was also no change in the roundness of the cells after 72 h, regardless of whether the cells were treated (Figures 3.16 C and 3.16 C). In untreated cells, there were no changes in solidity after 72 h. However, in treated cells, a significant increase in solidity was observed 48 h after treatment.

3.7 Apoptosis assay

Raw extracts of T. violacea have been shown to trigger apoptosis in triple-negative breast cancer (TNBC) cells. An experiment was conducted using an apoptosis detection kit and flow cytometry to determine the type of cell death during cell cycle analysis, distinguishing between apoptosis and necrosis as a result of *exposure to the T. violacea extract*. The cells were treated with *T. violacea* extract for 75 h at various concentrations: below, at, and above the IC_{50}. Subsequent application of annexin V and propidium iodide (PI) enabled the differentiation of live cells from those in the stages of apoptosis or necrosis. Heat-killed cells served as a positive control for necrosis, aiding in calibrating the Luminex Guava Muse® cell analyser as these cells predominantly fell into the dead quadrant (Figure 3.17A). In contrast, the untreated control MCF10A and MBA-MB 231 cells mostly resided in the live quadrant, with 86.5% and 79.2% viability, respectively (Figure 3.17B). Less than 10% of the cells in either line exhibited signs of apoptosis, and 4.75% of MCF10A cells died. In MBA-MB 231 cells, 19% of cells died, but the majority remained viable. treatment, a significant proportion of MBA-MB 231 cells either died or were in late-stage apoptosis (82%). Although the extract also induced apoptosis in MCF10A cells, over 58% were still viable after 72 h, compared to only 4.7% in MDA-MB231 cells. Therefore, *treatment with T. violacea extract* led to higher apoptosis rates in TNBC cells than in normal breast cancer cells.

Further experiments using various concentrations of this extract revealed that this increase in apoptosis levels in TNBC cells was concentration-dependent, with concentrations half that of the IC_{50} causing little to no apoptosis. In this context, the count of viable cells resembled that of untreated cells (Figure 3.18). Notably, treatment led to the majority of cells undergoing necrosis, whereas most untreated cells experienced apoptosis as the primary mode of cell death. Treatment with concentrations at or exceeding the IC_{50} resulted in substantial apoptosis and a significant reduction in cell viability. Notably, when normal MCF10A breast cells were treated, there was a noticeable increase in cell death; however, this effect was considerably less pronounced when compared to TNBC cells subjected to the same concentration.

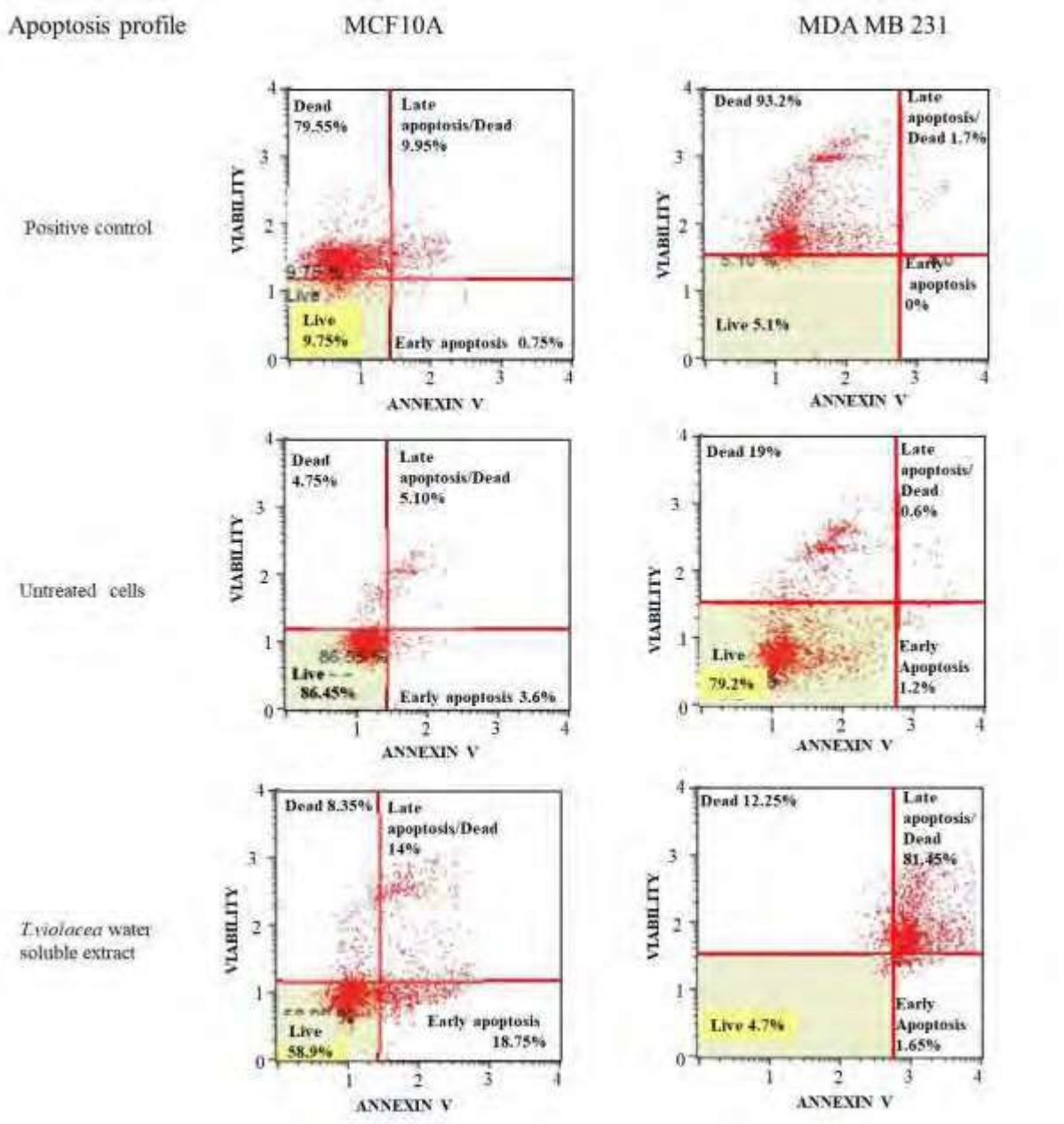

Figure 3.17 depicts the flow cytometry analysis of apoptosis in MCF10A and MDA-MB-231 cells treated with the *T. violacea* water-soluble extract at the corresponding IC50 concentration for 72 h. A) Positive control of heat-killed cells, predominantly in the dead cell quadrant. B) Representative untreated control cells, with the majority viable in both cell lines. C) Illustrates the effect of the extract treatment, inducing high levels of late apoptosis and cell death in MDA-MB-231 triple-negative breast cancer cells, while normal MCF10A cells remained more viable.

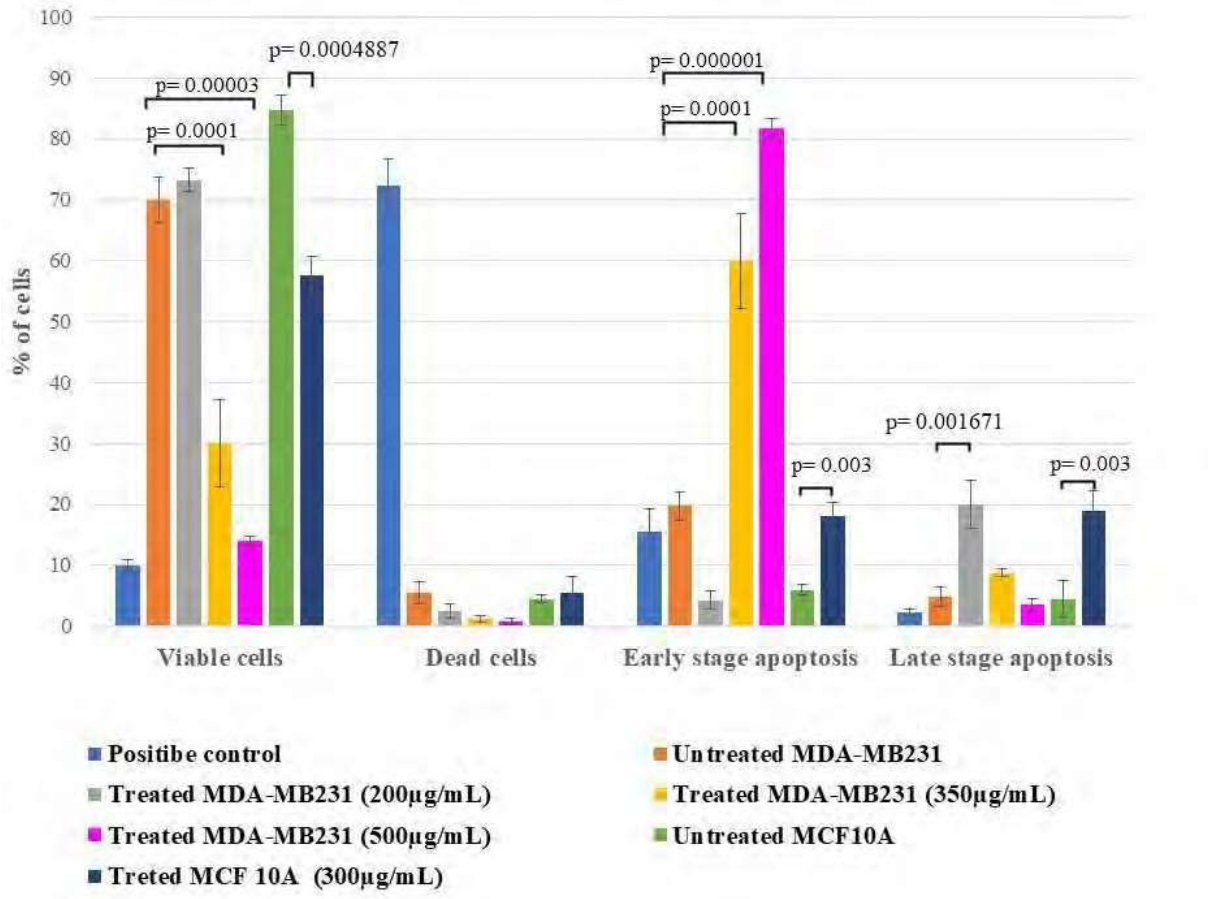

Figure 3.18 depicts the results of an Annexin V apoptosis assay performed on triple-negative breast cancer (TNBC) cells and normal breast cells after treatment with varying concentrations of the *T. violacea* water-soluble extract The cells were stained with Annexin V, which binds to phosphatidylserine exposed on the surface of apoptotic cells, and a dead cell marker. Flow cytometry analysis was used to quantify the percentages of viable cells, early apoptotic cells, late apoptotic cells, and dead cells based on their distinct staining patterns. This assay allowed the evaluation of the pro-apoptotic effects of *T. violacea* extract on both cancer and normal cells at different concentrations.

3.8 Cell cycle assay

The DNA content of the treated cells was evaluated using flow cytometry and propidium iodide (PI) staining to determine the effect of active plant extracts on cell cycle progression. This approach is critical for determining the first phase of the cell cycle, which is often known as the resting phase. This phase encompasses the gap 0 (G0) stage, characterised by cellular dormancy, where cell division is paused. This is followed by the Gap 1 (G1) stage, during which the cells undergo growth. The next phase, known as the synthesis (S) phase, is where the DNA replication occurs. The third stage, the Gap 2 (G2) phase, occurs between DNA synthesis and mitosis, with the cell continuing to grow. The

final phase, mitosis (M), occurs when cell growth stops and the cell divides into two daughter cells. The course of the cell cycle is controlled by cyclin-dependent kinases (CDKs), with checkpoints controlling the entrance of the cell into each phase.

The DNA content of a cell indicates its current cell cycle stage. Cells in the S-phase, which actively synthesises DNA, have a higher DNA content than those in the G1 phase. Consequently, cells in the G2 phase, ready for division, should show nearly double the DNA content of G1 cells, resulting in brighter fluorescence under DNA staining.

The cells underwent the same treatment regimen as previously, with three distinct concentrations of *T. violacea* water-soluble extract: one below, one at, and another above the IC_{50} value. After 48 h of treatment, cells were harvested and fixed in ice-cold absolute ethanol. Subsequently, cells were rehydrated and treated with RNase at 37°C. RNase treatment is crucial, as propidium iodide (PI) can bind to RNA similar to DNA, which might influence the precision of fluorescence measurements. After RNA elimination, the cells were stained with a 1 mg/mL solution of PI, and the stained cells were evaluated using the cell cycle program on a Muse flow cytometer. incubated at 4 °C in the dark overnight.

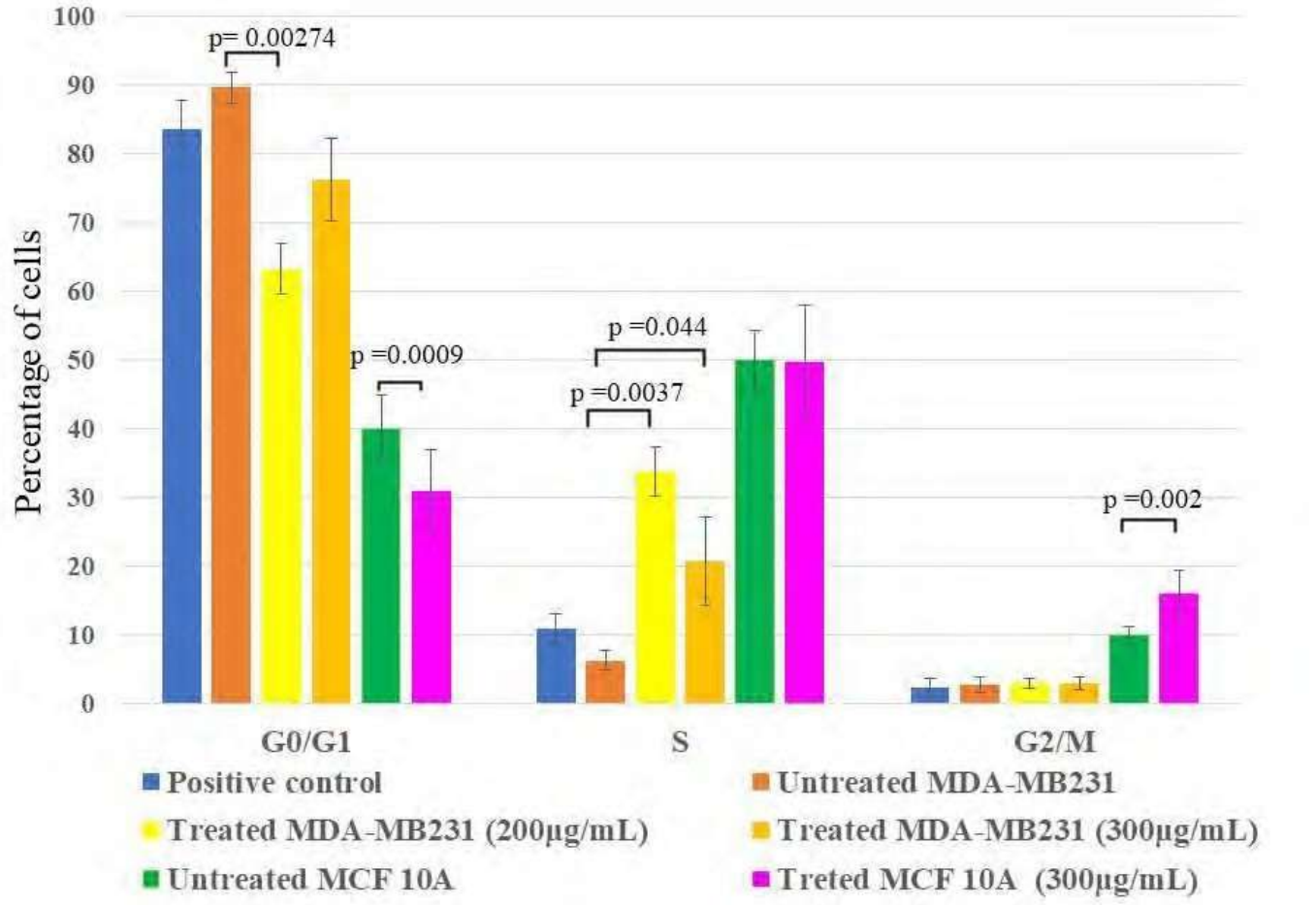

Figure 3.19 depicts the results of a cell cycle analysis performed on both triple-negative breast cancer (TNBC) and normal breast cell lines using flow cytometry. The data illustrate the distribution of cells across different phases of the cell cycle (G0/G1, S, and G2/M) following treatment with *T. violacea* water-soluble extract at varying concentrations. In untreated TNBC cells, a high proportion of cells was observed in the G0/G1 phase. However, upon treatment with the extract, there was a dose-dependent decrease in the number of cells in this phase, accompanied by a significant shift towards the S phase. A similar trend was observed in normal breast cells, where initially a smaller fraction of cells was in the G0/G1 phase, but treatment with the extract induced progression into the S phase. This shift towards the S phase in both cell lines suggests the activation of an S-phase checkpoint in response to the extract treatment, potentially due to DNA damage or replication stress induced by the extract.

Figure 3.19 presents the outcomes of a cell cycle assay performed on both TNBC and normal breast cell lines, demonstrating the impact of treatment with two distinct concentrations of the extract. In the case of TNBC cells, the treatments were applied at a concentration marginally below the IC_{50} and at half the IC_{50} concentration, whereas normal breast cells received the highest concentration. After treatment, both TNBC and normal breast cells showed an increase in the S-phase cell population. This

increase is most likely due to activation of the intra-S-phase checkpoint, which is accompanied by a reduction in the number of cells in the G0 or G1 phases. This checkpoint is normally activated in response to the termination of replication forks due to DNA damage, implying that one ingredient of the extract may directly or indirectly cause this response inside the cells [234].

3.9 Measuring the effect, the active plant extract had on cell invasion and migration

In solid tumours, the predominant cause of mortality is the capability of cancer cells to disseminate from their initial location to diverse regions of the body, forming new neoplasms. Known as metastasis, this process relies on the increased mobility of cancer cells, their diminished adhesion to other cells or the extracellular matrix, and their ability to invade different tissue layers.

3.10 Migration assays

Cell mobility is critical for maintaining homeostasis and for directing the development of multicellular organisms. Cell migration is critical in the setting of homeostasis because it ensures the proper placement of cells and facilitates the execution of their duties, such as immune surveillance. However, when the regulation of cell migration is disrupted, it often becomes a hallmark of pathological states, particularly in conditions such as cancer [235]. Cell migration is vital in every stage of the metastatic process, which includes intratumoural movement, invasion into the neighbouring stromal compartment, and establishment of metastases at distant locations. During the initial phases of carcinoma metastasis, cancer cells penetrate the basement membrane and encase the tumour. Following that, these cancer cells invade the surrounding stromal compartment, which contains stromal cells as well as the extracellular matrix (ECM)Following that, these cancer cells invade the surrounding stromal compartment, which contains stromal cells as well as the extracellular matrix (ECM) [236]. Following intravasation into the bloodstream, malignant cells circulate within the vasculature and eventually halt in distant tissues [237]. Indeed, after extravasation, cancer cells depart from the bloodstream and migrate into the stromal tissue of newly colonised organs or tissues. These cells must undergo particular changes in this foreign milieu to survive and proliferate,

eventually leading to the development of metastatic lesions. (Wang et al., 2019).

Cell motility can be classified into two primary modes. The first is referred to as mesenchymal, and is characterised by a lamellipodial protrusion driven by actin polymerisation. The second mode is known as amoeboid, in which rapid protrusions called blebs, corresponding to bulges in the cell cortex, facilitate movement [238, 239]. Indeed, physical constraints can modify migration patterns. For example, confinement can instigate fast migration by triggering the consistent formation of a "constant bleb" at the forefront of the cell [240, 241]. Tumour cells display a diverse array of migration mechanisms [242, 243]. Therefore, assessing the capacity of the extracts to impede cell migration will provide additional insights into the anticancer potential of these extracts.

3.11 Scratch assay for migration analysis

The wound-healing or scratch assay was one of the earliest techniques developed to study cell migration in an in vitro setting [244]. This technique involves monitoring cell movement into a "wound" created in a cell monolayer. While it does not precisely replicate in vivo cell migration, it approximates the cellular movement observed in wound healing to a certain degree. Compared to other popular in vitro methods such as time-lapse microscopy and Boyden chamber assays, the wound-healing assay is especially useful for studying directional cell migration and its influence on cell interactions. To investigate the effects of the crude extract on cell migration, this method entailed creating a cell-free area within a dense cell layer and observing the closure of this gap using differential interference contrast (DIC) microscopy over 72 h. A scratch was first made with a 200-µl micropipette tip, and the degree of gap closing was measured at 0, 6, and 24 h (see Appendix C for more details).

Figure 3.20 presents a series of micrographs illustrating the closure of a scratch in MDA-MB231 cells after treatment with different extracts, captured at 0, 12, and 24-hours post-treatment. *T. violacea* methanol-soluble and C. *orbiculata* water-soluble extracts caused consistent complete closure of the scratch in MDA-MB231 cells 24 h after treatment. The cell migration patterns displayed by these extracts were very similar to those observed in untreated cells, as shown in Figures 3.21 and 3.22. Exposure of the MDA-MB231 cells to the *C. orbiculata* methanol-soluble extract invariably resulted

in cell mortality, as evidenced by the progressive decrease in the cell count on the glass slide, culminates in cessation of cell migration. This outcome was unexpected, given that the cells were subjected to concentrations marginally below the IC_{50} established for this extract in the cytotoxicity tests. The quantitative assessments of cell movement are shown in Figures 3.21 and 3.22.

by calculating the scratch size (Figure 3.20) and the distance between the two opposing leading edges of the scratch (Figure 3.21). Alterations in the area of the scratch within the MDA-MB231 monolayer indicated that both the *T. violacea* methanol-soluble extract and the C. orbiculate water-soluble extract had no statistically significant impact on cell migration when compared to untreated cells. After 12 h of treatment, the methanol-soluble extract of *C. orbiculata* and water-soluble extract of *T. violacea* significantly affected cell migration. This effect was evident from the marked difference in the scratch area compared to untreated cells, with statistical significance observed ($p = 0.008$ and 0.01, respectively, at 12 h for each extract; $p = 0.002$ and 0.003, respectively, at 24 h). The absence of scratch closure in the case of *C. orbiculata* methanol-soluble extract is likely attributed to cell death. The asterisk indicates that there was no discernible change between the treated and untreated control cells.

The lack of cell closure in the cells treated with the extract appeared to be due to increased cell death, as seen by the reduced number of cells visible on the slide 24 h after treatment. This was surprising because of the large IC_{50} determined for this extract in cytotoxicity assays. The water-soluble extract of *T. violacea* was the only extract that consistently inhibited cell migration.

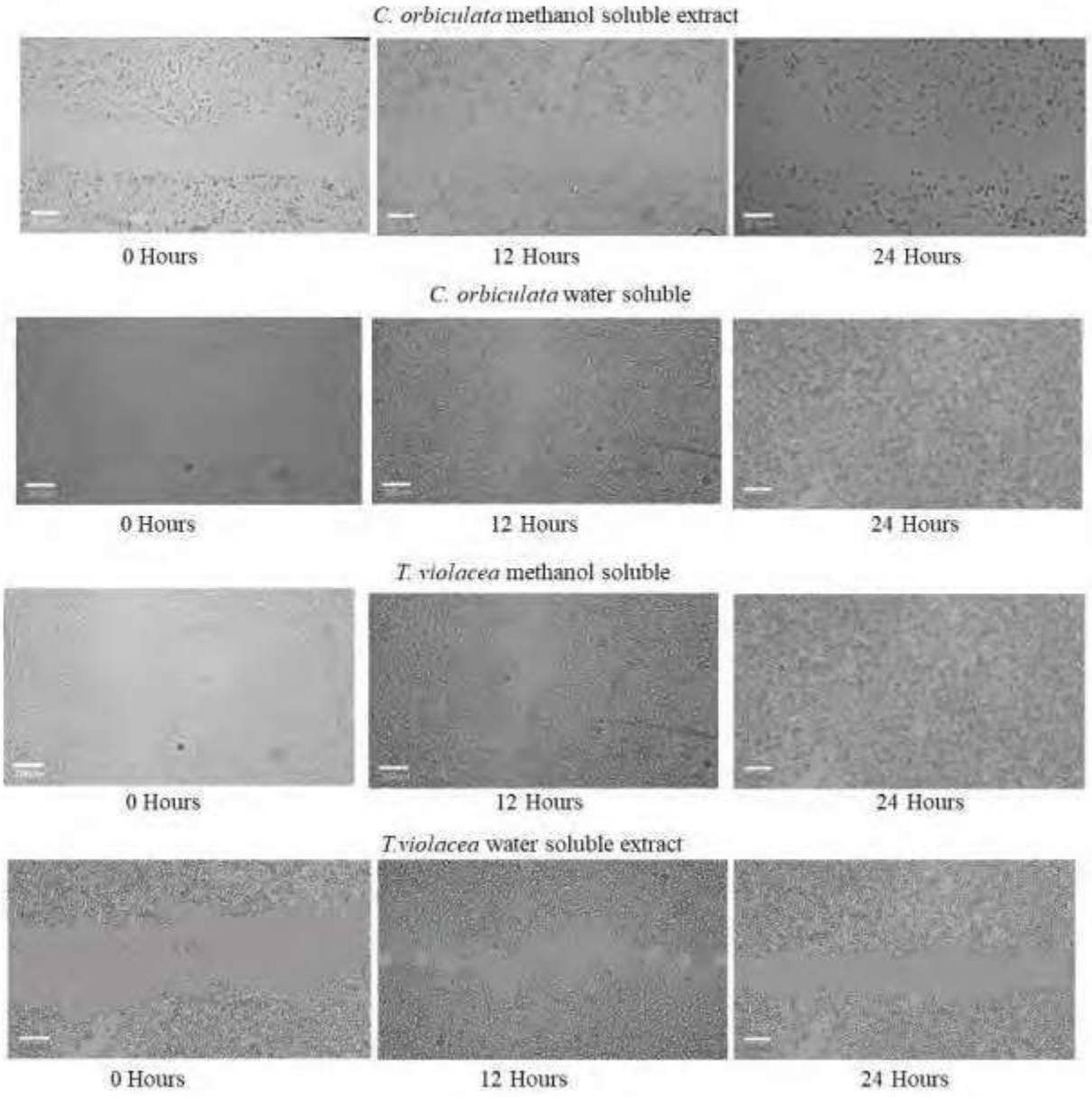

Figure 3.20 depicts the results of a scratch assay performed to evaluate the impact of different plant extracts on the migration of MDA-MB-231 triple-negative breast cancer cells. The assay involves creating a cell-free "scratch" in a confluent monolayer of cells and monitoring the closure of this gap over time under different treatment conditions. The micrographs show the progression of gap closure at 0, 12, and 24 h after treatment with the various extracts. Substantial scratch closure was observed in cells treated with the methanol-soluble extract of *T. violacea* and water-soluble extract of *C. orbiculata*, indicating that these extracts did not significantly impede cell migration. In contrast, cells treated with the methanol-soluble extract of *C. orbiculata* displayed no gap closure, likely due to the increased cell death induced by this extract. Notably, the water-soluble extract of *T. violacea* consistently inhibited cell migration, as evidenced by the lack of scratch closure. The white scale bars in the images represent the reference distance for comparison.

100 µm.

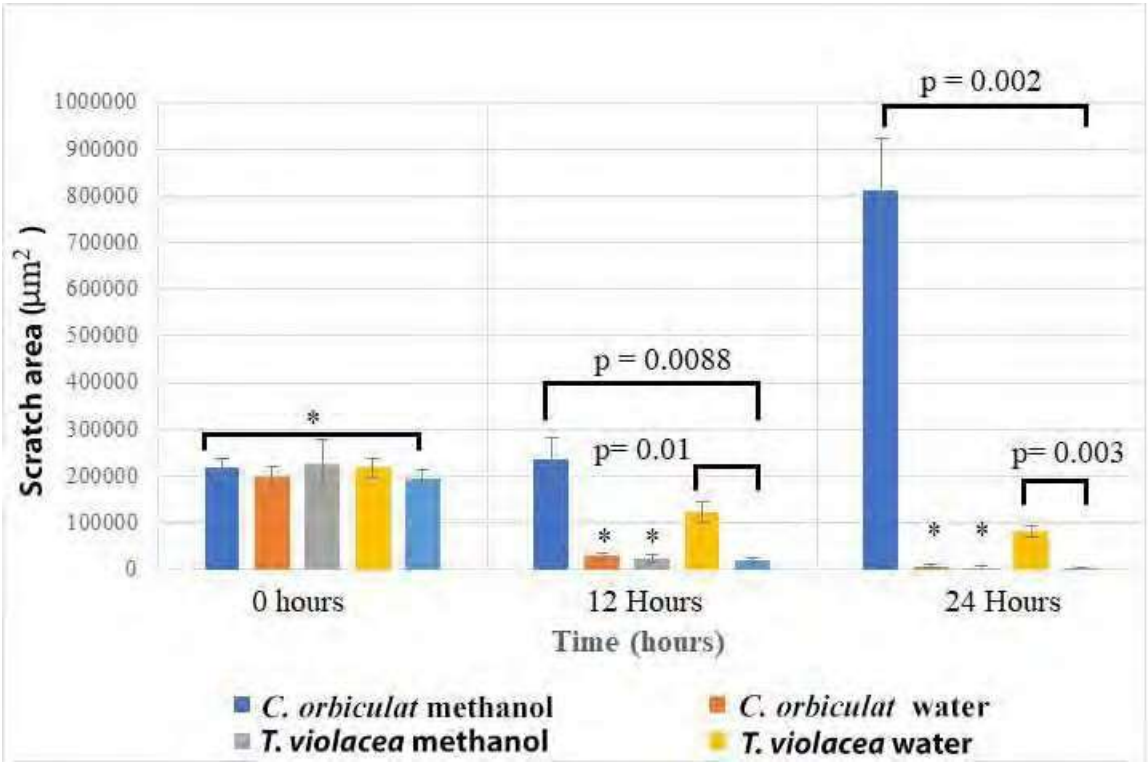

Figure 3.21 depicts the changes in the area of a scratch created in a monolayer of MDA-MB231 cells following treatment with various plant extracts. The graph shows the scratch area at different time points (0, 12, and 24 h) after treatment. At the start of the experiment (0 h), there was no significant difference in the scratch area between untreated cells and cells treated with the different extracts. However, after 12 h of treatment with *T. violacea* water-soluble extract and *C. orbiculata* methanol-soluble extract, a significant reduction in the scratch area was observed compared to untreated cells, indicating inhibition of cell migration. This effect persisted at the 24-hour time point for these two extracts. The complete absence of scratch closure in the cells treated with the *C. orbiculata* methanol-soluble extract was likely due to increased cell death induced by the extract. An asterisk (*) indicates no significant difference in the scratch area compared to untreated control cells.

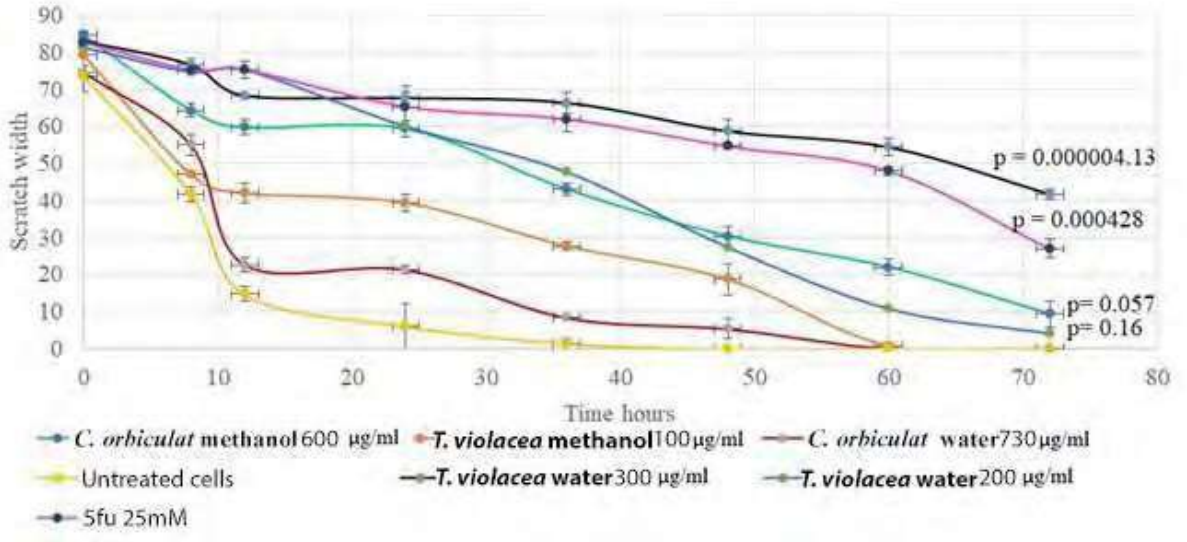

Figure 3.22 depicts the assessment of the effects of various extracts on the migration of triple-negative breast cancer (TNBC) cells using a scratch assay. The distance between the leading edges of a scratch created on the cell monolayer was measured over 72 h. The assay included a positive control (5FU) and two different concentrations of the *water-soluble T. violacea* extract. Notably, treatment with *T. violacea* extract at a concentration slightly below the IC50 value (300 µg/ml) significantly impeded cell migration, effectively halting it completely. At lower concentrations, cell migration was delayed by up to 13 h compared with that in the untreated control. The effects observed with the *T. violacea* extract were comparable to those observed with the positive control, 5FU. Remarkably, at the end of the 72-hour period, none of the other extracts tested, even at concentrations below their respective IC50 values, exhibited any discernible influence on TNBC cell migration.

Figure 3.23 displays the results of the scratch assay on normal MCF-10A breast cells treated with *T. violacea* water-soluble crude extract, while Figure 3.24 shows the temporal changes in the scratch area for both treated and untreated MCF-10A cells. These results indicate that the scratches in untreated MCF-10A cells healed more rapidly than those treated with the extract. However, as anticipated, the closure rate did not match that of MDA-MB231 cells (Figure 3.21). The treated MCF-10A cells exhibited slower migration than untreated cells, yet the wound in both was nearly completely healed within 3 h post-treatment. This suggested that the extract affected the migration of MCF-10A cells, although the effect was less pronounced than on MDA- MB231 cells.

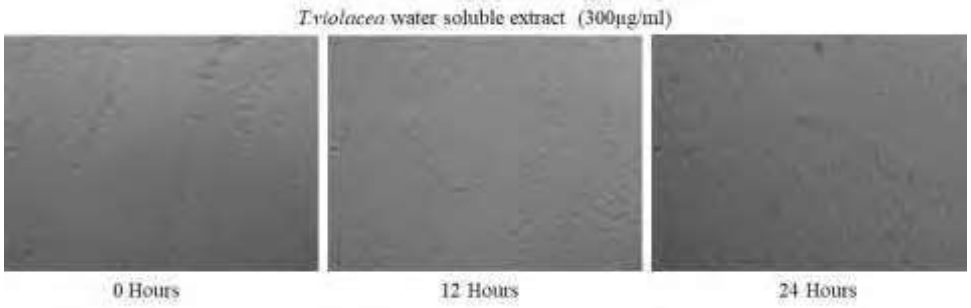

Figure 3.23 depicts the results of a scratch assay performed on MCF-10A cells, which are normal breast cells. The assay was used to test the effect of the *water-soluble T. violacea* extract on cell migration in normal cells. The figure consists of three panels, each representing different time points: 0, 12, and 24 h. The panels show the progression of scratches and wounds over time. At the 0-hour time point, a clear scratch or wound was visible in the cell monolayer. By the 12-hour time point, the wound had started to close, and by the 24-hour time point, the wound was nearly completely closed. The figure legend provides a concise and informative description of the experiment and its results. A scratch assay was performed on MCF-10A cells to test the effect of the *T. violacea* water-soluble extract on cell migration in normal breast cells. The legend also shows that the wound was nearly completely closed by 24 h, suggesting that the extract had only a minimal impact on cell migration.

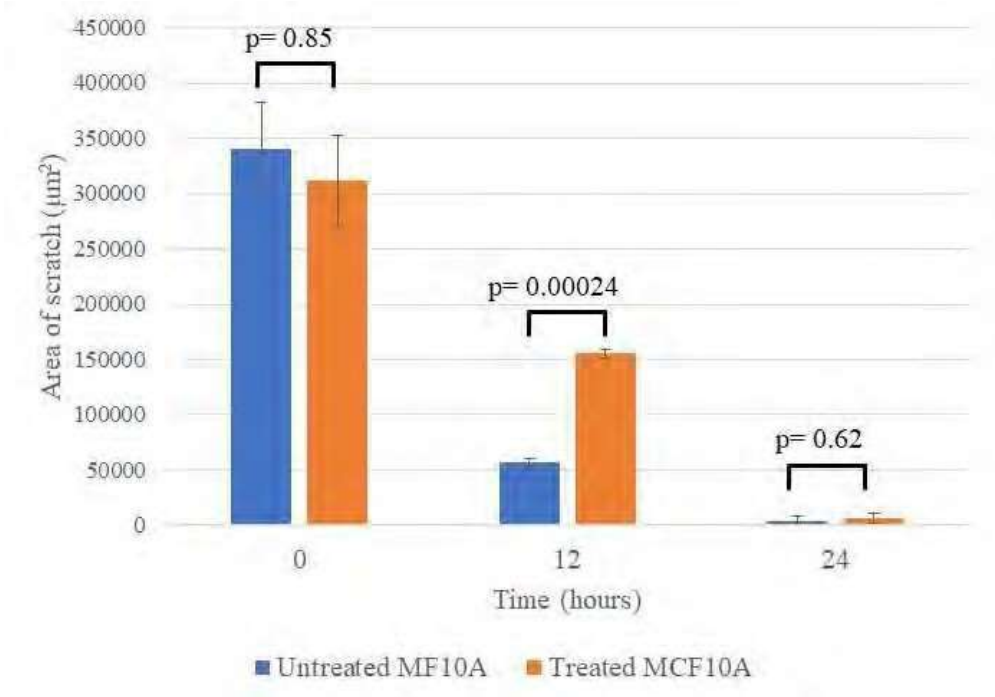

Figure 3.24 depicts the results of a scratch assay performed on MCF-10A cells, which are normal breast cells. The assay was used to test the effect of the *T. violacea* water-soluble extract on cell migration in these normal cells. The figure consists of three panels, each representing a different time point: 0 hours, 12 hours, and 24 hours. The panels show the progression of the scratch or wound over time. At the 0-hour time point, a clear scratch or wound is visible in the cell monolayer. By the 12-hour time point, the wound has started to close, and by the 24-hour time point, the wound is nearly completely closed. The figure legend provides a concise and informative description of the experiment and its findings. It states that the scratch assay was performed on MCF-10A cells to test the effect of the *T. violacea* water-soluble extract on cell migration in normal breast cells. Untreated normal breast cancer cells migrate at a slower rate than triple-negative breast cancer (TNBC) cells. Additionally, the treatment of cells with the water-soluble *T. violacea* extract resulted in a

reduced migration rate at 12 h post-treatment, but by the 24-hour mark, the wound was nearly fully closed in both treated and untreated cells.

3.12 Migration assay using RTCA cell invasion and migration assay plates

The RTCA Cell Invasion and Migration Plate uses RTCA technology to track the migration of cells from the upper chamber into the lower chamber through a membrane filter. This leads to an elevation in the cell impedance reading, which serves as a direct measure of the cell population on the surface of the plate in the lower chamber. Consequently, it serves as a reliable indicator of the number of migrating cells. The experiment was configured using MDA-MB231 TNBC cells treated with *T. violacea* water extract, one at a concentration slightly lower than the IC_{50} concentration, and a control lacking any media containing serum as a chemoattractant in the lower chamber. Figure 3.25 depicts the results of this assay. The graph depicts the increase in cell impedance following the movement of MDA-MB231 cells into the lower chamber. The cells with no chemoattractant in the lower wells showed very low levels of migration, with a CI at 50 h after treatment, less than a quarter that of the untreated cells with chemoattractant. When TNBC cells were treated with the extract at a concentration of 300 µg/ml, their ability to migrate into the bottom chamber was significantly reduced.

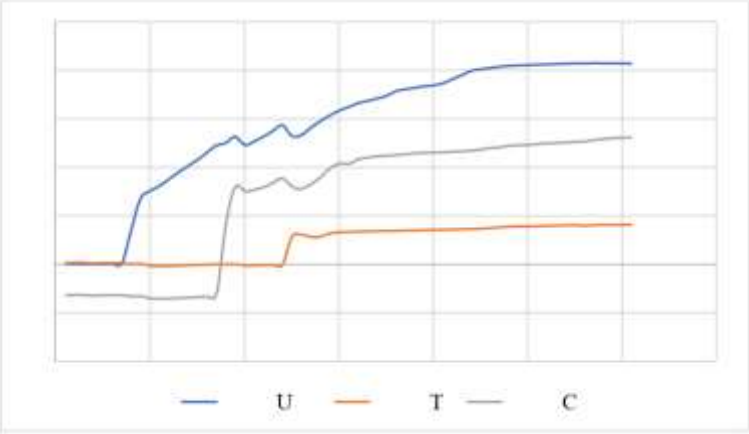

Figure 3.25 Figure 3.25 depicts the results of an RTCA cell migration assay examining the effect of the *T. violacea* water-soluble crude extract on MDA-MB231 triple-negative breast cancer cells. The graph shows the changes in cell index over time, which correlates with cell migration, for three conditions: untreated cells with a chemoattractant in the lower chamber to induce migration, untreated cells without a chemoattractant as a control, and cells treated with *T. violacea* extract in the presence of a chemoattractant. Untreated cells exposed to the chemoattractant exhibited the highest

increase in cell index, indicating robust migration. In contrast, the extract-treated cells showed the lowest cell index values, even in the presence of a chemoattractant, demonstrating potent inhibition of cancer cell migration by the plant extract.

3.13 Cell invasion assays

The ability to infiltrate, as observed by the forceful penetration of the thick extracellular matrix (ECM), which comprises basement membranes and stromal compartments, is a key factor in why metastasis is the major cause of cancer death [245]. To develop strategies to effectively inhibit cancer cell invasion, it is essential to establish assays that offer quantitative and reproducible assessments of the invasive behaviour of cancer cells. These assays are vital for uncovering the molecular mechanisms driving cancer cell invasion and for identifying potential therapeutic targets. These were also used to select the most effective inhibitors. Considering the complex nature of cancer cell invasion in vivo, which involves dynamic interactions with various microenvironmental components, such as angiogenic blood vessels, fibroblasts, and inflammatory cells, which are indispensable tools in enhancing my understanding and formulating intervention strategies [246]. While it is difficult to replicate the complexity of cancer cell invasion in simple in vitro assays, it is possible to create assays that focus on different parts of the invasion process. In this context, two specific assays were conducted to determine whether treatment with water-soluble *T. violacea* extract had any impact on the invasive potential of TNBC cells through an extracellular matrix (ECM) analogue.

3.14 Boyden dye-based assay

These experiments were performed using Boyden assay. Boyden's chamber experiment is a commonly used technique to study cellular migration and invasion in response to a range of stimuli [247]. Readily accessible polymeric inserts, tailored for multi-well plates and typified by Transwell® Permeable Supports, provide a method for performing exact and consistent invasion experiments. When these inserts were placed in a multi-well tissue culture plate, they created a dual-chamber system partitioned by a cell-permeable membrane. This membrane, measuring 10 µm in thickness, incorporates uniformly distributed pores with a preset diameter. The pore dimensions were

intentionally selected to be narrower than the diameters of both the MCF-10A and MDA-MB231 cells. Following this, the pores were lined with an ECM-simulative gel crafted to emulate the typical matrices confronted by neoplastic cells during the invasion process in vivo. MCF-10A and MDA-MB231 cells were added to the upper wells with media containing no serum. Serum-containing media was added to the bottom well as a chemoattractant. Both cell lines were subjected to either no treatment or treatment with 350 µg/ml water-soluble *T. violacea* extract. Quantitative invasion was evaluated by tallying the cells that traversed the cell-permeable barrier by infiltrating the ECM layer. The absorbance of the dye picked up by invading cells in the lower chamber was used to calculate the number of cells. Figure 3.20 illustrates the results of this assay. The ability of MCF-10A cells to penetrate the ECM layer and invade was unaffected by the extract. This ability of the NCF10A cells was less than that of the untreated MDA-MB231 cells, which readily invaded the lower chamber and penetrated the ECM as they moved towards the chemoattractant. Treatment with a concentration of the water-soluble extract lower than the IC_{50}, on the other hand, leads in a considerable decrease in the capacity of TNBC cells to invade the lower chamber is observed. This suggests that the *water-soluble extract of T.* violacea inhibits TNBC cell invasiveness.

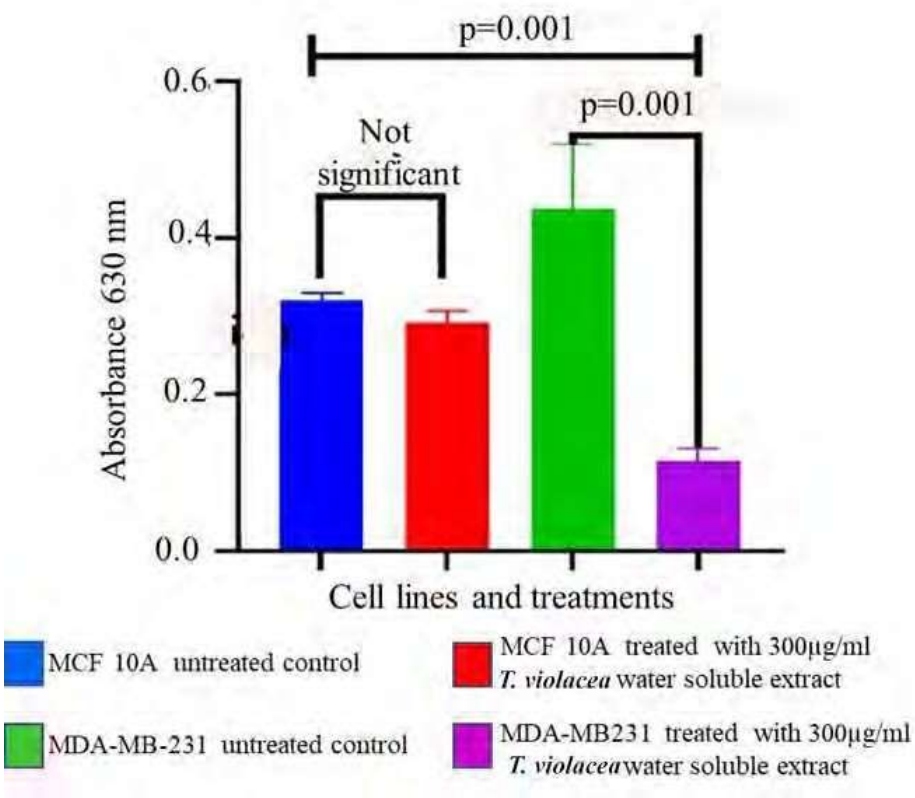

Figure 3.26 presents a bar graph depicting the results of a cell invasion assay that measured the ability of MDA-MB-231 triple-negative breast cancer cells and MCF-10A normal breast cells to invade through an extracellular matrix (ECM) analogue called Geltrex™. The y-axis represents absorbance values, which correlate with the number of cells that successfully invaded the ECM layer. Untreated MDA-MB-231 cancer cells exhibited high absorbance readings, indicating robust invasion through the matrix. In contrast, when MDA-MB-231 cells were treated with *T. violacea* water-soluble plant extract, the absorbance values were significantly lower, suggesting potent inhibition of cancer cell invasion by the extract. Importantly, extract treatment did not affect the invasion of normal MCF-10A breast cells, as evidenced by the comparably low absorbance values in both untreated and treated conditions for this cell line.

3.15 3.4.2.2.Invasion assay using RTCA cell invasion and migration assay plates

The RTCA Cell Invasion and Migration Plate operated in a manner similar to the inserts used in the previously described assay. However, it utilises RTCA technology to track the migration of cells into the lower chamber, where they infiltrate an ECM analogue and attach to the surface of the lower chamber. As a result, there is an increase in the cell impedance reading, which serves as a direct indicator of the number of cells present on the surface of the plate. The experiment was set up in a similar way to the above experiment, with the MDA-MB231 TNBC cells treated with a concentration of *T. violacea* water extract at a concentration slightly lower than the IC_{50} concentration and a control

lacking any media containing serum as a chemoattractant in the lower chamber. Figure 3.21 depicts the results of this assay. The graph depicts the increase in cell impedance following the movement of MDA-MB231 cells through the ECM into the lower chamber. The cells with no chemoattractant in the lower wells showed very low levels of invasion, with a CI at 50 hours after treatment less than a fifth that of the untreated cells with chemoattractant present. TNBC cells were significantly less able to penetrate the bottom chamber after exposure to of 300 µg/ml. The behaviour of the treated and untreated cells remained comparable for up to 20 h following treatment.

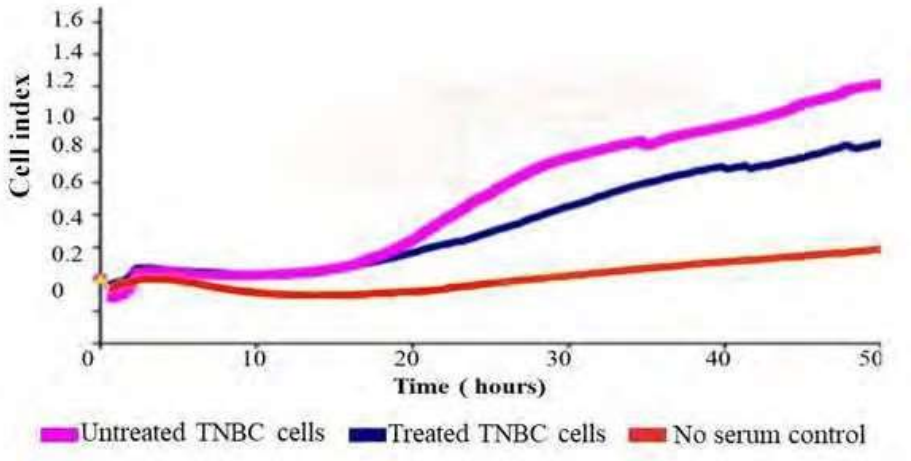

Figure 3.27 depicts the results of an invasion assay examining the effect of the water-soluble extract of *T. violacea* on the invasive ability of MDA-MB-231 triple-negative breast cancer cells. The graph shows the changes in the cell index over time, which correlates with the number of cells invading through an extracellular matrix (ECM) layer. There are three lines representing different conditions: untreated TNBC cells allowed free invasion, TNBC cells treated with *T. violacea* water extract, and a control condition without any chemoattractant in the lower chamber to induce invasion. The untreated TNBC cells exhibited a steady increase in the cell index, indicating robust invasion through the ECM layer. In contrast, *T. violacea* water extract substantially inhibited this invasive capability, as evidenced by the significantly lower cell index values for extract-treated cells compared to untreated controls over the course of the experiment.

3.16 Cell adhesion assays

Cellular attachment is critical for controlling cell activity and tissue formation. Cellular attachment is critical in controlling cell activities and tissue formation. Diminished cell stickiness in cancerous cells leads to the disruption of the histological architecture, a significant characteristic of malignant neoplasms. The control of cellular adhesion involves intricate interplay among cells, the extracellular matrix (ECM), and signaling pathways, and understanding these processes is vital for devising

targeted therapeutic strategies. Furthermore, signals from adhesion junctions can interact with traditional signal transduction pathways to assist in the control of cell growth and differentiation. Furthermore, signals from adhesion junctions can interact with traditional signal transduction pathways to assist in the control of cell growth and differentiation [248]. Dynamic management of cellular attachments to the ECM is vital for cell proliferation, differentiation, and mobility, whereas attachments between adjacent cells facilitate sorting, rearrangement, and polarisation within multicellular structures [249].

Neoplastic cells demonstrate alterations in their attachment to the ECM and these modifications are frequently linked to their invasive and metastatic capabilities. An adhesion experiment was performed to assess the effect of *water-soluble T. violacea* leaf extract on cell attachment in the triple-negative breast cancer cell line MDA-MB-231 and the normal breast cell line MCF-10A. This assay utilised GeltrexTM as an ECM substitute and measured the number of cells capable of adhering to this substrate, both before and after treatment. Adherent cells were quantified using a dye-uptake assay. Figure 3.28 presents the findings of this assay, showing that the extract increases the attachment of MDA-MB-231 cells to an ECM substitute, resulting in a greater number of these cells adhering to the matrix compared to both treated and untreated normal breast cells. Moreover, treatment of normal cells did not affect their attachment to the ECM. As anticipated, untreated MDA-MB-231 cells exhibited less attachment to the synthetic ECM than normal breast cells. These observations suggest that *T. violacea* crude water-soluble extracts bolster cell attachment in TNBC cells.

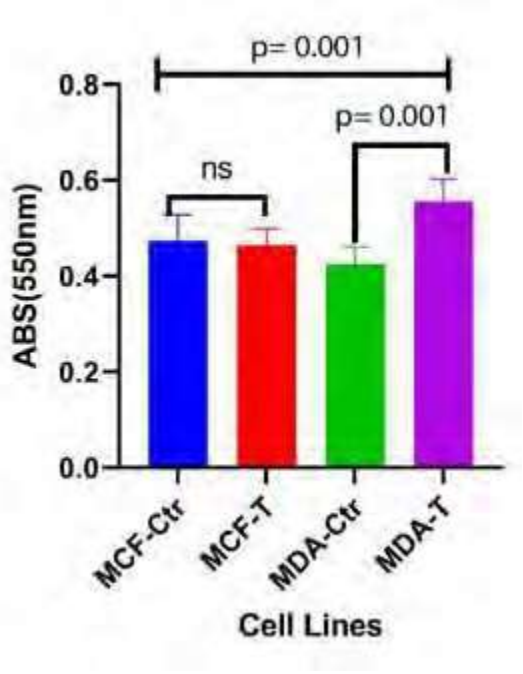

Figure 3.28 a bar graph depicting the cell adhesion levels of different cell lines to the Geltrex™ matrix. The y-axis represents cell adhesion in arbitrary units (A.U.), whereas the x-axis lists the different cell lines. The graph shows that the MDA-MB-231 cell line had the lowest adhesion to the Geltrex™ matrix in the control group, as indicated by the blue bar. However, the adhesion of this cell line significantly increased after treatment with the *water-soluble extract of T. violacea*, as shown by the purple bar. The figure legend provides a clear and concise description of the key findings, stating that MDA-MB-231 cells had the least adhesion to the matrix surface in the control group, but this adherence was notably increased following treatment with the *T. violacea* water-soluble extract.

3.17 Determination of Antioxidant Activity Using the 2,2-Diphenyl-1-picrylhydrazyl (DPPH) Radical Scavenging Method

The antioxidant capability of the extracts was evaluated using the stable DPPH radical to determine their hydrogen-donating or radical-scavenging activity (2,2-diphenyl-1-picrylhydrazyl). Experiments were conducted following the methodology established by Blois [224]. The decrease in the radical concentration was accompanied by a reduction in the absorbance at 517 nm. A volume of 2 mL of either a methanolic or aqueous methanolic stock solution of the extracts was placed into test tubes, after which 2 mL of a 1 mM DPPH solution was added. The tubes were wrapped in Parafilm and incubated in the dark for one hour. incubation, the absorbance at 517 nm was recorded using a UV-vis spectrophotometre (Jasco V-530). and subsequently compared with the ascorbic acid calibration curve. The results are expressed in milligrams of ascorbic acid equivalent per gram of dried sample.

Each assay was performed in triplicate to ensure precision and consistency. A formula was used to determine the percentage DPPH radical inhibition.

$$I\ \% = ((A0 - A) / A0) \times 100$$

Where:

• I% represents the percentage of DPPH inhibition,

• A0 is the absorbance of the control sample at the beginning of the reaction (t = 0 hours),

• A is the absorbance of the tested sample after the reaction (t = 2 h).

The IC50 value, defined as the amount of sample required to reduce DPPH absorbance by 50%, was graphically estimated for *T. violacea* and *C. orbiculata* water and methanolic solutions at various

concentrations.

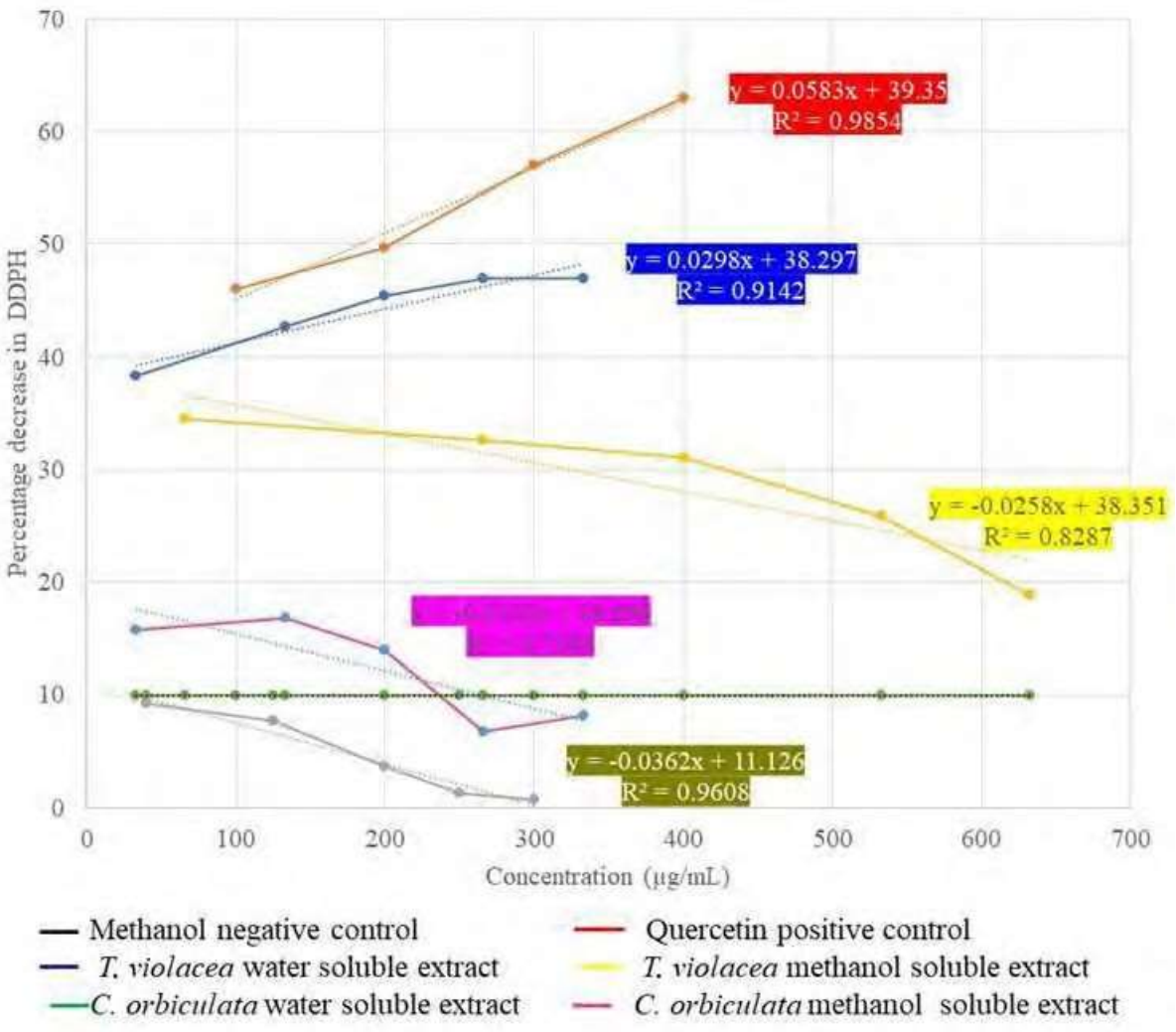

Figure 3.29 depicts the antioxidant activity of various plant extracts, including the *T. violacea* water-soluble extract, *T. violacea* methanol-soluble extract, C. orbiculata water-soluble extract, and C. orbiculata methanol-soluble extract, as determined by the DPPH antioxidant assay. The graph presents the percentage decrease in DPPH, a measure of antioxidant activity, plotted against the extract concentration. Linear regression equations and R-squared values for each extract are provided, indicating the strength of the relationship between the extract concentration and antioxidant activity. Notably, the *water-soluble extract of T. violacea* exhibited antioxidant activity comparable to that of the positive control quercetin, as evidenced by their similar slopes and R-squared values, suggesting that this extract possesses potent antioxidant properties.

Figure 3.29 represents the results of this assay. The negative control should have very little antioxidant activity, as reflected by the near-flat line with a very small slope. The height of the intercept reflects that the reaction conditions most likely have a slight antioxidant activity. Most of

the extracts, except for the *water-soluble T. violacea* extract, showed antioxidant activity. This extract had a Y-intercept similar to that of the positive control, quercitin. However, as the concentration of quercetin increased, the antioxidant activity increased rapidly, whereas an increase in the concentration of the extract resulted in only a small increase in anti-oxidant activity. All other extracts showed an inverse relationship between the concentration and antioxidant activity. The methanol extract of *T. violacea* showed high activity at low concentrations, and this decrease with increasing concentration may be due to the solvent. The other two extracts showed lower activity than the methanol control, even at the lowest concentrations.

3.18 Determination of the molecular composition of the *T. violacea* water soluble extract

Indeed, *T. violacea* contains allylsulfur compounds, typical of the onion and garlic families. Among these compounds, marasmicin is one of the most prevalent in *T. violacea* [206]. The range of chemicals found in *T. violacea* was impressive. Beyond the allylsulfur compounds previously mentioned, the plant also harbours free sugars, such as arabinose, rhamnose, and xylose, along with glycosides, such as methyl-D-glucopyranoside. Adding to *T. violacea*'s chemical diversity, it contains phenolic substances including flavonoids, gallotannins, condensed tannins, and saponins. These compounds, known for their varied biological activities, may contribute significantly to the potential medicinal attributes of the plant [250].

3.19 FITR to examine the biological materials.

Fourier-transform infrared spectroscopy (FTIR) has distinct advantages over conventional dispersive spectroscopy offered an enhanced signal-to-noise ratio at specific resolutions and achieved greater frequency accuracy by employing mathematical data conversion from the time domain to the frequency domain. This conversion allows for the interpretation of the percentage of light transmitted through a sample plotted against the wavelength of light. The dips observed in this spectrum indicate the wavelengths at which the sample absorbs light, and different chemical bonds and compounds are known to absorb light at different wavelengths.

Figure 3.29 shows the Fourier spectra obtained from the FITR analysis of the extracts from *C. orbiculata.* These spectra were obtained for light with wavelengths ranging from 600 cm1 to 4000 cm1. The water-soluble *C. orbiculata extract* contained compounds with amine and amide bonds, as well as ethers. Overall, the spectrum contained very few absorbance peaks, which may indicate either the presence of very few compounds or a fairly homogenous mixture of very similar compounds with very similar chemical bonds. The spectrum of the methanol-soluble extract showed a much more diverse collection of compounds with many absorption peaks. The peak at 3400 cm1 is representative of alcohols, the N-H bond of amines, or the OH stretch of carboxylic acid. The peaks observed at 300 cm^{-1} in the spectrum correspond to CH3 bonds typically found in alkanes. This assignment is corroborated by the presence of a peak at 1500 cm^{-1}, which further supports the presence of alkanes in the sample. Moreover, the spectral peak observed at 1200 cm^{-1} can be attributed to the carbon-hydrogen bonds characteristic of alkanes, providing additional evidence for their presence in the sample. Finally, the peak detected at 1050 cm^{-1} is indicative of the carbon-oxygen bonds commonly associated with ketones or the CO bond typically found in ethers.

Figure 3.30 displays the Fourier spectra acquired through FITR analysis of the extracts derived from *T. violacea* leaves. These spectra were obtained for light with wavelengths ranging from 600 Cm^{-1} op 4000 Cm^{-1}. Both the water-soluble *and* methanol-soluble *T. violacea* extracts were shown to be diverse collections of compounds with many absorption peaks. In both extracts, there is a common peak between 3500 and 3250 $cm^{-1,}$ which represents the OH bond of alcohols or the NH bond of amides. This peak was slightly shifted in the methanol extract and may also represent the OH stretch of carboxylic acid or the N-H bond of amines. At 3000 Cm^{-1} in the methanol-soluble extract, there was a peak that could represent the OH stretch of carboxylic acid once again and a peak at 2900, which could represent the CH stretch of alkanes. The presence of carboxylic acid in this extract was indicated by the peak at 1600 cm^{-1} which may represent the compound's CO bonds. The range of small peaks in the methanol-soluble extract that occurred around 1500 cm^{-1} represented the C-H stretch of alkenes, CN stretch of amines, CF stretch of alkyl halides, and nitro group of various compounds. The large peak at 100 cm^{-1} in this sample may represent the PH bond of phosphates, the C-O-C bond

of ethers, the CN stretch of amines, or the C-F stretch of alkyl halides. The presence of alkyl halides in the water-soluble extract is also indicated by a peak at 1400 cm^{-1}. Peaks at 1600 cm^{-1} and 100 cm^{-1} indicate the presence of the NH bond of amines and the C-O-C bond of esters, respectively.

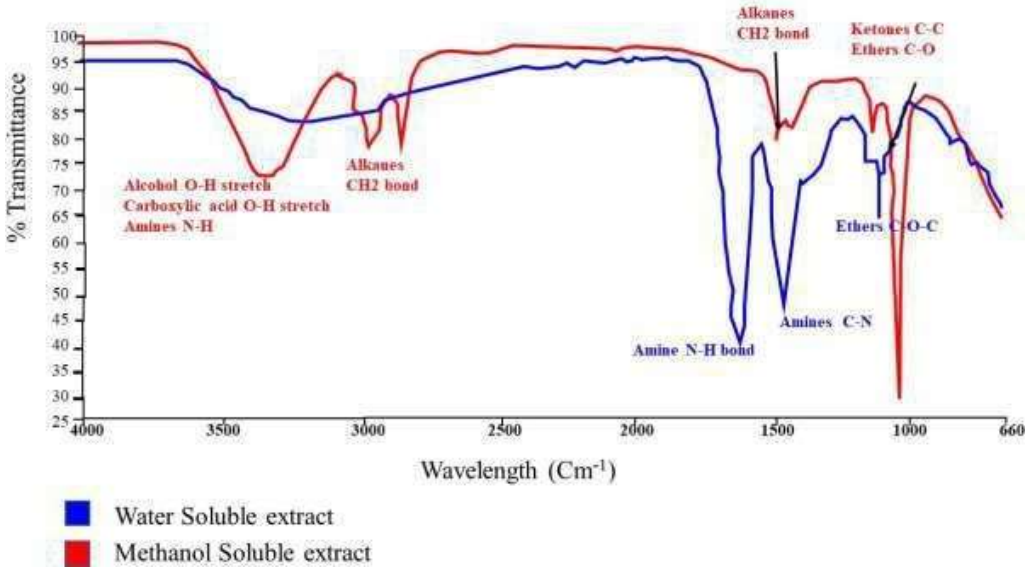

Figure 3.30 shows the Fourier-transform infrared (FTIR) spectra of the water-soluble and methanol-soluble extracts from *C. orbiculata*. The blue line represents the water-soluble extract, which appears relatively featureless with a few distinct absorption peaks, suggesting that it contains either a limited number of compounds or a mixture of very similar compounds belonging to a few chemical classes. In contrast, the red line depicts the methanol-soluble extract, exhibiting a much more complex spectrum with numerous absorption peaks, indicating the presence of a diverse array of different compounds, likely representing a wider range of chemical classes.

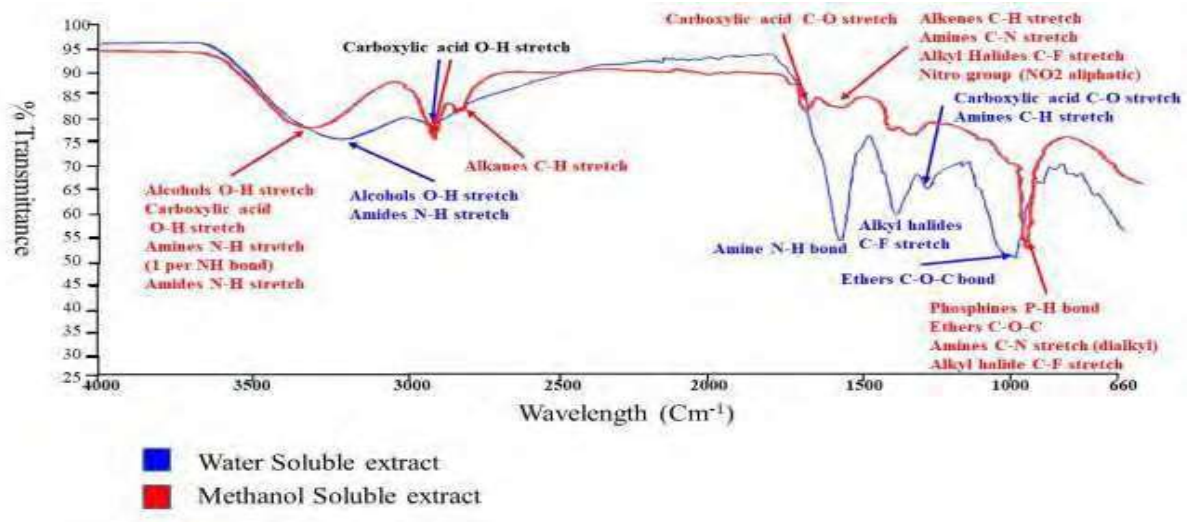

Figure 3.31 shows the Fourier-transform infrared (FTIR) spectra of the water-soluble and methanol-soluble extracts from Tulbaghia violacea. The blue line represents the water-soluble extract, which appears relatively

featureless with few distinct absorption peaks, suggesting it contains either a limited number of compounds or a mixture of very similar compounds belonging to a few chemical classes. In contrast, the red line depicts the methanol-soluble extract exhibiting a much more complex spectrum with numerous absorption peaks, indicating the presence of a diverse array of different compounds likely representing a wider range of chemical classes.

3.20 Gas Chromatography mass spectrophotometry

Gas chromatography-mass spectrometry (GC-MS) is a well-known and widely used technology for the identification of a wide range of chemicals in plant extracts. This method has proven to be effective in detecting and characterising a range of substances, including alkaloids, flavonoids, organic acids, and amino acids [251]. GC-MS has solidified its role as a crucial tool in secondary metabolite profiling across various biological species, both plant-based and otherwise [252]. Renowned for its combined analytical approach, GC-MS is acclaimed for its speed, accuracy, and precision in identifying diverse chemicals in medicinal plants [253]. This approach is also useful for identifying the overall chemical composition of plant extracts [254], and has been particularly useful for the separation and analysis of specific compounds, such as galanthamine-type alkaloids [255]. Moreover, its proficiency in analysing organic and amino acids makes it invaluable for studies focusing on the efficacy and toxicity of these compounds [256].

Figure 3.31 illustrates the mass charge spectrum produced from the GC-MS analysis of the water-soluble *T. violacea* extract. Approximately 36 compounds were identified during this process. A catalogue of some of these compounds along with their respective spectra is provided in Table 2.3.

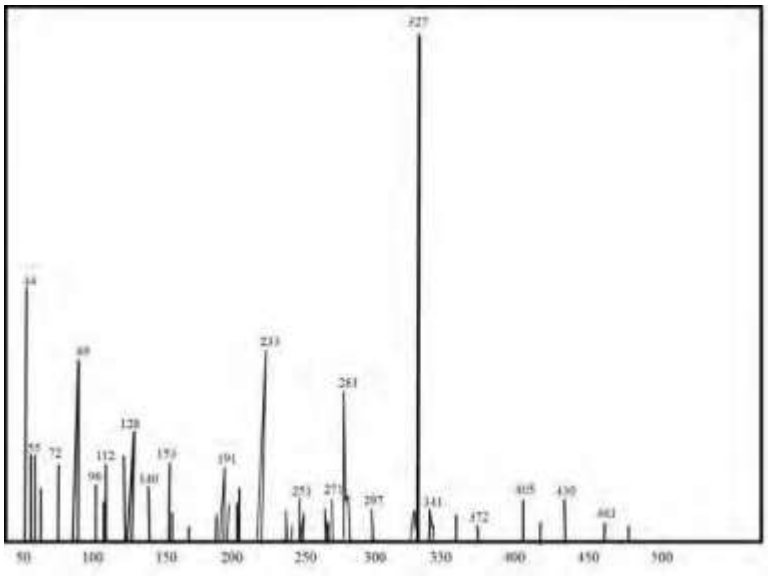

Figure 3.32 shows the mass charge spectrum for the water-soluble extract of *T. violacea*. The x-axis represents the mass-to-charge ratio (m/z) of the detected ions, and the y-axis indicates the relative abundance or intensity of the ions. The spectrum displayed a series of peaks, each corresponding to a specific ion or compound present in the water-soluble extract. Notable peaks were observed at m/z values of 327, 313, 281, 251, 227, 207, 191, 141, 130, 112, 72, and 50, with the largest peak at m/z 327 likely representing the most abundant compound in the extract.

Table 3.2 GC MS spectral of some compounds identified in the MS analysis of the methanol soluble fraction of *T*.

violacea

OXiMe-, methoxrphenyl	Vanillin
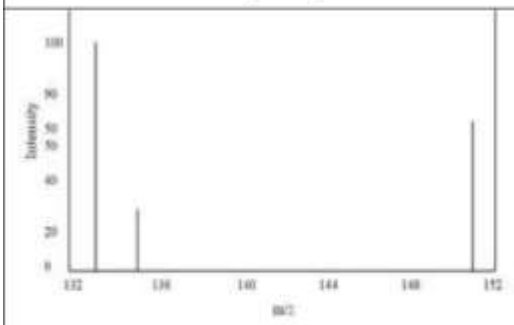	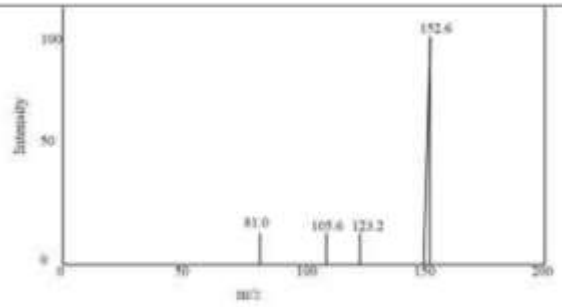
Benzaldehyde, 4-(I-methy-lethyl)-(cuminaldehyde)	4H-Pyran-4-one, 2,3-di hydro-3,5-dihydroxy-6-meth-yl-(DDMI)
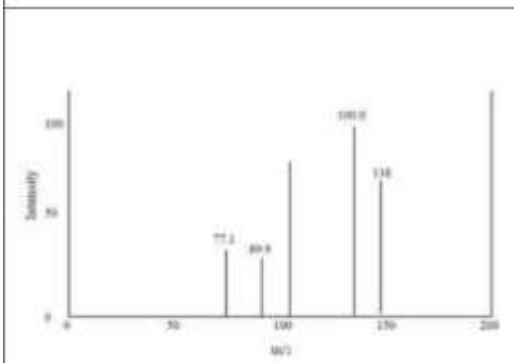	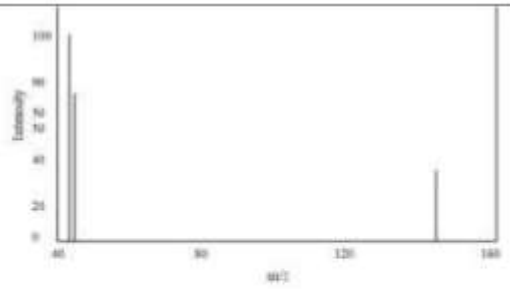
1,2,4-Triazine-3,5(21-1,4H)-di-one (6-a zauracil)	Pyrrolidine
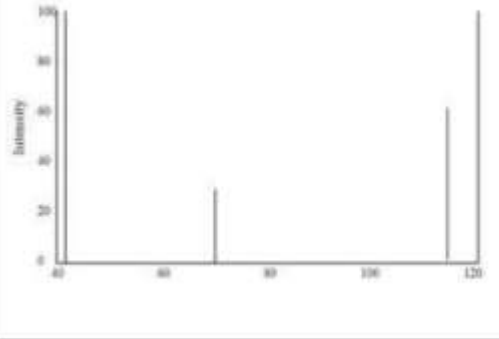	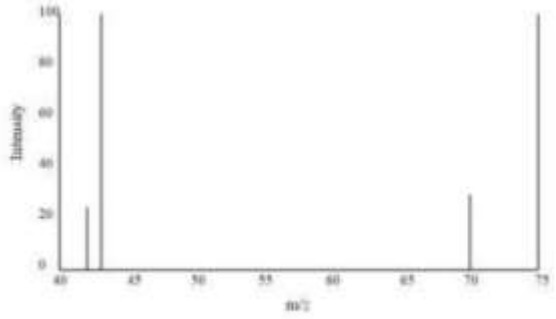
Schizandrin	Taurolidine

OXiMe-, methoxrphenyl	Vanillin
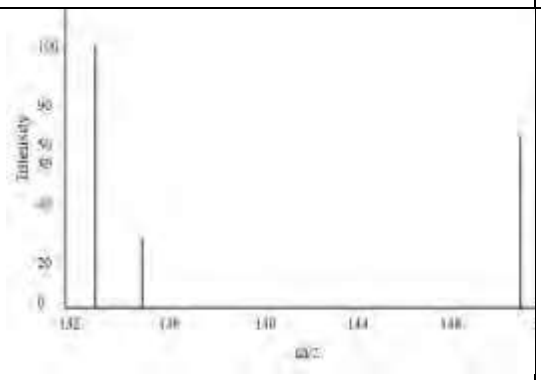	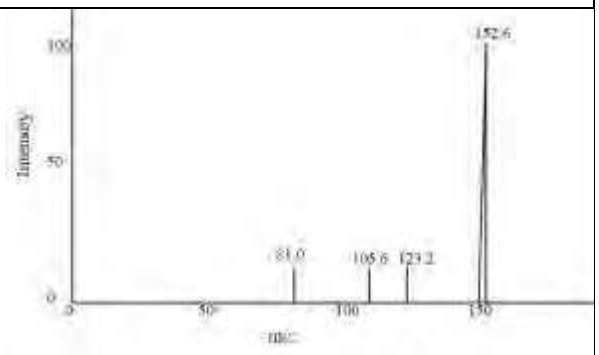
Benzaldehyde, 4-(I-methy-lethyl)- (cuminaldehyde)	4H-Pyran-4-one, 2,3-di hydro-3,5- dihydroxy-6-meth-yl-(DDMI)
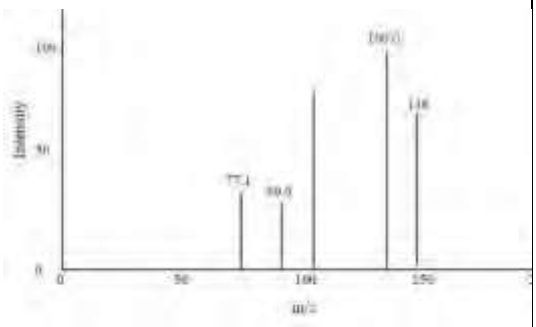	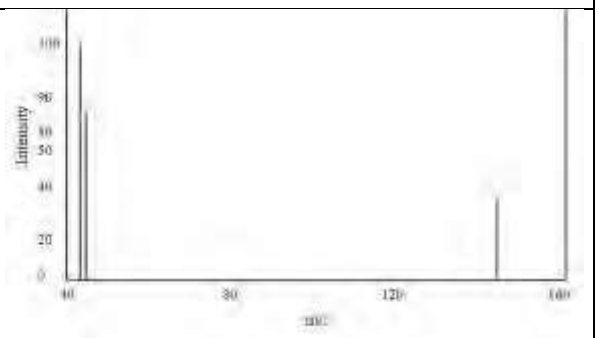
1,2,4-Triazine-3,5(21-1,4H)-di-one (6-a zauracil)	Pyrrolidine

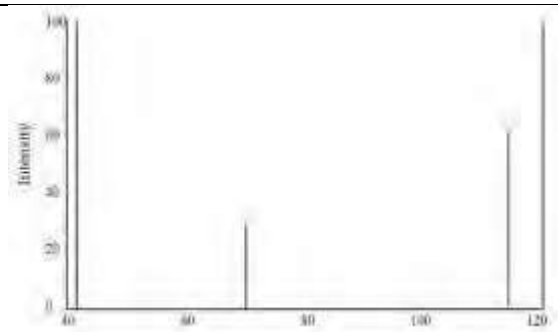	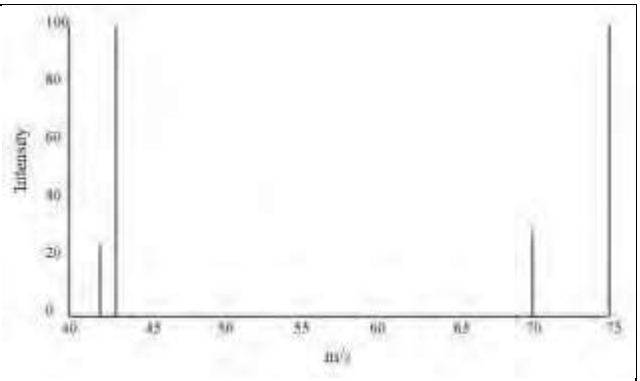
Schizandrin	Taurolidine
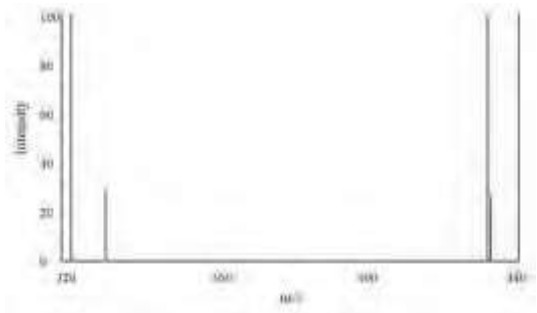	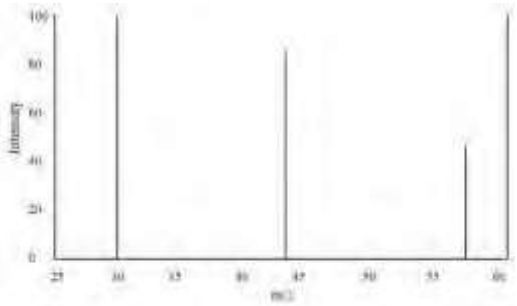
Alpha Pinene	
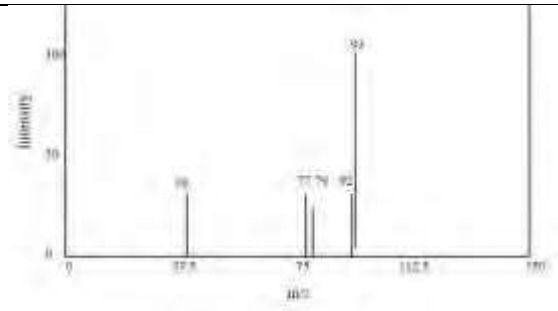	

3.21 NMR Spectroscopy

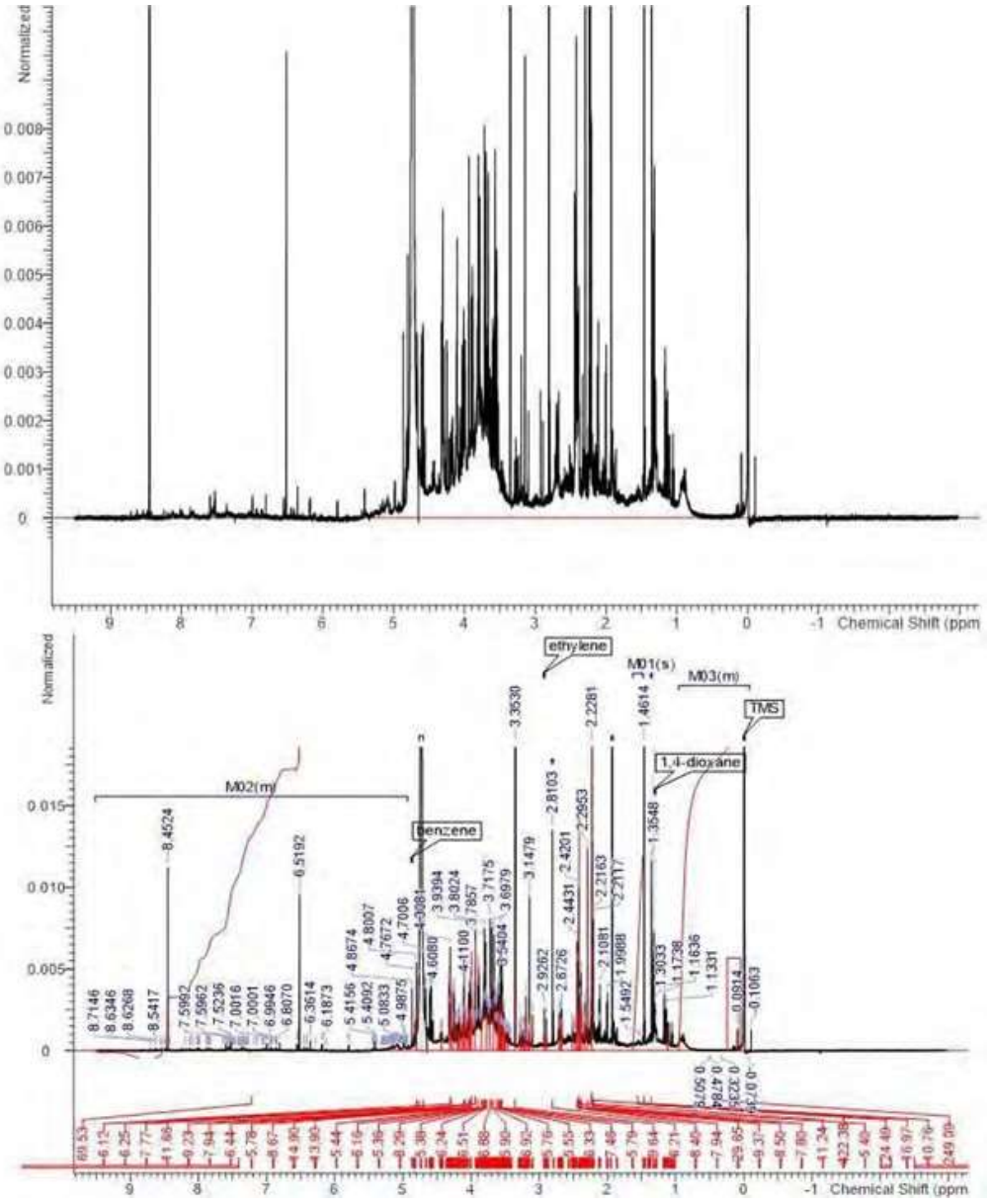

Figure 3.33 shows the nuclear magnetic resonance (NMR) spectrum of the water-soluble extract from the plant *T. violacea*. The x-axis represents the chemical shift in parts per million (ppm), indicating the magnetic environment of atomic nuclei in the molecules present in the extract. The y-axis displays the signal intensity or relative abundance of nuclei experiencing each chemical shift. The spectrum revealed a series of peaks at different chemical shift values, with the most prominent peaks labelled, suggesting the presence of various compounds or functional groups in the water-soluble extract of *T. violacea.* This NMR spectrum provides valuable information about the chemical composition and structure of the bioactive molecules present in the extract.

Table 3.3 Examples of compounds detected by NMR analysis of the crude water-soluble *T. violacea* extract.

Compound	Formula	FW	MF (multi spec)	Max $d_N(^1H)$	Acquisition time (sec)
4H-Pyran-4-one, 2,3-dihydro-3,5-dihydroxy-6-methyl-	C6H4O2	96.0841	0.90	0.353	2.1999
1,2,4-Triazine-3,5(2H,4H)-dione	C3H3H3O2	113.0748	0.91	0.179	2.1889
d-Glycero-d-galacto-heptose	C7H16O7	212.1977	0.86	0.144	2.1889
Benzaldehyde, 4-(1-methylethyl)-	C7H6O	106.1219	0.88	0.468	2.1889
Vanillin	C8H8O3	152.1473	0.34	0.347	2.1889
Oxime-, methoxy-phenyl	C21H32O2	332.4770	0.942	0.347	2.1889
Pyrrolidine	C4H9N	71.1210	0.83	0.615	2.1889
Schizandrin	C23H25O7	416.4642	0.81	1.017	2.1889
Taurolidine	C7H16N4O4S2	284.3563	0.87	0.487	2.1889
alpha.-Pinene	C15H16Cl3N3O2	376.6654	0.00	0.229	2.1889

Figure 3.33 shows the NMR spectrum obtained from the analysis of the water-soluble *T. violacea* extract. This analysis identified approximately 61 separate compounds, including all the compounds initially identified using GC-MS. While the GC-MS spectra only clearly indicated the presence of 31 compounds, the small, unclear peaks indicated that there may be other compounds present in smaller amounts or that they were not being effectively separated by GC. These compounds appeared to be easily identified by NMR analysis. A list of some compounds exclusively detected by NMR analysis is presented in Table 3.1

Combining the results of the GC-MS and NMR analyses, I obtained a list of 51 compounds. Some of these compounds have known anticancer activities. These compounds and the details of their anticancer activities of the compounds are listed in Table 3.4. Other compounds have known

medicinal uses and applications. These are listed in Table 3.5 with the known medical applications. Table 3.6 lists those compounds with known applications that are not medical in nature, while Table 3.7 lists those compounds identified with no known application.

Table 3.4 Compounds with known anti-cancer activity.

Phytochemical compound	RT (min)	Exact mass	Formula
4H-Pyran-4-one, 2,3-dihydro-3,5-dihydroxy-6-methyl- (DDMP)	4.4	144.12	C6H8O4
4H-Pyran-4-one, 2,3-dihydro-3,5-dihydroxy-6-methyl (DDMP) exhibits significant antioxidant properties, effectively neutralizing free radicals [257]. It also has anti-proliferative and pro-apoptotic actions in cancer cells via blocking the NF-B pathway [258]. This inhibition helps to modulate apoptosis, affecting cell growth and survival [259]. The compound's ability to inhibit NF-B signaling underlines its potential for cancer treatment, particularly in oesophagus and lung malignancies [258]. Overall, DDMP's multifaceted action on oxidative stress and apoptosis underlines its therapeutic promise.			
1,2,4-Triazine-3,5(2H,4H)-dione	4.5	113.08	C3H3N3O2
The compound 1,2,4-Triazine-3,5(2H,4H)-dione has been found to possess diverse biological activities. It has been shown to suppress the proliferation of microorganisms. Additionally, it has demonstrated the capacity to inhibit tumour progression in both animal models and instances of human acute leukemia [260]. Furthermore, it diminishes the effects of inhibitors on protein and RNA synthesis, and simultaneously obstructs the degradation of chlorophyll and proteins [261]. These findings emphasise the multifarious potential of 1,2,4-triazine-3,5(2H,4H)-dione as an antibacterial, anticancer, and protein synthesis regulating molecule.			
d-Glycero-d-galacto-heptose	4.8		C7H14O7

According to the sources, d-glycero-d-galacto-heptose modulates NF- κB activation, whereas d-mannoheptulose influences d-glucose metabolism in pancreatic islet cells [262] These discoveries highlight the potential of these compounds in influencing both innate immune responses and metabolic processes. Further research is warranted to elucidate the precise mechanisms underlying their effects and to explore their potential therapeutic applications. Additionally, studies have shown that d-mannoheptulose inhibits the metabolism of D-glucose in pancreatic islets [263]. This glucose metabolism inhibition by d-mannoheptulose suggests its potential as a modulator of insulin secretion and glucose homeostasis. Therefore, these compounds hold promise for further investigation in the context of immune modulation and metabolic regulation.

Benzaldehyde, 4-(1-methylethyl)	8.1791	- 148.20	C10H12O

Benzaldehyde, 4-(1-methylethyl), has demonstrated multifaceted effects on various cellular processes, particularly with relation to cancer. Nitoda et al. found that it suppresses melanin formation in cultured murine B16-F10 melanoma cells [264]. Additionally, Kubo et al. isolated benzaldehyde, 4-(1-methylethyl) from cumin and demonstrated its inhibitory effect on mushroom tyrosinase [265]. Furthermore, Ghosh et al. highlighted its anti-neoplastic effect against breast cancer [264]. Tsai et al. also discovered that it can cause apoptosis in human colorectal adenocarcinoma cells by activating pro-apoptotic proteins such caspase 3 and 9, affecting mitochondrial integrity, and decreasing the action of DNA integrity- preserving enzymes [266]. Similarly, Yang et al. and Morshedi et al. demonstrated its capability to suppress human lung squamous cell carcinoma by extensively activating the apoptosis pathway [266]. These findings collectively underscore the potential of benzaldehyde, 4-(1-methylethyl) as a promising candidate for further investigation in cancer therapy.

Vanillin	5.4	152.15	C8H8O3

Vanillin, a natural component found in food, has been shown to possess various beneficial properties. It has been demonstrated to exhibit anti-mutagenic and anti-metastatic characteristics [267]. Vanillin acts to suppress mutagenesis and cytotoxicity by interacting			
with DNA repair mechanisms [267]. Additionally, it serves as an agent for chemoprevention [268]. Furthermore, vanillin acts as an antioxidant, providing protection to cell membranes against lipid peroxidation (LPO) and preserving DNA from strand breaks [269]. Vanillin has also been shown to inhibit the activation of NF-κB and the production of the cyclooxygenase-2 gene in mice macrophages activated by lipopolysaccharide [270]. Furthermore, vanillin has been shown to limit the invasion and migration of mammary adenocarcinoma cancer cells as well as decrease NF-kappaB activation, hence enhancing TRAIL-induced death [271]. It has also been noted to diminish the expression of metalloproteinase-9 [272]. Vanillin suppresses DNA-PK, an enzyme involved in non-homologous end joining, thereby hindering the process of DNA end-joining [267]. It prevents both in vitro and in vivo metastasis of mouse breast cancer cells [273].			
Oxime-, methoxy-phenyl	5.4	151.16	C8H9NO2
The oxime- and methoxy-phenyl compounds have been found to possess various biological activities. They have been reported to have antibacterial and antioxidant properties [274] and to act as novel anticancer agents [275]. Additionally, the vanillin- derived piperidin-4-one oxime esters have demonstrated antioxidant and antimicrobial properties, with the phenyl ester substituents playing a significant role in their activity [274]. These findings point to the potential of oxime- and methoxy-phenyl compounds in a variety of biological applications, including antibacterial, antioxidant, and anticancer agents.			
Pyrrolidine	5.9	71.12	C4H9N

Pyrrolidine and its derivatives have received substantial research due to its broad biological and pharmacological value, notably in cancer therapy. Pyrrolidine has been shown to inhibit cancer cell proliferation by triggering cell cycle arrest and apoptosis in a time and dosage-dependent way. [276]. Additionally, pyrrolidine compounds have exhibited cytotoxicity against pancreatic cancer cells, although they lacked selectivity for tumour cells [277]. These findings highlight pyrrolidine's ability to reduce oxidative stress and its cytotoxic effects on cancer cells, indicating its potential as a therapeutic agent in cancer treatment. [277].			
Schizandrin	6.0	432.5	C24H32O7

chisandrin B's pharmacological effects have been widely researched. It has been demonstrated to reduce liver fibrosis via modulating the Nrf2-ARE and TGF-/Smad signaling pathways. [278]. Furthermore, Schisandrin B has been shown to decrease the growth of airway smooth muscle cells and to have anti-asthmatic properties [279]. Furthermore, it has been identified for its ability to reduce chondrocyte inflammation and osteoarthritis by suppressing the NF-B and MAPK signal pathways [280]. Schisandrin B has also been found to protect against beta-amyloid and homocysteine neurotoxicity, indicating its potential neuroprotective effects [281]. Furthermore, it has been proposed as a hormetic agent for the prevention of age-related neurodegenerative illnesses through the reduction of oxidative stress and mitochondrial dysfunction [282]. Additionally, Schisandrin B has been reported to alleviate diabetic cardiac autonomic neuropathy Zhang et al. [283] and has showed potential in suppressing osteoclastogenesis and guarding against ovariectomy-induced bone loss [284]. It has also been studied for its ability to reduce the inflammatory response, oxidative stress, and apoptosis caused by traumatic spinal cord damage [285]. Schisandrin B has also been studied for its inhibitory effects on the pharmacokinetics of poziotinib Wang et al. [286] and its potential in reducing Aβ generation by restraining beta-secretase 1 transcription and translation [287]. Furthermore, it has been demonstrated to have anticancer effects on human gastric cancer cells via ROS-mediated MAPK, STAT3, and NF-B pathways [288]. Additionally, Schisandrin B has been found to inhibit epithelial- mesenchymal transition and stemness of large-cell lung cancer cells and tumorigenesis in xenografts via inhibiting the NF-κB and p38 MAPK signaling pathways [288]. It has also been shown to cause G1 arrest and death in human leukaemia U937 cells [289]. These findings illustrate Schisandrin B's broad pharmacological effects, which range from anti-
inflammatory and antioxidant capabilities to possible anticancer and neuroprotective effects.

Taurolidine	7.6	284.4	C7H16N4O4S2

Taurolidine has been shown to induce apoptosis in several cancer cell lines, including osteosarcoma, colon carcinoma, esophageal carcinoma, glioblastoma, melanoma, mesothelioma, and malignant mesothelioma [290]. This action is due to the escalation of DNA

fragments in the cell cycle's sub-G0/G1 phase, externalisation of phosphatidylserine, and the release of apoptosis-inducing factor [291]. Furthermore, taurolidine has been shown to increase the concentrations of the proapoptotic protein Bax while decreasing the amounts of Bcl-2, Mcl-1, and survival, as well as activating p53 [290]. Furthermore, taurolidine has been shown to induce autophagy as well as necroptosis in glioma cell lines [292]. Taurolidine's anti-neoplastic activity appears to be mediated via the inhibition of tumour angiogenesis [292]. Furthermore, taurolidine has been proven in vitro and in vivo to suppress the development of rat metastatic colorectal tumour cell lines [291].

alpha-Pinene	11.3	136.23	C10H16

α-Pinene, a bicyclic monoterpene compound, has demonstrated significant potential as an antineoplastic agent. -pinene has been proven in studies to increase the antineoplastic efficacy of natural killer cells via the ERK/AKT signaling cascade, showing its capacity to boost the immune response against cancer cells [293]. Furthermore, α-pinene has been shown to cause apoptosis by stopping the cell cycle in the G2/M phase in human ovarian cancer and hepatocellular carcinoma, hence inhibiting cancer cell growth [294]. Furthermore, it has been shown to inhibit the manufacture of matrix metalloproteinase-9 in human breast cancer cells, hence preventing malignant invasion [295]. Furthermore, α-pinene displays synergistic antitumor efficacy with paclitaxel against non-small cell lung carcinoma, indicating its potential for combination treatment [296]. -pinene inhibited the growth of human prostate cancer in a mouse xenograft model, highlighting its potential as a therapeutic agent [278]. Furthermore, -pinene was shown to lower miR-221 expression in HepG2 cells, showing its capacity to influence gene expression in cancer cells [297]. These findings imply that α-pinene has the potential to be an effective antineoplastic drug with the capacity to control multiple cellular processes involved in cancer growth.

Thymol	5.8005	150.22	C10H14O

Thymol, a natural phenol derivative, has been extensively studied for its wide range of therapeutic applications. It is widely used as an antiseptic, antioxidant, and stabilizer in harmaceuticals, agriculture, cosmetics, and food industry. Research has shown that thymol possesses antimicrobial, antifungal, and antioxidant properties, making it a sturdy antimicrobial agent [298]. Furthermore, thymol has been shown to have antioxidant activity, reduce oxidative stress, and ameliorate inflammation-related reactions, implying its potential to lower aortic intimal lipid lesions and inhibit the progression of hyperlipidaemia and atherosclerosis [299]. Furthermore, thymol has demonstrated cytotoxicity against melanoma cells, indicating its potential for cancer treatment ([300]. However, it is important to note that thymol has also been reported to induce chromosome aberrations in certain conditions [301].

Rhodanine	5.5591	C3H3NOS2	133.20

Rhodanine, also known as 2-thioxo-4-thiazolidinone, is a thiazolidinone molecule with a wide range of biological activities [302]. It has been studied for its potential anticancer [302], antimicrobial, and antiparasitic properties [303]. Rhodanine is a privileged heterocycle in medicinal chemistry, making it a valuable scaffold for drug discovery [304]. Furthermore, the structure of rhodanine has been explored for the development of novel inhibitors of viral enzymes, such as the NS5B polymerase of the hepatitis C virus, indicating its potential as a scaffold for antiviral agents [305].

Table 3.5 Compounds with known medical applications.

Exact mass	Formula
537.8	C23H42F3NO4Si3
424.5	C28H28N2O2
246.26	C13H14N2O3
257.24	C10H15N3O5
188.23	C11H12N2O
151.25	C10H17N
150.22	C10H14O
276.4	C17H24O3
150.17	C9H10O2
144.60	C7H9ClO
102.09	C3H6N2O2
145.20	C7H15NO2
57.09	C3H7N

Table 3. 1: Examples of compounds detected by NMR analysis of the crude water-soluble *T. violacea* extract.

Compound	Formula	FW	MF (multi spec)	Max $d_N(^1H)$	Acquisition time (sec)
4H-Pyran-4-one, 2,3-dihydro-3,5-dihydroxy-6-methyl-	C6H4O2	96.0841	0.90	0.353	2.1999
1,2,4-Triazine-3,5(2H,4H)-dione	C3H3H3O2	113.0748	0.91	0.179	2.1889
d-Glycero-d-galacto-heptose	C7H16O7	212.1977	0.86	0.144	2.1889
Benzaldehyde, 4-(1-methylethyl)-	C7H6O	106.1219	0.88	0.468	2.1889
Vanillin	C8H8O3	152.1473	0.34	0.347	2.1889
Oxime-, methoxy-phenyl	C21H32O2	332.4770	0.942	0.347	2.1889
Pyrrolidine	C4H9N	71.1210	0.83	0.615	2.1889
Schizandrin	C23H25O7	416.4642	0.81	1.017	2.1889
Taurolidine	C7H16N4O4S2	284.3563	0.87	0.487	2.1889
alpha.-Pinene	C15H16Cl3N3O2	376.6654	0.00	0.229	2.1889

Table 3. 4: Compounds with known anticancer activity.

According to the sources, d-glycero-d-galacto-heptose modulates NF- κB activation, whereas d-mannoheptulose influences d-glucose metabolism in pancreatic islet cells [262] These discoveries highlight the potential of these compounds in influencing both innate immune responses and metabolic processes. Further research is warranted to elucidate the precise mechanisms underlying their effects and to explore their potential therapeutic applications. Additionally, studies have shown that d-mannoheptulose inhibits the metabolism of D-glucose in pancreatic islets [263]. This glucose metabolism inhibition by d-mannoheptulose suggests its potential as a modulator of insulin secretion and glucose homeostasis. Therefore, these compounds hold promise for further investigation in the context of immune modulation and metabolic regulation.

Benzaldehyde, 4-(1-methylethyl)	8.1791	-148.20	C10H12O

Benzaldehyde, 4-(1-methylethyl), has demonstrated multifaceted effects on various cellular processes, particularly with relation to cancer. Nitoda et al. found that it suppresses melanin formation in cultured murine B16-F10 melanoma cells [264]. Additionally, Kubo et al. isolated benzaldehyde, 4-(1-methylethyl) from cumin and demonstrated its inhibitory effect on mushroom tyrosinase [265]. Furthermore, Ghosh et al. highlighted its anti-neoplastic effect against breast cancer [264]. Tsai et al. also discovered that it can cause apoptosis in human colorectal adenocarcinoma cells by activating pro-apoptotic proteins such caspase 3 and 9, affecting mitochondrial integrity, and decreasing the action of DNA integrity- preserving enzymes [266]. Similarly, Yang et al. and Morshedi et al. demonstrated its capability to suppress human lung squamous cell carcinoma by extensively activating the apoptosis pathway [266]. These findings collectively underscore the potential of benzaldehyde, 4-(1-methylethyl) as a promising candidate for further investigation in cancer therapy.

Vanillin	5.4	152.15	C8H8O3

Vanillin, a natural component found in food, has been shown to possess various beneficial properties. It has been demonstrated to exhibit anti-mutagenic and anti-metastatic characteristics [267]. Vanillin acts to suppress mutagenesis and cytotoxicity by interacting

with DNA repair mechanisms [267]. Additionally, it serves as an agent for chemoprevention [268]. Furthermore, vanillin acts as an antioxidant, providing protection to cell membranes against lipid peroxidation (LPO) and preserving DNA from strand breaks [269]. Vanillin has also been shown to inhibit the activation of NF-κB and the production of the cyclooxygenase-2 gene in mice macrophages activated by lipopolysaccharide [270]. Furthermore, vanillin has been shown to limit the invasion and migration of mammary adenocarcinoma cancer cells as well as decrease NF-kappaB activation, hence enhancing TRAIL-induced death [271]. It has also been noted to diminish the expression of metalloproteinase-9 [272]. Vanillin suppresses DNA-PK, an enzyme involved in non-homologous end joining, thereby hindering the process of DNA end-joining [267]. It prevents both in vitro and in vivo metastasis of mouse breast cancer cells [273].

Oxime-, methoxy-phenyl	5.4	151.16	C8H9NO2
The oxime- and methoxy-phenyl compounds have been found to possess various biological activities. They have been reported to have antibacterial and antioxidant properties [274] and to act as novel anticancer agents [275]. Additionally, the vanillin- derived piperidin-4-one oxime esters have demonstrated antioxidant and antimicrobial properties, with the phenyl ester substituents playing a significant role in their activity [274]. These findings point to the potential of oxime- and methoxy-phenyl compounds in a variety of biological applications, including antibacterial, antioxidant, and anticancer agents.			
Pyrrolidine	5.9	71.12	C4H9N

Pyrrolidine and its derivatives have received substantial research due to its broad biological and pharmacological value, notably in cancer therapy. Pyrrolidine has been shown to inhibit cancer cell proliferation by triggering cell cycle arrest and apoptosis in a time and dosage-dependent way. [276]. Additionally, pyrrolidine compounds have exhibited cytotoxicity against pancreatic cancer cells, although they lacked selectivity for tumour cells [277]. These findings highlight pyrrolidine's ability to reduce oxidative stress and its cytotoxic effects on cancer cells, indicating its potential as a therapeutic agent in cancer treatment.
[277].

Schizandrin	6.0	432.5	C24H32O7

Schisandrin B's pharmacological effects have been widely researched. It has been demonstrated to reduce liver fibrosis via modulating the Nrf2-ARE and TGF-/Smad signaling pathways. [278]. Furthermore, Schisandrin B has been shown to decrease the growth of airway smooth muscle cells and to have anti-asthmatic properties [279]. Furthermore, it has been identified for its ability to reduce chondrocyte inflammation and osteoarthritis by suppressing the NF-B and MAPK signal pathways [280]. Schisandrin B has also been found to protect against beta-amyloid and homocysteine neurotoxicity, indicating its potential neuroprotective effects [281]. Furthermore, it has been proposed as a hormetic agent for the prevention of age-related neurodegenerative illnesses through the reduction of oxidative stress and mitochondrial dysfunction [282]. Additionally, Schisandrin B has been reported to alleviate diabetic cardiac autonomic neuropathy Zhang et al. [283] and has showed potential in suppressing osteoclastogenesis and guarding against ovariectomy-induced bone loss [284]. It has also been studied for its ability to reduce the inflammatory response, oxidative stress, and apoptosis caused by traumatic spinal cord damage [285]. Schisandrin B has also been studied for its inhibitory effects on the pharmacokinetics of poziotinib Wang et al. [286] and its potential in reducing Aβ generation by restraining beta- secretase 1 transcription and translation [287]. Furthermore, it has been demonstrated to have anticancer effects on human gastric cancer cells via ROS-mediated MAPK, STAT3, and NF-B pathways [288]. Additionally, Schisandrin B has been found to inhibit epithelial- mesenchymal transition and stemness of large-cell lung cancer cells and tumorigenesis in xenografts via inhibiting the NF-κB and p38 MAPK signaling pathways [288]. It has also been shown to cause G1 arrest and death in human leukaemia U937 cells [289]. These findings illustrate Schisandrin B's broad pharmacological effects, which range from anti-
inflammatory and antioxidant capabilities to possible anticancer and neuroprotective effects.

Taurolidine	7.6	284.4	C7H16N4O4S2

Taurolidine has been shown to induce apoptosis in several cancer cell lines, including osteosarcoma, colon carcinoma, esophageal carcinoma, glioblastoma, melanoma, mesothelioma, and malignant mesothelioma [290]. This action is due to the escalation of

DNA

fragments in the cell cycle's sub-G0/G1 phase, externalisation of phosphatidylserine, and the release of apoptosis-inducing factor [291]. Furthermore, taurolidine has been shown to increase the concentrations of the proapoptotic protein Bax while decreasing the amounts of Bcl-2, Mcl-1, and survival, as well as activating p53 [290]. Furthermore, taurolidine has been shown to induce autophagy as well as necroptosis in glioma cell lines [292]. Taurolidine's anti-neoplastic activity appears to be mediated via the inhibition of tumour angiogenesis [292]. Furthermore, taurolidine has been proven in vitro and in vivo to suppress the development of rat metastatic colorectal tumour cell lines [291].

alpha-Pinene	11.3	136.23	C10H16

α-Pinene, a bicyclic monoterpene compound, has demonstrated significant potential as an antineoplastic agent. -pinene has been proven in studies to increase the antineoplastic efficacy of natural killer cells via the ERK/AKT signaling cascade, showing its capacity to boost the immune response against cancer cells [293]. Furthermore, α-pinene has been shown to cause apoptosis by stopping the cell cycle in the G2/M phase in human ovarian cancer and hepatocellular carcinoma, hence inhibiting cancer cell growth [294]. Furthermore, it has been shown to inhibit the manufacture of matrix metalloproteinase-9 in human breast cancer cells, hence preventing malignant invasion [295]. Furthermore, α-pinene displays synergistic antitumor efficacy with paclitaxel against non-small cell lung carcinoma, indicating its potential for combination treatment [296]. -pinene inhibited the growth of human prostate cancer in a mouse xenograft model, highlighting its potential as a therapeutic agent [278]. Furthermore, -pinene was shown to lower miR-221 expression in HepG2 cells, showing its capacity to influence gene expression in cancer cells [297]. These findings imply that α-pinene has the potential to be an effective antineoplastic drug with the capacity to control multiple cellular processes involved in cancer growth.

Thymol	5.8005	150.22	C10H14O	

Thymol, a natural phenol derivative, has been extensively studied for its wide range of therapeutic applications. It is widely used as an antiseptic, antioxidant, and stabilizer in Pharmaceuticals, agriculture, cosmetics, and food industry. Research has shown that thymol possesses antimicrobial, antifungal, and antioxidant properties, making it a sturdy antimicrobial agent [298]. Furthermore, thymol has been shown to have antioxidant activity, reduce oxidative stress, and ameliorate inflammation-related reactions, implying its potential to lower aortic intimal lipid lesions and inhibit the progression of hyperlipidaemia and atherosclerosis [299]. Furthermore, thymol has demonstrated cytotoxicity against melanoma cells, indicating its potential for cancer treatment ([300]. However, it is important to note that thymol has also been reported to induce chromosome aberrations in certain conditions [301].

Rhodanine 5.5591 C3H3NOS2 133.20

Rhodanine, also known as 2-thioxo-4-thiazolidinone, is a thiazolidinone molecule with a wide range

of biological activities [302]. It has been studied for its potential anticancer [302], antimicrobial, and antiparasitic properties [303]. Rhodanine is a privileged heterocycle in medicinal chemistry, making it a valuable scaffold for drug discovery [304]. Furthermore, the structure of rhodanine has been explored for the development of novel inhibitors of viral enzymes, such as the NS5B polymerase of the hepatitis C virus, indicating its potential as a scaffold for antiviral agents [305].

Methyl formate, a chemical compound with the formula CH3O2CH, has been widely used as a fumigant and larvicidal agent in agriculture. In addition, Yagi et al. [306] highlighted the significance of agricultural soil fumigation as a source of atmospheric methyl bromide, thereby emphasising the role of fumigants in agricultural practices. Ren & Mahon [307] conducted fumigation trials using ethyl formate on wheat, split faba beans, and sorghum, demonstrating the potential of formate compounds as effective fumigants. In addition, Seo et al. [308] developed cellulose nanocrystal-stabilised Pickering emulsions of massoia and nutmeg essential oils for the control of Aedes albopictus, indicating the ongoing research and development of novel fumigants and larvicidal agents for agricultural pest management. Collectively, these studies underscore the importance of methyl formate and related compounds in agricultural fumigation and pest control, highlighting the need for continued research and innovation in this field.

Cyclo heptas iloxan e, tetrad ecame thyl-	7.736 7	519.0 7	C14H 42O7 Si7
Cycloheptasiloxane tetradecamethyl is a marine xenobiotic metabolite that has been reported to exhibit various biological activities. detected antibacterial activity of this compound in sea			

urchin extracts [309]. Similarly, identified cycloheptasiloxane tetradecamethyl as a xenobiotic of interest in cord plasma and placental tissue of monochorionic twins complicated with selective intrauterine growth restriction [310]. Moreover, reported the anticancer and antimicrobial effects of this compound [311]. Additionally, identified cycloheptasiloxane tetradecamethyl in the fractions of Peristrophe bivalvis leaf, indicating its presence in plant material [312]. Furthermore, highlighted the anti-inflammatory, antibacterial, antifungal, and anti-aging properties of cycloheptasiloxane tetradecamethyl, which is used in personal care products [313]. These findings collectively demonstrate the diverse biological activities associated with cycloheptasiloxane tetradecamethyl, ranging from antibacterial and anticancer
effects to its presence in plant material and personal care products.

Cyanogen chloride	6.9260	61.47	CNCl or ClCN or CClN

Cyanogen chloride (CNCl) is a highly toxic lachrymator that has been utilised as tear gas because of its ability to induce tearing. It is important to note that its vapour is denser than air, which can cause it to persist at lower levels and pose a risk to individuals in enclosed spaces. CNCl is a disinfection byproduct found in chlorinated and chloraminated drinking water and is formed by the reaction of free chlorine or chloramines with natural organic matter [314]. It is a colourless to pale yellow liquid that turns into a gas near room temperature [315]. This substance is highly toxic and volatile, and its damage potential depends mainly on the concentration and duration of exposure [316]. In addition, CNCl hydrolyzes the base to produce cyanate and chloride ions. It has been shown to be difficult to effectively remove CNCl via porous substances such as activated carbon due to the weak interaction between CNCl and the adsorbent surface [317]. Furthermore, CNCl can cause rapid death when inhaled, highlighting its extreme toxicity [314].

Table 3. 7: Other identified compounds.

Phytochemical compound	RT (min)	Formula	Exact mass
1,3,5-Benzenetriol	3.8560	C6H6O3	126.11

1,3,5-Benzenetriol, a natural product found in Ecklonia cava and Alpinia blepharocalyx, has been identified as an algal metabolite [318]. Clinical studies have been conducted to assess the diagnostic effectiveness of this compound in colonoscopy. [319]. Additionally, 1,3,5-benzenetriol has been found to have potential α-glucosidase inhibitory activity [320] and has been detected as an alpha-glucosidase inhibitor in previous research [320]. Furthermore, 1,3,5- benzenetriol has been utilised in the synthesis of a copper 1,3,5-triamino-2,4,6-benzenetriol metal–organic framework [321]. Moreover, it has been reported that 1,3,5- benzenetriol can selectively bind and precipitate Cs + ions from aqueous solutions [322]. These findings highlight the diverse potential applications and biological activities of 1,3,5-benzenetriol.

2-Piperidinecarboxamide, l-butyl-N-(2,6-dimethylphenyl)-	4.087	C19H31ClN2O	338.9

The compound 1-butyl-N-(2,6-dimethylphenyl)-2-piperidinecarboxamide, commonly known as bupivacaine, is a local anesthetic agent that has been widely used in both human and equine medicine for many years [323]. The chemical structure of bupivacaine includes a 2,6-dimethylphenyl group, which has been the focus of various chemical studies [324].

1-Butanol, 3-methyl-, acetate	5.0608	C7H14O2 or CH3COO(CH2)2CH(CH3)2	130.18

Isoamyl acetate, also known as 3-methyl-1-butanol acetate, is a significant metabolite produced by Saccharomyces cerevisiae during primary alcoholic fermentation [325]. This acetate ester is formed from isoamylol, and its production is influenced by various factors, including the addition of specific amino acids. For instance, the addition of L-isoleucine and L-phenylalanine during longan juice fermentation leads to significantly higher concentrations of isoamyl acetate and its corresponding acetate esters [326]. The expression levels of yeast alcohol acetyltransferase genes, such as ATF1 and ATF2, have been found to control the formation of a broad range of volatile esters, including isoamyl acetate [327]. Additionally, the enzymatic synthesis of isoamyl esters, including isoamyl acetate, has been investigated, demonstrating the feasibility of using fusel oil as an alternative. Furthermore, Candida antarctica lipase B immobilisation has been investigated for the synthesis of isoamyl acetate in solvent-free and organic medium esterification, showing its potential utility in the manufacturing of this flavour molecule [328].

Morphinan-6-one, 4,5- epoxy-3,14-dihydroxy-17- (2-propenyl)-, (S. alpha.)	5.102	C19H21NO4	327.4

Morphinan-6-one, 4,5-epoxy-3,14-dihydroxy-17-(2-propenyl)-, (S. alpha.), is a member of the morphinan alkaloid group that has received a lot of attention due to its pharmacological potential.Morphinan-6-one, 4,5-epoxy-3,14-dihydroxy-17-(2-propenyl)-, (S. alpha.), is a member of the morphinan alkaloid group that has received a lot of attention due to its pharmacological potential. Different morphinan-6-one derivatives were synthesised and analysed, emphasising the effect of different substituents on their in vitro and in vivo activity [329]. Similarly, reported on chemically innovative modifications of N-methylmorphinan-6-ones, leading to the development of a novel class of morphinans with acrylonitrile incorporated substructures, demonstrating the potential for chemical modifications to generate new morphinan derivatives with pharmacological relevance [330]. Furthermore, focused on developing centrally acting mu-opioid receptor antagonists through structural modifications of morphinan derivatives, indicating the potential for designing compounds with specific pharmacological actions
[331].

Benzeneethanamine, 4-methoxy	5.667	C9H13NO	151.21

The compound 4-methoxybenzeneethanamine is a derivative of ethylamine with a 4-methoxyphenyl substituent at the 2-position, derived from a hydride of 2- phenylethylamine. This compound has been studied for its inhibitory properties against quorum sensing proteins of Salmonella enterica serovar Typhi [332].
Additionally, the presence of 4-methoxyphenyl substituents has been shown to affect the

reactivity and selectivity of organic compounds in various reactions [333]. Furthermore, the effects of introducing methoxy groups into the auxiliary ligands of copper (I) dyes on dye-sensitized solar cells have been studied [334]. The compound has also been implicated in the synthesis of chiral palladium β-diimine complexes [335]. Moreover, the presence of 4-methoxyphenyl lateral substituents has been linked to the enhanced efficiency of perovskite solar cells [336]. This research shows the chemical 4- methoxybenzeneethanamine's broad uses and implications in a variety of domains,
including medicine, catalysis, and materials science.

Schizandrin	5.9817	C24H32O7	432.5

Schisandrin is a natural product found in Schisandra rubriflora, Schisandra bicolor, and other organisms with available data. It has been demonstrated to have a variety of pharmacological characteristics, including anti-inflammatory [337], neuroprotective [338], and anti-HIV activities [339]. Additionally, Schisandrin inhibits oxidative stress (Bend et al., 2015), reduces Aβ generation [287], and inhibits osteoclastogenesis [284]. Furthermore, it has been identified as a potential therapeutic agent for diabetic cardiac autonomic neuropathy [283]. Schisandrin has also been investigated for its possible use in the treatment of Alzheimer's disease Maia et al. [340] and has been found to have antioxidant potential [341]. Moreover, research has shown that schisandrin can restore mitochondrial function, energy metabolism, biogenesis, and dynamics in rat primary hippocampal neurones [338]. These studies emphasise the diverse pharmacological properties of schisandrin and its potential therapeutic application in various diseases.

Benzoic acid, 2,4-dihydroxy-6-methyl-	6.0284	C8H8O4	168.15

Benzoic acid, also known as 2,4-dihydroxy-6-methyl-, is a naturally occurring chemical found in plant and animal tissues, fruits, and vegetables [342]. It is known to
function in plants as a defensive mechanism against fungal diseases [343].

In fact, benzoic acid has been identified as a major aromatic acid present in cranberry fruit [344]. Furthermore, it has been reported that benzoic acid is converted into 1,2- dihydro-1,2-dihydroxybenzoic acid by benzoate-1,2-dioxygenase, and then transformed into catechol by the function of the gene benD-xylL [345]. Additionally, benzoic acid has been suggested as the biosynthetic precursor of salicylic acid in tobacco [346]. Furthermore, investigations have detected and measured 2,4- dihydroxy-6-methylbenzoic acid in human plasma following cranberry juice ingestion [347]. Furthermore, benzoic acid has been found to be excreted mainly as the glycine conjugate, hippuric acid, in marsupials [348]. It is important to note that benzoic acid has been reported to be a natural constituent of plants, with high amounts being found in fruits and berries [344].

2,4(1H,3H)-Pyrimidinedione, 5-amino-	6.7927	C4H5N3O2	127.10

Riboflavin is synthesised by the conversion of GTP to 5-amino-6-ribitylamino-2,4(1H,3H)-pyrimidinedione via a series of enzymatic processes [349]. This intermediate is essential for the production of riboflavin and its coenzymes. It has also been found to be a precursor for the manufacture of powerful GPR84 agonists [350]. The conversion of 5-amino-6-ribitylamino-2,4(1H,3H)-pyrimidinedione to riboflavin is catalysed by specific enzymes, highlighting its significance in the riboflavin biosynthetic pathway [351]. Additionally, 5-amino-6-ribitylamino-2,4(1H,3H)- pyrimidinedione was prepared by phosphorylation of 5-nitro-6-ribitylamino-2,4(1H,3H)-pyrimidinedione, followed by reduction, further emphasising its role as an important intermediate in riboflavin biosynthesis [352].

Propanoic acid, 2-hydroxy, ethyl ester	7.3404	C5H10O3	118.13

Ethyl 2-hydroxypropanoate, also known as ethyl lactate, is a natural product found in Cocos nucifera and Camellia sinensis [353]. It is the ethyl ester obtained from 2- hydroxypropanoic acid and has been identified as a metabolite with potential biological roles [354]. Because of its occurrence in Cocos nucifera and its prospective uses in sectors like as cosmetics, food science, and biology, this chemical has been the topic of investigation. Because of its occurrence in Cocos nucifera and its prospective uses in sectors like as cosmetics, food science, and biology, this chemical has been the topic of investigation [355]. According to studies, ethyl lactate is found in the volatile profiles of various fermented items, indicating its involvement in adding to their scent and flavour [356]. Furthermore, the safety assessment of coconut-derived ingredients in cosmetics has been conducted, highlighting the relevance
of ethyl lactate in the context of product safety and application [357].

Tetrasiloxane, 3,5-diethoxy- 1,1,1,7,7,7-hexamethyl-3,5-bis(trimethylsiloxy)-	14.9229	C16H46O7Si6	519.0

Tetrasiloxane (3, 5-diethoxy-1, 1, 1, 7, 7, 7-hexamethyl-3, 5-bis (trimethylsiloxy)-) has been the subject of several chemical studies. Ondo et al. [358] discussed the growth rates and thickness increment of thin films grown from linear tetrasiloxane substituted with methyl groups, similar to the compound in question. This study provides insights into the properties and behaviour of similar tetrasiloxane compounds. In addition, Wang et al. [359] synthesised and characterised tetrasiloxane-tailed gemini surfactants, which are relevant for understanding the chemical properties and potential applications of tetrasiloxane compounds. Additionally, Abe et al. [360] discussed the synthesis and structure of a related cyclotetrasiloxane and provided valuable information on the rmation and properties of such compounds. Computational modelling of the interaction of COX -2 and components of the *T. violacea* water soluble extract. The aqueous crude extract of *T. violacea* leaves was effective against the TNBC cell line MDA-MB231, indicating its therapeutic potential in the treatment of triple-negative breast cancer. GC-MS and NMR analyses confirmed the presence of several bioactive

compounds with various pharmacological effects. The ability of these bioactive substances to trigger apoptosis in the TNBC cell line was explored through in silico molecular docking studies with COX-2, a protein known to impede apoptosis.

Computer-aided methods have matured into advanced techniques for drug discovery, aiding the identification of bioactive elements in medicinal plants for pharmacological applications [361]. In silico predictive algorithms play a critical role in predicting the pharmacological, pharmacokinetic, and toxicological profiles of substances, and are critical in the decision-making process that drives pharmaceutical and technological breakthroughs [362]. Molecular docking is a rapid and cost-effective strategy for the development and evaluation of drugs. It yields insightful data regarding drug-receptor interactions, assisting in forecasting how drug candidates will bind to target proteins [363], leading to effective engagement at ligand-binding sites [364]. Analysis of the interactions between COX-2 and various ligands revealed that their binding patterns were influenced by ligand characteristics. Figures 3.33, 3.34, and Table 3.8 illustrate the docking results for these bioactive molecules.

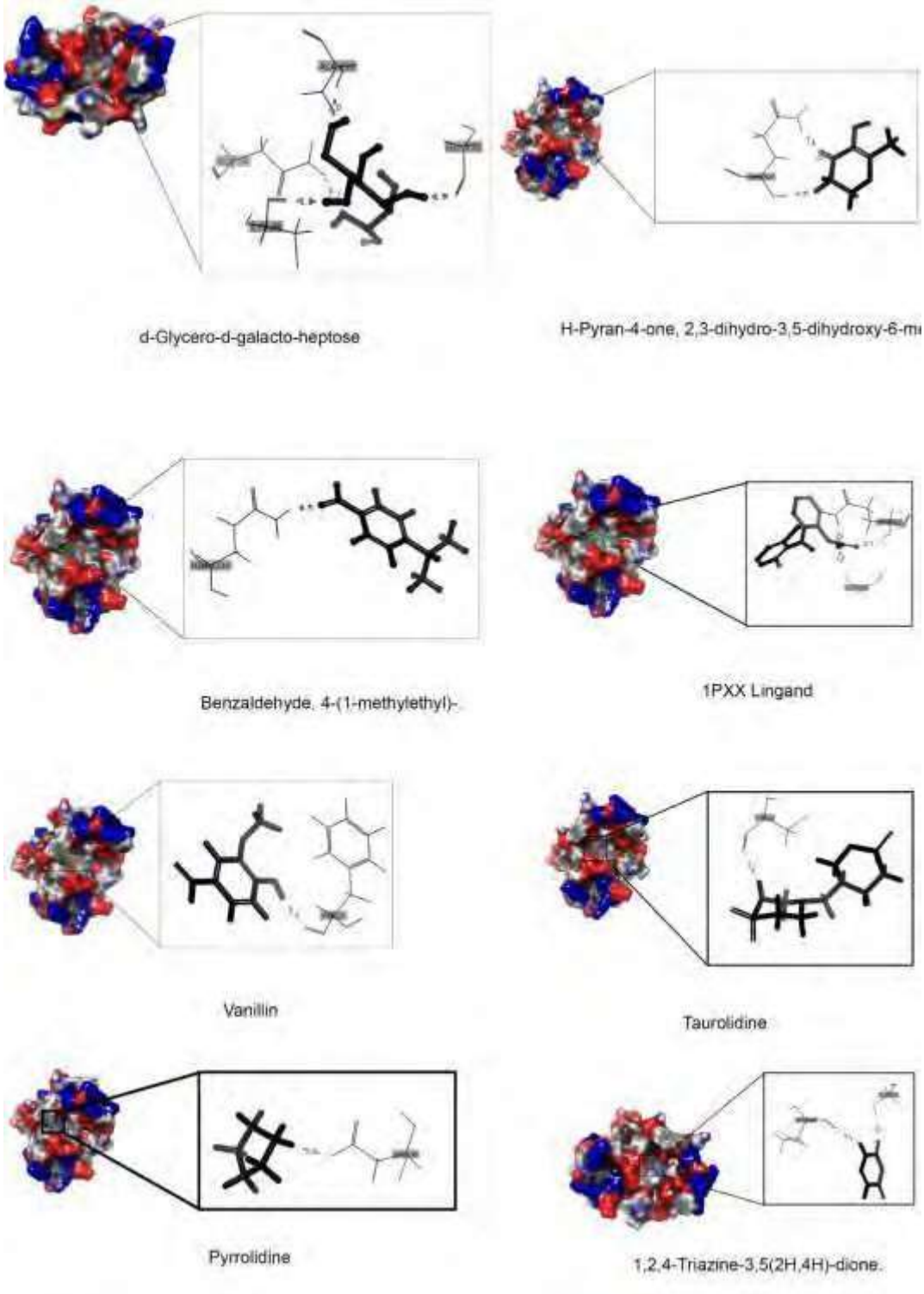

Figure 3.34 depicts the molecular docking of various bioactive anticancer compounds identified from Tulbaghia violacea extracts with the cyclooxygenase-2 (COX-2) protein

The individual panels show the three-dimensional structures and interactions between the COX-2 protein and different bioactive molecules, such as d-glycero-d-galacto-hepimages showan-4-one, 2,3-dihydro-3,5-dihydroxy-6-methyl-4H-pyran-4-one, benzaldehyde 4-(1-methylethyl)-, 1PXX Ligand, Vanillin,,Tauroldine, and Pyrolidine. These compounds docked with the COX-2 protein target, which is known to be a tobenzaldehyde in modulating apoptosis and inflammation pathways relevant to cancer. Docking analysis provides insights into the potential binding interactions and affinities of these phytochemicals from *T. violacea* with the COX-2 protein, aiding in understanding their anticancer mechanisms. The pink dashed lines represent the hydrogen bond interactions between the compounds and proteins.

Table 3.6 Molecular docking score for the anticancer bioactive compounds of *T. violacea* water crude extract with COX-2 protein

Title	docking score
1PXX - minimized_protein	-7.660
d-Glycero-d-galacto-heptose	-4.895
H-Pyran-4-one, 2,3-dihydro-3,5-dihydroxy-6-methyl	-4.69
Benzaldehyde, 4-(1-methylethyl)	-4.432
Diclofenac ligand	-3.990
H-Pyran-4-one, 2,3-dihydro-3,5-dihydroxy-6-methyl	-3.933
Vanillin	-

	3.820
Taurolidine	-3.715
-Taurolidine	-3.690
Taurolidine	-3.685
Vanillin	-3.051
Pyrrolidine	-2.573
2,4-Triazine-3,5(2H,4H)-dione	-2.396
Taurolidine	-2.322
T aurolidine	-2.130
Triazine-3,5(2H,4H)-dione	-2.104
alpha.-Pinene	-1.953
Oxime-, methoxy-phenyl	-0.637

A more negative docking score signifies a stronger affinity of the ligand for the receptor, suggesting that bioactive compounds with lower scores demonstrate enhanced efficacy in interacting with COX2. The docking scores for the anticancer ligands varied between -4.9 and -0.6. Molecules such as d-glycero-d-galacto-heptose, H-Pyran-4-one, 2,3-dihydro-3,5-dihydroxy-6-methyl, and benzaldehyde, 4-(1-methylethyl) showcased the most prominent docking scores among the bioactive compounds evaluated in this study, indicating superior binding at the 1XPP site 1 (Fig. 3.5). This site encompasses

amino acids Ser 49, Asn 34, Gly 135, Cy 36, and Ala 156.

The crystallographic structure of a diclofenac complex with murine COX-2 demonstrates that diclofenac adheres to COX-2 in a reversed orientation, with its carboxylate group forming hydrogen bonds with Tyr-385 and Ser-530 [365], possessing a binding score of -3.9 compared to 4.9, 4.4, and 4 for glycero-d-galacto-heptose, H-Pyran-4-one, 2,3-dihydro-3,5- dihydroxy-6-methyl, and benzaldehyde, 4-(1-methylethyl). In the docking model, all important residues formed hydrogen bonds with carboxylate groups on d-glycero-d-galacto-heptose.

H-Pyran-4-one, 2,3-dihydro-3,5-dihydroxy-6-methyl, connects with TCOX-2 at Gln B:1327 and Gly B:1324, whereas 4-(1-methylethyl) benzaldehyde attaches to COX-2 at Gln B:1327. Despite having the least favourable score, oxime, methoxy-phenyl, and alpha-pinene demonstrated effectiveness as anti-inflammatory and anticancer therapeutic agents.

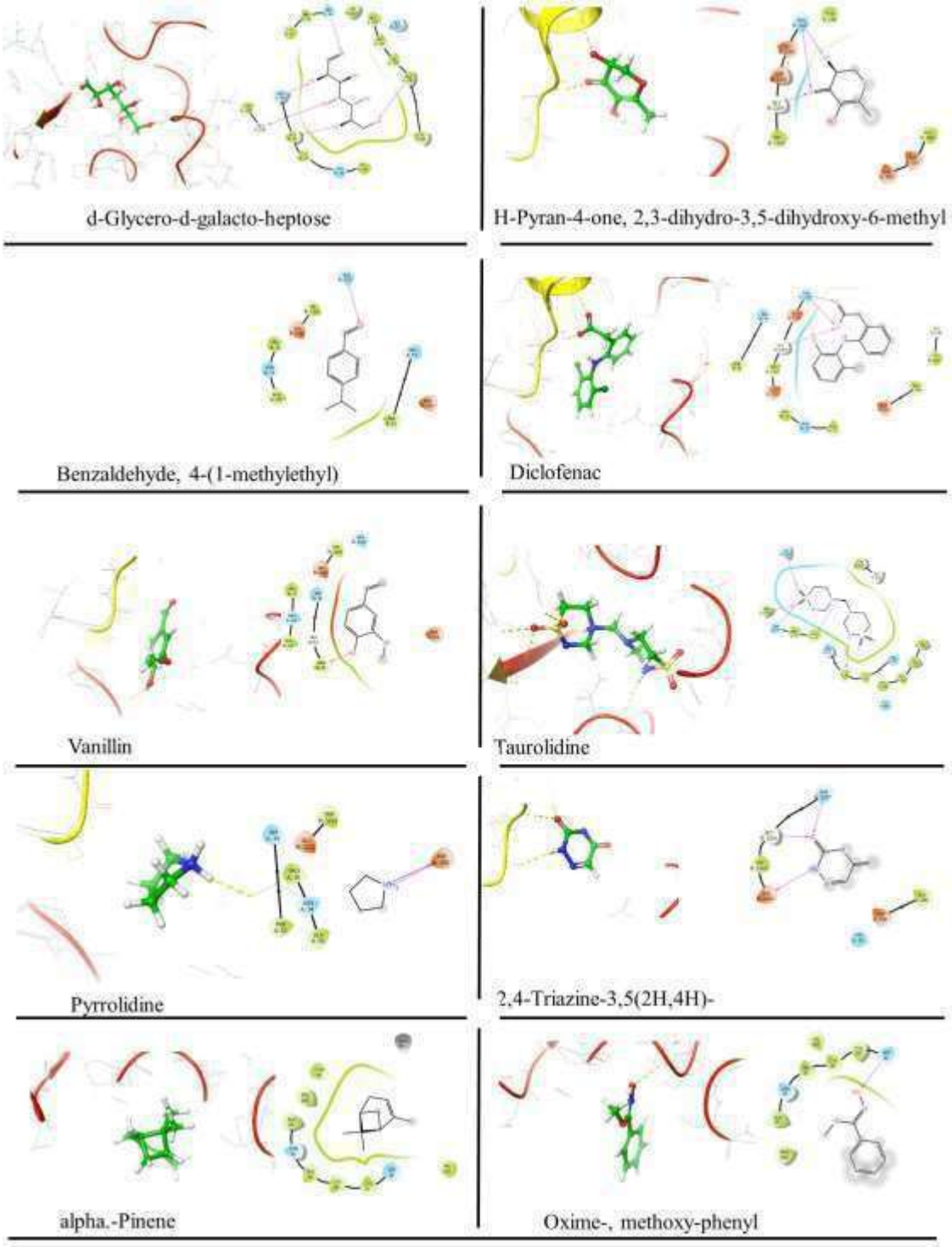

Figure 3.35 depicts the molecular docking analysis of various compounds identified in the crude extracts of *Tulbaghia violacea* with the cyclooxygenase-2 (COX-2) protein. The image shows the three-dimensional structures and interactions between the COX-2 protein target and different bioactive molecules such as d-Glycero-d-galacto-heptose, H-Pyran-4-one, 2,3-dihydro-3,5-dihydroxy-6-methyl-4H-pyran-4-one, Benzaldehyde 4-(1-methylethyl)-, 1PXX

Ligand, Vanillin, Tauroldine, and Pyrolidine. These compounds are docked onto the COX-2 protein, which is known to play a role in regulating apoptosis and inflammation pathways relevant to cancer. Docking analysis provides insights into the potential binding interactions and affinities of these phytochemicals from *T. violacea* with the COX-2 protein target, aiding in understanding their proposed anticancer mechanisms.

3.22 Proteomic analysis of the RTK pathway

The protein profiler system relies on antibodies attached to polyvinylidene fluoride (PVDF) membranes. The samples were then used to wash the membrane under binding conditions, and the proteins present in the sample were bound to the antibodies raised against these proteins. The levels of these proteins in the sample can then be determined by the strength of the fluorescent signal due to a secondary HRP antibody. To perform this, proteins were extracted from MDA-MB231 and MCF10A cells before and after treatment with 400 μg/mL water-soluble *T. violacea* extract for 24 h. Figure 3.35 represents the results of SDS-PAGE analysis of the protein extracts. The extracted proteins were of high quality. Nevertheless, 20 μg of total protein was loaded per lane, as equal volumes of protein were applied to the gel. The samples derived from MDA-MB231 cells were substantially more abundant than those derived from MCF10A cells. Following determination of the concentration of the extracts, an equal amount of each protein sample was used in the protein profiler assay. Figure 3.36 shows the membranes visualised with a ChemiDoc imaging system using a fluorescent camera. The loading and signal controls are shown at positions A1, A2, A23, A24, F', and F2. These showed similar staining intensities across samples. All signals were normalised based on the signals from the controls. shows the intensities of the samples plotted for each protein antibody that was fixed to the membrane. The samples were categorised into three plots. Plot (A) depicts samples with a greater signal intensity in normal cells than in TNBC cells. Plot (B) depicts data where the signal intensity in TNBC cells was greater than that in normal cells but remained below 4/0 on the scale. Plot (C) shows the samples with significantly higher signal intensities.

The results of the quantitative analysis, along with the roles of various RTKs and their protein interactions, are detailed in Table 3.9. The STRING online tool was used to identify the interacting proteins. In addition, we examined the expression levels of additional proteins involved in this signaling cascade. Figure 3. 36 SDS-PAGE analysis of proteins extracted from TNBC and normal

breast cells before and after treatment with *T. violacea* water-soluble extract The protein samples extracted were shown to be of good quality, with discrete bands. However, the gel highlighted that were amplified at different concentrations.

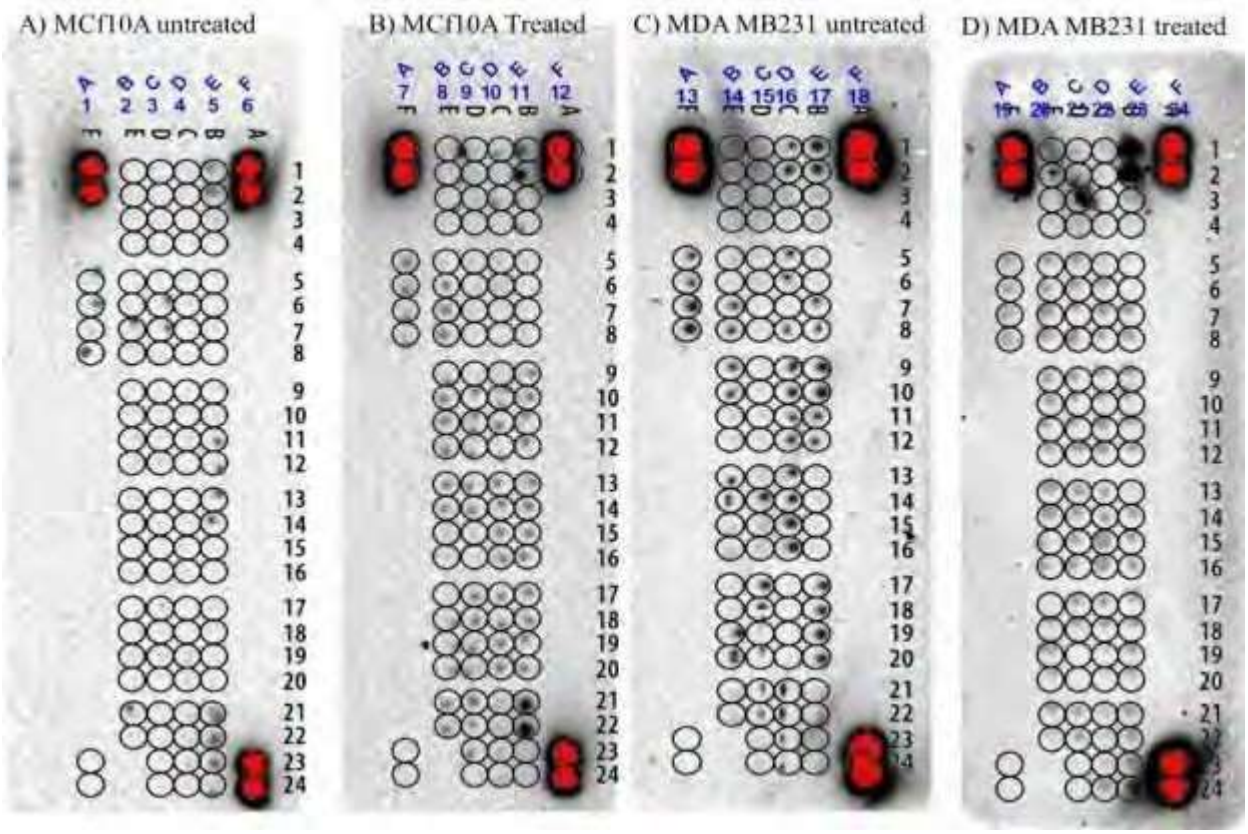

Figure 3.36 shows the results of a protein profiler array, which allows for the detection and semi-quantitative analysis of the relative levels of phosphorylation of 43 receptor tyrosine kinases (RTKs) and two2 additional proteins. The image displays multiple membranes, each containing an array of capture antibodies, printed in duplicate. Upon incubation with cell lysates, the phosphorylated RTKs present in the samples bind to their corresponding capture antibodies on membranes. Subsequent chemiluminescence detection revealed the presence and relative levels of phosphorylated RTKs as indicated by the signal intensities observed at each capture antibody spot. The consistent signal intensities across the control membranes suggested proper functioning of the assay and allowed for a comparative analysis between different treatment conditions or cell types.

The majority of the receptors decreased when cells were treated with the water-soluble *T. violacea* extract.

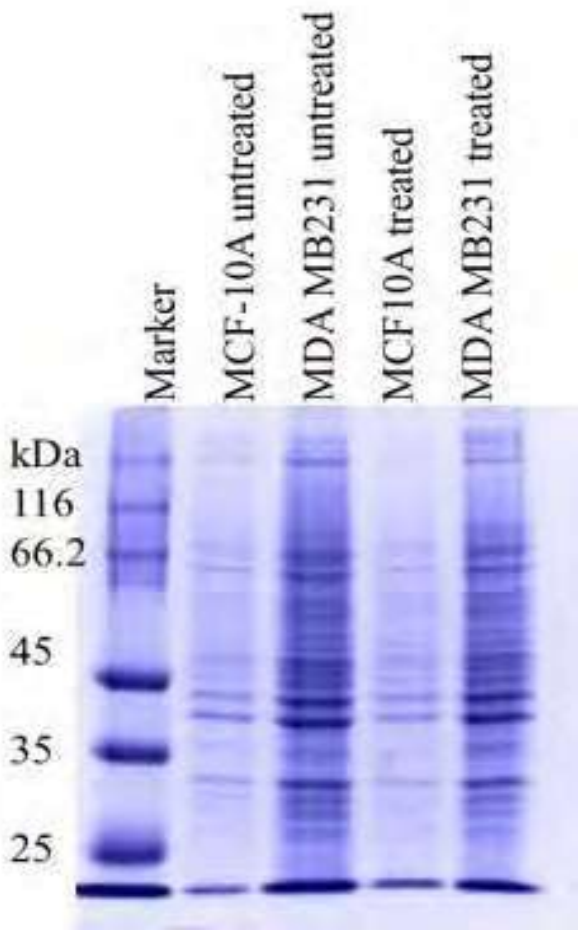
Marker
MCF-10A untreated
MDA MB231 untreated
MCF10A treated
MDA MB231 treated
kDa
116
66.2
45
35
25

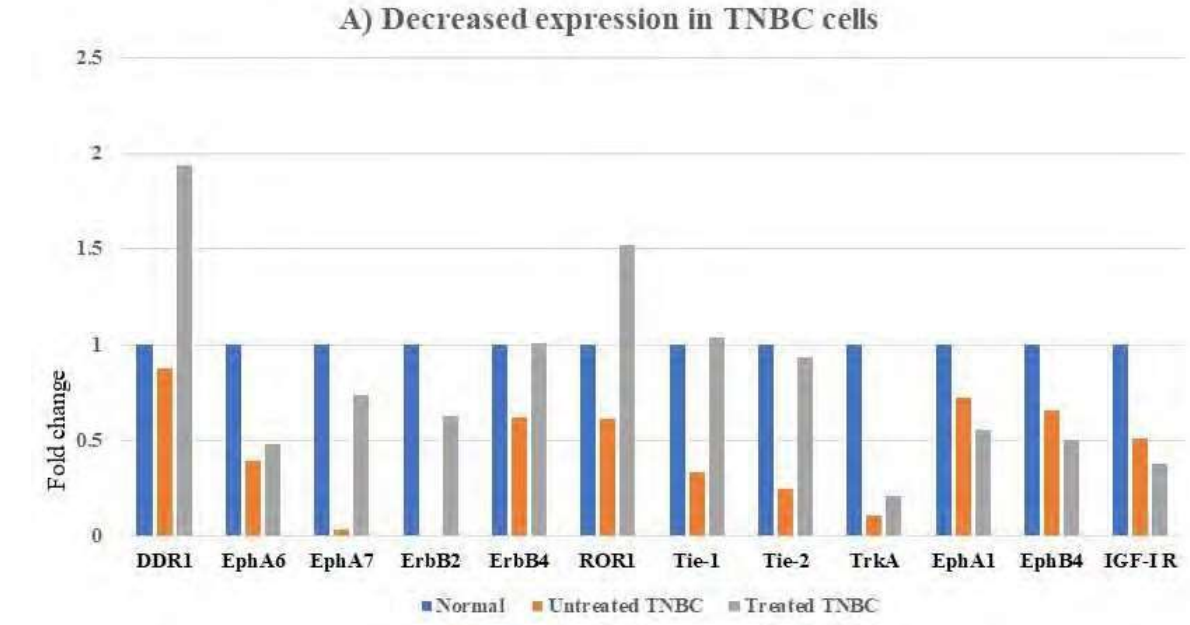
A) Decreased expression in TNBC cells
Fold change
2.5
2
1.5
1
0.5
0
DDR1
EphA6
EphA7
ErbB2
ErbB4
ROR1
Tie-1
Tie-2
TrkA
EphA1
EphB4
IGF-I R
Normal
Untreated TNBC
Treated TNBC

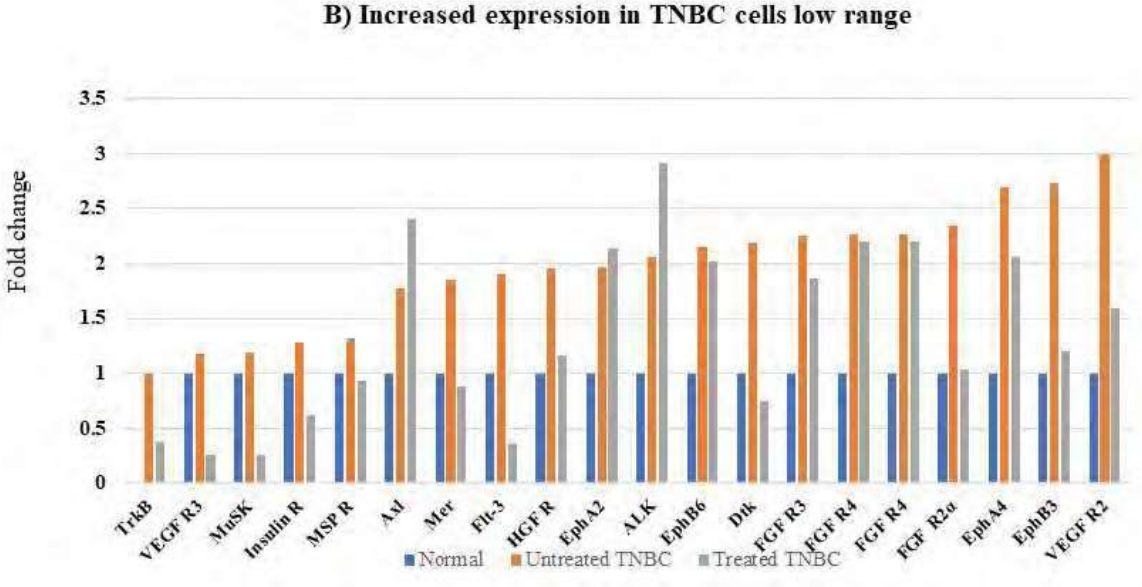
B) Increased expression in TNBC cells low range
Fold change
3.5
3
2.5
2
1.5
1
0.5
0
TrkB
VEGF R3
MuSK
Insulin R
MSP R
Axl
Mer
Flt-3
HGF R
EphA2
ALK
EphB6
Dtk
FGF R3
FGF R4
FGF R4
FGF R2a
EphA4
EphB3
VEGF R2
Normal
Untreated TNBC
Treated TNBC

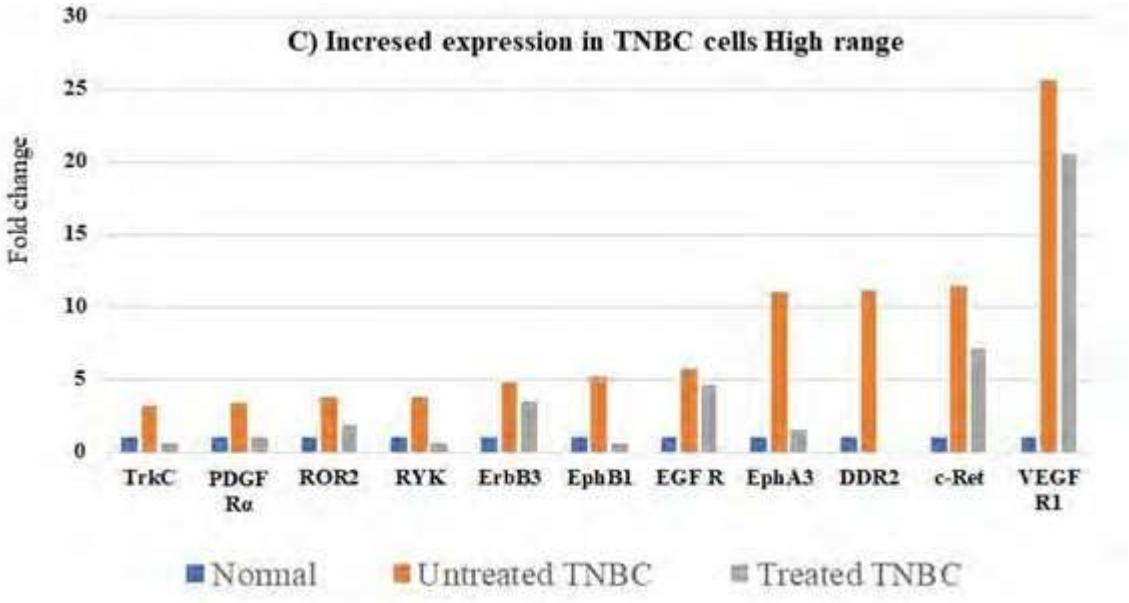

Figure 3.37 Fold changes in the expression of the different tyrosine kinases. The figure is divided into multiple panels, with each panel representing a specific tyrosine kinase or protein. The y-axis indicates the molecular weight in kilodaltons (kDa), while the x-axis represents the different cell lines or treatments, such as MCF10A (normal breast cells), MDA MB231 (breast cancer cells), untreated, and treated cells. The intensity of the bands corresponds to the expression levels of the respective tyrosine kinases or proteins. The figure legend shows that the fold-changes in expression were calculated based on the optical density of chemiluminescent signals detected using a chemi-doc system, with normalisation performed against the optical density of normal breast cell samples.

Table 3.7 Function protein interactions and the result of exposure to the water-soluble *T. violacea*

AKT

• Controls a variety of functions, including metabolism, cellular proliferation, survival, growth, and angiogenesis, as well as glucose absorption.. • Exhibits the capability to attenuate insulin signaling but can also enhance insulin-mediated glucose uptake. • Controls the conversion of glucose into glycogen for storage. • Catalyzes the phosphorylation of GSK3, fostering cellular proliferation. • Initiates phosphorylation of MAP3K5, supporting cellular survival. • Facilitates insulin-induced protein synthesis. • Determines the cytoplasmic positioning of the Forkhead family of transcription factors. • Influences NF-kappa-B-mediated gene transcription and positively impacts CREB1, leading to the expression of pro-survival genes like BCL2 and MCL1. • The AKT-mTOR signaling pathway is essential for cellular proliferation and neurogenesis. • Operates downstream of PI3K, amplifying the effects of various growth factors including PDGF, EGF, and IGF-I. • SPATA13-dependent cell mobility and	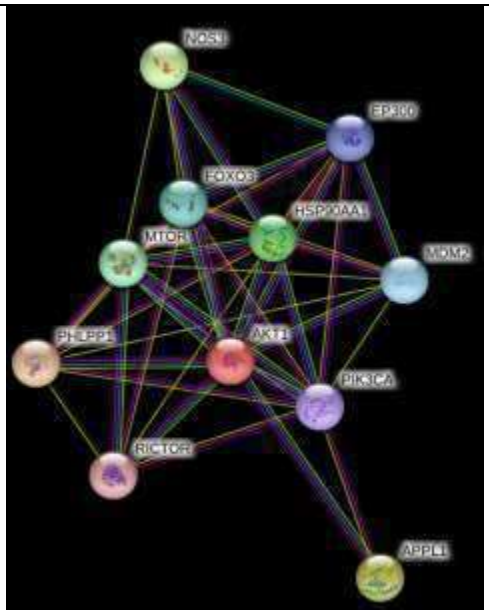

adhesion regulation is required. • Encourages the nuclear import of SRPK2. • Activates the pro-apoptotic functions of BAD. • Inversely affects the acetylation of p53. • Changes the cytoskeleton's structure and cellular motility. • [366, 367]	
Upregulated in TNBC following treatment where it is already upregulated in untreated TNBC cells compared to normal breast cells	
ALK	

• A neuronal receptor tyrosine kinase (RTK) is a protein that is found in certain parts of the central and peripheral nervous systems and is required for nervous system maturation and specialisation. • Promotes cell proliferation via the IRS1, MAPK, and PI3- kinase pathways. Stimulates NF-kappa-B, most likely via IRS1. • Integral to the autocrine signaling that promotes development and sustenance in MDK.	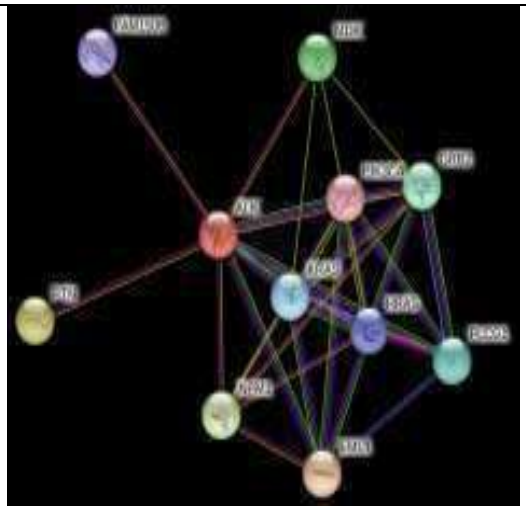
Up-regulated in TNBC following treatment where it is already upregulated in untreated TNBC cells compared to normal breast cells	
c-Ret	
• Involved in cellular growth, neuron guidance, cellular motility, and cellular differentiation. • Engages with glial cell-derived neurotrophic factor (GDNF) ligands [368]. • Regulates the balance between apoptosis and cell survival [369]. • Affects cell adhesion and promotes cellular migration	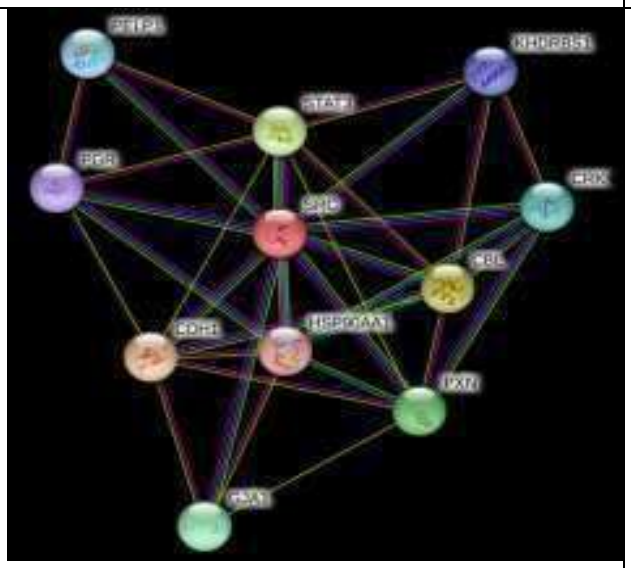

through integrin-mediated mechanisms [369]. • In the presence of GDNF, it promotes cell survival and decreases growth hormone synthesis in somatotrophs, while in the absence of it, it induces apoptosis [370]. • Activates the MAPK and AKT signaling cascades [371]. •	
Exhibited lower expression in treated triple-negative breast cancer (TNBC) cells compared to untreated TNBC cells, with expression levels in normal breast cells significantly lower than in TNBC cells.	
DDR1	
• The interaction with collagen initiates the activation of MMPs, specifically MMP2, MMP7, and MMP9. • Assists in cellular motility [372]	

Expression in untreated TNBC cells is lower than in normal breast cells. Increase in TNBC following treatment
DDR2

• Operates as a cell membrane receptor for fibrillar collagen, overseeing cell differentiation, extracellular matrix (ECM) reorganization, cell motility, and proliferation. • Directs ECM remodelling by boosting collagenase MMP1, MMP2, and MMP13 expression, allowing for cell mobility and tumour cell invasion. • Encourages fibroblast mobility and development, which aids in the repair of skin damage [373]. • . •	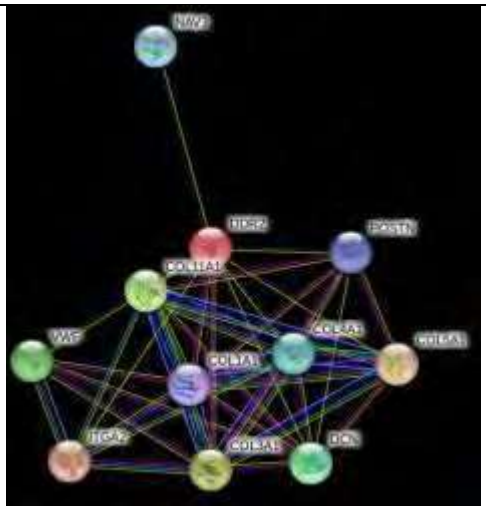
Absent in treated TNBC yet highly high in untreated TNBC	
Dtk	
• Engages with various ligands, including TULP1 and GAS6 [374]. • Governs cellular survival, motility, and differentiation [375]. • Amplifies the functionality of PI3-kinase [376]. • The AKT survival pathway is activated, which includes the translocation of NF-kappa-B into the nucleus [376]. • Changes the cytoskeleton's structure [377]. • Activates STAT1 to suppress the TLR innate immune response [377].	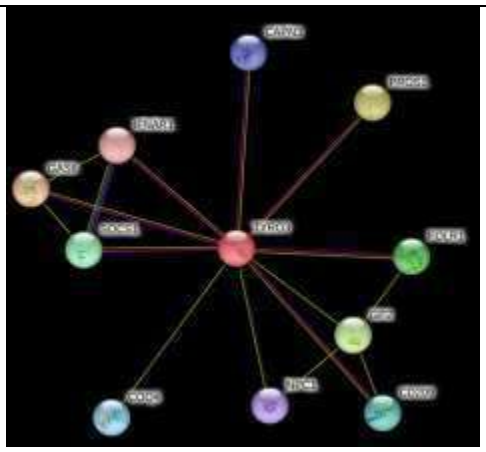

Downregulated in TNBC following treatment lower than normal breast cells. Very high expression in untreated TNBC
EphA family
By interacting with ephrin-binding proteins, the EphA family of receptor tyrosine kinases (RTKs) mediates contact-mediated signaling [378]. A ligand family on nearby cells influences cellular proliferation, motility, and programmed cell death [379]. The involvement of EphA receptors in tumorigenesis is complex and context-dependent, as they can either facilitate or inhibit tumour development [380, 381].
EphA1

• Binds to EFNA3, EFNA4, and EFNA1 to cause cell adherence to the extracellular matrix (ECM) and to inhibit cell dispersion and motility [382]. • Furthermore, it promotes angiogenesis and regulates cellular proliferation. It may potentially play a role in programmed cell death (apoptosis) [382].	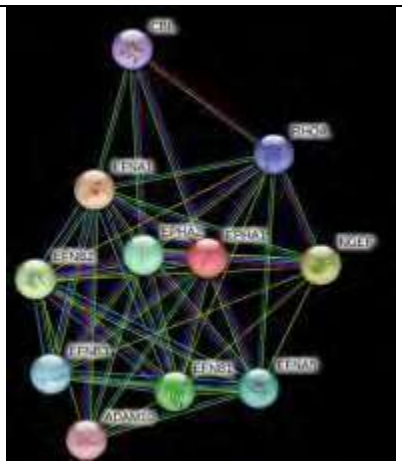
Following therapy, there was a reduction in expression in triple-negative breast cancer (TNBC), with expression levels in normal breast cells being greater than in TNBC cells.	
EphA2	
• Activated by the ligand ephrin-A1/EFNA1 [383]. • Cell migration, adhesion, growth, and specialisation are all regulated by this protein [383]. • Suppresses the ERK1/ERK2 signaling	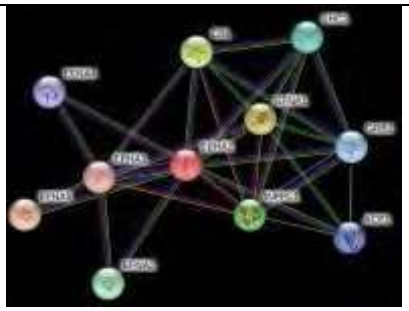

cascade [384]. • It contributes to the creation of new blood vessels (angiogenesis) [384].	
Following therapy, expression in TNBC cells is substantially greater than in normal breast cells.	
EphA3	
• Oversees cell-cell adhesion, cytoskeleton organisation, and cellular motility [385]. • Contributes to the migration and specialisation of heart cells [386]. • Directs the separation of motor and sensory axons during the creation of neuromuscular circuits, but not their navigation [387]. •	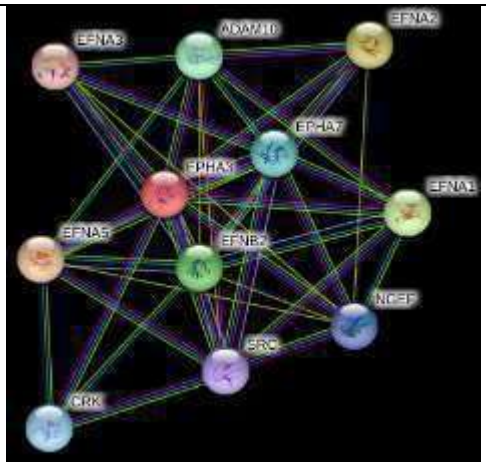
TNBC expression was reduced after therapy with levels comparable to normal breast cells.	
EphA4	
• As the sole Eph receptor activated by both GPI-anchored ephrin-A and transmembrane ephrin-B ligands, it demonstrates significant adaptability [388]. • Controls cell shape and integrin-dependent cell adhesion [389]. • Oversees various stages of axonal navigation [389].	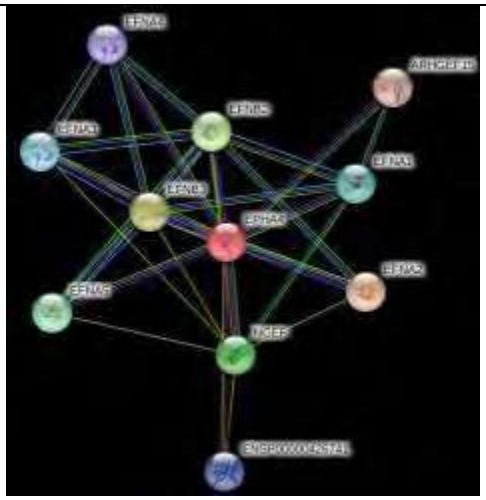

• Interferes with adherens junctions by severing cadherins [390]. •	
Decreased expression in treated TNBC cells. Expression in TNBC higher than in normal breast cells	
EPHA6	
• Can have either a tumour-promoting or tumour-suppressing effect [391]. • Cell proliferation, migration, and death are all facilitated by this protein. cell proliferation, migration, and death are all facilitated by this protein [392].	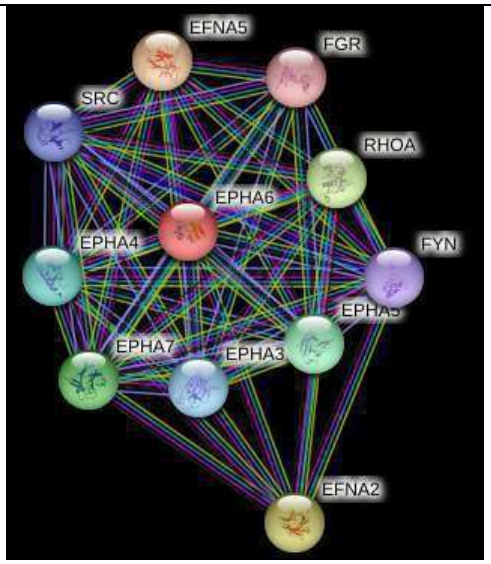
Following therapy, there is a slight rise in expression in triple-negative breast cancer (TNBC). Normal breast cells have much greater levels of expression than TNBC cells.	
EPHA7	

• It has the capacity to either accelerate or prevent tumour growth [393, 394]. • Cellular proliferation, migration, and programmed cell death are all regulated by this protein (apoptosis) [393].	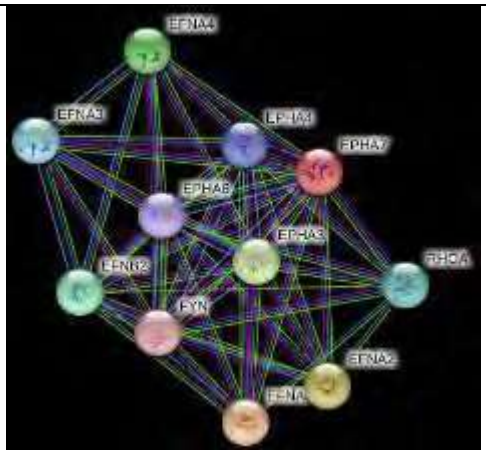
Shows increased expression in triple-negative breast cancer (TNBC) cells after therapy, but not in untreated TNBC cells. Normal breast cells have much greater levels of expression than TNBC cells.	
EphB family	
An RTK (Receptor Tyrosine Kinase) that binds to membrane-bound ephrin family ligands on nearby cells, resulting in contact-dependent bidirectional signaling (Conover et al., 2000). Forward signaling refers to the signaling cascade downstream of the receptor, whereas reverse signaling refers to the signaling cascade downstream of the ephrin ligand [395].	
EphB1	

• Directs the growth of axons in the retina. • Oversees chemotaxis [396]. • Possibly governs the process of angiogenesis [397]. • It is possible that it has a function in focused cell migration and adhesion [398, 399].	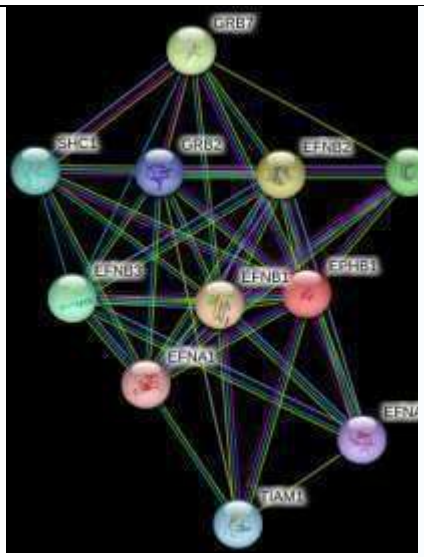
Following therapy, it was downregulated in triple-negative breast cancer (TNBC), reaching levels comparable to normal breast cells.	
EphB3	

• Orchestrates axon navigation during developmental stages [400]. • Regulates cellular migration and positioning, along with angiogenesis [400]. • Supervises the movement and adhesion of cells responsible for forming tubes in the urethra and partitioning the cloaca [401].	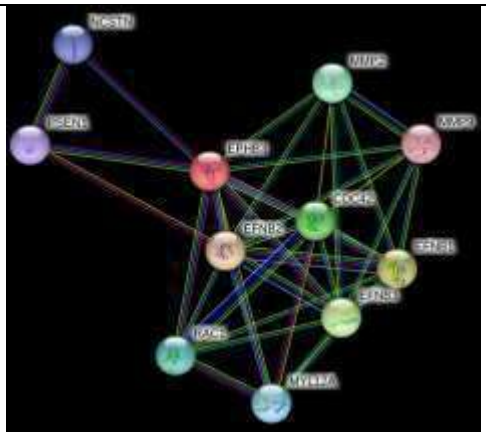
Following therapy, there is a reduction in expression in triple-negative breast cancer (TNBC).	
EphB4	

EphB4

- Cell adhesion and migration are regulated, and it is important in angiogenesis, blood vessel remodelling, and vascular permeability. Forward signaling via EPHB4 regulates cellular repulsion and segregation from EFNB2-expressing cells [402].

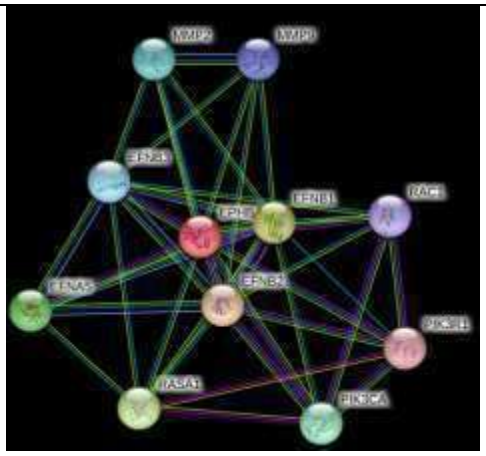

Although there is an increase in expression in triple-negative breast cancer (TNBC) cells after therapy, the level of expression in TNBC cells remains lower than in normal breast cells.

EphB6

- Affects cell adhesion and migration, exerting both stimulating and inhibitory impacts [403].
- When triggered by ephrin-B2, it inhibits JNK activation, T-cell receptor-induced IL-2 release, and CD25 expression [404].

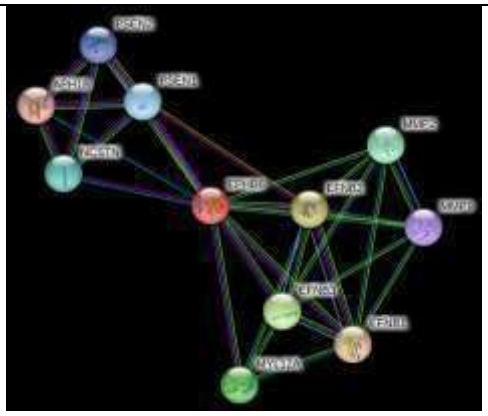

Following therapy, there is a small reduction in expression in triple-negative breast cancer (TNBC). TNBC has much greater levels of expression than normal breast cells.

EGFR

• Binds to ligands from the EGF family, such as EGF, TGFA/TGF-alpha, AREG, epigen/EPGN, and HBEGF/heparin-binding EGF [405]. • Signaling pathways such as RAS-RAF-MEK-ERK, PI3 kinase- AKT, PLC gamma-PKC, and STATs are activated [406]. • The NF-kappa-B signaling pathway may also be activated [407]. • Enhances cell movement via interactions with BTC/betacellulin and epiregulin/EREG [408].	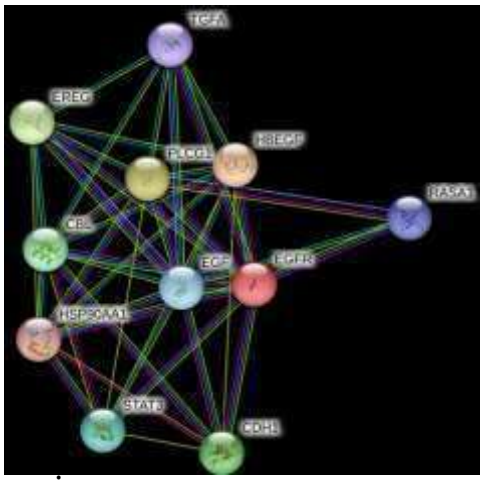
Following therapy, shows reduced expression in triple-negative breast cancer (TNBC), with TNBC cells exhibiting much greater expression levels than normal breast cells.	
ErbB family	
Functions as a cell membrane receptor for neuregulins [409].	
ErbB2	

Increases cancer metastasis by amplifying numerous metastasis- associated features [410].	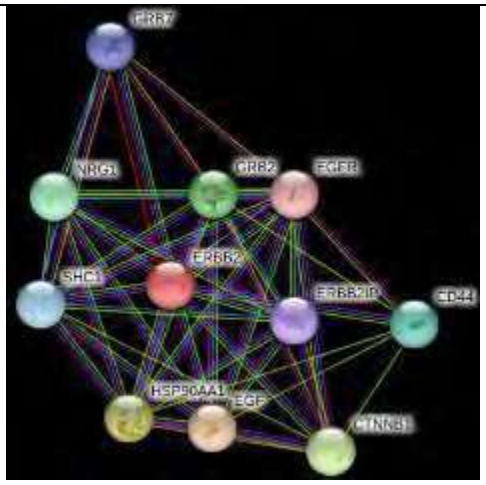
Following therapy, the amount of expression in triple-negative breast cancer (TNBC) cells rose, although it remained half that of normal breast cells. The expression was undetectable in untreated TNBC cells.	
ErbB3	

• Binds to neuregulin-1 (NRG1) [411, 412]. • Phosphatidylinositol 3-kinase activation is initiated (PI3K) [412]. • Myeloid cell differentiation is regulated by this protein [413].	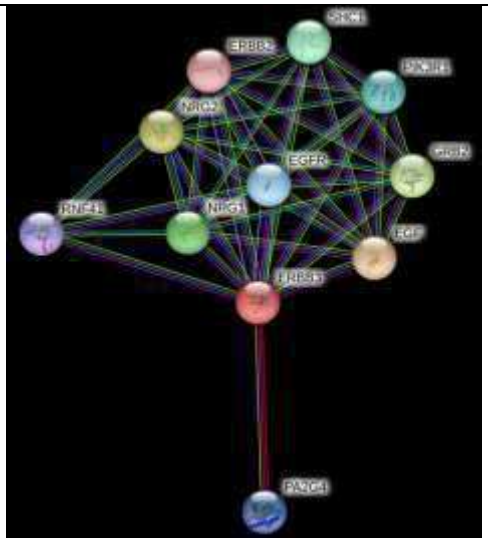
After therapy, the expression in triple-negative breast cancer (TNBC) cells decreases but stays greater than in normal breast cells.	
ErbB4	

ErbB4 stands out among its receptor peers, being the only one recognized for having properties that inhibit growth [414].	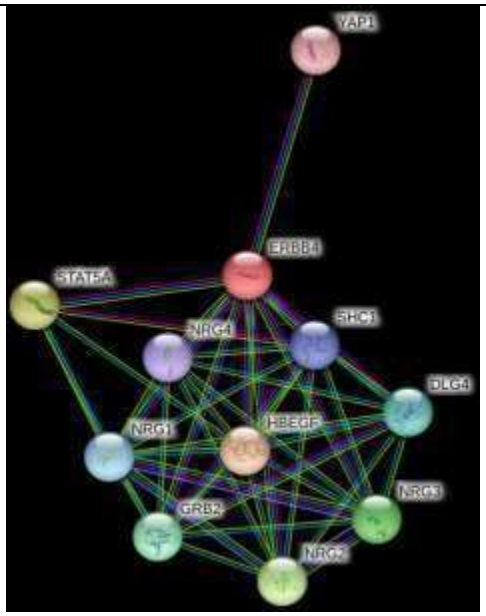
There is an increase in expression in treated triple-negative breast cancer (TNBC) cells, approaching normal breast cell levels. Untreated TNBC cells, on the other hand, continue to express less than normal breast cells.	
FGFR family	
• A tyrosine-protein kinase that acts on the cellular membrane as a receptor for fibroblast growth factors, helping to regulate cellular proliferation, differentiation, and motility [415]. • Promotes PLCG1 and FRS2 phosphorylation. This PLCG1 activation stimulates FRS2, resulting in the participation of GRB2, GAB1, PIK3R1, and SOS1, allowing the activation of RAS, MAPK1/ERK2, MAPK3/ERK1, and the MAP kinase cascade, as well as the AKT1 signaling pathway [416].	
•	
FGFR2a	

- Participates in the process of apoptosis [1].
- It stimulates cellular proliferation in keratinocytes and immature osteoblasts, while it causes apoptosis in adult osteoblasts [2].
- Anomaly signaling is caused by changes that cause continuous kinase activity or hinder normal FGFR2 synthesis, internalisation, and breakdown [1].
- Increased FGFR2 concentrations enhance STAT1 activation [1].

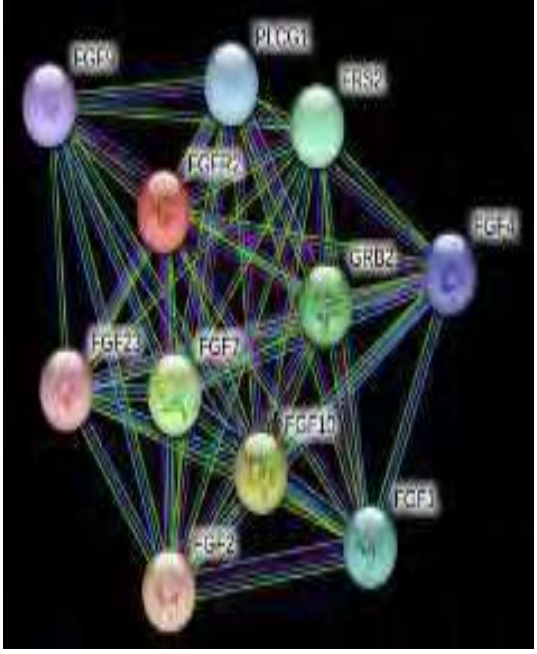

Following therapy, there is a decrease in expression inside triple-negative breast cancer (TNBC) cells, resulting in levels comparable to those found in normal breast cells.

FGF-R3

- Essential in controlling the differentiation, growth, and programmed cell death of chondrocytes.
- Induces programmed cell death in chondrocytes, but can also promote cancer cell growth.
- Excessive expression or persistent activation of FGFR3 results in the

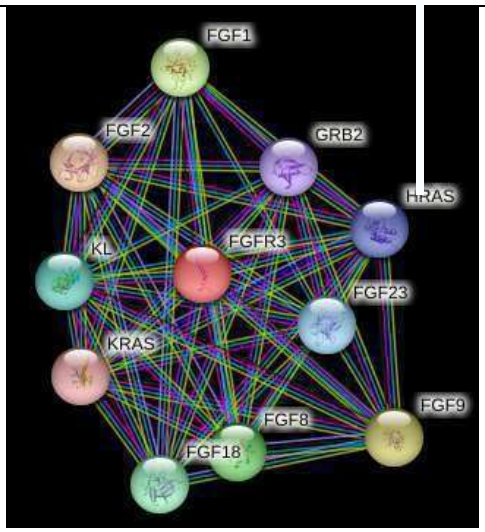

family, has been implicated in various cancers, including rhabdomyosarcoma, hepatocellular, lung, breast, nasopharyngeal, colorectal, esophageal, oral, oropharyngeal, and prostate cancers. Studies have shown that dysregulated FGFR4 activity is associated with advanced-stage, high-grade serous ovarian carcinoma [417], adult epithelial cancers [418], hepatocellular carcinoma [419], rhabdomyosarcomas [420], non-small-cell lung cancer (Huang et al., 2015), and colorectal cancer [421].

<table>
<tr><td></td><td>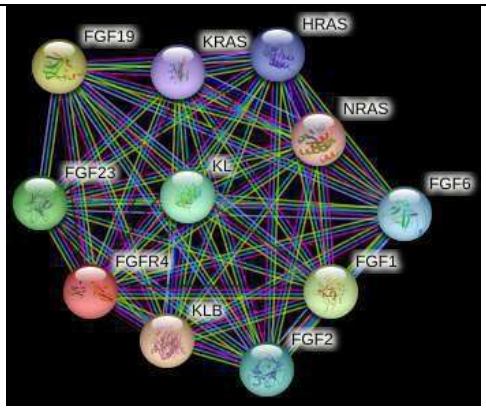
</td></tr>
<tr><td colspan="2">Following therapy, triple-negative breast cancer (TNBC) expression decreases. Untreated TNBC cells have much greater expression levels than ordinary breast cells.</td></tr>
<tr><td colspan="2">Flt-3</td></tr>
<tr><td>Interacts with FLT3LG to influence hematopoietic progenitor cell differentiation, proliferation, and survival [422].
MTOR and RAS signaling pathways are activated, resulting in MAPK1/ERK2 signaling [423].
Genetic modifications leading to continuous kinase activity enhance cellular proliferation and inhibit apoptosis [424].</td><td>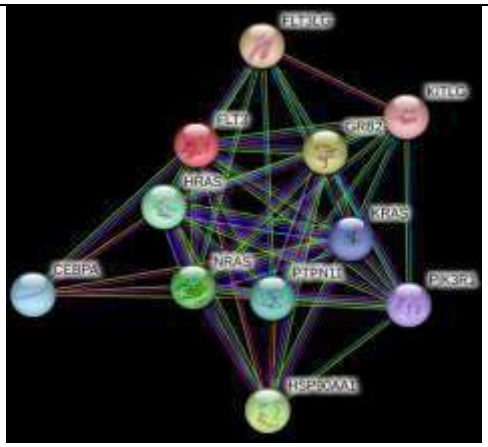
</td></tr>
<tr><td colspan="2">Following treatment, expression decreases in triple-negative breast cancer (TNBC) cells. The highest level of expression is found in
untreated TNBC cells. TNBC cell expression levels drop significantly after therapy, dropping below those of normal breast cells.</td></tr>
<tr><td colspan="2">HGFR</td></tr>
</table>

• Governs cellular proliferation, migration, differentiation, and survival processes [425]. • Activates PIK3R1, PLCG1, SRC, GRB2, STAT3, or the adaptor GAB1, triggering a variety of signaling pathways such as RAS-ERK, PI3 kinase-AKT, and PLC gamma-PKC [2]. • Induces morphogenetic alterations and enhances cell viability [426].	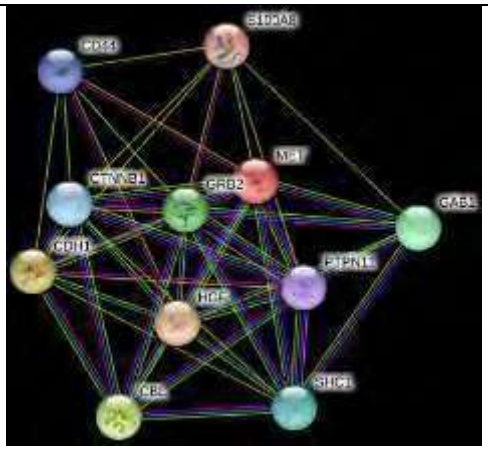

After therapy, expression in triple-negative breast cancer (TNBC) cells reduces dramatically, nearing normal breast cell levels. Expression is extremely high in untreated TNBC cells.
IGF-IR

• It binds to insulin-like growth factor 1 (IGF-1) (IGF1). • Plays a role in regulating cellular growth and survival. • Essential for tumour formation and cancer cell survival. Activates the PI3K-AKT/PKB and Ras-MAPK pathways, increasing cellular proliferation, decreasing apoptosis, and increasing protein synthesis. • Interacts with Grb2/SOS to initiate the Ras-MAPK pathway. • Activates JNK, which in turn stimulates STAT proteins crucial for the oncogenic	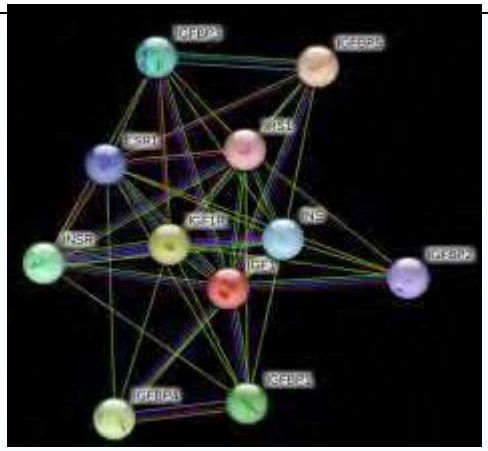

effect of IGF1R. • [427-433]	
The expression of triple-negative breast cancer (TNBC) decreases after therapy. Normal breast cells have the highest levels of expression.	
Insulin receptor	
• It binds to insulin-like growth factor 1 (IGF-1) (IGF1). • Involved in the control of cell growth and survival. Vital for tumour transformation and the persistence of cancerous cells [426]. • The PI3K-AKT/PKB and Ras-MAPK pathways are activated, resulting in enhanced cell proliferation, reduced programmed cell death, and increased protein output [426]. • Stimulates AKT/PKB, leading to mTOR-driven protein synthesis and anti-apoptotic actions [426]. • Initiates the JNK pathway, subsequently activating transcription (STAT) proteins	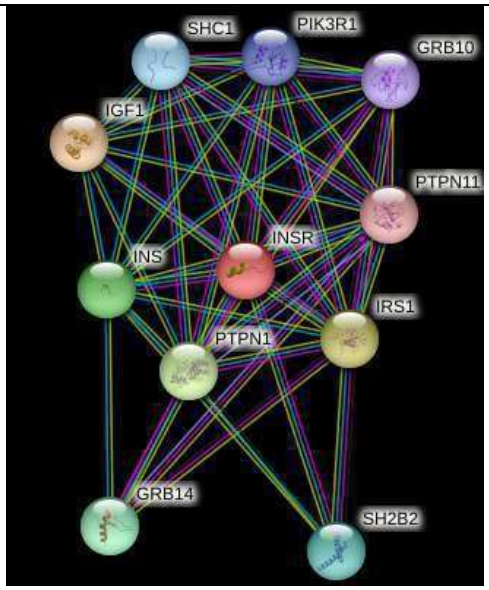

[434]. • STAT3 may be required for IGF1R's transformational action [434].	
After therapy, expression in triple-negative breast cancer (TNBC) cells decreases considerably, falling to levels far lower than in normal breast cells. Expression levels are much greater in untreated TNBC cells.	
MspR	

• Oversees cellular survival, motility, and differentiation mechanisms [435]. • Influences PIK3R1, PLCG1, or the adaptor GAB1, causing the RAS-ERK, PI3 kinase-AKT, or PLC gamma-PKC pathways to be activated [436]. • Helps wound healing by promoting epithelial cell motility, proliferation, and survival [437]. • Contributes to the innate immune response by controlling macrophage motility and phagocytic activity [438].	

• Controls macrophage motility and phagocytic activity, which contributes to the innate immune response [437]. • In response to growth factors other than the MST1 ligand, it generates signals for cellular migration and proliferation [438].	
Following therapy, expression in triple-negative breast cancer (TNBC) cells decreases significantly, reducing to levels far lower than in normal breast cells. Expression levels are much greater in untreated TNBC cells.	
Mer	
• Activates LGALS3, TUB, TULP1, or GAS6 [439]. • Controls cellular survival, motility, differentiation, and apoptotic cell phagocytosis (efferocytosis) [440]. • Activates GRB2 or PLCG2, causing MAPK1, MAPK2, FAK/PTK2, or RAC1 to be activated [441]. • Plays a function in macrophage clearance of apoptotic cells, platelet aggregation, cytoskeleton reorganisation, and phagocytic activities [442]. • Inhibits the TLRs innate immune response through STAT1 [443].	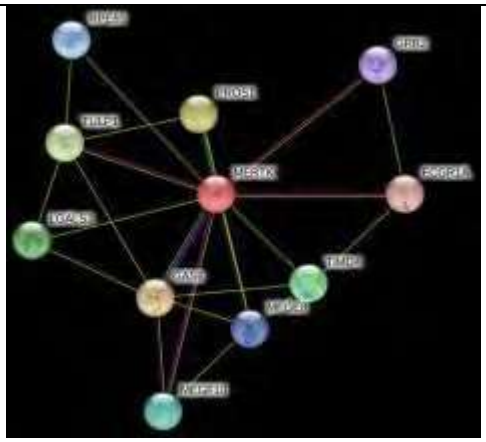
Following therapy, expression in triple-negative breast cancer (TNBC) cells decreases significantly, reducing to levels far lower than in	

normal breast cells. Untreated TNBC cells had much higher expression levels.
MuSK

• Participates in the operations of the neuromuscular junction (NMJ) [444]. • Aids in actin cytoskeleton reorganisation and acetylcholine receptor (AChR) clustering in the postsynaptic membrane [445]. • May improve the function of Rho family GTPases [446]. • Could potentially be involved in the central nervous system [447].	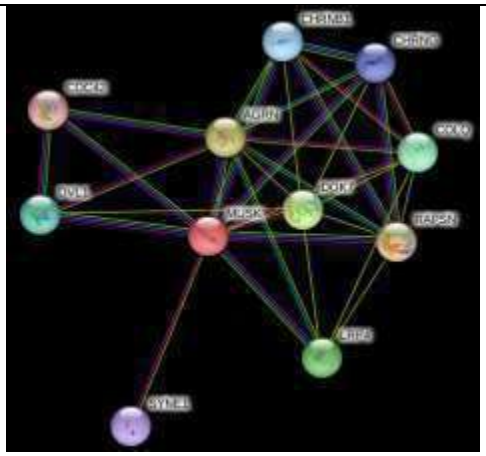
Following therapy, expression in triple-negative breast cancer (TNBC) cells declines considerably, falling to levels far lower than in normal breast cells. Expression levels are much greater in untreated TNBC cells.	
PDGFRα	
• Engages with PDGFA, PDGFB, and PDGFC [448]. • Oversees cellular proliferation, survival, and chemotaxis [448] • Either promotes or inhibits cellular growth and migration. Involved in cellular motility and guided movement during wound repair [449]. • Affects platelet activation, the release of mediators from platelet granules, and platelet clumping triggered by thrombin.	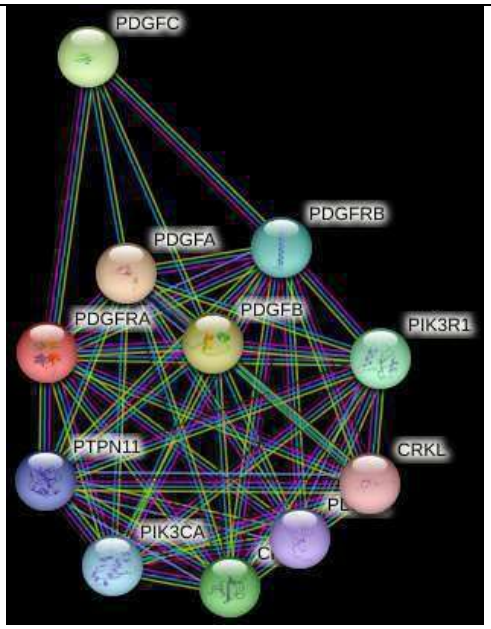

• The activation of PKC and PIK3R1 leads to the stimulation of AKT1 [2]. • Helps to activate HRAS and the MAP kinases MAPK1/ERK2 and/or MAPK3/ERK1 [450]. • Activates STAT family proteins STAT1, STAT3, and STAT5A and/or STAT5B [448].	
Following therapy, expression in triple-negative breast cancer (TNBC) cells decreases to levels equivalent to those in normal breast cells. TNBC cells that have not been treated have much higher levels of expression.	
ROR1	

• Functions as a receptor for the WNT5A ligand, activating subsequent NFkB signaling and perhaps inhibiting WNT3A-mediated signaling [451]. • ROR1-positive TNBC cells have been reported in studies to have increased tumour cell proliferation and to have a shorter disease duration. -free existence [451]. • has been linked to the inhibition of cellular growth and the promotion of apoptosis in TNBC cellshas been linked to the inhibition of cellular growth and the	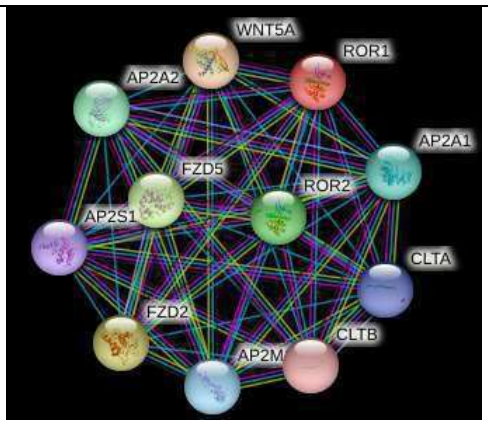

promotion of apoptosis in TNBC cells [452]. • ROR1 inhibition has been found to prevent breast cancer epithelial-mesenchymal transition and metastasis [452] • has been associated to basal-like breast cancer cell line invasiveness [453].	
Following therapy, expression is increased in triple-negative breast cancer (TNBC) cells, resulting in greater levels in treated TNBC relative to normal breast cells. Untreated TNBC cells had the lowest expression levels.	
ROR2	
• The receptor tyrosine kinase-like orphan receptor 2 (ROR2) has been discovered as a receptor for the Wnt ligand WNT5A, which has implications for suppressing WNT3A-mediated signaling [454].	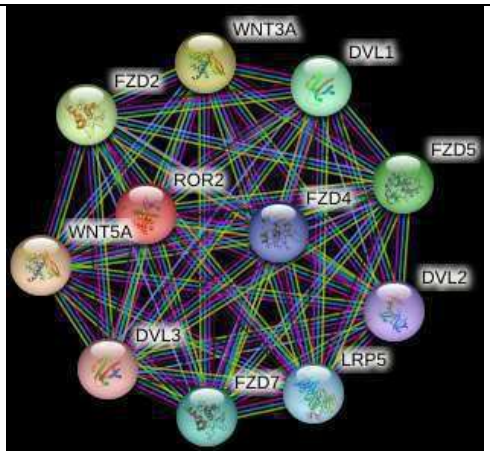
Following therapy, expression diminishes in triple-negative breast cancer (TNBC) cells. Untreated TNBC cells had much higher expression than normal breast cells, and even after therapy, TNBC cells have higher expression than normal breast cells.	
RYK	

- Contributes to neuron differentiation, axon navigation, and neurite outgrowth by interacting with WNT1, WNT3, WNT3A, and WNT5A [455].
- This receptor is cleaved at its C-terminus in the transmembrane domain upon WNT3 activation, allowing the intracellular C-terminal fragment to move from the cytoplasm to the nucleus, where it plays an important role in neuronal development [456].

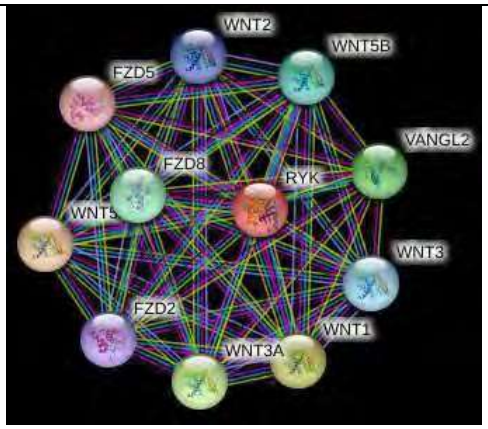

After therapy, expression is decreased in triple-negative breast cancer (TNBC) cells. Untreated TNBC cells had much greater expression
than normal breast cells. The expression level in treated TNBC cells is lower than in normal breast cells.

Tie-1

- A transmembrane tyrosine-protein kinase that may control TEK/TIE2 activity and is implicated in angiogenesis regulation.A transmembrane tyrosine-protein kinase that may control TEK/TIE2 activity and is implicated in angiogenesis regulation.
- [457-468].

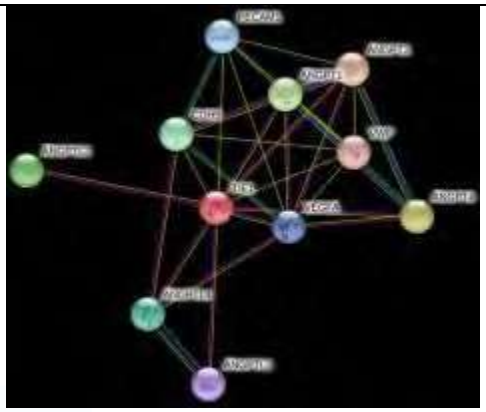

Following therapy, expression rises in triple-negative breast cancer (TNBC) cells. Untreated TNBC cells had lesser expression than
normal breast cells. TNBC cell expression somewhat outperforms normal cell expression after therapy.

Tie-2

- Functions as an ANGPT1, ANGPT2, and ANGPT4 receptor .
- Endothelial cell angiogenesis, survival, proliferation, motility, adhesion, and spreading, as well as actin cytoskeleton remodelling and vascular quiescence, are all regulated by this protein.
- Anti-inflammatory properties are demonstrated.
- Depending on the environmental setting, it either stimulates or inhibits angiogenesis postnatally.
- Reduces angiogenesis in areas where endothelial cells are densely packed.
- It stimulates PTK2/FAK, MAPK1/ERK2, and MAPK3/ERK1 in migrating endothelial cells that lack cell-cell adhesions to promote sprouting angiogenesis.
- DOK2, GRB7, GRB14, PIK3R1, SHC1, and TIE1 are all

phosphorylated.

[469-471]

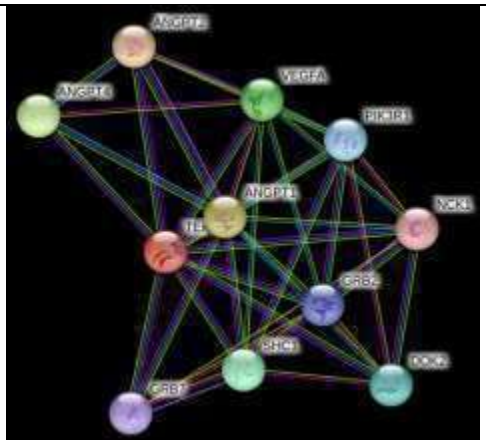

After therapy, expression is increased in triple-negative breast cancer (TNBC) cells. Expression levels in untreated TNBC cells are lower

than in normal breast cells. TNBC cell expression somewhat exceeds that of normal cells after therapy.

Trk family

This receptor tyrosine kinase (RTK) is involved in both the central and peripheral nervous systems' development and maturation. It regulates a wide range of neuronal processes, including survival, proliferation, migration, differentiation, and the formation and plasticity of synapses [472].

TrkA

- Acts as a receptor for nerve growth factor (NGF), influencing neuronal development, neural cell proliferation, nociceptor function, and apoptosis avoidance [473].

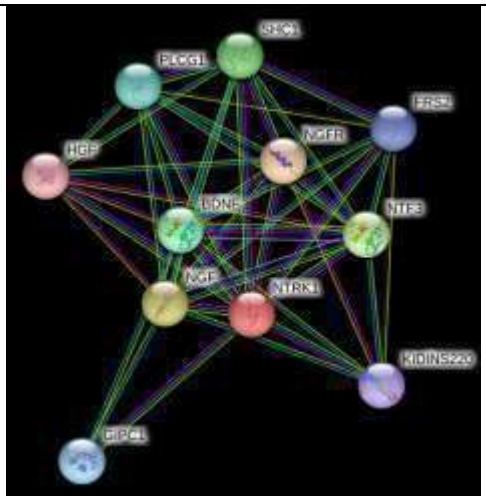

Following therapy, expression rises in triple-negative breast cancer (TNBC) cells. Expression is lower in untreated TNBC cells than in normal breast cells. Nonetheless, even after therapy, TNBC cell expression remains much lower than in normal cells.

Trk B

- It is a BDNF/brain-derived neurotrophic factor and NTF4 receptor [474].
- Regulates the survival of neurons [475].
- Activates SHC1, FRS2, SH2B1, SH2B2, and PLCG1, which are involved in regulatory processes [476].
- Dictates neuronal differentiation, including neurite outgrowth [477].
- Oversees both cell development and survival [477].

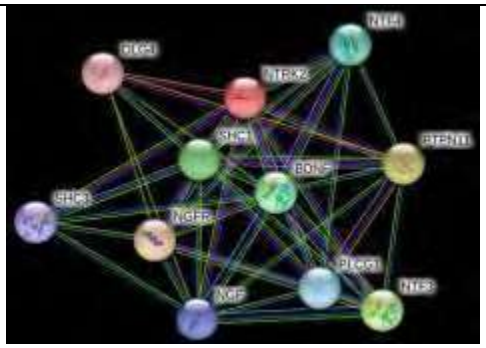

• Participates in the activation of NF-Kappa-B and cell survival [477].	
Following therapy, expression in triple-negative breast cancer (TNBC) is downregulated. TNBC cells had high levels of expression prior to therapy, but untreated normal breast cells do not.	
TrkC	

• The neurotrophic receptor tyrosine kinase 3 (NTRK3) is important in the development of the nervous system and perhaps the heart. When NTRK3 binds to its ligand NTF3/neurotrophin-3, it autophosphorylates and begins multiple signaling pathways, including the phosphatidylinositol 3-kinase/AKT and MAPK pathways, which are important for governing cell survival and differentiation. Furthermore, NTF3 promotes anoikis resistance in cancer cells, and NTRK gene deregulation can result in oncogenesis. Neurotrophins exert biological effects by activating the tropomyosin-related kinase (Trk) family of receptor tyrosine kinases (TrkA, TrkB, and TrkC) [478]. NTRK3 is also a transmembrane receptor tyrosine kinase that	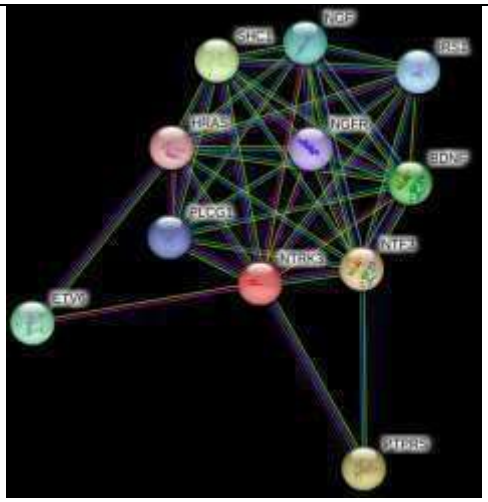

interacts to neurotrophin-3 (NT-3) [479]. These findings emphasise the importance of NTRK3 and its ligand NTF3 in a variety of physiological and pathological processes, as well as their potential as therapeutic targets in a variety of disorders.	
Expression decreases in triple-negative breast cancer (TNBC) following treatment. Before treatment, TNBC cells exhibit significantly elevated expression levels compared to normal cells. After treatment, expression in TNBC cells falls below that in normal breast cells.	
VEGFR family	
Allows MAPK1/ERK2, MAPK3/ERK1, and the MAP kinase signaling pathways, as well as the AKT1 signaling pathway, to be activated. It catalyses SHC1 phosphorylation and enables PIK3R1 phosphorylation, which is a regulatory component of phosphatidylinositol 3-kinase. Furthermore, it promotes the phosphorylation of MAPK8 at 'Thr-183' and 'Tyr-185', as well as AKT1 at 'Ser-473' [480].	
VEGFR1	
Expression decreases after treatment. In normal breast cells, expression levels are higher compared to those in triple-negative breast cancer (TNBC) cells.	
VEGF R2	

• Functions as a VEGFA, VEGFC, and VEGFD cell-surface receptor [483]. • Manages the control of angiogenesis and vascular permeability [483]. • Promotes cellular proliferation, survival, migration, and differentiation [483]. • Aids in the reorganisation of the actin cytoskeleton [484]. • PLCG1 activation causes protein kinase C to be activated [483]. • Indispensable for VEGFA-induced stimulation of NOS2 and NOS3, leading to NO signaling [485].	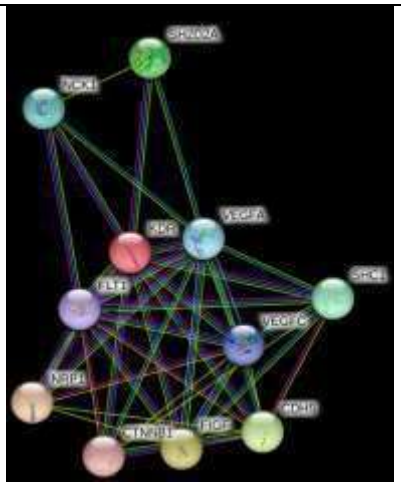
Following therapy, expression diminishes. Expression levels in normal breast cells are much lower than in triple-negative breast cancer (TNBC) cells.	

VEGFR3

• Plays an important function in adult lymphangiogenesis by acting as a cell-surface receptor for VEGFC and VEGFD [486]. • Endothelial cell proliferation, survival, and migration are promoted, and angiogenic sprouting is coordinated [487]. • Modifies KDR signaling via forming heterodimers [488]. • Aids in the activation of the JUN signaling pathway and the AKT1 signaling pathway [489].	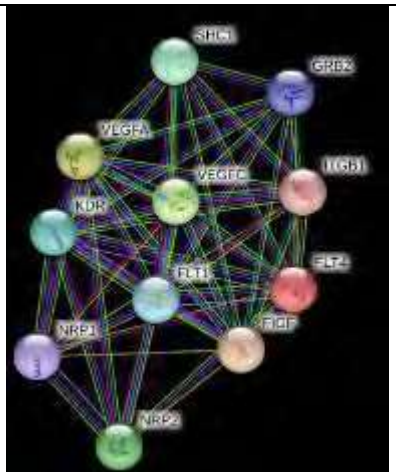
Following therapy, expression diminishes. Expression levels in normal breast cells are much lower than in triple-negative breast cancer	

(TNBC) cells.

3.23 Whole transcriptome analysis of treated and untreated TNBC and normal breast cells

RNA was isolated from MDA-MB-231 and MCF10A cells before and after exposure to 350 µg/mL of *water-soluble T. violacea* extract. RNA sample concentrations were determined using a Qubit RNA concentration kit and Qubit instrument. RNA samples were sent to Inqaba Biotec for sequencing. The data returned from Inqaba Biotec included a list of genes with the number of counts for each transcript, as well as the gene identities and their p-values, as well as their ranking.

The fold-change values were calculated and the corresponding p-values were plotted in a volcano plot. In Figure 3.38, the genes exhibiting significantly increased or decreased expression are highlighted in the plot. Notably, a larger number of genes displayed altered expression patterns following treatment with MDA-MB231 cell extract (Plot A).

When comparing the treated and untreated normal breast cells (Plot B), only a few genes showed statistically significant upregulation or downregulation. In the comparison between untreated TNBC and normal breast cells (Plot C), a substantial number of genes were significantly downregulated in the TNBC cells. Lastly, when comparing treated and untreated TNBC cells (Plot D), significant downregulation of gene transcription was observed following treatment, whereas a smaller number of genes exhibited significantly increased expression levels.

Apart from genes coding for proteins, sequencing has also detected a number of non-coding RNAs, the transcription of which is affected by treatment. To identify which genes and ncRNAs with altered transcript levels were shared between samples, Venn diagrams were plotted for the number of genes with significantly altered transcript levels. Figure 3.39 shows these Venn diagrams for the coding genes (A), miRNA (B), and lncRNA (C). The greatest number of gene expression alterations were observed in the upregulated genes in normal breast cells (2995), followed by the downregulated genes

in TNBC cells (1435), upregulated genes in TNBC cells (1117), and downregulated genes in normal breast cells (821). Although many genes are commonly upregulated in both TNBC and normal breast cells following treatment (223), a nearly equal number of genes that are upregulated in normal breast cells following treatment are downregulated in TNBC cells following treatment. In contrast, the number of shared genes downregulated in both TNBC and normal breast cells was relatively small (69).

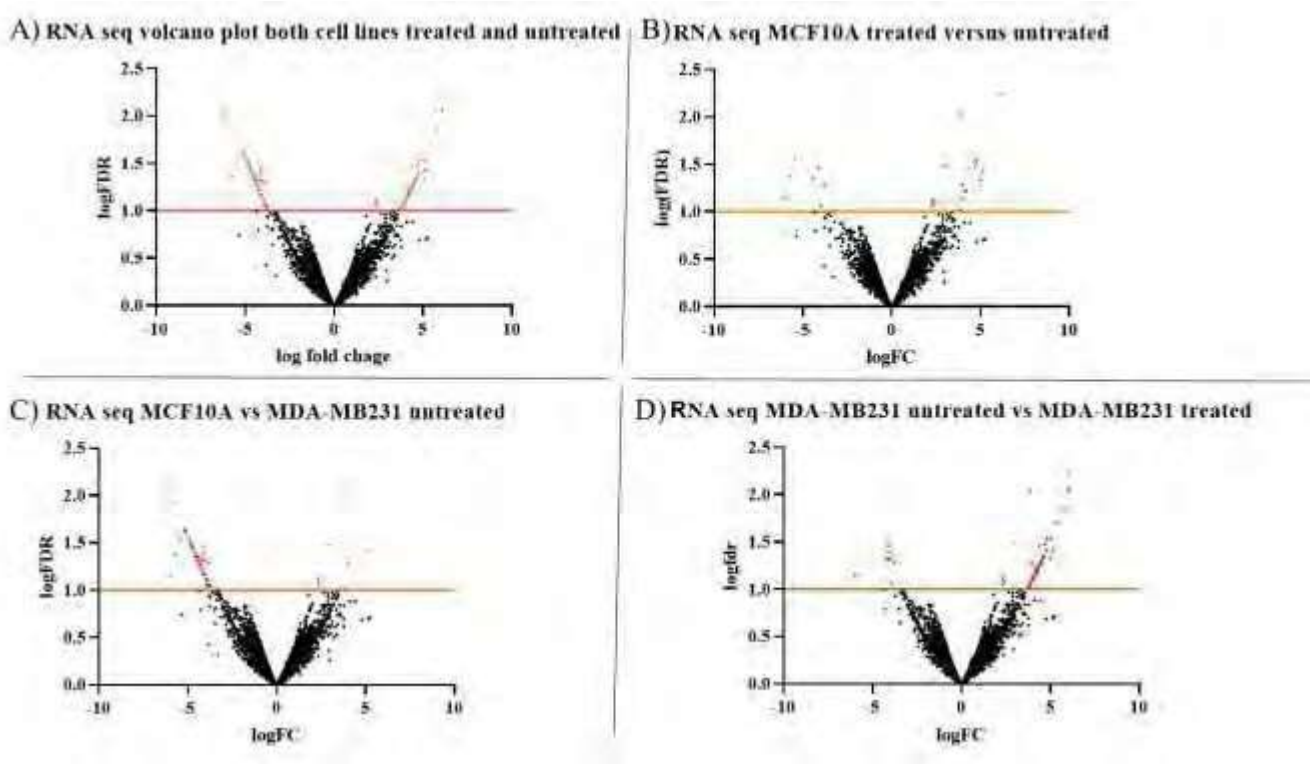

Figure 3.38 presents a series of volcano plots representing the differential gene expression analysis between various cell lines and treatment conditions

Figure 3.38 (A) Comparison of TNBC (MDA-MB-231) and normal breast (MCF-10A) cells showing significant upregulation and downregulation of genes in TNBC cells. (B) Comparison of treated and untreated MCF-10A cells, indicating relatively few changes, but upregulation after *T. violacea* extract treatment. (C) TNBC cells were compared with normal cells, revealing limited altered genes, with the most significant being down-regulated in TNBC cells. (D) Comparison of treated and untreated TNBC cells showing considerable upregulation or downregulation of genes following treatment. The red dots represent statistically significant changes in gene expression.

A

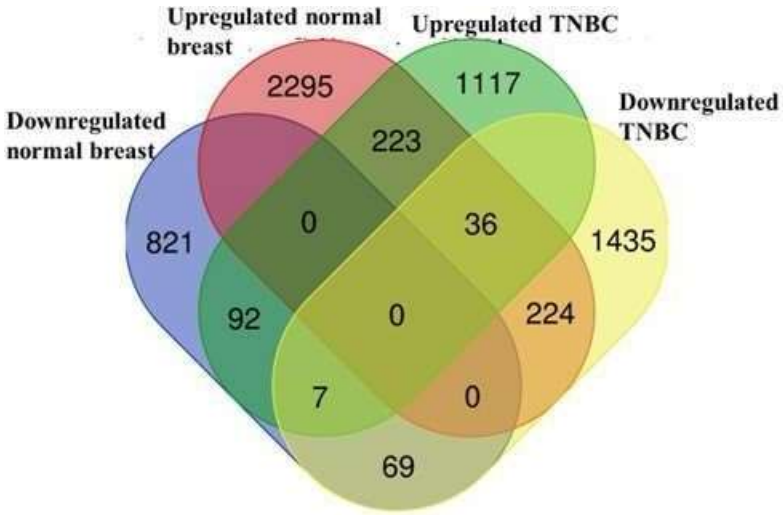
Upregulated normal breast
Upregulated TNBC
Downregulated normal breast
Downregulated TNBC
2295
1117
223
821
0
36
1435
92
0
224
7
0
69

B

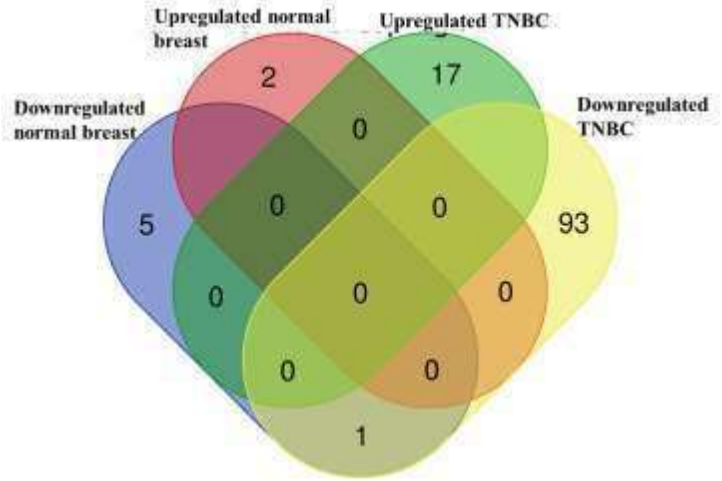
Upregulated normal breast
Upregulated TNBC
Downregulated normal breast
Downregulated TNBC
2
17
0
5
0
0
93
0
0
0
0
0
1

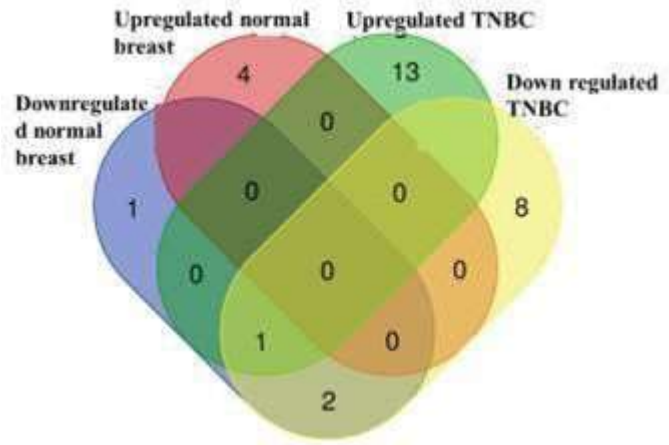

Figure 3.39 39 illustrates the expression changes shared between treated and untreated normal breast and triple-negative breast cancer (TNBC) cell lines. (A) The Venn diagram showingshows the overlap of genes whose expression changed after treatment ofin TNBC A significant number was upregulated in both cell types, but this represented only a fraction of those upregulated in TNBC cells. Many genes upregulated in normal cells were downregulated in TNBC cells. Few genes were downregulated in both cell lines, indicating differential gene responses to treatment. (B) and (C) reveal virtually no overlap in differentially expressed miRNAs and lncRNAs between the cell lines, likely due to the RNA extraction methods not targeting these small RNA molecules, identifying only highly expressed ones. Another 3.39 shows how treated triple-negative breast cancer (TNBC) and normal breast cells share gene expression patterns. The data revealed that 223 genes were upregulated in both TNBC and normal breast cancer cells treated with the water-soluble extract. Conversely, 69 genes were consistently downregulated in both the cell types following treatment. Interestingly, 92 genes showed divergent responses; they were increased after therapy in TNBC cells but were downregulated in normal breast cells. Furthermore, after treatment with the water-soluble extract, 224 genes showed an inverted pattern, being downregulated in TNBC cells, but upregulated in normal breast cells. The overall number of independently elevated genes in each cell type significantly outnumbered the number of shared genes, suggesting that a large number of genes were singularly upregulated or downregulated in either TNBC or normal breast cells following therapy.

Figure 3.40 shows a PANTHER analysis of genes with altered expression grouped by biological function. Cancer-associated pathways constituted the largest percentage in these categories. These cancer-associated pathways include the Wnt, cadherin, and CCKR signaling pathways. The CCKR pathway centres on gastrin, which primarily stimulates the secretion of hydrochloric acid (HCl).

Additionally, it functions as a mitogenic factor in the gastrointestinal epithelial cells. The expression of this hormone is elevated in precancerous tissue.This pathway also involves downstream components that affect cell survival and angiogenesis. The Hh signaling pathway, which controls cell adhesion, is also represented.

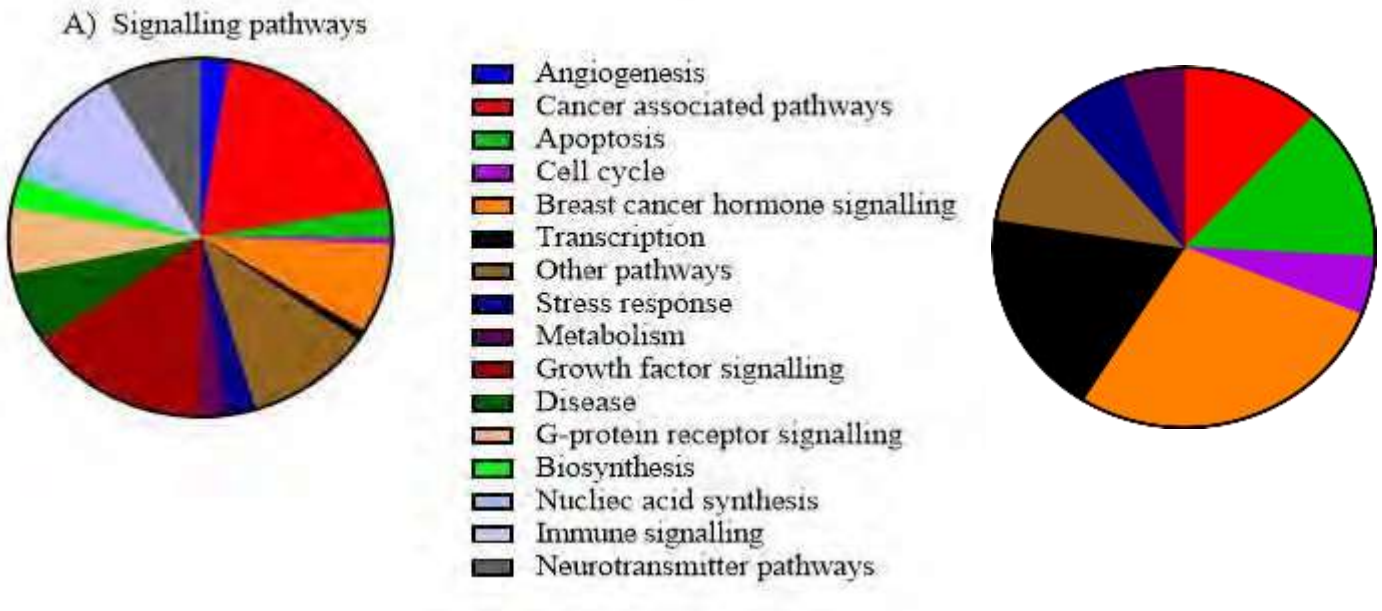

A) Growth factor signaling

EGF receptor signaling pathway FGF signaling pathway

Insulin/IGF pathway-protein kinase B Integrin signaling pathway

PDGF signaling pathway TGF-beta signaling pathway VEGF signaling pathway

Insulin/IGF pathway-MAP kinase

B) Hormone signaling involved in breast cancer

Androgen/estrogene/progesterone biosynthesis Gonadotropin-releasing hormone receptor

Oxytocin receptor mediated signaling Androgen/estrogene/progeste rone biosynthesis

- Thyrotropin-releasing hormone receptor
- PI3 kinase pathway
- Plasminogen activating cascade Cadherin signaling
- CCKR signaling map FAS signaling
- Hedgehog signaling JAK/STAT signaling p38 MAPK pathway p53 pathway
- p53 pathway glucose deprivation p53 pathway feedback loops 2 Ras Pathway
- Ubiquitin proteasome pathway Wnt signaling
- Notch signaling
- Endothelin signaling

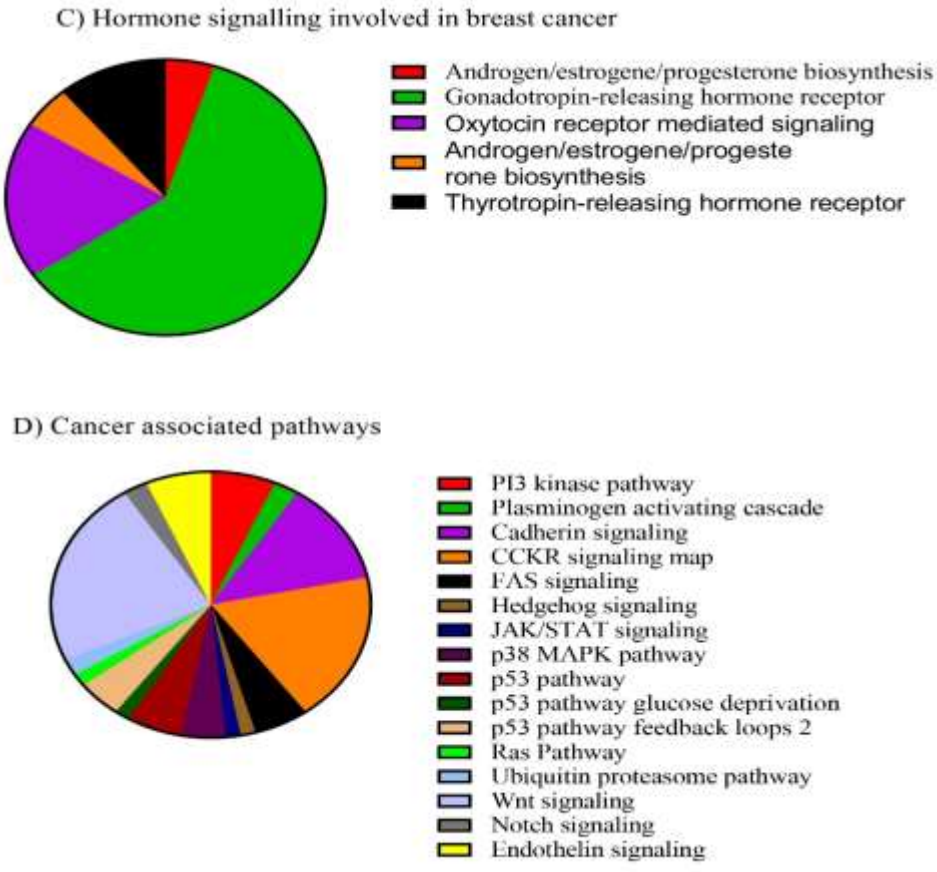

Figure 3.40 4039 illustrates the expression changes shared between treated and untreated normal breast and triple-negative breast cancer (TNBC) cell lines

Figure 3.40 shows a PANTHER analysis of the genes with altered expression grouped by biological function. Cancer-associated pathways make up the largest percentage of these categories. These cancer-associated pathways include Wnt signaling pathways, cadherin signaling pathways, and CCKR signaling pathways. The CCKR pathway centers on the gastrin hormone, which primarily stimulates the secretion of hydrochloric acid (HCl). Additionally, it functions as a mitogenic factor for gastrointestinal epithelial cells. The expression of this hormone is elevated in pre-cancerous tissue. The pathway also involves downstream components that affect cell survival and angiogenesis. The Hh signaling pathway, which controls cell adhesion) Growth factor is also represented.

- EGF receptor signaling pathway
- FGF signaling pathway
- Insulin/IGF pathway-protein kinase B
- Integrin signaling pathway
- PDGF signaling pathway
- TGF-beta signaling pathway
- VEGF signaling pathway
- Insulin/IGF pathway-MAP kinase

B) Altered hormone signaling pathways involved in breast cancer include the following:

- Androgen/estrogene/progesterone biosynthesis
- Gonadotropin-releasing hormone receptor
- Oxytocin receptor mediated signaling
- Thyrotropin-releasing hormone receptor

C) Other cancer-associated pathways showing altered gene expression include the following:

- PI3 kinase pathway
- Plasminogen activating cascade
- Cadherin signaling
- CCKR signaling map
- FAS signaling

- Hedgehog signaling
- JAK/STAT signaling
- p38 MAPK pathway
- p53 pathway
- p53 pathway glucose deprivation
- p53 pathway feedback loops 2
- Ras Pathway
- Ubiquitin proteasome pathway
- Wnt signaling
- Notch signaling
- Endothelin signaling

Figure 3.40 illustrates the expression changes shared between treated and untreated normal breast and triple-negative breast cancer (TNBC) cell lines:(A) The Venn diagram shows the overlap of genes whose expression changed after treatment in TNBC and normal cells. A significant number was upregulated in both, but this represented only a fraction of those upregulated in TNBC cells. Many genes upregulated in normal cells were downregulated in TNBC cells. Few genes were commonly downregulated across both cell lines, indicating differential gene responses to treatment.(B) and (C) reveal virtually no overlap in differentially expressed miRNAs and lncRNAs between the cell lines, likely due to the RNA extraction methods not targeting these small RNA molecules, identifying only highly expressed ones.Another class of genes whose expression is altered among TNBC and normal breast cancer cells following treatment are those coding for components of growth receptor pathways. This confirmed the changes in growth factor receptors observed using a protein profiler. Alterations in the transcription of genes related to hormone signaling, as well as genes in the gonadotrophin pathway, are closely associated with TNBC. Predictably, numerous genes associated with apoptosis and angiogenesis exhibited changes, and a set of genes encoding elements of growth receptor pathways exhibited altered expression in both TNBC and normal breast cancer cells after treatment. These treatment-induced alterations have implications for tumour growth and metastasis. Cancer progression and metastasis also involve neurogenesis and axonogenesis. This aspect sheds light on the observed changes in gene expression related to axonogenesis, neurogenesis, axon guidance, and

the neurotransmitters that regulate these processes. The modifications in these gene expressions highlight the complex interplay between cancerous growth and neural development pathways, underlining the multifaceted nature of cancer biology and its treatment responses.

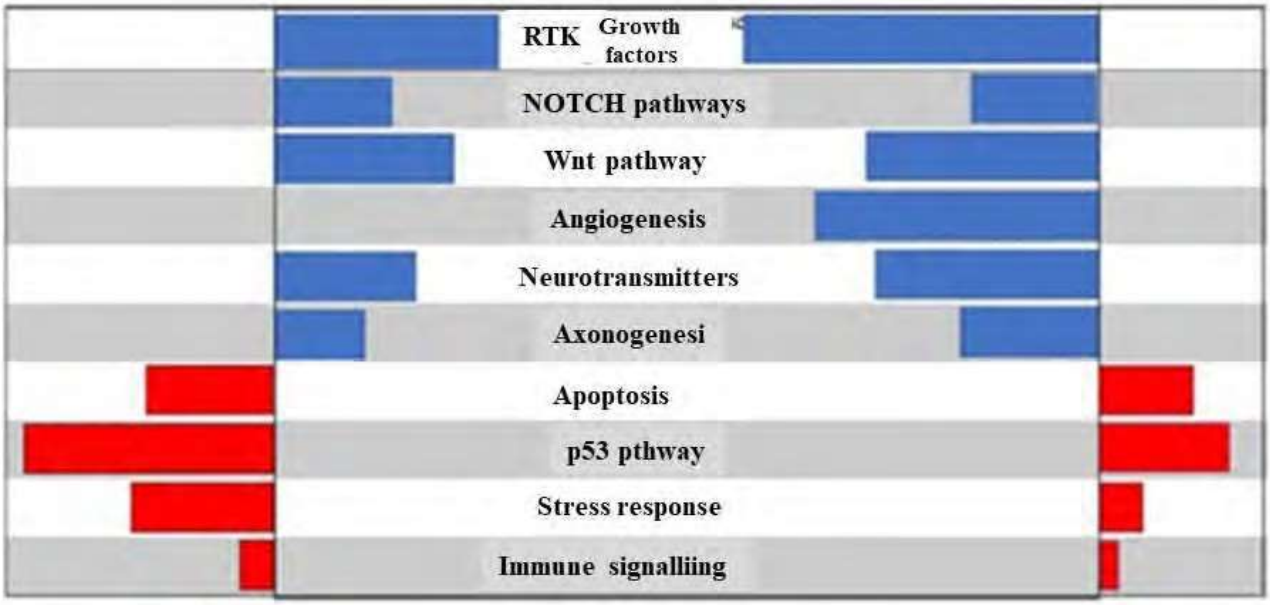

Figure 3.41 presents a heatmap visualisationvisualization of the functional enrichment analysis performed using the DAVID online tool The analysis focused on identifying up- and down-regulated genes involved in various biological pathways and signaling mechanisms, such as RTK growth factors, NOTCH pathways, Wnt signaling, angiogenesis, neurotransmitters, apoptosis, and immune signaling. The heatmap reveals that the transcription of genes associated with RTK (receptor tyrosine kinase) signaling is reduced after treatment with the extract, with this decrease being more pronounced in normal breast cells compared to triple-negative breast cancer (TNBC) cells. This finding suggests that RTK signaling is more active in untreated normal breast cancer cells than in TNBC cells.

Moreover, elements of both the Notch and Wnt signaling pathways exhibited decreased transcription after treatment in both normal and TNBC cells. In the context of angiogenesis, no significant enrichment was observed in either the treated or untreated normal breast cells. However, notably high transcription levels of genes involved in angiogenesis were detected in untreated TNBC cells, indicating a treatment-induced reduction in the transcription of these genes. Genes associated with apoptosis exhibited increased transcription in both TNBC and normal breast cells. This trend also applies to p53-related signaling pathways, suggesting an enhanced apoptotic response due to treatment. Similarly, the transcription of genes associated with stress responses increased in both types of treated cells, indicating the cytotoxic effect of the extract, particularly on TNBC cells and, to a lesser extent, on normal cells.

Additionally, the transcription of genes in immune signaling pathways, encompassing those linked to integrin and T-cell activation, increased following treatment in both TNBC and normal breast cells. This upregulation suggests potential activation of immune-related pathways in response to treatment. The analysis presented the outcomes of an expression enrichment assessment conducted using the DAVID online tool. These findings are consistent with predictions, suggesting a decrease in the expression of genes implicated in pro-oncogenic signaling in both TNBC and normal breast cells. The evident contrast in the expression of angiogenesis-related genes between the two cell types was striking: normal breast cells showed no significant change in these genes after treatment, but TNBC cells showed a considerable decrease in their expression. Furthermore, this study revealed an increase in the expression of apoptosis-related genes in both normal and TNBC cells. This indicates a shared response mechanism to the treatment across both cell types, underscoring the potential therapeutic efficacy of the treatment in triggering apoptotic pathways in both cancerous and normal cells.

The apoptosis assay revealed that the extract promoted apoptosis in triple-negative breast cancer (TNBC) cells and normal breast cells, with the former having a more substantial impact. This conclusion was supported by comparing the fold changes in transcript levels of pro-apoptotic and anti-apoptotic genes, as detected by Next-Generation Sequencing (NGS), in both pre- and post-treatment cell lines. Such a comparison is crucial for understanding the degree to which changes in the transcriptome correspond to the increased apoptosis rate post-treatment. It also helps identify the specific apoptotic pathways involved in this response. This method validates the cytotoxic potential of the extract and sheds light on its molecular mechanisms, particularly how it differentially affects TNBC and normal breast cells at a genetic level. As shown in Figure 3.42, the extract caused a significant increase in the expression of proapoptotic genes in TNBC cells. The data also suggest that both the extrinsic and intrinsic apoptotic pathways are activated.

A. Pro-apoptotic genes transcribed in TNBC cells

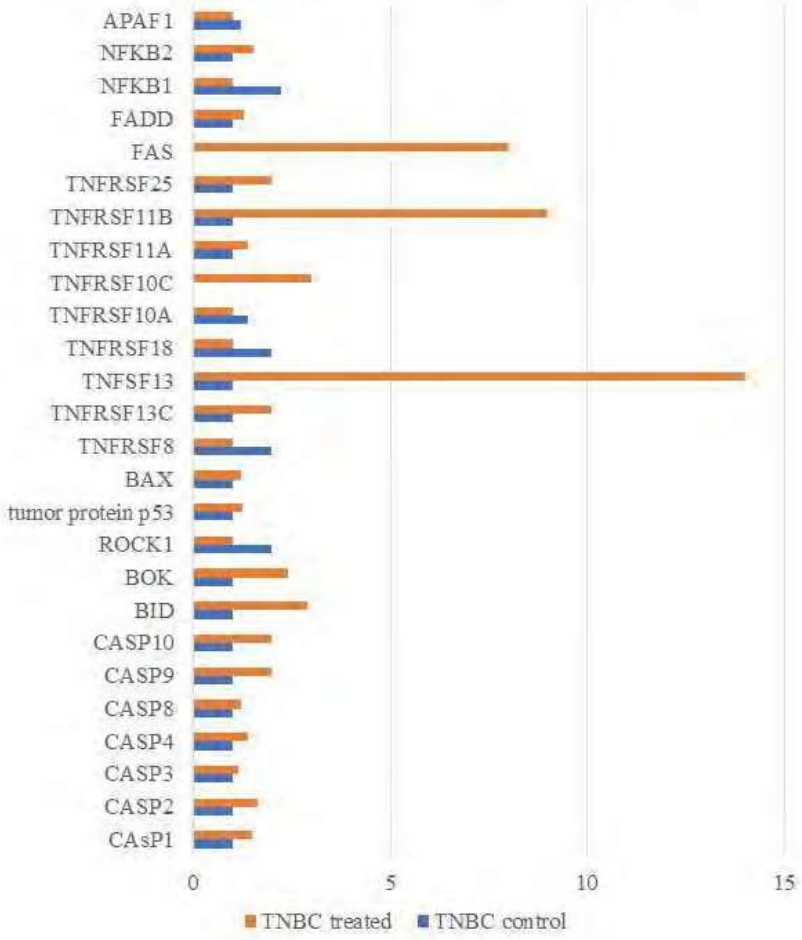

B. Anti-apoptotic genes transcribed in TNBC cells

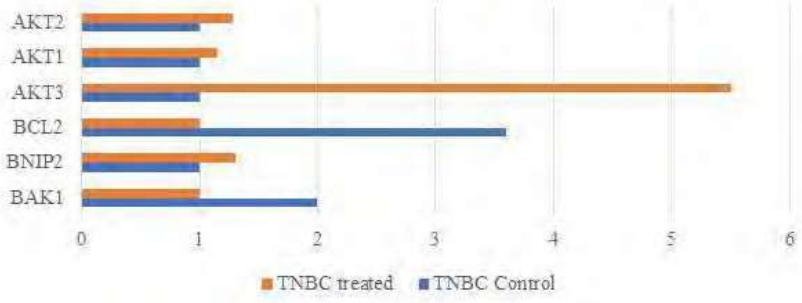

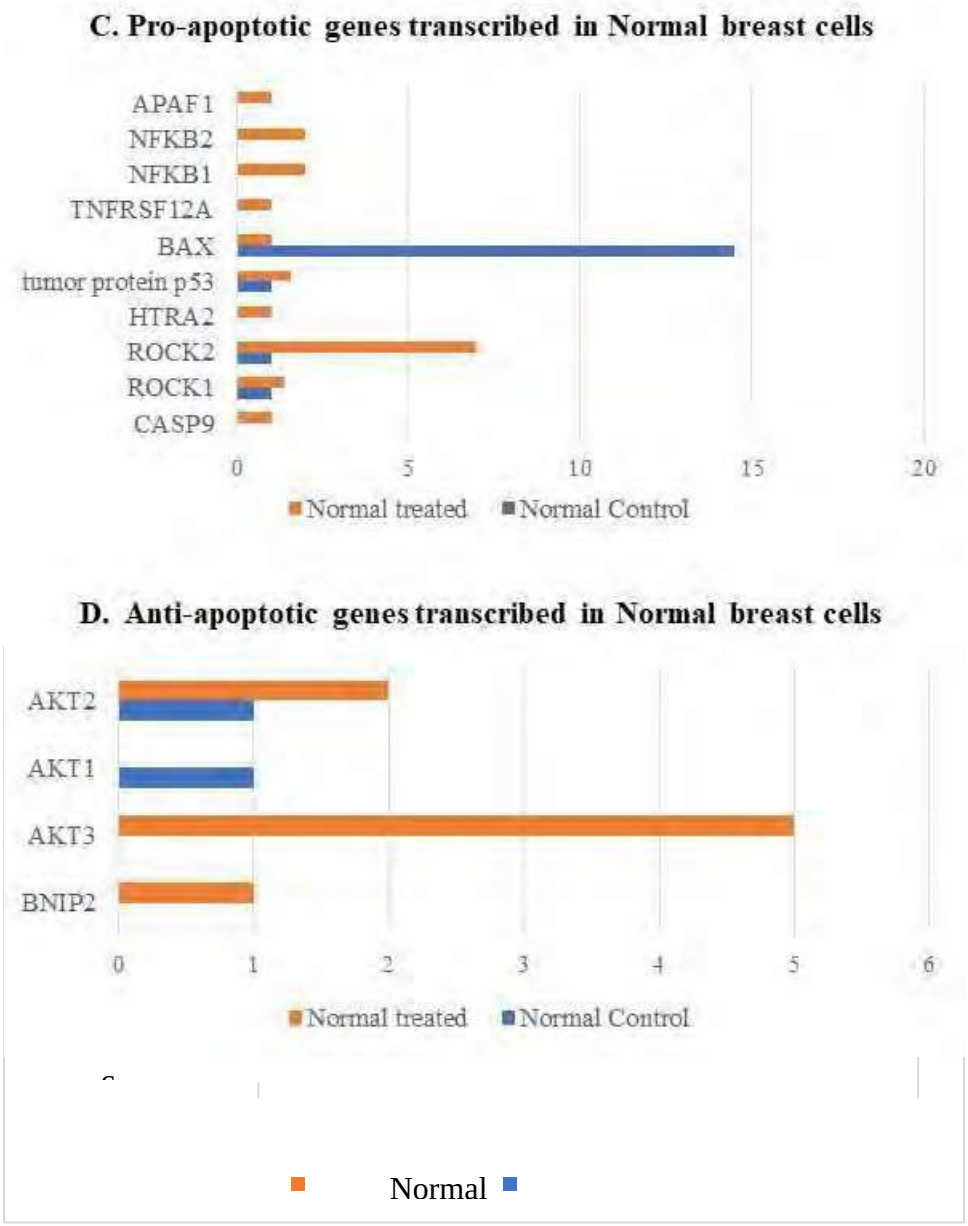

Figure 3.42 depicts the mRNA expression levels of pro-apoptotic and anti-apoptotic genes in normal breast cells and triple-negative breast cancer (TNBC) cells, before and after treatment with a water-soluble extract from *Tulbaghia violacea*. (A) Differential expression of pro-apoptotic genes, such as APAF1, NFKB2, and BAX, in TNBC cells upon treatment. (B) Changes in the expression of anti-apoptotic genes, including AKT2, AKT1, and AKT3, in TNBC cells. (C) Upregulation of pro-apoptotic genes such as BAX and downregulation of ROCK1 in normal cells after treatment. (D) Alterations in anti-apoptotic genes such as AKT2 and BNIP2 in normal cells. Data were obtained using next-generation sequencing (NGS) analysis.

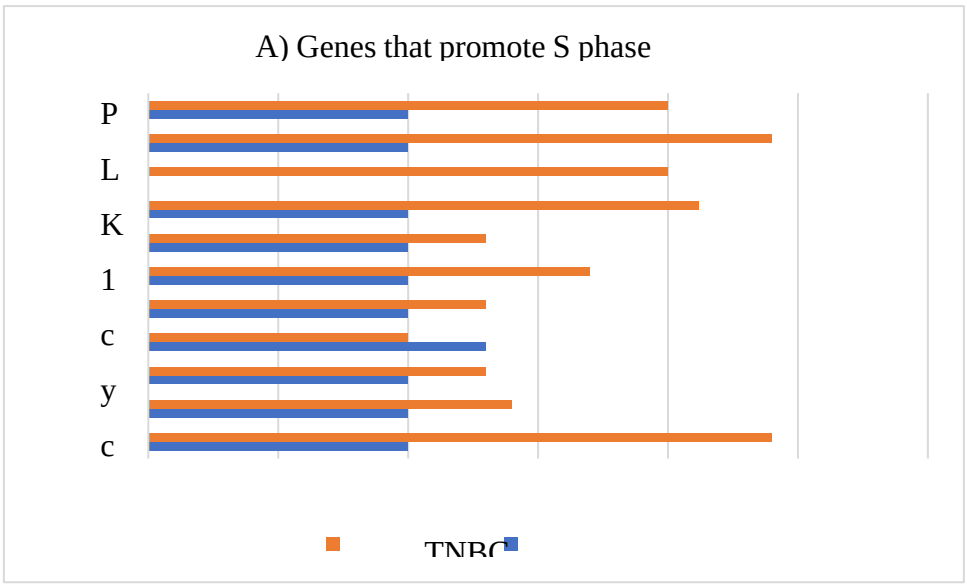
A) Genes that promote S phase
P
L
K
1
c
y
c
TNBC

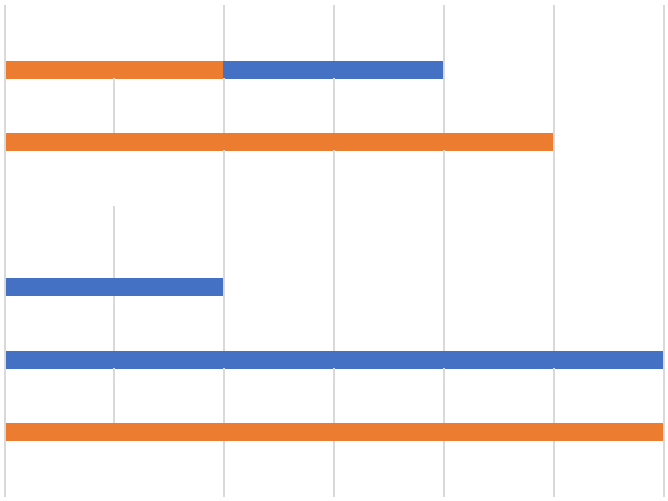

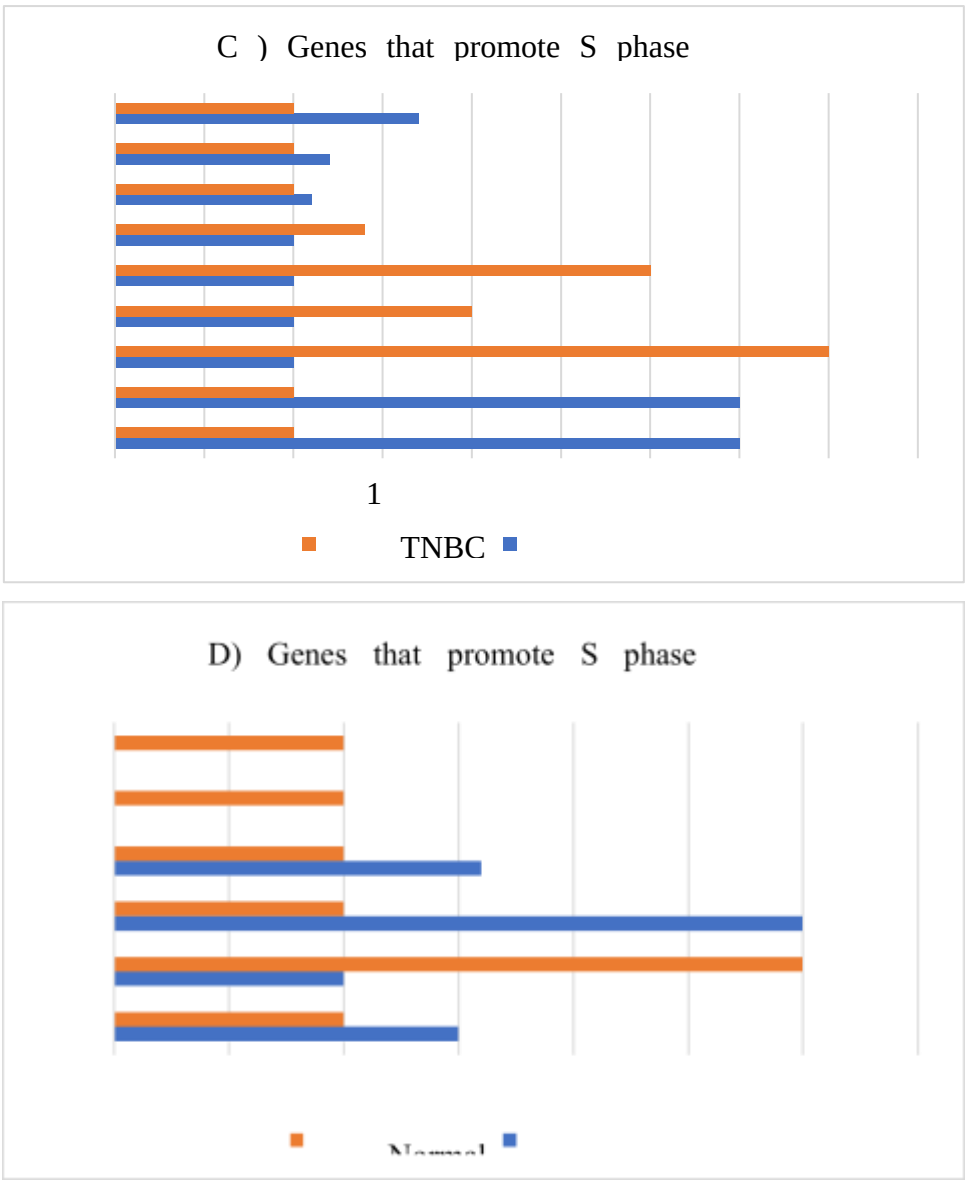

Figure 3.43 The figure depicts the mRNA levels of various cell cycle genes involved in S phase progression or arrest, as determined by next-generation sequencing before and after treatment with water-soluble *T. violacea* extract. Panel A shows genes promoting S-phase arrest in triple-negative breast cancer (TNBC) cells, whereas panel B focuses on these genes in normal breast cancer cells. Panel C displays genes that enhance S-phase progression in TNBC cells after treatment, highlighting the altered regulatory mechanisms. Lastly, panel D illustrates genes promoting S phase progression in normal breast cells, indicating potential changes in cell cycle regulation due to treatment. The legend effectively explains the purpose and findings of each panel, providing insights into the impact of treatment on the cell cycle dynamics in both TNBC and normal breast cancer cells.

The cell cycle assay verified that the extract led to a suspension in the S phase of the cell cycle, causing an accumulation of cells in this phase in both TNBC and normal breast cells. By evaluating the fold

changes in transcript levels of genes that are instrumental in promoting S phase progression and those responsible for inducing S phase arrest, as identified by Next-Generation Sequencing (NGS) in both cell types before and after treatment, I determined the correlation between transcriptomic changes and S phase arrest observed post-treatment. This comparison, depicted in Figure 3.43, offers valuable insights into how alterations in gene expression influence the cell cycle, particularly the S phase, in response to treatment. This analysis is crucial for understanding the molecular mechanisms underlying the effect of treatment on cell cycle regulation.

Chapter 4 Discussion

In this study, I examined the anticancer effects of *T. violacea* on triple-negative breast cancer cell lines and healthy breast cells, especially MCF10A and MDA-MB-231. According to current research, effective therapies for triple-negative breast cancer should attempt to initiate apoptosis or activate cell cycle checkpoints. This study investigated extracts from *T. violacea* and *C. orbiculata,* but only the water-soluble extract of *T. violacea* showed consistent effectiveness against cancer cells at concentrations not exceeding 400 µg/mL. Following treatment, the cells exhibited signs of apoptosis, such as shrinkage, spikes, and other indicators of DNA fragmentation. My research also analysed the chemical constituents of dried leaf extracts and their cytotoxic effects. *Water-soluble extracts of T. violacea* displayed substantial cytotoxicity against TNBC cells, highlighting the potential of *T. violacea* leaves as a source of natural antioxidants and/or anticancer drugs. *Water-soluble T. violacea extracts exhibit* pro-apoptotic and anti-proliferative properties.

4.1 Background

In this study, I conducted a series of tests to determine how water- and methanol-soluble extracts from two plant species affect MDA-MB231 and MCF10A cell lines, which represent triple-negative breast cancer (TNBC) cells and normal, healthy breast cells, respectively. My findings show that the water-based extract derived from *T. violacea* leaves has the capacity to limit cell growth. Additionally, this extract was found to have pro-apoptotic properties, as confirmed by the Annexin V-FITC/propidium iodide labelling method(Figure4.1).

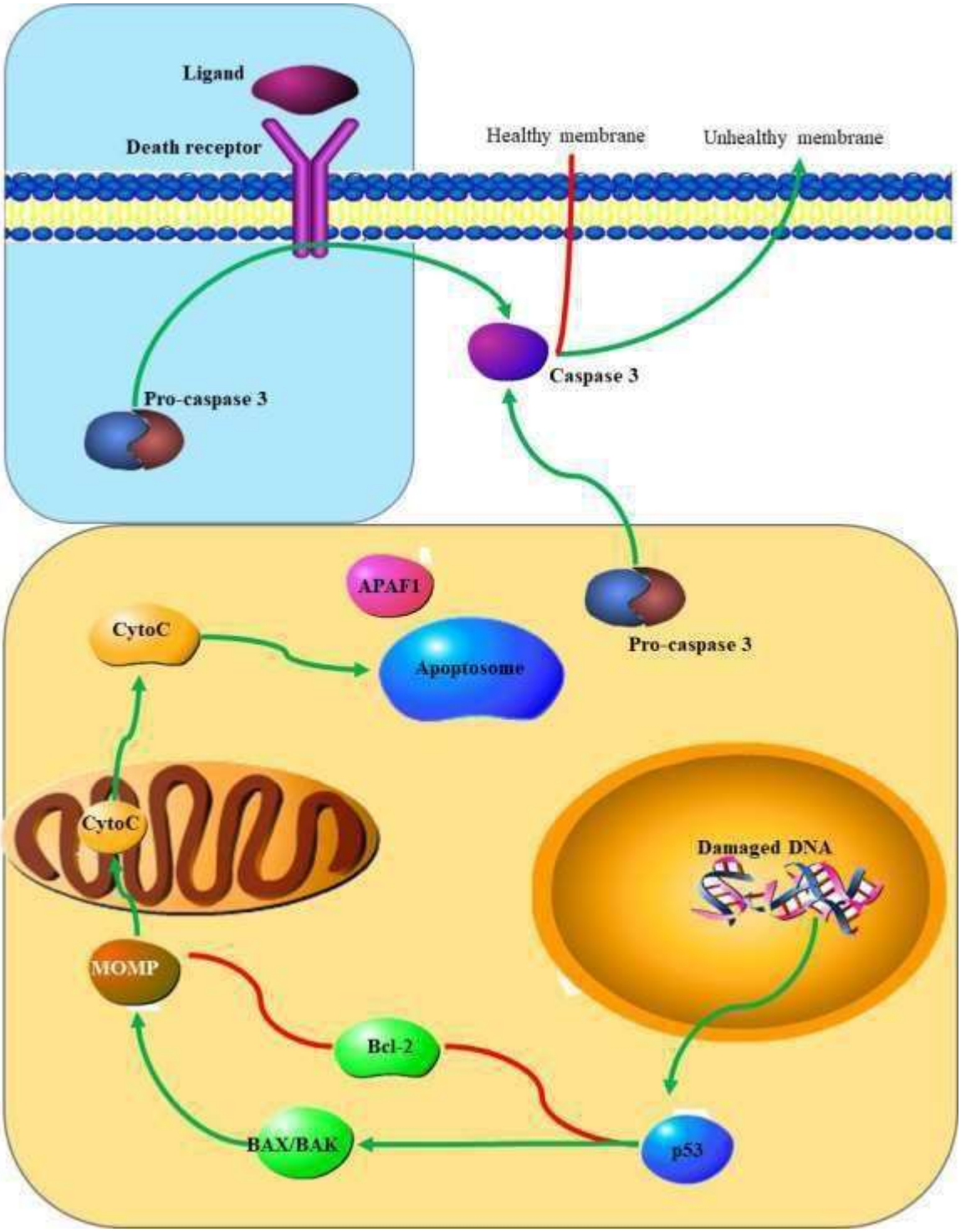

Figure 4.1depicts the extrinsic (blue box) and intrinsic (orange box) pathways of apoptosis, a form of programmed cell death . The extrinsic pathway is initiated by the binding of a ligand to a death receptor, activating pro-caspase 3 and caspase 3, which induces apoptosis. The intrinsic pathway is triggered by internal cellular stress, leading to the release of cytochrome c from mitochondria. Cytochrome c binds to Apaf1 to form an apoptosome that activates pro-caspase 3 and caspase 3, culminating in apoptosis. This diagram illustrates the key molecular players and events in both pathways,

providing a conceptual understanding of the mechanisms underlying the regulated cell death process.

These pathways, which include both internal and extrinsic processes, culminate in caspase activation, which is required to initiate morphological and biochemical alterations associated with apoptosis, such as phosphatidylserine externalization (PS). PS is normally found in the inner layer of the plasma membrane; however, during apoptosis, it moves to the outer layer. The Annexin-Renilla Fusion Protein (ArFP) is designed to attach to PS on the surface of apoptotic cells. This binding produces a bioluminescence signal in the presence of its substrate coelenterazine. This provides an innovative approach for the detection and quantification of apoptosis, as described by Brown [19]. This method can be particularly useful for elucidating the effectiveness of anticancer therapies, including the role of *T. violacea* extract in inducing apoptosis in cancer cells.

4.2 Determining the IC_{50} values

In this study, cytotoxicity tests were performed on extracts derived from *T. violacea* leaves and cotyledon orbiculate. The samples included soluble fractions in both aqueous and methanolic solutions. Cytotoxicity was evaluated using the RTCA xCELLigence system and alamar blue cytotoxicity assay.

According to xCELLigence research results, it is crucial to consider how cellular confluence might affect treatment results. Cell proliferation and confluence can affect cellular responses to various therapies. High confluence might lead to an underestimation of the antiproliferative effects of therapies, because cells spontaneously reduce their growth rate as a result of contact inhibition, making it challenging to differentiate treatment effects. Changes in the cellular microenvironment caused by higher cell density, such as decreased food supply, pH changes, and improved cell communication, may alter cell behaviour and affect their reaction to therapies. Highly confluent cells may show increased resistance to certain drugs. The extent of these collective effects may differ among cell lines, with certain cell lines displaying more sensitivity to contact inhibition than others. Cell lines exhibiting rapid proliferation were more susceptible to confluent effects in the xCELLigence experiment. Optimising the initial cell seeding density is crucial to reduce the effects of confluence. The objective was to introduce a sufficient number of cells to generate a strong

impedance signal, ensuring a sufficient time for the experiment to be conducted before the cells reached a state of excessive confluence. Conducting the first optimisation test was crucial. The Cell Index of the xCELLigence system enables continuous monitoring of cell confluence to detect critical levels that might impact test outcomes. Less sensitive methods, such as direct cytotoxicity tests, can be used to confirm putative confluence effects.

I created several dilutions of water extracts obtained from *T. violacea* and *C. orbiculata* leaves in cell culture medium. The diluted solutions were administered to MDA-MB-231 TNBC cells and a non-cancerous human breast cancer cell line (MCF10A). Cells were exposed to increasing concentrations of the extracts for 72 h. The cytotoxic effects of the extracts on these cell lines were evaluated. This approach allowed for a comprehensive assessment of the potential anticancer properties of the extracts, particularly for distinguishing their effects on cancerous and non-cancerous cells.

Both methods exhibited similar trends, with the water-soluble extract from *T. violacea* demonstrating the highest cytotoxicity and the water-soluble extract from C. violacea exhibiting the lowest cytotoxicity. The methanol-soluble extract of *C. orbiculata* showed significant differences between the two techniques, which was unusual.

Based on the results of the xCELLigence study, it is important to consider how cellular confluence affects treatment outcomes. The IC50 value of 400 μg/mL for the water-soluble extract of *T. violacea* was determined by merging results from the xCELLigence Real-Time Cell Analysis (395.2 μg/mL) and the Alamar Blue cytotoxicity assay (350 μg/mL). Although the IC50 value may be higher than that of conventional chemotherapeutic medications, it is not uncommon for crude plant extracts to have higher IC50 values owing to their complex chemical composition. The water-soluble extract of *T. violacea* demonstrated a dose-dependent cytotoxic effect on MDA-MB-231 triple-negative breast cancer cells with a higher IC50.

The study also examined the effect of the extracts on the non-tumourigenic MCF-10A breast epithelial cell line in normal cells. The *T. violacea* water-soluble extract showed reduced cytotoxicity in normal cells compared to cancer cells. For example, when exposed to 350 μg/mL of the extract, over 80% of MDA-MB-231 cells underwent apoptosis in the apoptosis assay, but more than 50% of MCF-10A

cells survived at similar doses. The difference in cell death rates between cancerous and healthy cells indicates that the water-soluble extract from *T. violacea* may include substances that specifically attack cancer cells while showing some level of protection against regular cells. Additional studies are needed to identify the exact bioactive chemicals responsible for this action and to enhance their selectivity and efficacy.

The RTCA method provided precise results but was limited by the cost of the E16 plates, which restricted the number of replicates that could be performed. In contrast, the alamar blue assay is cost-effective and allows for more replicates, potentially leading to a more accurate assessment.

Considering these factors, I decided to carefully analyse the results of both methods before determining the IC_{50} value. The inconsistent performance of the *C. orbiculata* methanol-soluble extract, along with the variation in the results between replicates, led us to exclude this from future experiments. We also noted that different preparations of this extract performed differently, possibly because of the difficulties in solubilising the dry powder in low concentrations of DMSO, resulting in insoluble clumps that had to be filtered out before use. Future research involving this plant should address these solubility issues, because a well-prepared methanol-soluble extract may exhibit promising cytotoxic activity.

4.3 Morphological studies on normal and TNBC cancer cell lines treated leaf extracts from *T. violacea*

highlighted the apoptotic potential of the *T. violacea* extract in TNBC cells. Morphological features such as cell shrinkage, nuclear disintegration, and cell detachment are classic markers of apoptosis [490]. This pioneering work has laid the foundation for understanding programmed cell death, and my findings align with this historical perspective. The resemblance of these morphological changes to those induced by 5-fluorouracil (5FU), a known apoptosis inducer, further validated our observations. This parallel not only strengthens the credibility of my study but also positions *T. violacea* extract as a promising agent for inducing apoptosis, particularly in the context of cancer treatment.

The detailed analysis of MDA-MB-231 cells treated with *T. violacea* extract, as described in Section 2.2.2 of my study revealed a heightened sensitivity of TNBC cells to this treatment. The rapid decline in cell count and distinct morphological alterations in treated TNBC cells compared to untreated and normal breast cells is particularly noteworthy. The quantitative assessment of cell area and perimeter provides a deeper understanding of apoptotic features, such as blebbing and shrinkage, in response to the extract.

My findings, enriched by the visual representation in Figures 3.10 to 3.16, not only demonstrate the cytotoxic efficacy of *T. violacea* extract against TNBC cells, but also offer a comprehensive view of its impact at the cellular level. The significant reduction in cell count and pronounced apoptotic features after 72 h of treatment highlight the potential of *T. violacea* as a natural source for developing anticancer therapies. The similarity with 5FU therapy emphasises the significance of these discoveries in the context of cancer research and treatment techniques.

4.4 The water-soluble crude extract of *T. violacea* induced apoptosis in TNBC cells.

My investigation into the anticancer properties of *T. violacea* leaf aqueous extract, particularly its efficacy against TNBC (MDA-MB-231) cells, is compelling and methodologically sound. The decision to focus on this extract, given its lowest IC_{50} value and significant impact on TNBC cell morphology, is well-justified. The IC_{50} values, which indicate the efficacy of the extract as well as the morphological alterations found in TNBC cells, strongly support the concept that *T. violacea* triggers apoptosis in these cells. These findings highlight *the therapeutic potential of T. violacea for* the treatment of TNBC.

The use of annexin-V and propidium iodide (PI) staining, combined with the Muse TM flow cytometry system, provided a clear distinction between viable, apoptotic, and necrotic cells. This approach is crucial for accurately quantifying the effect of the extract on cell viability. My findings that *T. violacea* aqueous extract induces dose- and time-dependent apoptosis, particularly in the TNBC cell line, while exhibiting reduced effectiveness in non-malignant MCF10A cells, are significant. This differential response, as depicted in Figures 3.17 and 3.18, suggests a selective

mechanism of action of the extract on TNBC cells, which is a critical attribute for any anticancer agent.

It is also notable that *T. violacea* leaf aqueous extract may selectively trigger apoptosis in cancer cells while sparing normal cells. This selectivity is a key characteristic of an effective anticancer agent as it targets malignant cells without causing undue harm to normal tissues. The irreversible nature of apoptosis, especially beyond the early stages, and the lack of cell recovery observed even after 72 h post-treatment further reinforce the potency of the extract. Although the half-life of the extract in cellular environments was not determined, the sustained effect observed indicated its lasting impact.

Overall, my research adds to our understanding of the potential of *T. violacea* as a natural anticancer drug with particular potency against TNBC cells. The ability to effectively trigger apoptosis in cancer cells is a promising indicator of therapeutic potential. Future research could further elucidate the molecular mechanisms underlying this selective action and explore the efficacy of the extract in other cancer cell lines or in in vivo models. My findings lay a strong foundation for further exploration and the potential development of *T. violacea*-based anticancer therapies.

4.5 *T. violacea* crude water-soluble extracts altered the cell cycle of TNBC and normal breast cancer cells.

Malfunction of the cell cycle is a pivotal element in the multifaceted progression of cancer. Several regulators that control the onset and progression of the cell cycle are frequently altered in cancer cells. Notably, abnormalities in cell cycle regulation are a common feature in nearly all types of human cancers. This results in cancer cells bypassing the standard regulatory mechanisms of the cell cycle, leading to uncontrolled proliferation, a fundamental characteristic of cancer. Understanding these alterations in cell cycle control is crucial for developing targeted oncological therapies [491]. The majority of cancers exhibit irregularities that disrupt normal cell cycle processes, resulting in enhanced cellular growth. These irregularities can affect various aspects of the cell cycle, including its inherent components and preceding signaling pathways that regulate cell cycle functions. Such

disruptions are instrumental in fuelling the proliferation and division of cancer cells, emphasising the need to examine and address these deviations in cancer research and treatment [492]. You have highlighted this important aspect of cell biology. The correct duplication of the genome during the S-phase and its subsequent division into two daughter cells during mitosis, also known as the M-phase, are required for the transfer of genetic material from one cell generation to the next. These stages, S and M, are essential in a cyclical process that guarantees accurate cell replication while reducing the probability of genetic anomalies. Preserving the fidelity of these processes is critical for maintaining the stability and functionality of the genetic content of an organism [493]. Cell cycle checkpoints during the G1/S transition, throughout

The S-phase, and throughout the G2/M phase, examines the timing and sequence of cell cycle activities [494].

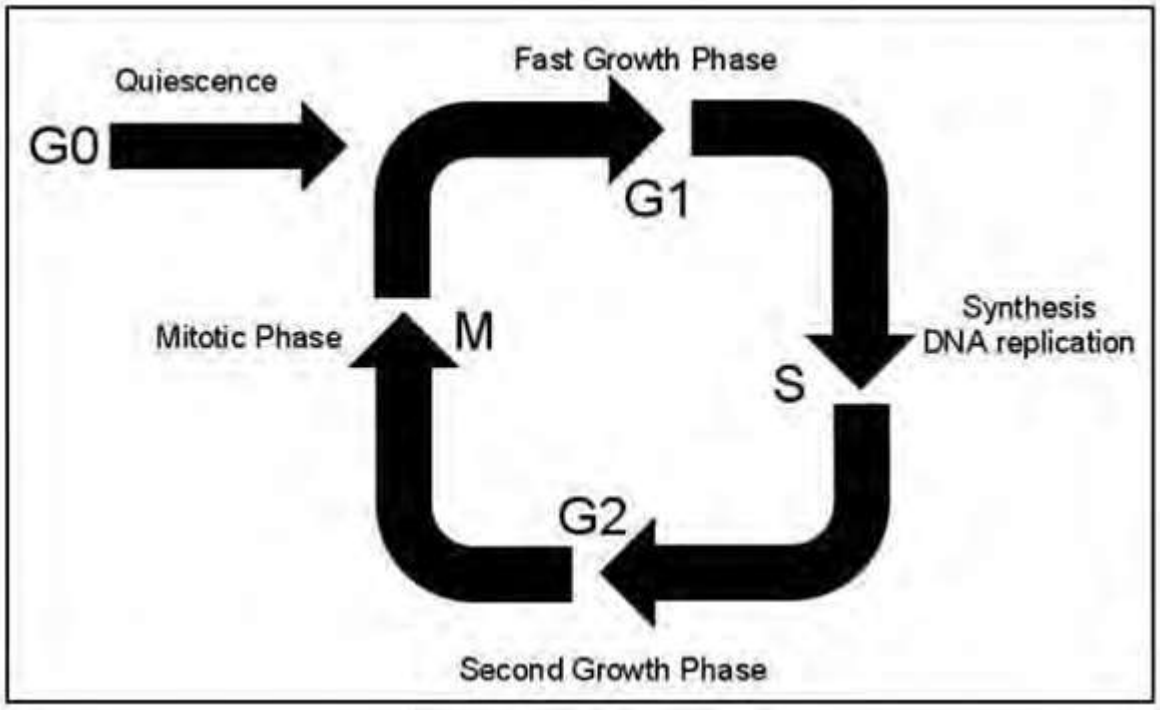

Figure 4.2 2depicts a circular diagram illustrating the different phases of the cell cycle

.

The cell cycle begins with the quiescence (G0) phase, followed by the Mitotic Phase (M), where cell division occurs. The cells then enter the Fast Growth Phase (G1), where they prepare for DNA

synthesis. The Synthesis (S) phase followed, during which DNA replication occurred. After the S phase, cells progress to the Second Growth Phase (G2) before re-entering mitosis (M) to complete the cycle. The diagram effectively visualizes the sequential stages cells go through during the cell cycle, providing a clear overview of this fundamental biological process

In the normal cell cycle, the synthesis phase always occurs after the mitotic phase, and mitosis starts only when the synthesis phase is completed. Two intermediary halts occur between these stages: G1, which separates mitosis from synthesis, and G2, which connects synthesis and mitosis. When a cell develops, it departs from the G1 phase of the cell cycle and enters a dormant condition known as G0.

Cell cycle checkpoints are regulatory systems that allow cell division only when activation signals such as growth factors are present. These checkpoints are critical for guaranteeing the correct transmission of genetic information from one generation to the next [495]. Activation of cell cycle checkpoints can be triggered by DNA damage or chromosomal misalignment of the mitotic spindle. In such situations, the growth halt induced by checkpoints allows for cell repair. If the repair is successful, the cell cycle proceeds; otherwise, the cell undergoes apoptosis, leading to programmed cell death [496]. Emerging research suggests that modulation of the cell cycle can either suppress or induce an apoptotic response, depending on the specific biological context [497]. Numerous genes that oversee the cell cycle also play essential roles in apoptosis control. Key examples include c-myc, c-fos, p53, and various kinases and phosphatases [498]. The signals that induce cell proliferation can also initiate apoptosis. When cell survival signals effectively suppress apoptosis, cell counts increase, potentially leading to the formation of cancer [499]. When DNA damage or disruption of the cell cycle occurs, the tumour suppressor protein p53 is activated and interacts with the transcription factor p21. This activates p21, which binds to the G1-S/cyclin-dependent kinase 2 (CDK2) complex, thereby slowing cell cycle progression and providing time for DNA repair. If DNA damage is irreversible, the cells die and genetic stability is preserved. However, if p53 is mutated or altered, cancer cells can divide, proliferate, invade particular organs, bypass protective processes, and promote tumour development [500].

The water-soluble extract of T. violacea triggered an S-phase checkpoint in both normal breast and TNBC cells, resulting in fewer cells in the G0/G1 phase. In contrast, the bulk of untreated normal and TNBC cells was in the G0/G1 phase. The cell cycle is controlled by cyclin-dependent kinases (CDKs) [501]. The S-phase replication checkpoint is activated in response to DNA replication forks that have slowed or stopped, which can be caused by DNA damage or replication disturbances, assuring precise chromosomal replication [502]. p53's role as a transcription factor is critical for arresting the cell cycle and initiating apoptosis [503].

p53 regulates the transcription of several biological genes. When p53 is active in dividing cells, it stops the cell cycle in both the G1 and G2 phases, mostly through transcriptional activation of p21, which inhibits cyclin-dependent kinases that are required for cell cycle progression [504].

In mammalian cells, checkpoints are governed by ATR and Chk2. Notably, the expression of these kinases is reduced in cancer cells [505-507]. RNA sequencing shows a 2.4-fold increase in Chk2 transcription in MDA-MB231 cells post-treatment, and a 1.5-fold increase in MCF-10A cells, with no ATR transcripts observed under these conditions.

Precise regulation of the cell cycle is crucial for controlling cell proliferation, and its dysregulation has been linked to numerous cancers [508]. Thus, targeting the cell cycle in cancer cells may be an effective approach for the development of anticancer medications [509].

4.1.1 Summary

This innovative study offers substantial proof of *the untapped potential of T. violacea* as an anti-cancer agent. In a field with limited research, this study stands out for its solid evidence of its effectiveness. Notably, we demonstrated the potent cytotoxic effect of the water-soluble extract on the aggressive TNBC cell line MDA-MB231, demonstrating its selective action against these cancer cells while sparing normal breast cells. This selective toxicity highlights *the potential of T. violacea in the treatment* of TNBC.

Through comprehensive cell death assays and in-depth examination of morphological alterations, the mechanism underlying the cytotoxic effect of *T. violacea* extract was elucidated. *T. violacea* components uniquely cause apoptosis, a step required for cancer cell elimination. These findings provide a solid foundation for future investigations aimed at identifying the specific bioactive compounds responsible for the pronounced anticancer efficacy.

Further research is imperative to validate the safety and therapeutic viability of the extracts. Immunotoxicity assessments are crucial to ensure that the extracts do not provoke adverse immune reactions. Such an exhaustive evaluation will bolster the credibility and potential clinical applicability of *T. violacea* as an efficacious option for cancer treatment. This direction of research not only contributes to our understanding of *the medicinal properties of T. violacea,* but also potentially paves the way for novel cancer therapies derived from natural sources.

4.2 Effect of *T. violacea* water-soluble leaf extract on the metastatic potential of MDA- MB231 cells.

4,5.1 Background

The ability of cancer cells to infiltrate and spread to other tissues is a defining feature of this disease. This feature results from the altered capacity of cancer cells to migrate, attach to the extracellular matrix (ECM), and penetrate the ECM or other cellular layers, which is frequently related to changes in gene expression or mutations. Thus, analysing the influence of unprocessed water-soluble *T. violacea* extracts on the attachment, movement, and invasive potential of MDA-MB231 cells is pivotal. In the present study, both MDA-MB231 and MCF10A cells were used in a range of tests to observe how the extract affected their adhesive, invasive, and migratory characteristics in a laboratory setting.

4.2.1 The *water-soluble crude extract of T. violacea* inhibited the migration of TNBC cells.

Two different methods were used to test the effect of the extracts on the migratory potential of MDA-MB231 cells: a wound healing (scratch) assay and an invasion and migration assay using the XCelligence RTCA analysis system. The scratch test was used to evaluate the effects of all four extracts, including the methanol and water extracts from *T. violacea* and *C. orbiculata*, as shown in Figures 3.20 and 3.21. The findings from the scratch assay indicated that the scratch area was reduced rapidly in untreated cells or those treated with *C. orbiculata water*-soluble extract or *T. violacea* methanol-soluble extract, suggesting that these extracts had a minimal impact on the migratory ability of the cells. This was further corroborated by measuring the distance between the two cell fronts as a measure of wound closure (Figure 3.22). In contrast to the IC50 data, the *C. orbiculata* methanol-soluble extract killed the cells continuously over time, limiting wound closure. However, when this was repeated using different preparations of the extract, lower levels of cell death and increased levels of wound closure were observed. This is indicated by the large error bars associated with this extract in Figures 3.21 and 3.22. This was most likely due to the poor solubility of this extract in the 1 percent DMSO solution used to dissolve the powdered extract. This was the highest concentration of DMSO that could be used before DMSO itself contributed to cell death and interfered with various assays. In addition to this, the highest mass of powder that could bedissolved was 2 mg in a 1 percent solution DMSO solution to obtain a 2 mg/ml concentration of the extract. The remaining clumps had to be filtered out, and it is likely that the poorly soluble components of the extract were cytotoxic. This inconsistent preparation was most likely the cause of the differences in cytotoxicity observed in migration and cytotoxicity assays.

The effect of *the water-soluble extract of T. violacea* on the migration of MDA-MB231 cells was consistent and occurred without significant cell death. This impact was noticeable within the first 12 h after treatment and continued beyond 24 h, up to approximately 35 h post-treatment, at which point the effect started to diminish and cell migration began to increase. The absence of additional extract application during this period suggests the active duration of the extract components or recovery time of the cells. When half of the IC_{50} concentration of the extract was used, the migration inhibitory

effect ceased after 24 h. However, complete wound closure was observed after 72 h, even at a reduced concentration.

This observation indicates that the capacity of the extract to inhibit cell migration was likely due to a prolonged effect on the cells, necessitating a recovery period rather than continuous extract activity. Furthermore, the influence of *water-soluble T. violacea* extract on cell migration was not solely a result of increased cell death, as shown in Figure 3.20. It seems that the extract affects the migratory abilities of cells, possibly by targeting specific molecules or pathways. This was verified by the RTCA VIM plate study, which revealed a significant decrease in the number of cells moving from the upper to lower chamber in the presence of the extract. This drop was so significant that it resulted in fewer migrating cells compared with the negative control, which lacked a chemoattractant in the lower chamber. Based on these findings, future studies should aim to replicate RTCA analysis with more plates, which was restricted in this study because of the cost of CIM plates.

The scratch assay using normal MCF-10A breast cells (Figure 3.24) showed that the extract negatively affected the migration of these cells, although the effect was less pronounced and shorter than that observed in TNBC cells. Notably, MCF-10A cells migrated naturally at a slower pace than cancer cells, consistent with the established trait of heightened cell migration in cancerous cells. This implies that the extract may affect cell migration by targeting molecules and pathways that are more active in the cancer cells.

4.2.2 Effect of *T. violacea* crude water-soluble extract on the adhesion of TNBC cells.

Following the migration investigation, we focused on cell adherence to the laminin-based extracellular matrix (ECM). Understanding the features and spreading tendencies of triple-negative breast cancer cells requires investigation of the attachment of MDA-MB-231 cells to GeltrexTM, a synthetic analogue of laminin ECM components. This evaluation is critical for determining the effect of water-soluble *T. violacea* extracts on cell adhesion to ECM. The cell adhesion pathway is essential for epithelial-to-mesenchymal transition and the activation of metastasis-related genes such as SNAIL

[510, 511]. Cell adhesion was significantly affected by the Sonic Hedgehog (SHH) signaling. Impairing this pathway or diminishing the expression of its components has been demonstrated to limit the ability of cells to adhere to the extracellular matrix (ECM), thereby effectively inhibiting this essential process [512].

Adhesion between cells and the extracellular matrix (ECM) is required for appropriate cell function and signaling. These adhesive interactions are key to preserving the structural integrity of tissues, providing cells with physical support, and facilitating communication between cells and their surrounding environment. Importantly, two fundamental features of cancer— the reduction of cell-to-cell adhesion and the capacity for anchorage-independent growth—rely heavily on cell adhesion molecules.

Figure 3.25 presents the outcomes of the adhesion assay conducted on both treated and untreated MCF10A and MDA-MB231 cells. The researchers discovered that crude water extracts of *T. violacea* decreased cell adhesion in MDA-MB-231 cells, but had little or no effect on normal breast cells. This suggests that treatments derived from *T. violacea* water crude extracts may be promising for the management of triple-negative breast cancer.

4.2.3 Effect of *T. violacea* crude extract on TNBC cell invasion.

To further understand the effects of *T. violacea* crude extract on the metastatic process, in vitro invasion assays were performed. In living organisms, cancerous cells must have the ability to invade surrounding tissues or enter the blood or lymphatic system after adhering to cell membranes. Following attachment to the target basement membrane, these cells engage in enzymatic breakdown using Type IV collagenase, which allows entry into the circulatory system. By reattaching migratory cells to the blood artery, they migrate and eventually form a metastatic (secondary) tumour [513]. Therefore, invasion assays that mimic this process provide insights into the capacity of cells to move through an extracellular matrix (ECM) coated with Laminin-1, akin to the basal lamina.

The untreated MDA-MB-231 cells demonstrated the ability to migrate through the matrix-coated

membrane and adhere to the underside. The addition of *T. violacea* water crude extracts to the experiment, on the other hand, greatly hampered cell invasion, resulting in a much lower number of cells passing through the membrane. These results corroborate the results of adhesion assays, considering that cell adhesion is a fundamental step in invasion. Previous studies involving breast, lung, cervical, prostate, and colon cancer cell lines have demonstrated a direct relationship between cell adhesion and invasion [514]. These observations hold significant therapeutic implications, as compounds targeting cancer cell adhesion might also reduce their ability to invade and migrate to the surrounding tissues (as illustrated in Figures 3.23 and 3.24).

4.2.4 The effect of *T. violacea* crude extracts on cell migration in triple-negative breast

It has been previously noted that cancerous cells need to infiltrate adjacent tissues, re-adhere, and multiply to form a secondary tumour following their passage through the basement membrane. This complex process depends on the ability of cells to move and engage in the epithelial-mesenchymal transition (EMT). For effective movement, cellular signaling pathways are activated, resulting in changes in their shape and structure [515, 516]. Cells move from epithelial to mesenchymal-like properties during the epithelial-mesenchymal transition (EMT), which may lead to changes in protein expression, such as E-cadherin. This process is governed by various signaling pathways, comprising multiple molecules and receptors that respond to external stimuli or were influenced by the inhibitors. To explore these networks and their impact on cellular behaviour, in vitro methods such as cell migration and wound healing assays have been employed [517]. The considerable role of the Wnt/-catenin pathway in boosting cell migration and metastatic tumour growth was revealed in studies analysing the impact of *crude T. violacea water* extracts on the triple-negative breast cancer cell line, MDA-MB-231.

In this study, *crude extracts of T. violacea water* showed notable efficacy in inhibiting cell migration over a period of 24 h, especially when the hedgehog pathway was suppressed. These data demonstrated that *T. violacea* extracts can inhibit the processes involved in MDA-MB-231 cell motility and invasion into cell-free environments. As a result, *T. violacea* water crude extracts have

the capacity to inhibit cell adhesion, resulting in a reduction in their migratory capacities (as depicted in Figures 3.26 to 3.32).

4.2.5 Summary

The observed alterations in the migration, invasion, and adhesion of TNBC cell lines after exposure to *T. violacea* crude water-soluble extract suggested that the extract may reduce the metastatic potential of cancer cells. The capacity of the extract to limit cell migration prevents cells from infiltrating ECM layers and diminishes cell adherence.

4.3 Antioxidant activity of *water-soluble T. violacea* extract.

The IC50 of the *T. violacea* water-soluble extract was determined using the 2,2-diphenyl-1-picrylhydrazyl (DPPH) assay, which is a free radical scavenging activity test. When oxygen reacts with specific chemicals, it typically produces free radicals that are atoms or clusters with unpaired electrons. They can arise from various sources, including normal metabolic processes, such as mitochondrial respiration, liver oxidase activities, and xanthine oxidase, as well as environmental pollutants, medications, and xenobiotics [518]. Free radicals are divided into reactive oxygen species (ROS) and reactive nitrogen species (RNS). Secondary metabolites from plants are abundant natural antioxidants, and polyphenolic chemicals are well known for their antioxidant properties. These function through multiple mechanisms, like quenching singlet oxygen, scavenging free radicals, chelating metal ions, and serving as reducing agents, effectively combats oxidative stress [519, 520]. The IC_{50} of the water-soluble extract of *T. violacea* was analysed using the 2,2-diphenyl-1-picrylhydrazyl (DPPH) assay, a free radical-scavenging activity test. Free radicals, atoms, and clusters with unpaired electrons are often produced when oxygen interacts with specific molecules. They can arise from various sources, including normal metabolic processes such as mitochondrial respiration, liver oxidase activities, and xanthine oxidase, as well as environmental pollutants, some medications, and xenobiotics [518]. Free radicals are divided into reactive oxygen species (ROS) and reactive nitrogen species (RNS). Secondary metabolites from plants are notably abundant in natural

antioxidants, with polyphenolic compounds particularly recognised for their strong antioxidant capabilities. This antioxidative characteristic underscores its potential as a source of natural antioxidants and as a foundation for new medications that scavenge free radicals. Cell viability is influenced by the nature and type of the stress applied. Cells can undergo prolonged lipid peroxidation in response to an apoptotic signal, connecting oxidative damage and Reactive Oxygen Species (ROS) to the beginning of apoptosis [521]. Bcl-2 has been suggested to regulate antioxidant pathways at sites of free radical production using a unique mechanism [522, 523]. Bcl-2 largely protects against apoptosis by blocking cytochrome c release from the mitochondria, especially when overexpressed, and it also serves as an antioxidant [524, 525].

Oxidative stress is a major cause of apoptosis, and can be induced by either a decrease in intracellular glutathione levels or an increase in cellular ROS concentrations [526, 527]. Even at low concentrations, hydrogen peroxide can trigger apoptosis by generating hydroxyl radicals and inducing changes in the oxidant/antioxidant pathways [519].

This study focused on analysing the phytochemicals and evaluating the antioxidant activity of crude extracts of *Tulbaghia*. Phytochemical analyses have identified several compounds, including flavonoids, glycosides, tannins, terpenoids, saponins, and steroids. These biologically active chemicals are potential contributors to the antioxidant activity of the *Tulbaghia* species. The presence of flavonoids and terpenoids implies that plant extracts may have antioxidant properties. Flavonoids are renowned for their antioxidant actions, which include scavenging or chelating free radicals [528]. Scavenging ROS can lead to multiple beneficial outcomes such as inhibiting lipid oxidation in vitro, enhancing the activity of antioxidant enzymes within the body, and decreasing the formation of peroxides in vivo [529]. Terpenoids act as primary antioxidants and effectively slow lipid oxidation by donating hydrogen to radicals [530]. The discovery of phytochemicals recognised for their antioxidant properties, such as flavonoids and terpenoids, in extracts opens the door to their extraction, purification, and extensive research, possibly leading to novel therapeutic developments. In the DPPH assay, methanol violet solution represents a stable free radical at room temperature. When antioxidants react with this radical, it disrupts the chain, changing the colour from violet to lighter

yellow. Extracts that turned yellow against violet setting showed antioxidant activity. Additionally, a shift to a yellow-white hue typically indicates a decrease in the formation of oxidised products, highlighting the role of antioxidants in curbing free radical production (Figure 3.33).

The antioxidant effects of plant extracts are commonly associated with the presence of phenolic compounds. *T. violacea*, with its high total phenol and flavonoid content, demonstrated strong antioxidant activity in the DPPH assay. Plant phenols, the most common antioxidants, interact with active oxygen radicals, such as hydroxyl, superoxide anion, and lipid peroxyl radicals to prevent early lipid peroxidation by scavenging hydroxyl groups. The phytochemicals discovered in the extracts used in this investigation are likely to contribute to the bioactivity of the Tulbaghia species. The significant polyphenolic and flavonoid contents of the extracts imply that the Tulbaghia species might be a good source of antioxidants. The antioxidant activity of these extracts in vitro shows that they can address oxidative stress and related health concerns. However, further research is needed to isolate and identify the individual molecules responsible for this action, with in vivo confirmation of the antioxidant efficacy of these pure compounds necessary before therapeutic use.

4.4 Determination of the molecular composition of the *T. violacea* water soluble extract

Background

Phytochemical research often employs a variety of analytical techniques including nuclear magnetic resonance (NMR), X-ray crystallography, mass spectrometry (MS), ultraviolet (UV), and infrared (IR) spectroscopy. Liquid chromatographic separation followed by spectroscopic detection is an excellent procedure for the thorough profiling (fingerprinting) of complicated mixtures. However, the combination of liquid chromatography and mass spectrometry (LC-MS) has grown in popularity owing to its comprehensive nature and capacity to work independently of physicochemical qualities, such as chromophoric attributes [531]. Table 1 shows the primary compounds isolated from the leaf fractions of *T. violacea*, which are detailed in Tables 3.3, 3.4, 3.5, and 3.6. The role of fatty acids in biological systems is critical, especially in reducing the risk factors associated with diseases such as

cancer, diabetes, and cardiovascular disease. Table 3.3 is solely devoted to identifying anticancer compounds that piqued my attention. To establish the presence of these anticancer medicines in *T. violacea* water-soluble extracts, the compounds identified using gas chromatography-mass spectrometry (GC-MS) were validated using NMR analysis.

4.4.1 4 H-Pyran-4-one, 2,3-dihydro-3,5-dihydroxy-6-methyl (DDMP)

In this study, I hypothesised that hydrophilic radical scavengers present in water-soluble extracts would be effective against DPPH radicals. This was confirmed when DDMP (5-Hydroxymethylfurfural) was identified as a major water-soluble radical scavenger, as indicated in Tables 3.2 and 3.3 and Figure 3.41. DDMP is known for its potent antioxidant properties [532]. It can form non-enzymatically from hexose sugars [532]. DDMP can be produced through thermal degradation of D-glucose, typically under high-temperature conditions [533]. It inhibits tyrosinase activity, an enzyme involved in the early stages of melanin synthesis from phenolic substrates. This property makes DDMP a promising compound for applications in cosmetics and medicine, particularly for targeting pigmentation processes [534]. DDMP, formed non-enzymatically from hexose sugars, has been identified as a significant water-soluble radical scavenger in *T. violacea* extracts [257, 480]. It has anticancer properties, most notably reducing colon cancer cell proliferation by causing apoptosis, principally by blocking the NF-kB pathway, which is essential for cell survival and development [535].

In my study, I discovered that different concentrations of DDMP (0.5 to 1.5 m, such as efficiently suppressed the proliferation of colon cancer cellsuch asW620 and HCT116) and triggered apoptoPARP.radeanoyl phorbol acetate-stimulated transcriptional and DNA-binding activities of NF-kB is also affected by DDMP (TPA). Furthermore, DDMP reduced the expression of NF-kB target anti-apoptotic genes, such as Bcl-2, while increasing the expression of pro-apoptotic genes, such as Bax, cleaved caspase-3, and cleaved PARP. I discovered that different concentrations of DDMP (0.5 to 1.5 mg/mL) efficiently suppressed the proliferation of colon cancer cells (SW620 and HCT116) and triggered apoptosis. TNF-α and tetradeanoyl phorbol acetate-stimulated transcriptional and DNA-

binding activities of NF-kB are affected by DDMP (TPA). Furthermore, DDMP reduced the expression of NF-kB target anti-apoptotic genes, such as Bcl-2, while increasing the expression of pro-apoptotic genes, such as Bax, cleaved caspase-3, and cleaved PARP [535].

Recent research has revealed the importance of NF-kB activation in numerous aspects of oncogenesis, such as the control of apoptosis, cell proliferation, differentiation, and cellular migration [536]. NF-kB activation promotes cancer cell proliferation, inhibits apoptosis, and enhances angiogenesis and metastatic potential [537].

NF-kB has been shown to be constitutively active in many cancer cell types, including pancreatic, breast, prostate, lung, and colorectal carcinomas. Continuous stimulation promotes the growth and development of cancer cells in various disorders. NF-kB has been shown to be constitutively active in many cancer cell types, including pancreatic, breast, prostate, lung, and colorectal carcinomas. This continuous stimulation leads to proliferation and growth of cancer cells in these disorders [538, 539]. Inhibition of NF-kB by DDMP may be critical for preventing the growth of MDA-MB 231 human TNBC cells. According to previous research, decreasing NF-κB activation can successfully decrease cancer cell proliferation, demonstrating DDMP's possible function of DDMP in controlling TNBC cell growth via NF-kB regulation of genes linked to cell death. NF-κB typically protects cells from various apoptotic triggers, such as chemotherapy, by deactivating anti-apoptotic gene pathways. The specific mechanisms through which DDMP achieves this suppression are yet to be thoroughly elucidated [540]. NF-kB controls both pro- and anti-apoptotic genes, including anti-apoptotic Bcl-2 and pro-apoptotic proteins such as Bax, cleaved caspase-3, cleaved caspase-9, and PARP. The balance between pro- and anti-apoptotic components is essential to determine whether a cell dies or survives. Therefore, targeting NF-kB can tilt the balance towards trigger apoptosis, which is desirable in cancer treatment [541]. This study investigated the effects of DDMP treatment on the levels of apoptosis-regulating proteins in human colon cancer cells (SW620 and HCT116). DDMP reduced the expression of anti-apoptotic proteins such as Bcl-2, while boosting the expression of pro-apoptotic proteins including Bax, cleaved caspase-3, and cleaved PARP. This shift in protein expression indicated DDMP's role of DDMP in driving cancer cell apoptosis by prioritising apoptotic processes

over anti-apoptotic signals.

A significant observation was that DDMP was non-toxic to normal colon cells at concentrations of up to 1.5 mg/mL, demonstrating its selective action on cancer cells and suggesting its potential as a safe therapeutic agent. The study also linked DDMP's impact of DDMP on apoptosis and cell growth inhibition to the deactivation of NF-kB, indicating that its anti-cancer properties might operate by modulating the NF-kB pathway. These findings emphasise the importance of onion-derived DDMP in exhibiting anti-cancer effects, with apoptosis induction being a central mechanism in its efficacy as a cancer treatment approach.

4.4.2 1,2,4-Triazine-3,5(2H,4H)-dione (6-azauracil)

This compound is a pyrimidine analogue that has demonstrated substantial antitumour effects against various transplantable mouse tumours [542]. 6-Azauracil (6AU), also known as as-triazine-3,5-dione, is an analogue of uracil that inhibits the growth of specific microorganisms. 6-Azauracil (6AU) has demonstrated significant antitumour effects against various experimental tumours, including sarcoma 180 (S-180) and mice [542].

6-Azauridine was marginally effective against L1210 tumours but ineffective against L5178Y tumours [543]. Cytosine arabinoside is one of the three most important pyrimidine antimetabolites used in cancer chemotherapy [544].

Indeed, 5-fluorouracil (5FU), 6-mercaptopurine (6MP), 6-thioguanine (6-TG), cytosine arabinoside (ARA-C), and methotrexate (MTX) are well-established chemotherapeutic agents used to treat various malignant diseases. Each of these drugs operates through different mechanisms to inhibit cancer cell proliferation and survival, making them essential components of chemotherapy regimens for various cancers. These drugs target different aspects of cancer cell growth and replication, making them valuable tools in cancer chemotherapy [545, 546]. 6-Azauracil (6AU) is a synthetic analogue of uracil that has shown significant antitumour activity in animal tumour models. Its promising preclinical results have led to its approval for human clinical trials, in which its potential as a cancer treatment

has been further investigated. The development of novel antitumor agents like 6AU is crucial in the ongoing efforts to combat cancer effectively [547]. Investigating the anticancer effect of 6-Azauracil (6AU) by monitoring mortality curves in animal models, such as white mice inoculated with Ehrlich ascites carcinoma cells, is a common approach in preclinical research. This type of study helps assess the potential of a compound to inhibit tumour growth and improve survival outcomes. The results obtained from these experiments provide valuable information regarding the efficacy of the compound as a potential cancer treatment [548]. 6-Azauraell has demonstrated a significant inhibitory effect on various experimental cancer tumours [549].

Pioneering research conducted by the National Cancer Institute on 6-azauridine (6AU) has demonstrated its significant effectiveness in experimental animals. Results from this investigation pointed to haematological enhancements in patients, indicating that 6AU might represent a potential therapeutic avenue for individuals newly diagnosed with certain types of cancer. This potential was inferred from its performance in preclinical models and early clinical observations [550].

1,2,4-triazines and their derivatives are important in medicinal chemistry owing to their substantial potential for biological action [551]. The 1,2,4-triazine ring is a prominent structural motif in many naturally occurring and synthetically derived, biologically active compounds. These compounds include anti-cancer and anti-inflammatory agents [552]. Indeed, azanucleosides, such as 6-azacytosine (6AU), which are structurally built on the 1,2,4-triazine nucleus, have demonstrated a broad spectrum of biological activities [553]. Azanucleosides such as 6-azacytosine (6AU), which are based on the 1,2,4-triazine nucleus, have shown a wide range of biological activities [554]. The biological activities of azanucleosides, nucleoside analogues with a furanose ring substituted by a nitrogen-containing ring or chain, have been a topic of interest [554]. In conclusion, the 1,2,4-triazine ring is a flexible structural motif with a wide range of biological actions, These include anticancer, anti-inflammatory, antifungal, and antiviral activities. The synthesis and evaluation of various derivatives and fused-ring structures have contributed to our understanding of their potential pharmacological applications. 6AU inhibits transcription by depleting the intracellular pool of guanosine monophosphate (GMP) and uridine monophosphate (UMP) [555]. 6AU is a drug that suppresses

cellular nucleoside triphosphate levels [556]. 6AU, an inhibitor of IMP dehydrogenase, decreases GTP pools, thereby causing transcriptional arrest [557]. The ribonucleosides of 6AU have demonstrated various biological properties, including antiviral, antitumour, and antifungal activities [558]. 6AU exhibits anticancer activity against several experimental tumours [559].

4.4.3 Benzaldehyde, 4-(1-methylethyl)-(cuminaldehyde)

The enzymatic activity of tyrosinase has been associated with its anticarcinogenic properties in melanoma [560]. Cuminaldehyde obstructed the enzymatic transformation of L-3,4-dihydroxyphenylalanine (L-DOPA) by tyrosinase, as demonstrated by spectrophotometric evaluation of enzyme activity [265].

Cuminaldehyde has numerous significant effects, including suppression of cell growth and induction of apoptosis. A decrease in mitochondrial membrane potential, activation of caspase-3 and caspase-9, and apparent apoptotic morphological alterations were all part of these effects. Cuminaldehyde also caused lysosomal vacuolation, acidic compartment enlargement, cytotoxicity, and inhibited topoisomerase I and II activity. An in vivo study using a nude mouse model demonstrated the ability of cuminaldehyde to significantly decrease tumour size, suggesting its potential clinical benefits. These effects were consistently observed across different cell lines, suggesting the potential of cuminaldehyde in chemoprevention or cancer therapy [561, 562].

Agents that impede cell development and cause cell death often target mitochondria in a number of ways. Two examples include the formation of holes in the mitochondrial membrane, which causes swelling and increased membrane permeability, leading to the release of pro-apoptotic cytochrome c into the cytoplasm. When cytochrome C reaches the cytosol, it interacts with Apaf-1 to form the apoptosome complex, which activates pro-caspase-9 and initiates a proteolytic cascade that results in apoptosis. Understanding these pathways is critical for understanding how certain substances trigger programmed cell death [563, 564].

Topoisomerases, which are crucial in managing DNA's topological state of DNA, are essential for genomic integrity [565, 566]. They relieve DNA entanglement by creating temporary protein-linked breaks in one strand for topoisomerase I or two strands for topoisomerase II [567, 568]. Topoisomerase I assists in DNA processing, maintaining genome integrity, and surveillance systems [569].

Elevated enzymatic activity, along with increased levels of the corresponding proteins and mRNA, has been observed in various human cancers. For example, both Akt3 enzymatic activity and mRNA are increased in breast cancer cell lines and tumours lacking the oestrogen receptor (ER), as well as in androgen-insensitive prostate cancer cell lines [570]. The involvement of topoisomerase I in chromosomal instability in colorectal cancer (CRC) and its potential as a prognostic marker have been suggested [571].

Topoisomerase II expression is upregulated in colorectal cancer (CRC) and correlates with cell proliferation and peaks in the G2/M phase of the cell cycle. This observation has prompted investigations into the potential of increased topoisomerase II gene copy number as a biomarker for anticancer therapies [572]. Topoisomerase II is important not only for cell cycle control but also as a main target for antiproliferative medicines, which are essential components of cell growth and proliferation strategies [573]. Increased expression of this enzyme is associated with the amplification of the TOP2A gene in CRC, a phenomenon under study for its potential as an anticancer biomarker [574]. This finding indicated that the correlation between gene amplification and protein expression may differ across various cancer types.

Following topoisomerase inhibition, apoptotic cell death is recognised as the most efficient cell death pathway in cancer [575]. In both in vitro and in vivo experiments, cuminaldehyde promoted apoptosis, thereby reducing cell growth [561]. Moving forward, I intend to broaden our research to investigate the impact of these compounds in a mouse model and use these systems to develop innovative drugs. Cuminaldehyde, a fundamental molecule, will lead to the development of safer and more effective chemopreventive and/or anticancer agents.

4.4.4 Vanillin

Vanillin, chemically known as 4-hydroxy-3-methoxybenzaldehyde, has shown anticancer properties, particularly owing to its strong antimutagenic activity. It is notably effective in diminishing the mutagenic effects of various heterocyclic amines [576].

Vanillin inhibits DNA repair by targeting DNA-dependent protein kinase (DNA-PK), an important component of the non-homologous end-joining (NHEJ) pathway, which is responsible for mending double-strand breaks (DSBs) in DNA. This interference with DNA-PK activity disrupts the NHEJ mechanism and potentially affects DNA damage repair [577].

The ability of vanillin to prevent cancer cell invasion and migration at non-lethal dosages may be due to its ability to inhibit DNA repair mechanisms. Furthermore, vanillin has been demonstrated to decrease MMP-9, an enzyme responsible for extracellular matrix disintegration, which aids cancer cell invasion and metastasis. Vanillin, by inhibiting MMP-9, may further limit cancer cell invasion and metastasis by downregulating the nuclear factor-B (NF-B) signaling pathway in human hepatocellular carcinoma cells [578]. Vanillin has also been investigated as a potential therapeutic agent for sickle cell anaemia [579] and exhibits antioxidant properties. It inhibits DNA-dependent protein kinases and enhances cancer cell sensitivity to cisplatin. Cell migration, influenced by various growth factors, involves interactions with cell surface receptors and activation of signaling pathways that lead to cytoskeletal changes and cell mobility mechanisms [580].

Cell migration offers numerous molecular targets for therapeutic agents aimed at inhibiting cancer progression [581]. Several molecular targets that reduce cancer cell migration have been identified, including miR-450. It has been shown to reduce cell proliferation, migration, and invasion in gastric cancer by targeting CREB1 and altering the AKT/GSK-3 signaling pathway [582]. Furthermore, hsa-miR-15a-5p has been proven to decrease colon cancer proliferation, migration, and invasion by targeting CCND1, indicating its potential as a molecular target for colon cancer diagnostics and treatments [583]. Furthermore, hsa-miR-15a-5p has been proven to inhibit colon cancer proliferation, migration, and invasion by targeting the CCND1 gene, indicating its potential as a molecular target for

colon cancer diagnosis and therapy [584].

The structural similarities between vanillin and aspirin and their potential anti-invasive effects in different cancer cell lines call for further research on their therapeutic capabilities in impeding cancer cell invasiveness [585]. Advances in machine learning and computational methods have significantly contributed to medical research, particularly in the diagnosis of complex diseases [586].

Aspirin has been shown to decrease prostate cancer cell motility by modifying actin cytoskeletal topologies and suppressing persistently active NF. -kB [587]. Aspirin and other nonsteroidal anti-inflammatory drugs may slow the spread of prostate cancer by inhibiting the cyclooxygenase (COX) pathway and its effects on cellular proliferation, apoptosis, and angiogenesis [588]. Aspirin also prevents IKK-β-mediated prostate cancer cell invasion by inhibiting matrix metalloproteinase-9 and urokinase-type plasminogen activator [589]. Furthermore, when used for several years, aspirin has been shown to reduce the long-term risk of various malignancies, notably colon cancer [590].

The mechanism by which vanillin impedes the migration of 4T1 cells might be similar to or different from that of aspirin. Previous studies confirmed the antimetastatic effectiveness of vanillin against breast cancer cells in laboratory and animal models [591]. Vanillin obstructs cell migration and breakdown of the extracellular matrix (ECM), which is crucial for cancer invasion. This suggests that vanillin can effectively prevent cancer invasion in experimental models and may help reduce metastasis in living organisms. Furthermore, vanillin has been shown to decrease cell growth in vitro, indicating its potential as an improved anti-metastatic drug. Notably, the antimetastatic effect of vanillin was evident in living organisms at a well-tolerated dosage in mice. Vanillin is a good option for the development of anticancer medication because of its safety and efficiency in preventing cancer cell proliferation [592]. At higher dosages, vanillin may alter gene expression in key biological processes, such as the cell cycle, apoptosis, cancer growth, and G2 phase arrest. Vanillin specifically has been demonstrated to control genes related to DNA damage and oxidative stress in colon cancer cell lines. HCT116 [576].
By blocking NF-κB activity, vanillin increases TRAIL-induced apoptosis in cancer cells [593]. This

made HeLa cells more susceptible to TRAIL-induced apoptosis by inhibiting NF-kB activity. This procedure involves inhibiting TRAIL-induced NF-kB activation, blocking TRAIL-induced NF-kB activation by interfering with p65 phosphorylation, and decreasing NF-kB transcriptional activity. Vanillin also inhibits NF-kB activation generated by inflammatory cytokines, such as TNF, LPS, and trinitrobenzene sulfonic acid (TNBS) [594], as well as the highly carcinogenic 12-O-tetradecanoylphorbol-13-acetate (TPA) [595]. The FDA considers vanillin safe for use in food and pharmaceutical products, as evidenced by an oral LD50 in rats ranging from 1.58 to 2.8 g/kg. Vanillin shows promise as a leader in the development of less harmful anticancer agents that offer multiple therapeutic benefits, including inhibiting metastasis and angiogenesis and increasing cancer cell sensitivity to TRAIL-induced apoptosis.

4.4.5 Oxime-, methoxy-phenyl

In the aqueous extracts of BMSE, a novel compound, methoxy-phenyl oxime (MPO), was found to induce apoptosis in HEK293T and HCT116 cells. The significance of this finding is uncertain, especially considering the complex relationship between p53 degradation and apoptosis [596].

P53 is essential for preserving genomic integrity and controlling cell cycle progression following DNA damage. When such damage occurs, p53 can stop the cell cycle at multiple checkpoints to allow repair. In cases of severe or irreversible damage, p53 can induce apoptosis, kill damaged cells, and prevent their transformation into malignant cells. The role of p53 as a tumour suppressor is critical for the prevention of cancer formation [597]. The processes that govern p53 stability and degradation are complex and include numerous proteins such as MDM2 and MDMX [598]. Evidence suggests that p53 plays a role in apoptosis under certain conditions [599]. The precise link between p53 degradation and apoptosis remains unknown [600].

However, as observed in cells treated with radicicol oxime, p53 degradation by one or more apoptosis-induced proteases occurs at later stages of apoptosis [601]. This observation might suggest a nuanced and potentially context-dependent relationship between p53

degradation and apoptotic process, underscoring the complexity of cellular responses to apoptotic signals and the need for further investigation to fully elucidate these mechanisms.

4.4.6 Pyrrolidine

Nitroxides are stable free radicals with unpaired electrons in their nitroxyl groups. They have been widely used in biology and medicine owing to their unique properties. The antioxidant activity of nitroxides is associated with their ability to undergo redox cycling. In this cycle, nitroxides accept electrons from reactive oxygen species (ROS), converting them into stable, non-radical forms. This process helps neutralise ROS and reduce oxidative stress, making nitroxides valuable as antioxidants and potentially useful in various medical and biological applications [602]. Many derivatives of piperidine, pyrroline, and pyrrolidine nitroxides are water-soluble, which makes them compatible with biological systems. This solubility allows them to be easily administered and to interact with cells and tissues. Additionally, one of the advantages of nitroxides is that they are generally considered non-toxic and non-immunogenic to normal cells, which is important for their use in medical or biological applications. This property enhances their safety profile and makes them suitable for various research and therapeutic purposes [602]. These findings suggest that pyrrolidine derivatives have promising anticancer properties. They have been demonstrated to cause G0/G1 cell cycle arrest and enhance cell death in HCT116 and HL60 cells. These results imply that compounds with a pyrrolidine structure could be potential candidates for future anticancer therapies [603, 604]. Additional structural and biological examinations involving nine distinct human cancer cell lines, coupled with apoptosis analysis, have indicated potential medicinal applications of pyrrolidines. This underscores the promise of pyrrolidine-based compounds as therapeutic agents, particularly in the context of medical interventions for diverse cancer types [605]. Furthermore, pyrrolidine compounds have shown significant cytotoxic effects against pancreatic cancer cells [606]. Pyrrolidines have received much research attention because of their antibacterial, antiviral, neurological, and prospective anticancer properties [606]. These findings highlight the potential of pyrrolidine-based compounds as cancer therapeutic agents.

4.4.7 Schizandrin

Schizandrin is renowned for its anticancer properties, including its capacity to act as a dual inhibitor of P-glycoprotein and multidrug resistance protein 1 (MRP1), which contributes to its effectiveness against cancer cells [607]. It enhances the effectiveness of doxorubicin-induced apoptosis in cancer cells by activating the mitochondrial apoptotic pathway while causing little harm to normal cells [608]. Schizandrin also suppresses ATR protein kinase, particularly in response to DNA damage [609].

Schizandrin has shown remarkable reduction in 4T1 lung metastasis and prolonged survival in mice. It significantly suppresses 4T1 cell metastasis at the local invasion stage and decreases epithelial-mesenchymal transition (EMT) in both 4T1 and primary human breast cancer cells, limiting their metastatic potential [228]. Schizandrin's role in inhibiting cancer cell metastasis, as well as its potential benefits when taken with other anticancer drugs, shows its broad pharmacological effects, which include antioxidant, anti-asthmatic, anti-inflammatory, and anti-cancer capabilities [610, 611] Schisandrin inhibits glioma cell growth and invasion by modulating several signaling pathways [612, 613], In addition to limiting the growth of lung cancer A549 cells by cell cycle arrest and death [614]. Schisandrin also inhibits TGF-1-induced epithelial-mesenchymal transition (EMT) in human A549 cells [615]. Schisandrin reduces the viability and growth of human gallbladder cancer cells [613]. It activates caspase-3 and caspase-9, inactivates several key proteases, and kills cancer cells. It induces apoptosis in these cells by increasing Bax expression and decreasing Bcl-2 expression and Bcl-2/Bax ratio. Schizandrin suppresses NF-kB activity, which is required for apoptosis suppression by downregulating its target genes in the Bcl-2 family [610].

The suppression of NF-kB nuclear translocation observed in this study, as well as the downregulation of its target genes in the Bcl-2 family, show that schizandrin inhibits NF-kB activation during tumour growth. The suppression of NF-kB nuclear translocation observed in this study, as well as the downregulation of its target genes in the Bcl-2 family, shows that schizandrin inhibits NF-kB activation during tumour growth [616]. Flow cytometry analysis revealed G0/G1 phase arrest and Apoptosis of GBC-SD and NOZ cells. Schizandrin-treated cells had higher levels of Bax, cleaved caspase-9, cleaved caspase-3, and cleaved PARP. Concurrently, the levels of Bcl-2, NF-kB, cyclin

D1, and CDK-4 have been reported [616]. Schizandrin causes apoptosis via the mitochondria-mediated intrinsic caspase pathway, as demonstrated by alterations in the expression of proteins such as Bax, Bcl-2, caspase-9, caspase-3, PARP, and other Bcl-2 protein family members. Schizandrin causes apoptosis via the mitochondrial-mediated intrinsic caspase pathway, as indicated by alterations in the expression of proteins including Bax, Bcl-2, caspase-9, caspase-3, PARP, and other Bcl-2 protein family members [617, 618]. Schisandrin has been shown to inhibit large-cell lung cancer cells via the NF-B and p38 MAPK signaling pathways. These findings suggest that schisandrin may be effective in the treatment of large-cell lung cancer. Schisandrin has been shown in tests to inhibit large-cell lung cancer cells via the NF-B and p38 MAPK signaling pathways. These findings suggest that schisandrin may be effective for the treatment of large-cell lung cancer [619]. Schisandrin has been shown to suppress cell migration, invasion, epithelial-mesenchymal transition (EMT), and cancer stem cells (CSC). Furthermore, it may control other signaling pathways associated with EMT, including SMAD, PI3K/AKT, Wnt, and Notch, indicating that Schisandrin has a greater regulatory influence on these cancer-related processes. Schisandrin inhibits cell cycle progression in A549 cells by downregulating cyclin D1, cyclin-dependent kinase (CDK) 4, and CDK6 while concurrently increasing p53 and p21 expression [620].

Furthermore, Schizandrin caused apoptosis in A549 cells by increasing the expression of Bax, cleaved caspase-3, cleaved caspase-9, and Cytochrome C, while lowering the expression of Bcl-2 and PCNA [616]. Additionally, Schisandrin therapy significantly lowered PCNA expression levels in A549 cells. Schisandrin also induces G0/G1 cell cycle arrest and cell death [621].

Furthermore, Schisandrin treatment dramatically decreased PCNA expression in A549 cells. Schisandrin also induced G0/G1 cell cycle arrest and death in these cells [338, 621]. Cell cycle arrest is associated with the inhibition of tumour cell growth [622].

In A549 cells, schisandrin administration significantly reduced CDK4, CDK6, and cyclin D1 expression, and increased p21 expression. This variation in the quantity of cyclins, CDKs, and CDK inhibitors is critical for controlling cell cycle progression and inhibiting tumour cell development. [623]. Cyclin D1, a key player in the G1 phase of cell division, is linked to the cancerous

characteristics of tumour cells [624].

Cyclin-CDK combinations have an important role in determining cell cycle phases, notably via assembling cyclin and CDK subunits. Proteins like p21 and p27 impede the transition from G1 to S phase by promoting the breakdown of cyclin/CDK complexes, hence influencing cell cycle progression [625].

Schisandrin's significant suppression of cyclin D1, CDK4, and CDK6, together with increased p21 expression, is likely to slow the transition from G1 to S phase during cellular division [289].

Furthermore, A549 cells treated with Schisandrin showed considerably higher levels of p53, which is associated with cell cycle arrest and programmed cell death [285]. p53 is necessary for regulating p21 expression [626]. Schisandrin treatment may boost p53 expression, which in turn increases p21 levels. This increase may inhibit the cyclin D1/CDK complex, causing A549 cell cycle arrest at the G0/G1 phase. Furthermore, Schisandrin decreases SIRT1 protein expression, and there is a negative correlation between SIRT1 and the activation of SMURF2, which inhibits colon cancer cell proliferation and spread [627].

4.4.8 Taurolidine

Taurolidine, renowned for its potent chemotherapeutic properties, is highly effective in managing inflammatory conditions via the methylation of amino groups on cellular membrane proteins (Schuller-Levis and Park, 2003). Taurolidine exhibits antiendotoxin, antimicrobial, anti-adhesive, and antifungal properties [628]. Taurolidine has been used topically and systemically to treat individuals with confirmed peritonitis in clinical settings [629] and as a peritoneal rinse to prevent infection after elective colorectal surgery. Taurolidine suppresses the development of a rat metastatic colorectal tumour cell lines in vitro and in vivo, suggesting that it may be effective in preventing peritoneal metastases [629].

Research on the influence of taurolidine on tumour cell apoptosis revealed that lower doses (5 µg/ml and 10 µg/ml) promote apoptosis in tumour cells, while higher doses (15 µg/ml and 25 µg/ml) lead to cellular necrosis. These in vitro results support the findings of Nici et al. [630], emphasising the suppressive effect of taurolidine on the DHD/K12/TRb tumour cell line. Taurolidine, which has antibacterial and antiendotoxin capabilities within the thiadiazine chemical group, has been shown to decrease a rat tumour cell line both in vitro and in vivo. Taurolidine inhibits the development of three human colon cell lines at therapeutic levels with higher efficacy than the recommended doses of 5FU [629, 631].

Investigations using optical and electron microscopy combined with flow cytometry suggested a mechanism of apoptotic cell death through previously unidentified pathways. In vitro studies have demonstrated direct and selective antitumour effects of taurolidine on glial and neuronal brain tumour cells [632]. Taurolidine likely acts by directly diminishing IL-1 production in peritoneal macrophages, thereby obstructing the response of tumour cells to growth signals. Additionally, taurolidine appears to directly affect tumour cell proliferation, possibly through the same mechanism employed to eliminate microorganisms [633]. Consequently, taurolidine undergoes enzymatic hydrolysis and decomposes into methyloltaurultam and taurultam, which further breaks down into methyloltaurinamid, ultimately producing taurin and an active methylol group. These active constituents are believed to induce cell death by interacting with the cell surface receptors. However, the precise mechanism underlying the suppression of tumour growth by taurolidine in various cancers remains unclear. The induction of cell death in DU145 human prostate tumours exemplifies this phenomenon [634]. In this model, TRD correlates with DNA fragmentation and heightened externalisation of membrane PS, which is indicative of apoptosis induction [635].

TRD's potential of TRD to activate PARP cleavage in these cells was validated when exposed to the pan-caspase inhibitor VAD-FMK at the same time. TRD also led to the detection of cytochrome c in the cytoplasm, the activation of procaspase 9 after 2 hours, and the subsequent activation of procaspase 8 after 4 h. TRD causes mitochondria-mediated apoptosis in DU145 human prostate tumour cells [636]. TRD causes apoptosis in human ovarian tumour and promyelocytic leukaemia

cells, indicating its therapeutic potential [637].

TRD's apoptotic mechanisms of TRD include activation of the mitochondrial cytochrome c-dependent pathway [638] and inhibition of protein synthesis [628]. TRD has shown good clinical results in patients with advanced gastric cancer and glioblastoma [632]. TRD affects the mitochondrial cytochrome c-dependent (intrinsic) pathway [639]. In addition, TRD obstructs protein synthesis [632]. Aurolidine induces cell death via both caspase-dependent and-independent mechanisms, increases the production of reactive oxygen intermediates, and reduces mitochondrial membrane permeability. The oxygen scavenger N-acetylcysteine has been found to prevent cell death. Taurolidine therapy activated p53 in two-thirds of MPM cell lines, while lowering survivin, Bcl-2, and Mcl-1 protein levels. Furthermore, taurolidine treatment increases the susceptibility of MPM cells to cisplatin-induced apoptosis. Taurolidine induces both apoptosis and necrosis, activates p53, and enhances sensitivity to cisplatin, whereas PVP-I primarily inhibits cell growth via necrosis. MPM cells carry wild-type p53 as well as the apoptosis inhibitors survivin, Bcl-xL, Bcl-2, and Mcl-1 [640].

MPM cell lines and tumours express Bcl-2 family members, most notably Bcl-xL and Mcl-1 [641], along with the apoptosis inhibitor protein, survivin [642]. Bcl-2 expression is rare; however, when present, it is inversely correlated with the apoptotic index [643]. Furthermore, taurolidine therapy reduces TNF synthesis and blocks the generation of growth-stimulating interleukin-1 (IL-1) in peripheral blood cells [644]. Taurolidine induces apoptosis in human ovarian and prostate cancer cell lines. [630]. Furthermore, in vivo studies have shown that taurolidine, when used as an abdominal rinse in a rat model of colon cancer, dramatically inhibits intraperitoneal tumour development [629]. Taurolidine enhanced the expression of the pro-apoptotic protein Bax and decreased the expression of the anti-apoptotic protein Bcl-2 in a dose- and time-dependent manner. This demonstrates that changes in Bcl-2 family protein expression may be a crucial mechanism underlying taurolidine-induced apoptosis in murine melanoma cells [645].

In a Syrian hamster model of pancreatic adenocarcinoma, taurolidine effectively inhibited primary tumour growth and reduced metastases at both the port site and liver [646].

Taurolidine affects apoptosis by modulating Bcl-2/Bax concentrations [647]

It exhibits anti-metastatic properties within the tumour microenvironment by blocking angiogenesis and endothelial cell adhesion [648]. IIn glioma cell lines, taurolidine triggered autophagy and necroptosis. Taurolidine appears to promote autophagy and necroptosis in glioma cell lines [292]. Taurolidine induces autophagy and necroptosis in glioma cell lines and has been used to treat glioblastoma and gastric cancer in humans [292].

4.4.9 Alpha-Pinene

Research indicates that α-pinene, a naturally occurring compound, exhibits anticancer properties [278]. Research has shown that α-pinene suppresses cell cycle progression from G2 to M phase in BEL-7402 cells. Treatment with -pinene reduced Cyclin B protein levels, a situation associated with G2/M cell cycle arrest [610]. Importantly, treatment with -pinene increases Chk1 and Chk2 levels, while lowering CDC25 and CDNK1 levels [649]. Thus, it is postulated that α-pinene-induced cell cycle arrest is controlled by pathways involving Chk2 and CDC25C [649].

Research indicates that α-pinene possesses anticancer properties in human ovarian and hepatocellular liver carcinoma cell lines [650]. -Pinene has also been shown in tests on N2A neuroblastoma cells to have antioxidant, anti-cancer, and genotoxic effects [651]. The potential of -pinene to limit tumour invasion was investigated in a research utilising highly metastatic MDA-MB-231 human breast cancer cells [278]. α-pinene may suppress TNFa-induced matrix metalloproteinase-9 gene promoter activation and mRNA production in a dose-dependent manner [650].

Treatment with α-pinene reduced TNF-α-triggered NF-kB activation and transcriptional activity. [652]. By inhibiting nuclear factor kappa B (NF-kB) activity, -pinene effectively reduced TNFα-induced MMP-9 gene expression and the invasive nature of MDA-MB231 cells [653].

Furthermore, -pinene inhibits cell proliferation and induces cell cycle arrest, resulting in a reduction in tumour cells. In accordance with these results, the present study shows that α-Pinene treatment of human ovarian cancer cells induces cell cycle arrest during the transition from the G2 to M phase [654]. α-Pinene has been shown to induce apoptosis in human leukaemia cells via a mitochondrial-mediated route [654]. These findings suggest that -pinene has a significant impact on tumour invasion and may be employed as an anti-metastatic agent for the treatment of triple-negative breast cancer.

4.6 RTK pathway analysis following treatment of cells with T. violacea crude water-soluble extract

In line with the observed alterations in apoptosis, cell cycle regulation, invasion, metastasis, and adhesion, there was a significant reduction in the expression of various receptor tyrosine kinases (RTKs). RTKs are integral to these cellular functions. Among them, Dtk1, which is known for its function in cell survival and motility [654], as well as EGFR and Flt-3, which are also recognised for their roles in cell proliferation and apoptosis suppression [655], exhibited reduced expression. Furthermore, HGFR is required for proliferation, dispersion, morphogenesis, and survival [656], and MspR is a protein involved in epithelial cell migration, proliferation, and survival [435] were similarly impacted. Mer has a role in cell survival, motility, differentiation, and phagocytosis of apoptotic cells. was also downregulated. PDGFR, renowned for its uncertain function in regulating cell proliferation, motility, survival, and chemotaxis, has been shown to have decreased expression. This finding is relevant as the PDGFR family is implicated in more aggressive forms of breast cancer, with overexpression in TNBC correlating with worse patient prognosis and increased recurrence risk [574].

The increase in AKT expression in TNBC cells post-treatment may indicate the activation of diverse mechanisms, including cell survival and angiogenesis, a paradox considering the observed increase in apoptosis and reduced migration. This complexity underscores the effects of treatment on cancer cell behaviour [657]. However, the precise role of AKT remains uncertain because of its involvement in various processes, such as enhancing BAD's pro-apoptotic activity of BAD, which complicates the identification of its specific function in response to treatment [413]. AKT also regulates p53 acetylation, increasing p53 transactivation potential and showing its complex regulatory roles [658]. These effects likely contribute to the observed increase in apoptosis, with AKT's heightened

transcription correlating with the protein profile assay results. Given AKT's critical function in neurogenesis, it is especially important to understand its role in the observed cellular responses [659].

The observed increase in gene transcription related to axon guidance and neurogenesis after treatment is linked to the activation of the AKT pathway. Upregulation of AKT underscores its significant impact on key cellular processes in response to treatment. The simultaneous tumour-promoting and-inhibiting properties of the ephrin family of RTKs reflect their function in regulating cell proliferation, migration, and death [660]. Following therapy, there is a notable drop in EphA1 expression, which is involved in cell adhesion and migration, and correlates with the reported impacts on these activities [661]. Similarly, reductions in EphA3 and EphA4 expression, which are involved in cell-cell adhesion, cytoskeleton organisation, and migration, have been noted [662]. EphA4's role in TNBC and its potential as a target to impede cell migration are highlighted, despite the high expression of other EphA family members. EphA2, which is overexpressed in TNBC, exhibits increased expression after treatment, indicating a possible mechanism by which the extract may counteract or override EphA2's impact, implying therapeutic promise in TNBC therapy [663].

treatment, downregulation of all three FGFR family members was observed. FGFRs are crucial in cell proliferation, differentiation, and migration regulation and serve as potential biomarkers in TNBC. FGFR2 overexpression is associated with poorer survival outcomes, indicating a therapeutic avenue for TNBC, especially in FGFR-upregulated cases [664]. The ROR family of RTKs, functioning as receptors for the WNT ligand WNT5A, potentially suppresses WNT3A-mediated signaling inhibits cell proliferation and promotes cell death. This interaction highlights the complex interplay between cellular signaling pathways in cancer development and progression (Reis et al., 2021). In TNBC cells, ROR1 expression increased significantly, whereas ROR2 expression decreased. Overexpression of ROR1 in TNBC is linked with more aggressive tumours and a greater risk of metastasis, revealing a complex regulation mechanism and potential therapeutic value for such extracts [665].

After treatment, there was a decrease in RYK expression, which is critical for Wnt signaling and neurogenesis, suggesting an influence on the Wnt signaling pathways involved in cell proliferation,

differentiation, and migration [666]. Trk family members showed differential regulation post-treatment, with upregulation of TrkA and downregulation of Trk B and Trk C. These receptors are vital for neurotrophic signaling in TNBC, and understanding these alterations could be critical for exploring new therapeutic strategies [667]. The heightened expression of TrkA after treatment correlates with the extract's inhibitory effects on metastasis and apoptosis induction, emphasising the downregulated roles of RTKs in neurogenesis, axon guidance, and neurotransmitter signaling [668].

Both Tie 1 and Tie 2 showed increased expression after treatment in TNBC cells, playing a key role in controlling angiogenesis. Under certain conditions, Tie 2 serves as an angiogenesis inhibitor. In particular, Tie 2 acts as an angiogenesis inhibitor [669]. A decrease in the expression of all three VEGF receptor family members, VEGFFR1, VEGFR2, and VEGFR3, was observed post-treatment. These receptors are integral in mediating various signaling pathways crucial for angiogenesis, cell survival, and migration, suggesting a potential therapeutic pathway in TNBC progression by targeting VEGF receptors [670].

4.4.10 Transcriptome analysis

Previous research on the effects of water-soluble chemicals isolated from *T. violacea* on triple-negative breast cancer (TNBC) cells has yielded a range of outcomes. These effects include influencing apoptosis and the cell cycle, as well as altering essential TNBC cell behaviours, such as migration, invasion, and adhesion. These findings indicate that *T. violacea* chemicals play a range of functions in controlling the pathophysiological behaviours of TNBC cells, which might have important implications for developing novel treatments for this aggressive type of breast cancer. These chemicals also exhibit cytotoxic and antioxidant effects. These findings indicate that *T. violacea* chemicals play a range of functions in controlling the pathophysiological behaviour of TNBC cells, which might have important implications for creating novel treatments for this aggressive type of breast cancer. These chemicals also exhibit cytotoxic and antioxidant effects. These findings indicate that *T. violacea* chemicals play diverse roles in influencing the pathophysiological behaviour of TNBC cells, which may have major implications for creating novel therapeutic options for this

aggressive type of breast cancer. The chemicals also have cytotoxic and antioxidant effects. These findings point to

T. violacea chemicals playing a diverse role in influencing the pathophysiological behaviours of TNBC cells, which might have major implications for creating novel therapeutic options for this aggressive type of breast cancer. The chemicals also have cytotoxic and antioxidant effects. Exposure to *T. violacea* compounds altered gene expression more extensively in TNBC cells than in normal breast cells. There was considerable overlap in the genes with modified expression in both cell types, as confirmed by functional enrichment analysis, identifying similar gene groups based on biological functions that were upregulated or downregulated in both cell types. Post-exposure, a reduction in gene expression associated with cancer-specific and RTK pathways was noted. In contrast, the gene expression associated with angiogenesis varied; it was mainly steady in normal breast cells but reduced dramatically in TNBC cells. The augmented expression of apoptosis-related genes after treatment aligns with the outcomes of the apoptosis assay. Previous theoretical models have shown that the components of the extract effectively bind to the anti-apoptotic protein COX-2. An increase in stress response gene expression post-exposure was surprising considering the antioxidant nature of the extract, but may not be sufficient to mitigate its cytotoxic effects.

For a more comprehensive understanding and additional experimental replicates for in-depth sequencing data analysis, further sequencing experiments on the impact of this extract on TNBC and normal breast cancer cells are essential. The identification of specific miRNAs and lncRNAs in these experiments indicates the potential for targeted sequencing of these non-coding RNAs. These initial findings shed light on how the extract alters gene expression, influencing cell survival and cancer-related behaviours, such as increased migration, invasion, and decreased adhesion. Further testing of the individual components within the extract is also suggested to identify potential lead compounds for TNBC treatment development.

4.4.11 The transcriptome and increased levels of apoptosis

The elevation of pro-apoptotic gene transcription in TNBC cells after treatment with *T. violacea* extract corresponded with the anticipated outcomes, primarily for two reasons. The observed increase in apoptosis, as shown by the apoptosis test, indicated a direct impact on the biological pathways that

lead to cell death. Second, the composition of the extract, which contains various apoptosis-inducing compounds, implies that these components likely act through diverse pathways to initiate apoptosis. This variation in mechanisms could account for the increased transcriptional activity of pro-apoptotic genes after treatment. Regarding anti-apoptotic genes, there was an equal mix of increased and decreased transcription in TNBC cells post-treatment, with two intrinsic pathway genes being notably downregulated.

In normal cells, the relatively moderate increase in apoptosis after treatment with the water-soluble *T. violacea* extract corresponds to the transcriptional alterations seen in figures c and D. Following therapy, transcription of most pro-apoptotic genes increases, as do numerous anti-apoptotic genes, and the particularly high transcript levels of these anti-apoptotic genes might signal the activation of protective pathways counterbalancing extract-induced apoptosis, culminating in lower apoptosis levels.

4.4.12 The transcriptome and S phase checkpoint activation

The cell cycle study demonstrated that the water-soluble extract of *T. violacea* induced S phase arrest in both TNBC and normal cells, resulting in a large number of cells in the S phase for each cell type. Cell cycle analysis revealed that the water-soluble extract of *T. violacea* promotes S phase arrest in both TNBC and normal cells, resulting in a significant concentration of cells in the S phase for each cell type. To gain a deeper understanding of this phenomenon, a comparative analysis was conducted on the alterations in the transcript levels of genes that either promote S phase progression or contribute to its arrest. The observed changes in gene expression were consistent with the S phase arrest observed post-treatment, particularly in the TNBC cell line. TNBC cells exhibited a considerable increase in the transcription of genes linked to S phase arrest, as seen in Figure 3.44A. In contrast, the effect on normal breast cells was less marked, potentially explaining the extract's relatively gentler inhibitory impact on the proliferation of these normal cells. This differential response between TNBC and normal cells underscore the specificity of the *T. violacea* extract in targeting cancer cell growth and highlight its potential therapeutic value in selectively inhibiting TNBC cell proliferation.

Chapter 5 Conclusion

The methanol-soluble extract from *T. violacea* has varying lethal effects on triple-negative breast cancer (TNBC) cells. The water-soluble and methanol-soluble extracts of C. orbiculate had distinct effects on TNBC cells. The water-soluble extract of *T. violacea* exhibited notable cytotoxic effects on TNBC cells, inducing more pronounced morphological alterations than in normal cells. This excerpt caused apoptosis and S-phase cell cycle arrest in both cell lines, with TNBC cells showing the most significant effect. It decreased cell migration, invasion, and adhesion in TNBC cells without affecting normal cells, and exhibited antioxidant capabilities.

The extract was analysed to determine its component makeup, which showed the presence of different compounds, some of which have known anticancer properties. In computational docking investigations, the chemicals showed strong binding affinity for COX2, an anti-apoptotic gene related to cell survival. The extract also affected the expression of several Receptor Tyrosine Kinases (RTKs) that play a role in cancer-related processes and neurogenesis. The extract treatment reduced the transcription of genes involved in neurogenesis, axonogenesis, and axon guidance while increasing the transcription of genes related to both extrinsic and intrinsic apoptotic pathways, thus promoting apoptosis. Genes linked to cancer advancement and formation of new blood vessels exhibit decreased expression.

This study highlights the effectiveness of water-soluble *T. violacea* extracts in TNBC cells. The water-soluble extract of *T. violacea* has been shown to be effective in triggering apoptosis in triple-negative breast cancer (TNBC) cells, with a notably greater rate of TNBC cell death than in normal breast cells. This selectivity is essential for cancer treatment to reduce the harm to healthy tissues. The ability of the extract to target cancer cells is likely due to chemicals that interact with the anti-apoptotic protein COX-2, which is frequently overexpressed in cancer cells and promotes cell survival. 5-Fluorouracil (5FU), a traditional chemotherapy medication, disrupts DNA and RNA synthesis in fast-growing cells and triggers cell death in cancer cells. 5FU is non-selective and can

damage normal tissues with high proliferation rates, leading to adverse effects.

Future studies should investigate the specific chemicals within this extract, either alone or in combination, against TNBC cells. Commercially manufactured compounds should be used to ensure uniformity.

This study examined the anticancer effects of extracts of C. orbiculata and *T. violacea*, two medicinal plants from Southern Africa, on TNBC cell lines in a laboratory setting. The water-soluble extract of *T. violacea* contains unique compounds that specifically induce apoptosis and hinder metastasis in TNBC cells. Alterations in gene transcription and protein signaling pathways pertinent to cancer contribute to these outcomes. D-Glycero-D-galacto-heptose exhibits a high affinity for COX2 and might serve as a promising lead chemical for treating TNBC.

Further research is needed to further our understanding of the apoptotic effects of *T. violacea* extract and its components, particularly their interactions with cellular targets and signaling networks. This study highlights the importance of investigating natural compounds obtained from medicinal plants for novel cancer treatment, creating opportunities for drug discovery targeting TNBC and other cancers.

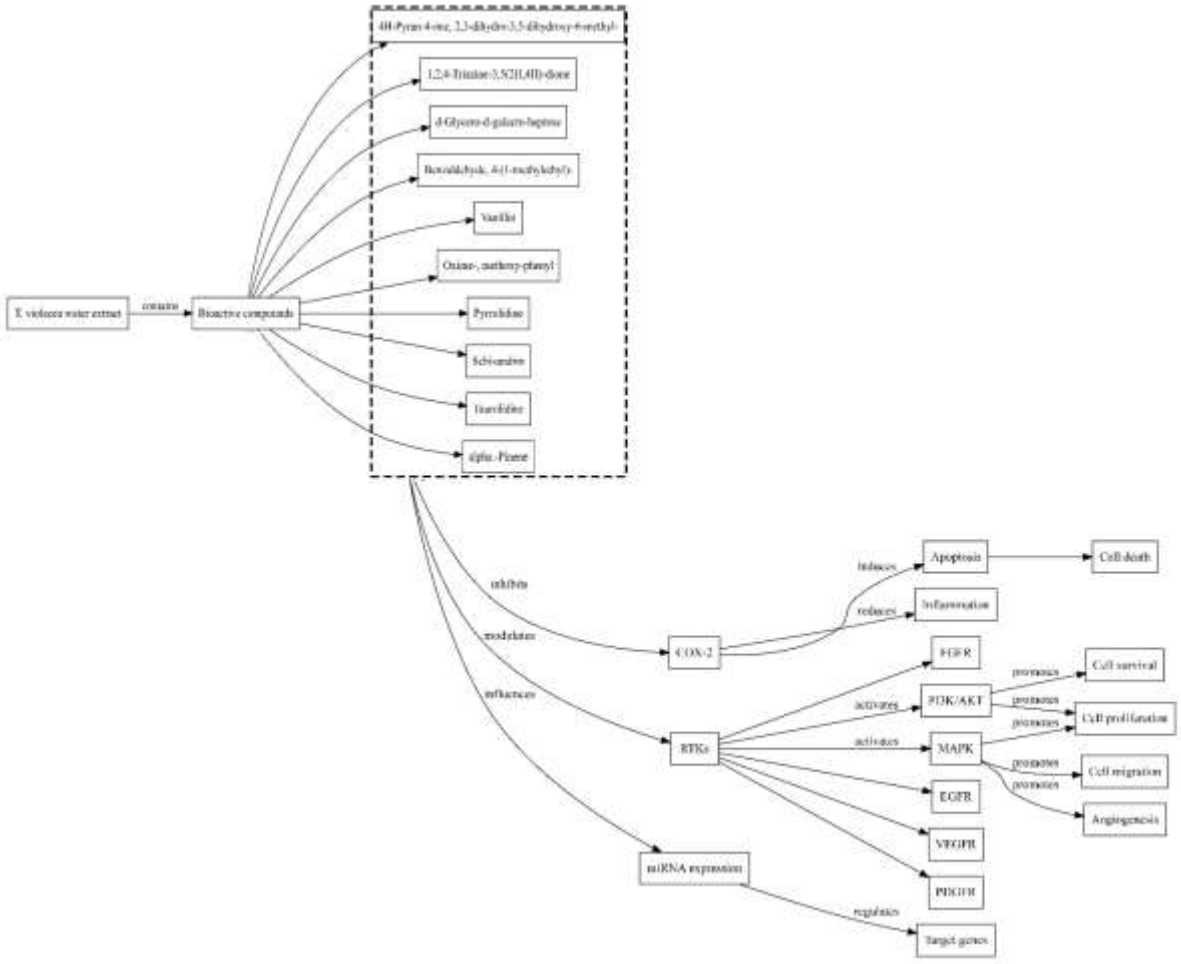

Figure 5.1 Signaling Pathway Network Regulating Cellular Processes, The figure depicts a complex network of interactions between various molecules, enzymes, and cellular processes involved in the regulation of key cellular functions such as apoptosis, inflammation, cell survival, proliferation, migration, and angiogenesis. The main components of the network include Small Molecules and Compounds:1,2-diacyl-sn-glycerol, 3-dehydroxy-3-dehydroxy-6-ethyl-3,4-dihydro-2H-pyran-2-one, and 1, 2, 3, 4-tetrahydro-3-isoquinolinecarboxylic acid. Enzymes and Proteins: COX-2, RTK, MAPK, VEGFR, PDGFR, and others.Cellular Processes and Responses: optosis, cell death, inflammation, cell survival, proliferation, migration, and angiogenesis

Table 5.1 List of Proteins in the Signaling Pathway Network

Protein	Function
COX-2	Enzyme involved in inflammation
RTK	Receptor tyrosine kinase, regulates cell signaling
MAPK	Mitogen-activated protein kinase, involved in cell proliferation and differentiation
VEGFR	Vascular endothelial growth factor receptor, regulates angiogenesis
PDGFR	Platelet-derived growth factor receptor, regulates cell growth and division

Note: This table provides an illustrative example, and the actual list of proteins and their functions may vary depending on the specific pathway or network being represented.

Chapter 6 Appendices

6.1 Appendices A

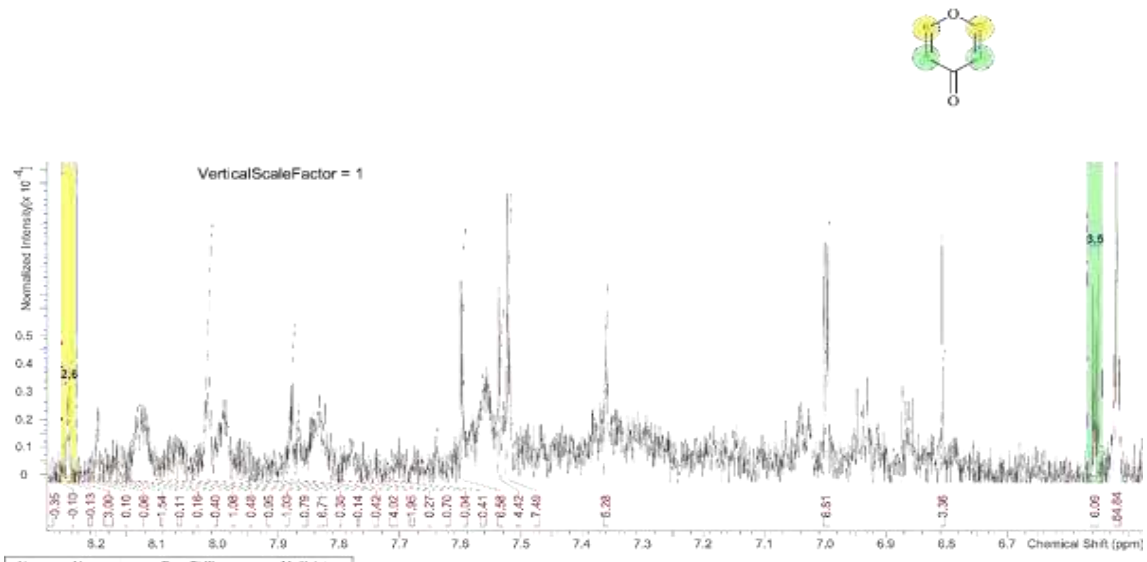

No.	Atom	Exp. Shift (ppm)	Multiplet
1	3	6.56	M216
2	5	6.56	M216
3	2	8.24	M183
4	6	8.24	M183

Figure 6.1 4H-Pyran-4-one, 2,3-dihydro-3,5-dihydroxy-6-methyl- T. violacea aqueous compound NMR spectrum.

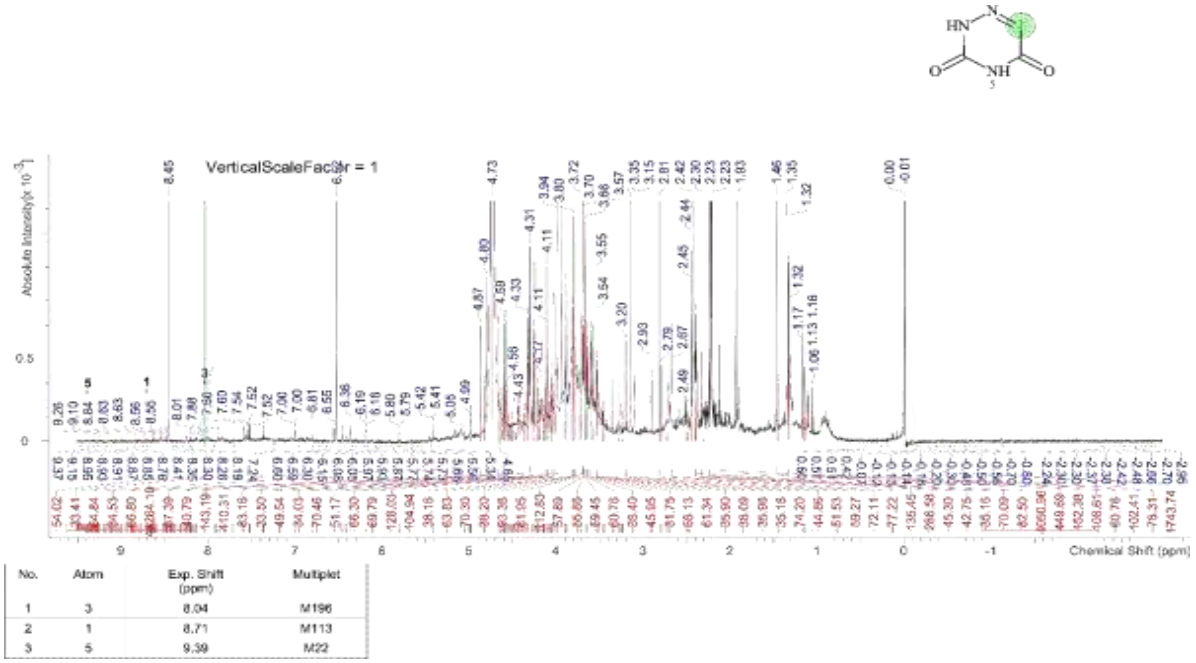

Figure 6.2 1,2,4-Triazine-3,5(2H,4H)-dione T. violacea aqueous compound NMR spectrum

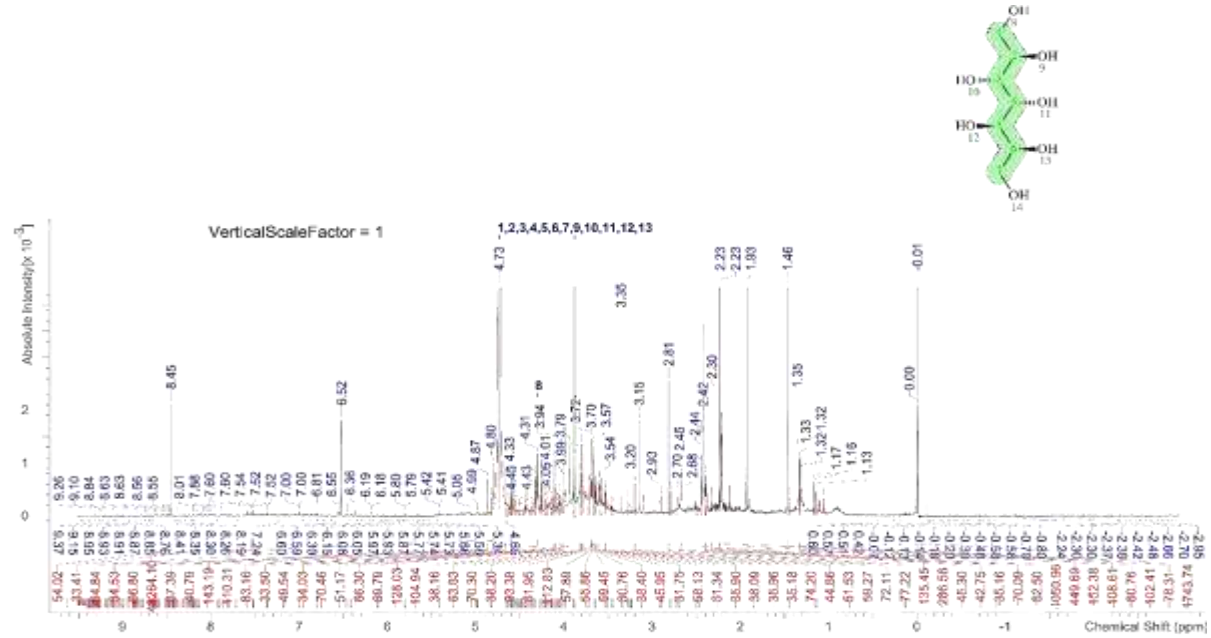

No.	Atom	Exp. Shift (ppm)	Multiplet	No.	Atom	Exp. Shift (ppm)	Multiplet	No.	Atom	Exp. Shift (ppm)	Multiplet
1	1	3.88	M315	6	6	3.88	M315	11	12	3.88	M315
2	2	3.88	M315	7	7	3.88	M315	12	13	3.88	M315
3	3	3.88	M315	8	9	3.88	M315	13	8	4.29	M274
4	4	3.88	M315	9	10	3.88	M315	14	14	4.73	M236
5	5	3.88	M315	10	11	3.88	M315				

Figure 6.3 1,2,4-Triazine-3,5(2H,4H)-dione T. violacea aqueous compound NMR spectrum

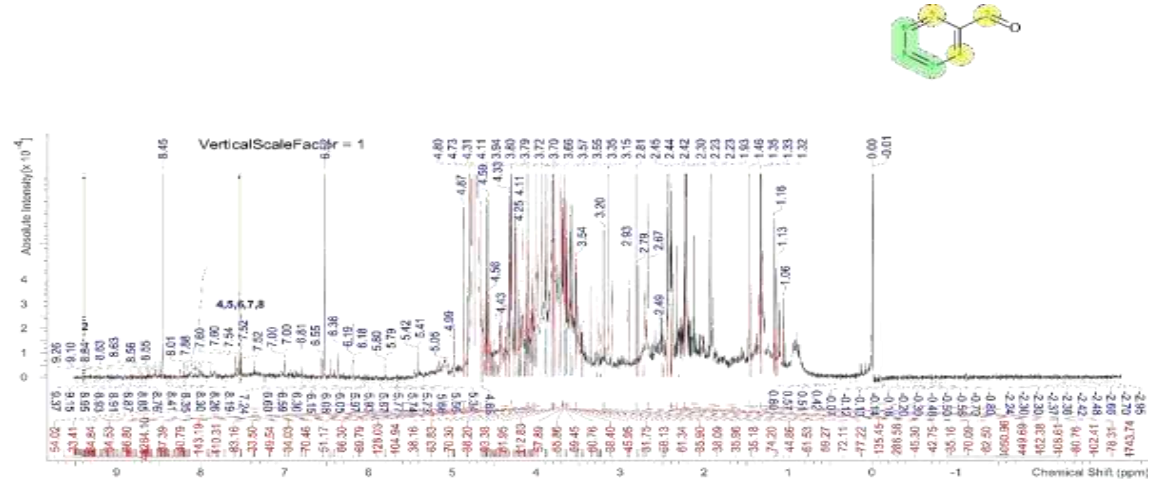

No.	Atom	Exp. Shift (ppm)	Multiplet
1	4	7.54	M207
2	5	7.54	M207
3	6	7.54	M207
4	7	7.54	M207
5	8	7.54	M207
6	2	9.39	M22

Figure 6.4 1,2,4-Triazine-3,5(2H,4H)-dione T. violacea aqueous compound

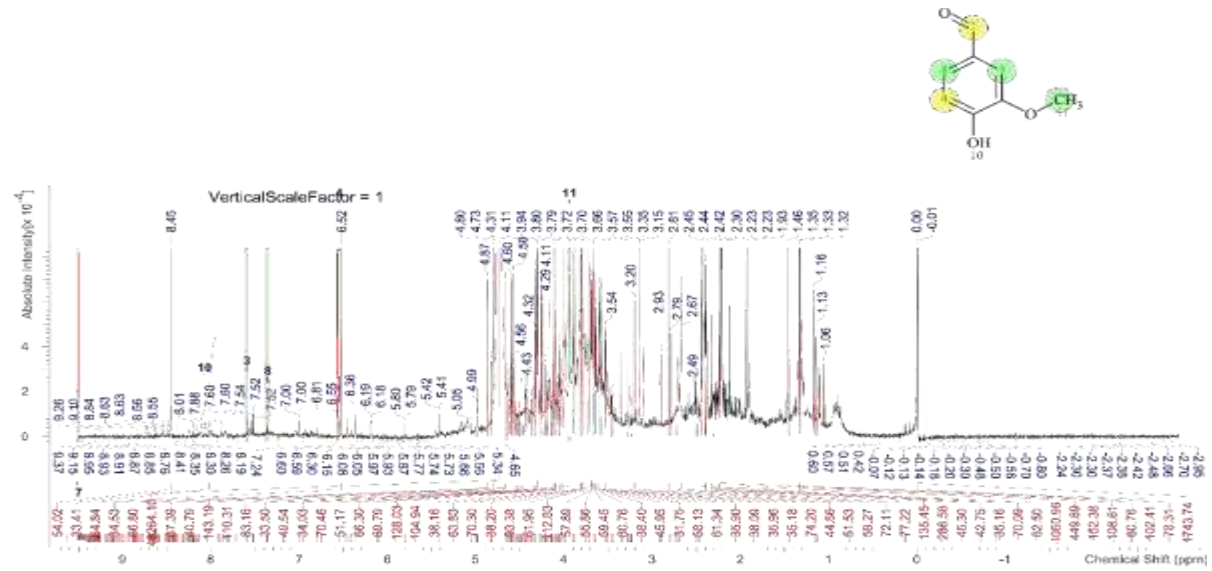

No.	Atom	Exp. Shift (ppm)	Multiplet
1	11	3.94	M311
2	4	6.56	M216
3	8	7.36	M209
4	3	7.80	M206
5	10	8.08	M193
6	7	9.51	M01

Figure 6.5 Vanillin T. violacea aqueous compound NMR spectrum.

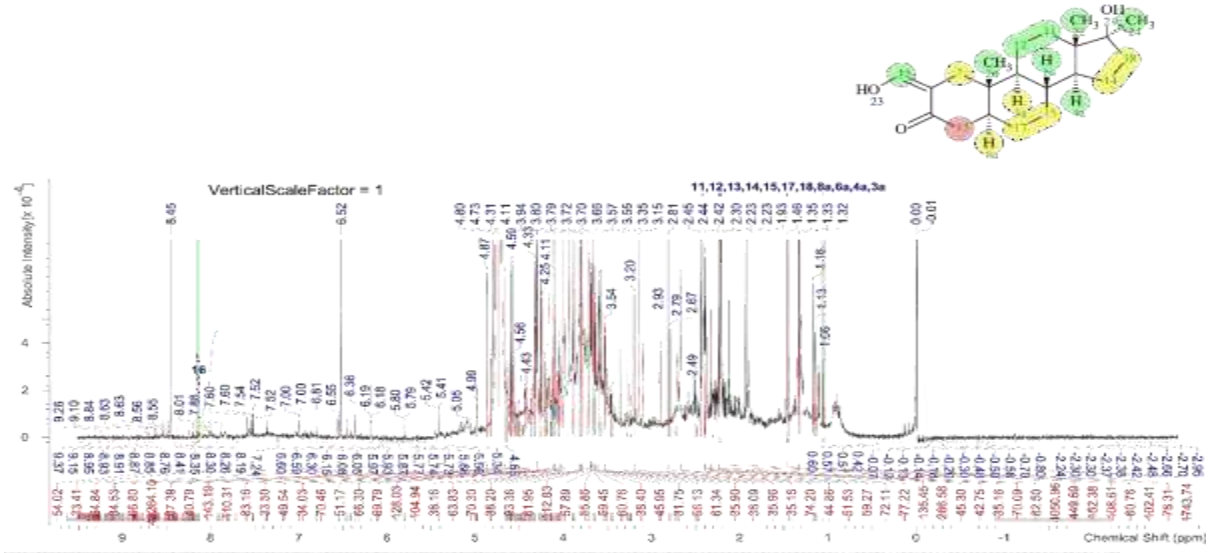

No.	Atom	Exp. Shift (ppm)	Multiplet	No.	Atom	Exp. Shift (ppm)	Multiplet	No.	Atom	Exp. Shift (ppm)	Multiplet
1	23	-	-	8	11	1.46	M376	15	17	1.46	M376
2	22	1.06	M385	9	13	1.46	M376	16	18	1.46	M376
3	24	1.06	M385	10	14	1.46	M376	17	18	1.46	M376
4	20	1.06	M385	11	14	1.46	M376	18	13	1.46	M376
5	11	1.46	M376	12	15	1.46	M376	19	8a	1.46	M376
6	12	1.46	M376	13	15	1.46	M376	20	6a	1.46	M376
7	12	1.46	M376	14	17	1.46	M376	21	4a	1.46	M376

Figure 6.6 Oxime-and methoxy-phenyl T. violacea aqueous compound NMR spectra.

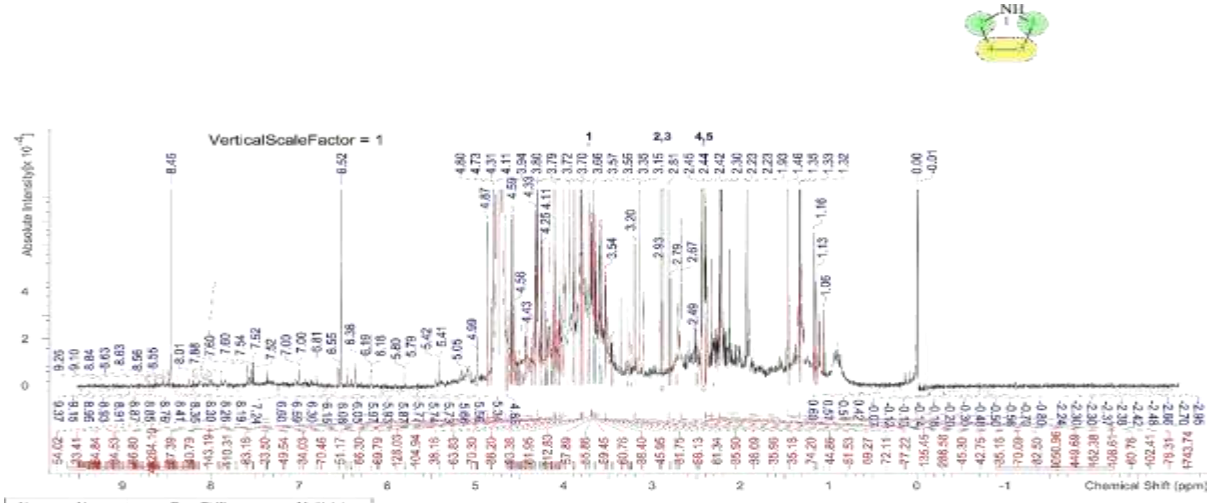

No.	Atom	Exp. Shift (ppm)	Multiplet
1	4	2.42	M368
2	5	2.42	M368
3	2	2.90	M356
4	3	2.90	M356
5	1	3.72	M324

Figure 6.7 Figure 5.7. Pyrrolidine T. violacea aqueous compound NMR spectrum.

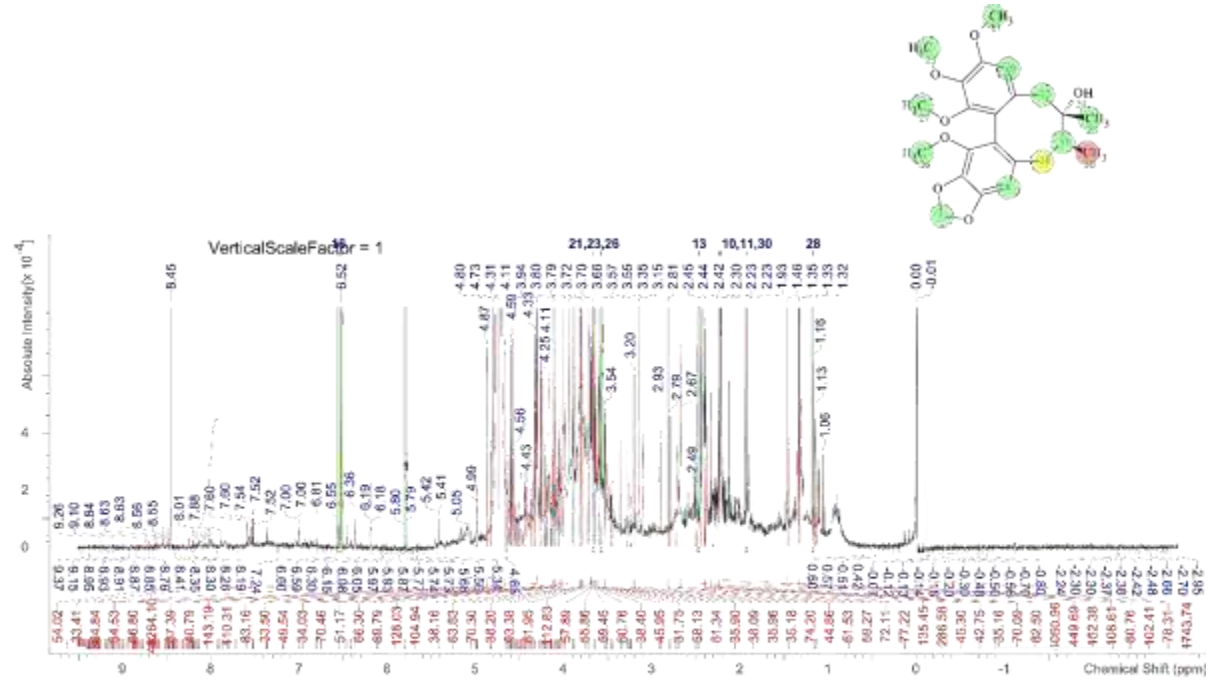

No.	Atom	Exp. Shift (ppm)	Multiplet	No.	Atom	Exp. Shift (ppm)	Multiplet	No.	Atom	Exp. Shift (ppm)	Multiplet
1	28	1.17	M381	6	13	2.47	M365	11	1	5.79	M226
2	10	1.93	M375	7	27	3.57	M338	12	6	6.52	M217
3	11	1.93	M375	8	21	3.66	M331	13	16	6.56	M212
4	30	1.93	M375	9	23	3.66	M331				
5	29	2.23	M374	10	26	3.66	M331				

Figure 6.8 Schizandrin T. violacea aqueous compound NMR spectrum

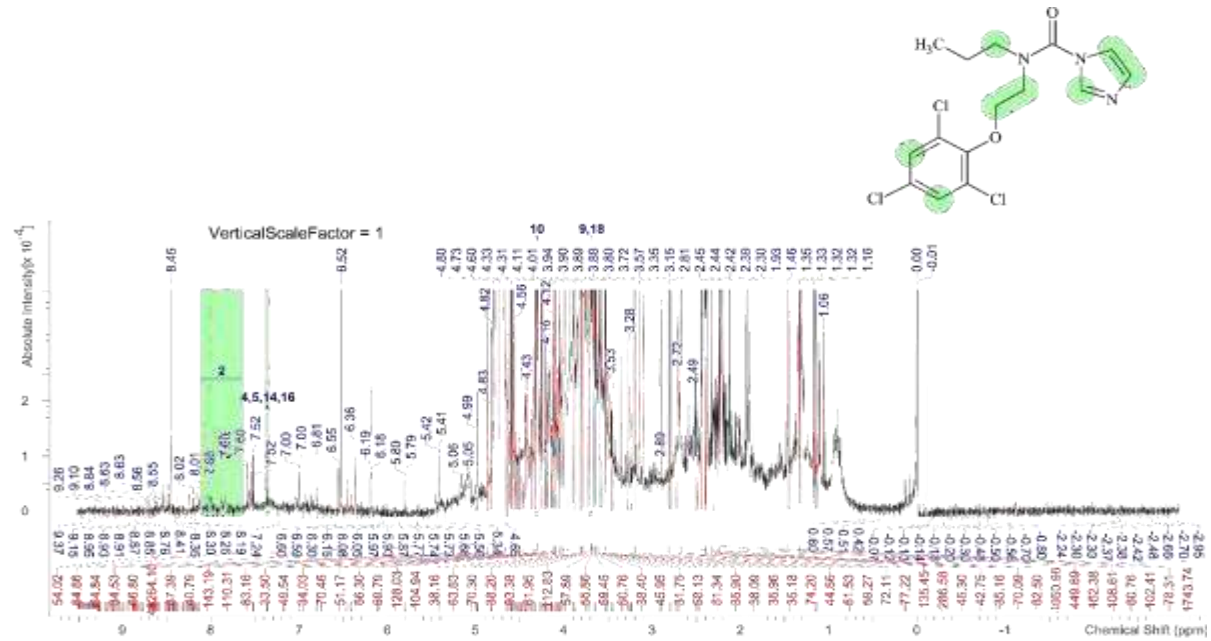

No.	Atom	Exp. Shift (ppm)	Multiplet	No.	Atom	Exp. Shift (ppm)	Multiplet	No.	Atom	Exp. Shift (ppm)	Multiplet
1	20	-	-	5	10	4.31	M272	9	5	7.36	M209
2	19	-	-	6	14	7.36	M209	10	2	7.89	M390
3	18	3.70	M326	7	18	7.36	M209				
4	9	3.70	M326	8	4	7.36	M209				

Figure 6.9. Alpha-Pinene *T. violacea* aqueous compound NMR spectrum

.

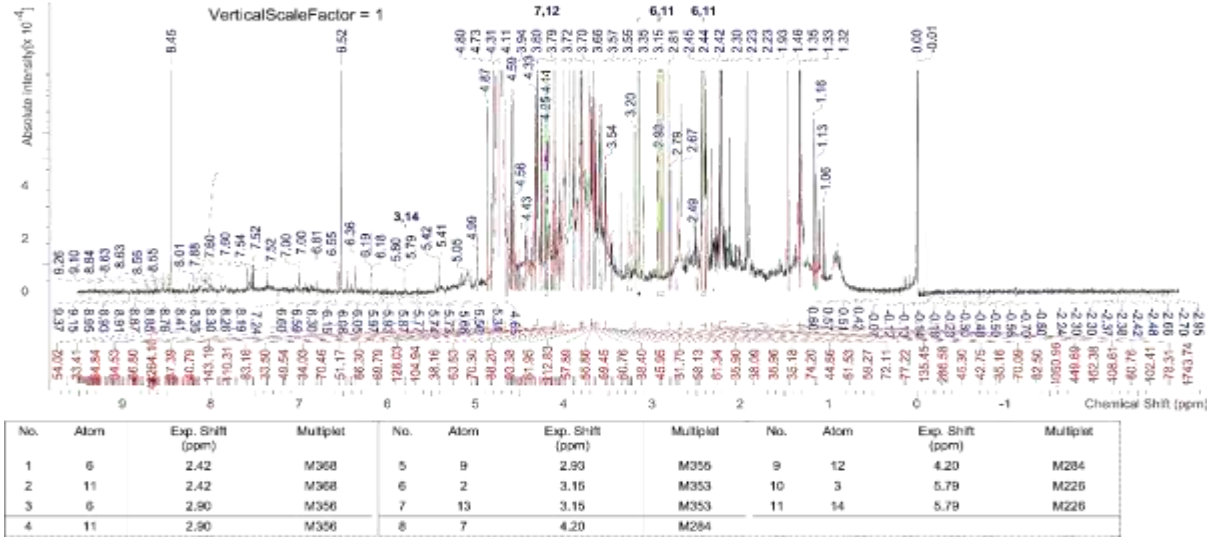

No.	Atom	Exp. Shift (ppm)	Multiplet	No.	Atom	Exp. Shift (ppm)	Multiplet	No.	Atom	Exp. Shift (ppm)	Multiplet
1	6	2.42	M368	5	9	2.93	M355	9	12	4.20	M284
2	11	2.42	M368	6	2	3.15	M353	10	3	5.79	M226
3	6	2.90	M356	7	13	3.15	M353	11	14	5.79	M226
4	11	2.90	M356	8	7	4.20	M284				

Figure 6.10 Taurolidine T. violacea aqueous compound NMR spectrum.

Table 6.1 Examples of compounds detected by NMR analysis of the crude water-soluble T.

Compound	Formula	FW	MF (multi spec)	Max $d_N(^1H)$	Acquisition time (sec)
4H-Pyran-4-one, 2,3-dihydro-3,5-dihydroxy-6-methyl-	C6H4O2	96.0841	0.90	0.353	2.1999
1,2,4-Triazine-3,5(2H,4H)-dione	C3H3H3O2	113.0748	0.91	0.179	2.1889
d-Glycero-d-galacto-heptose	C7H16O7	212.1977	0.86	0.144	2.1889
Benzaldehyde, 4-(1-methylethyl)-	C7H6O	106.1219	0.88	0.468	2.1889
Vanillin	C8H8O3	152.1473	0.34	0.347	2.1889
Oxime-, methoxy-phenyl	C21H32O2	332.4770	0.942	0.347	2.1889
Pyrrolidine	C4H9N	71.1210	0.83	0.615	2.1889
Schizandrin	C23H25O7	416.4642	0.81	1.017	2.1889
Taurolidine	C7H16N4O4S2	284.3563	0.87	0.487	2.1889
alpha.-Pinene	C15H16Cl3N3O2	376.6654	0.00	0.229	2.1889

6.2 Appendix B

6,2.1 Ethics waiver

UNIVERSITY OF THE WITWATERSRAND JOHANNESBURG

HUMAN RESEARCH ETHICS COMMITTEE (MEDICAL)

Office of the Deputy Vice-Chancellor (Research & Innovation)

26/08/2023

Ref: W-CBP-230626-02

TO WHOM IT MAY CONCERN

Waiver: This certifies that the following research does not require clearance from the Human Research Ethics Committee (Medical)

Investigator: Mr M Alaouna
Student No. (if appropriate): 321814
Staff No. (if appropriate):

Supervisor: Dr CB Penny

School: Clinical Medicine
Department: Medicine
Internal Medicine - Oncology
Medical School
University

Project title: *The effects of indigenous South African plant extracts (Cotyledon orbiculata and Tulbaghia violacea) in triple negative breast cancer cells*

Reason: In vitro laboratory study
No human participants will be involved in the study

Dr N Naran
Co-Chairperson: Human Research Ethics Committee (Medical)

Research Office Secretariat:
Third Floor, Philip Tobias Building, corner of St Andrews and York Roads, Parktown, Johannesburg 2193
Postal address: Private Bag 3, Wits 2050
Tel Nos: +27 (0)11 717 1234/1252/2656/2700
Office E-mail: HREC-Medical.ResearchOffice@wits.ac.za
Website:
https://www.wits.ac.za/research/researcher-support/research-ethics/ethics-committees/

Turnitin Report

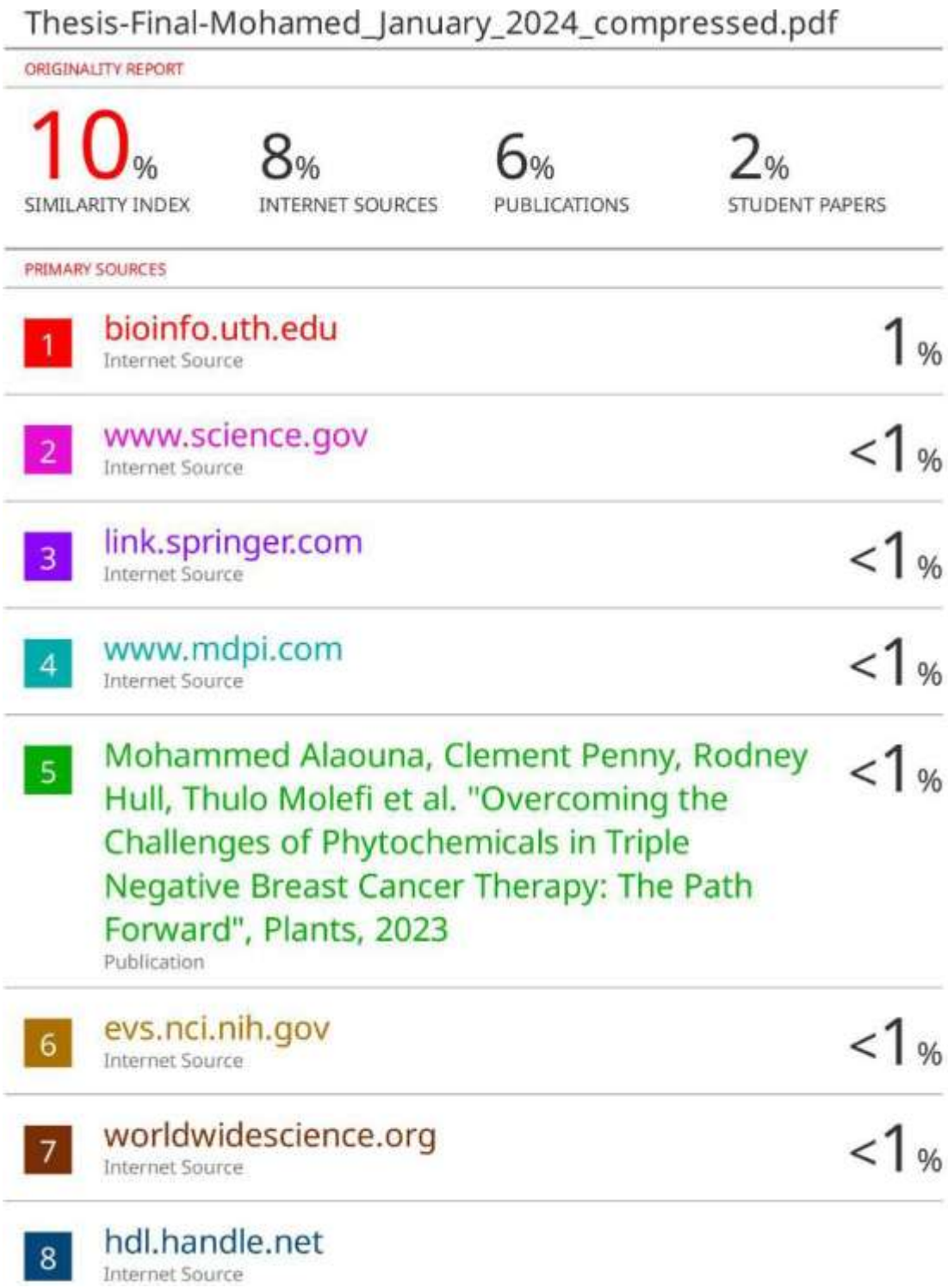

Thesis-Final-Mohamed_January_2024_compressed.pdf

ORIGINALITY REPORT

10%	8%	6%	2%
SIMILARITY INDEX	INTERNET SOURCES	PUBLICATIONS	STUDENT PAPERS

PRIMARY SOURCES

1	bioinfo.uth.edu Internet Source	1%
2	www.science.gov Internet Source	<1%
3	link.springer.com Internet Source	<1%
4	www.mdpi.com Internet Source	<1%
5	Mohammed Alaouna, Clement Penny, Rodney Hull, Thulo Molefi et al. "Overcoming the Challenges of Phytochemicals in Triple Negative Breast Cancer Therapy: The Path Forward", Plants, 2023 Publication	<1%
6	evs.nci.nih.gov Internet Source	<1%
7	worldwidescience.org Internet Source	<1%
8	hdl.handle.net Internet Source	

References

1. Boichuk, S., et al., *Targeting of FGF-Signaling Re-Sensitizes Gastrointestinal Stromal Tumors (GIST) to Imatinib in Vitro and in Vivo.* Molecules, 2018.

2. Schneider, A., et al., *Peritoneal Taurolidine Lavage in Children With Localised Peritonitis Due to Appendicitis.* Pediatric Surgery International, 2005.

3. Li, C., et al., *A Lys644Glu Substitution in Fibroblast Growth Factor Receptor 3 (FGFR3) Causes Dwarfism in Mice by Activation of STATs and Ink4 Cell Cycle Inhibitors.* Human Molecular Genetics, 1999.

4. Ferguson, H.R., M.P. Smith, and C. Francavilla, *Fibroblast Growth Factor Receptors (FGFRs) and Noncanonical Partners in Cancer Signaling.* Cells, 2021.

5. Ferlay, J., et al., *Estimating the Global Cancer Incidence and Mortality in 2018: GLOBOCAN Sources and Methods.* International Journal of Cancer, 2018. **144**(8): p. 1941-1953.

6. Luo, Z., et al., *A Qualitative Study on the Experience of Empowerment From the Perspectives of Breast Cancer Survivors.* Nursing Open, 2021. **8**(5): p. 2429-2438.

7. Li, C.-J., et al., *Advanced Evolution of Pathogenesis Concepts in Cardiomyopathies.* Journal of Clinical Medicine, 2019.

8. Ginsburg, O., et al., *The Global Burden of Women's Cancers: A Grand Challenge in Global Health.* The Lancet, 2017. **389**(10071): p. 847-860.

9. Sun, Y., et al., *Risk Factors and Preventions of Breast Cancer.* International Journal of Biological Sciences, 2017. **13**(11): p. 1387-1397.

10. Pan, K., et al., *Protein Intake by Source and Breast Cancer Incidence and Mortality: The Women's Health Initiative.* Jnci Cancer Spectrum, 2020. **4**(6).

11. Khameneh, S.C., et al., *Weighted Correlation Network Analysis Revealed Novel Long Non-Coding RNAs for Colorectal Cancer.* Scientific Reports, 2022. **12**(1).

12. Mirmalek, S.A., et al., *Comparison of in Vitro Cytotoxicity and Apoptogenic Activity of Magnesium Chloride and Cisplatin as Conventional Chemotherapeutic Agents in the McF-7 Cell Line.* Asian Pacific Journal of Cancer Prevention, 2016. **17**(sup3): p. 131-134.

13. Kreiter, E., et al., *Breast Cancer: Trends in International Incidence in Men and Women.* British Journal of Cancer, 2014. **110**(7): p. 1891-1897.

14. Qiu, J., et al., *Comparison of Clinicopathological Features and Prognosis in Triple-Negative and Non-Triple Negative Breast Cancer.* Journal of Cancer, 2016. **7**(2): p. 167-173.

15. Ebrahimi, E., et al., *The NCCN Criterion "Young Age at Onset" Alone Is Not an Indicator of Hereditary Breast Cancer in Iranian Population.* Cancer Prevention Research, 2019. **12**(11): p. 763-770.

16. Lynce, F., et al., *Deleterious BRCA1/2 Mutations in an Urban Population of Black Women.* Breast Cancer Research and Treatment, 2015. **153**(1): p. 201-209.

17. Cascione, L., et al., *Integrated MicroRNA and mRNA Signatures Associated With Survival in Triple Negative Breast Cancer.* Plos One, 2013. **8**(2): p. e55910.

18. Lacroix, M., R.A. Toillon, and G. Leclercq, *P53 and Breast Cancer, an Update.* Endocrine Related Cancer, 2006. **13**(2): p. 293-325.

19. Brown, M. and L.W. Cowart, *Evaluating the Effectiveness of Faith-Based Breast Health Education.* Health Education Journal, 2018. **77**(5): p. 571-585.

20. Amend, K.L., D.G. Hicks, and C.B. Ambrosone, *Breast Cancer in African-American Women: Differences in Tumor Biology From European-American Women.* Cancer Research, 2006. **66**(17): p. 8327-8330.

21. Millikan, R.C., et al., *Epidemiology of Basal-Like Breast Cancer.* Breast Cancer Research and Treatment, 2007. **109**(1): p. 123-139.

22. Villarreal-Garza, C., et al., *Significant Clinical Impact of Recurrent BRCA1 and BRCA2 Mutations in Mexico.* Cancer, 2014. **121**(3): p. 372-378.

23. Desmedt, C., et al., *Biological Processes Associated With Breast Cancer Clinical Outcome Depend on the Molecular Subtypes.* Clinical Cancer Research, 2008.

24. Braman, N., et al., *Association of Peritumoral Radiomics With Tumor Biology and Pathologic Response to Preoperative Targeted Therapy for HER2 (ERBB2) Positive Breast Cancer.* Jama Network Open, 2019. **2**(4): p. e192561.

25. Perou, C.M., et al., *Molecular Portraits of Human Breast Tumours.* Nature, 2000. **406**(6797): p. 747-752.

26. Weisman, P., et al., *Genetic Alterations of Triple Negative Breast Cancer by Targeted Next-Generation Sequencing and Correlation With Tumor Morphology.* Modern Pathology, 2016. **29**(5): p. 476-488.

27. Bianchini, G., et al., *Triple-Negative Breast Cancer: Challenges and Opportunities of a Heterogeneous Disease.* Nature Reviews Clinical Oncology, 2016. **13**(11): p. 674-690.

28. Gbenonsi, G., et al., *Health System Factors That Influence Diagnostic and Treatment Intervals in Women With Breast Cancer in Sub-Saharan Africa: A Systematic Review.* BMC Public Health, 2021. **21**(1).

29. Jedy-Agba, E., et al., *Stage at Diagnosis of Breast Cancer in Sub-Saharan Africa: A Systematic Review and Meta-Analysis.* The Lancet Global Health, 2016. **4**(12): p. e923-e935.

30. Won, K.A. and C. Spruck, *Triple-negative Breast Cancer Therapy: Current and Future Perspectives (Review).* International Journal of Oncology, 2020. **57**(6): p. 1245-1261.

31. Peng, F., et al., *Isoliquiritigenin Derivative Regulates miR-374a/BAX Axis to Suppress Triple-Negative Breast Cancer Tumorigenesis and Development.* Frontiers in Pharmacology, 2020. **11**.

32. Chen, L. and C.I. Li, *Racial Disparities in Breast Cancer Diagnosis and Treatment by Hormone Receptor and HER2 Status.* Cancer Epidemiology Biomarkers & Prevention, 2015. **24**(11): p. 1666-1672.

33. Keegan, T.H.M., et al., *Occurrence of Breast Cancer Subtypes in Adolescent and Young Adult Women.* Breast Cancer Research, 2012. **14**(2).

34. Gillespie, E.F., et al., *Obesity and Angiolymphatic Invasion in Primary Breast Cancer.* Annals of Surgical Oncology, 2009. **17**(3): p. 752-759.

35. Shet, D., et al., *The Clinicopathological Profile of Breast Cancer in Young Women From a Tertiary Care Center.* Asian Journal of Oncology, 2022.

36. Bjerkaas, E., et al., *Smoking Duration Before First Childbirth: An Emerging Risk Factor for Breast Cancer? Results From 302,865 Norwegian Women.* Cancer Causes & Control, 2013. **24**(7): p. 1347-1356.

37. Chin, S.N., C.F. Walters, and E.L. Williams, *Breast Cancer Receptor Profiles in Jamaica: A 6-Year Analysis.* West Indian Medical Journal, 2016.

38. Hoskins, K., et al., *Association of Social Determinants and Tumor Biology With Racial Disparity in Survival From Early-Stage, Hormone-Dependent Breast Cancer.* Jama Oncology, 2023. **9**(4): p. 536.

39. Yu, Q., et al., *Multiple Third-variable Analysis for Competing Risk Data—With an Application to Explore Racial Disparity in Breast Cancer Recurrence.* Stat, 2023. **12**(1).

40. Chilwesa, P.M., et al., *Comparison of 18 F-Fluorodeoxyglucose Positron Emission Tomography/Computed Tomography and Conventional Imaging for Locally Advanced Breast Cancer Staging: A Prospective Study From a Tertiary Hospital Cancer Centre in the Western Cape.* South African Journal of Oncology, 2020. **4**.

41. Viel, J.-F. and R. Rymzhanova, *Mammographic Density and Urbanization: A Population-Based Screening Study.* Journal of Medical Screening, 2012. **19**(1): p. 20-25.

42. Olaniyi, F.C., J. Ogola, and T.G. Tshitangano, *Efficiency of Health Care Risk Waste Management in Rural Healthcare Facilities of South Africa: An Assessment of Selected Facilities in Vhembe District, Limpopo Province.* International Journal of Environmental Research and Public Health, 2019. **16**(12): p. 2199.

43. Flaws, J.A., C.J. Newschaffer, and T.L. Bush, *Breast Cancer Mortality in Black and in White Women: A Historical Perspective by Menopausal Status.* Journal of Women S Health, 1998. **7**(8): p. 1007-1015.

44. Obeng-Gyasi, S., et al., *Purposeful Surgical Delay and the Coronavirus Pandemic: How Will Black Breast Cancer Patients Fare?* Breast Cancer Research and Treatment, 2020. **182**(3): p. 527-530.

45. Clegg, L.X., et al., *Impact of Socioeconomic Status on Cancer Incidence and Stage at Diagnosis: Selected Findings From the Surveillance, Epidemiology, and End Results: National Longitudinal Mortality Study.* Cancer Causes & Control, 2008. **20**(4): p. 417-435.

46. Dent, R., et al., *Triple-Negative Breast Cancer: Clinical Features and Patterns of Recurrence.* Clinical Cancer Research, 2007. **13**(15): p. 4429-4434.

47. Lundqvist, A., et al., *Socioeconomic Inequalities in Breast Cancer Incidence and Mortality in Europe—a Systematic Review and Meta-Analysis.* European Journal of Public Health, 2016. **26**(5): p. 804-813.

48. Yin, L., et al., *Triple-Negative Breast Cancer Molecular Subtyping and Treatment Progress.* Breast Cancer Research, 2020. **22**(1).

49. Siddharth, S. and D. Sharma, *Racial Disparity and Triple-Negative Breast Cancer in African-American Women: A Multifaceted Affair Between Obesity, Biology, and Socioeconomic Determinants.* Cancers, 2018. **10**(12): p. 514.

50. Zippel, D. and M.Z. Papa, *The BRCA Breast Cancer Patient: Treat the Tumor or the Problem?* Journal of Surgical Oncology, 2008. **97**(7): p. 561-562.

51. Saxena, S., et al., *Contribution of Germline BRCA1 and BRCA2sequence Alterations to Breast Cancer in Northern India.* BMC Medical Genetics, 2006. **7**(1).

52. Kirchhoff, T., et al., *Frequency of BRCA1 and BRCA2 Mutations in Unselected Ashkenazi Jewish Patients With Colorectal Cancer.* Jnci Journal of the National Cancer Institute, 2004. **96**(1): p. 68-70.

53. Fujisawa, F., et al., *Prevalence of BRCA1 and BRCA2 Mutations in Japanese Patients With Triple-negative Breast Cancer: A Single Institute Retrospective Study.* Molecular and Clinical Oncology, 2021. **14**(5).

54. Muendlein, A., et al., *Evaluation of BRCA1/2 Mutational Status Among German and Austrian Women With Triple-Negative Breast Cancer.* Journal of Cancer Research and Clinical Oncology, 2015. **141**(11): p. 2005-2012.

55. Rajagopal, T., et al., *Analysis of Pathogenic Variants in BRCA1 and BRCA2 Genes Using Next-Generation Sequencing in Women With Triple Negative Breast Cancer From South India.* Molecular Biology Reports, 2022. **49**(4): p. 3025-3032.

56. Palomba, G., et al., *Triple-Negative Breast Cancer Frequency and Type of BRCA Mutation: Clues From Sardinia.* Oncology Letters, 2014. **7**(4): p. 948-952.

57. Theodor, L., et al., *An Identical Novel Mutation in BRCA1 and a Common Haplotype in Familial Ovarian Cancer in Non-Ashkenazi Jews.* British Journal of Cancer, 1998. **77**(11): p. 1880-1883.

58. Pal, T., et al., *Early Onset Breast Cancer in a Registry-Based Sample of African-American Women:<i>BRCA</I>Mutation Prevalence, and Other Personal and System-Level Clinical Characteristics.* The Breast Journal, 2013. **19**(2): p. 189-192.

59. Kwong, A., et al., *Comprehensive Spectrum Of BRCA1 and BRCA2 deleterious Mutations in Breast Cancer in Asian Countries.* Journal of Medical Genetics, 2015. **53**(1): p. 15-23.

60. Nel, C., A. Mannel, and D. Kruger, *Triple-Negative Breast Cancer - A Retrospective Audit of 151 Cases Seen at the Charlotte Maxeke Johannesburg Academic Hospital Breast Unit.* South African Journal of Surgery, 2022. **60**(2): p. 115-118.

61. Weigman, V., et al., *Basal-Like Breast Cancer DNA Copy Number Losses Identify Genes Involved in Genomic Instability, Response to Therapy, and Patient Survival.* Breast Cancer Research and Treatment, 2011. **133**(3): p. 865-880.

62. Ademuyiwa, F.O., et al., *Differences in the Mutational Landscape of Triple-Negative Breast Cancer in African Americans and Caucasians.* Breast Cancer Research and Treatment, 2016. **161**(3): p. 491-499.

63. Gorodetska, I., I. Kozeretska, and A. Dubrovska, *BRCA genes: the role in genome stability, cancer stemness and therapy resistance.* Journal of Cancer, 2019. **10**(9): p. 2109.

64. Cimprich, K.A. and D. Chen, *ATR: An Essential Regulator of Genome Integrity.* Nature Reviews Molecular Cell Biology, 2008. **9**(8): p. 616-627.

65. Matsuoka, S., et al., *Ataxia Telangiectasia-Mutated Phosphorylates Chk2 in Vivo And in Vitro.* Proceedings of the National Academy of Sciences, 2000. **97**(19): p. 10389-10394.

66. Rodrigue, A., et al., *A Global Functional Analysis of Missense Mutations Reveals Two Major Hotspots in the PALB2 Tumor Suppressor.* Nucleic Acids Research, 2019. **47**(20): p. 10662-10677.

67. Martinez, J.S., et al., *BRCA2 Regulates DMC1-mediated Recombination Through the BRC Repeats.* Proceedings of the National Academy of Sciences, 2016. **113**(13): p. 3515-3520.

68. Filippo, J.S., et al., *Recombination Mediator and Rad51 Targeting Activities of a Human BRCA2 Polypeptide.* Journal of Biological Chemistry, 2006. **281**(17): p. 11649-11657.

69. Angeli, D., S. Salvi, and G. Tedaldi, *Genetic Predisposition to Breast and Ovarian Cancers: How Many and Which Genes to Test?* International Journal of Molecular Sciences, 2020. **21**(3): p. 1128.

70. Bapat, A., et al., *Assessing Germline Mutational Profile and Its Clinicopathological Associations in Triple Negative Breast Cancer.* 2022.

71. Franchet, C. and J.-S. Hoffmann, *Recent Advances in Enhancing the Therapeutic Index of PARP Inhibitors in Breast Cancer.* Cancers, 2021. **13**(16): p. 4132.

72. Yip, C.H. and L.A. Newman, *American Society of Clinical Oncology, American Society for Radiation Oncology, and Society of Surgical Oncology Guideline for Management of Hereditary Breast Cancer.* Jama Surgery, 2021. **156**(3): p. 284.

73. Hu, C., et al., *The Contribution of Germline Predisposition Gene Mutations to Clinical Subtypes of Invasive Breast Cancer From a Clinical Genetic Testing Cohort.* Jnci Journal of the National Cancer Institute, 2020. **112**(12): p. 1231-1241.

74. ElShamy, W.M., *The Protective Effect of Longer Duration of Breastfeeding Against Pregnancy-Associated Triple Negative Breast Cancer.* Oncotarget, 2016. **7**(33): p. 53941-53950.

75. Bauer, K., et al., *Descriptive Analysis of Estrogen Receptor (ER)-negative, Progesterone Receptor (PR)-negative, and HER2-negative Invasive Breast Cancer, the So-called Triple-negative Phenotype.* Cancer, 2007.

76. Shah, S.P., et al., *The clonal and mutational evolution spectrum of primary triple-negative breast cancers.* Nature, 2012. **486**(7403): p. 395.

77. Lakshmaiah, K.C., et al., *Role of Taxanes in Triple-Negative Breast Cancer: A Study From Tertiary Cancer Center in South India.* World Journal of Oncology, 2017.

78. Caramelo, O., et al., *The Effect of Neoadjuvant Platinum-Based Chemotherapy in BRCA Mutated Triple Negative Breast Cancers -Systematic Review and Meta-Analysis.* Hereditary Cancer in Clinical Practice, 2019.

79. Mahn, A. and A.d. Castillo, *Potential of Sulforaphane as a Natural Immune System Enhancer: A Review.* Molecules, 2021. **26**(3): p. 752.

80. Cook, L.A., J. Sachs, and N.G. Weiskopf, *The quality of social determinants data in the electronic health record: a systematic review.* Journal of the American Medical Informatics Association, 2022. **29**(1): p. 187-196.

81. Rydén, L., et al., *Vascular endothelial growth factor receptor 2 is a significant negative prognostic biomarker in triple-negative breast cancer: results from a controlled randomised trial of premenopausal breast cancer*. 2009, AACR.

82. Cohen, M.H., et al., *FDA drug approval summary: bevacizumab (Avastin®) as treatment of recurrent glioblastoma multiforme.* 2009. **14**(11): p. 1131-1138.

83. O'Shaughnessy, J., et al., *Comparison of Subgroup Analyses of PFS from Three Phase III Studies of Bevacizumab in Combination with Chemotherapy in Patients with HER2-Negative Metastatic Breast Cancer (MBC)*. 2009, AACR.

84. Conley, R.S., et al., *Antiangiogenic Agents Increase Breast Cancer Stem Cells via the Generation of Tumor Hypoxia.* Proceedings of the National Academy of Sciences, 2012. **109**(8): p. 2784-2789.

85. Mateo, J., et al., *A Decade of Clinical Development of PARP Inhibitors in Perspective.* Annals of Oncology, 2019. **30**(9): p. 1437-1447.

86. Jaspers, J.E., et al., *Loss of 53BP1 Causes PARP Inhibitor Resistance in Brca1-Mutated Mouse Mammary Tumors.* Cancer Discovery, 2013. **3**(1): p. 68-81.

87. Chan, S.K.W., M. Hill, and W.J. Gullick, *The Role of the Epidermal Growth Factor Receptor in Breast Cancer.* Journal of Mammary Gland Biology and Neoplasia, 2006.

88. Corkery, B., et al., *Epidermal growth factor receptor as a potential therapeutic target in triple-negative breast cancer.* 2009. **20**(5): p. 862-867.

89. Oliveras-Ferraros, C., et al., *Growth and molecular interactions of the anti-EGFR antibody cetuximab and the DNA cross-linking agent cisplatin in gefitinib-resistant MDA-MB-468 cells: new prospects in the treatment of triple-negative/basal-like breast cancer.* 2008. **33**(6): p. 1165-1176.

90. Carey, L.A., et al., *The triple negative paradox: primary tumor chemosensitivity of breast cancer subtypes.* Clinical cancer research, 2007. **13**(8): p. 2329-2334.

91. Baselga, J., et al. *The addition of cetuximab to cisplatin increases overall response rate (ORR) and progression-free survival (PFS) in metastatic triple-negative breast cancer (TNBC): results of a randomized phase II study (BALI-1).* in *Annals of Oncology*. 2010. OXFORD UNIV PRESS GREAT CLARENDON ST, OXFORD OX2 6DP, ENGLAND.

92. Twelves, C., et al., *Erlotinib in combination with capecitabine and docetaxel in patients with metastatic breast cancer: a dose-escalation study.* 2008. **44**(3): p. 419-426.

93. Liu, Y., et al., *MicroRNA-494 is required for the accumulation and functions of tumor-expanded myeloid-derived suppressor cells via targeting of PTEN.* The Journal of Immunology, 2012. **188**(11): p. 5500-5510.

94. Mordecai, J., S. Ullah, and I. Ahmad, *Sulforaphane and Its Protective Role in Prostate Cancer: A Mechanistic Approach.* International Journal of Molecular Sciences, 2023. **24**(8): p. 6979.

95. Newman, D.J. and G.M.J.J.o.n.p. Cragg, *Natural products as sources of new drugs over the 30 years from 1981 to 2010.* 2012. **75**(3): p. 311-335.

96. Cragg, G.M. and D.J. Newman, *Plants as a source of anti-cancer agents.* Journal of ethnopharmacology, 2005. **100**(1-2): p. 72-79.

97. Mottaghipisheh, J., *Sephadex® LH-20, Isolation, and Purification of Flavonoids From Plant Species: A Comprehensive Review.* Molecules, 2020. **25**(18): p. 4146.

98. Rao, Y.K., et al., *Antioxidant and cytotoxic activities of naturally occurring phenolic and related compounds: a comparative study.* 2007. **45**(9): p. 1770-1776.

99. Vineis, P. and D.J.E.J.o.C. Fecht, *Environment, cancer and inequalities—The urgent need for prevention.* 2018. **103**: p. 317-326.

100. Mans, D.R., A.B. Rocha, and G. Schwartsmann, *Anti-cancer drug discovery and development in Brazil:*

targeted plant collection as a rational strategy to acquire candidate anti-cancer compounds. 2000, Oxford University Press. p. 185-198.

101. Solowey, E., et al., *Evaluating Medicinal Plants for Anticancer Activity.* The Scientific World Journal, 2014.

102. Weinberg, R. and D. Hanahan, *The hallmarks of cancer.* Cell, 2000. **100**(1): p. 57-70.

103. Gerspach, J., K. Pfizenmaier, and H. Wajant, *Therapeutic Targeting of CD95 and the TRAIL Death Receptors.* Recent Patents on Anti-Cancer Drug Discovery, 2011.

104. Mohan, S., et al., *Involvement of NF-κB and Bcl2/Bax signaling pathways in the apoptosis of MCF7 cells induced by a xanthone compound Pyranocycloartobiloxanthone A.* 2012. **19**(11): p. 1007-1015.

105. Yang, W.H., et al., *Juxtacrine Signaling Inhibits Antitumor Immunity by Upregulating PD-L1 Expression.* Cancer Research, 2018.

106. Jin, J., et al., *Capsaicin mediates cell cycle arrest and apoptosis in human colon cancer cells via stabilizing and activating p53.* 2014. **10**(3): p. 285.

107. Kumar, M., et al., *Phytoconstituents as apoptosis inducing agents: strategy to combat cancer.* 2016. **68**(4): p. 531-563.

108. Tse, A.K.-W., et al., *Magnolol suppresses NF-κB activation and NF-κB regulated gene expression through inhibition of IkappaB kinase activation.* 2007. **44**(10): p. 2647-2658.

109. Colgate, E.C., et al., *Xanthohumol, a prenylflavonoid derived from hops induces apoptosis and inhibits NF-kappaB activation in prostate epithelial cells.* 2007. **246**(1-2): p. 201-209.

110. Sychrová, A., et al., *Prenylated flavonoids in topical infections and wound healing.* Molecules, 2022. **27**(14): p. 4491.

111. Manu, K. and G.J.I.i. Kuttan, *Ursolic acid induces apoptosis by activating p53 and caspase-3 gene expressions and suppressing NF-κB mediated activation of bcl-2 in B16F-10 melanoma cells.* 2008. **8**(7): p. 974-981.

112. Gambari, R., et al., *Corilagin is a potent inhibitor of NF-kappaB activity and downregulates TNF-alpha induced expression of IL-8 gene in cystic fibrosis IB3-1 cells.* 2012. **13**(3): p. 308-315.

113. Hengartner, M.O.J.N., *The biochemistry of apoptosis.* 2000. **407**(6805): p. 770-776.

114. Ambros, V., et al., *A uniform system for microRNA annotation.* Rna, 2003. **9**(3): p. 277-279.

115. Esquela-Kerscher, A. and F.J. Slack, *Oncomirs—microRNAs with a role in cancer*. Nature reviews cancer, 2006. **6**(4): p. 259.

116. Mohammadi-Dehcheshmeh, M., et al., *A Transcription Regulatory Sequence in the 5' Untranslated Region of SARS-CoV-2 Is Vital for Virus Replication With an Altered Evolutionary Pattern Against Human Inhibitory MicroRNAs.* Cells, 2021.

117. Lewis, B.P., C.B. Burge, and D.P. Bartel, *Conserved seed pairing, often flanked by adenosines, indicates that thousands of human genes are microRNA targets.* cell, 2005. **120**(1): p. 15-20.

118. Sharma, S., et al., *Round Cell Tumors: Classification and Immunohistochemistry*. Indian Journal of Medical and Paediatric Oncology, 2017.

119. Boufraqech, M., J. Kłubo-Gwieździńska, and E. Kebebew, *MicroRNAs in the Thyroid.* Best Practice & Research Clinical Endocrinology & Metabolism, 2016.

120. Frampton, J., *MYB transcription factors: their role in growth, differentiation and disease*. 2004: Springer.

121. Deng, S., et al., *Mechanisms of microRNA deregulation in human cancer.* 2008. **7**(17): p. 2643-2646.

122. Venkatadri, R., et al., *Role of apoptosis-related miRNAs in resveratrol-induced breast cancer cell death.* 2016.

7(2): p. e2104-e2104.

123. Ravindranath, V. and N.J.T. Chandrasekhara, *Absorption and tissue distribution of curcumin in rats.* 1980. **16**(3): p. 259-265.

124. González-Barrio, R., et al., *Bioavailability of anthocyanins and ellagitannins following consumption of raspberries by healthy humans and subjects with an ileostomy.* 2010. **58**(7): p. 3933-3939.

125. Papetti, M. and I.M. Herman, *Mechanisms of normal and tumor-derived angiogenesis.* American Journal of Physiology-Cell Physiology, 2002. **282**(5): p. C947-C970.

126. Melincovici, C.S., et al., *Vascular endothelial growth factor (VEGF)-key factor in normal and pathological angiogenesis.* Rom J Morphol Embryol, 2018. **59**(2): p. 455-467.

127. Pandya, N.M., N.S. Dhalla, and D.D. Santani, *Angiogenesis—a new target for future therapy.* Vascular pharmacology, 2006. **44**(5): p. 265-274.

128. Giavazzi, R., et al., *Distinct role of fibroblast growth factor-2 and vascular endothelial growth factor on tumor growth and angiogenesis.* The American journal of pathology, 2003. **162**(6): p. 1913-1926.

129. Braza-Boïls, A., et al., *MicroRNA expression profile in endometriosis: its relation to angiogenesis and fibrinolytic factors.* Human reproduction, 2014. **29**(5): p. 978-988.

130. Rust, R., C. Gantner, and M.E. Schwab, *Pro-and antiangiogenic therapies: current status and clinical implications.* The FASEB Journal, 2019. **33**(1): p. 34-48.

131. Balaji, S., et al., *The role of endothelial progenitor cells in postnatal vasculogenesis: implications for therapeutic neovascularization and wound healing.* Advances in wound care, 2013. **2**(6): p. 283-295.

132. Gonzalez-Avila, G., et al., *Matrix metalloproteinases participation in the metastatic process and their diagnostic and therapeutic applications in cancer.* Critical reviews in oncology/hematology, 2019. **137**: p. 57-83.

133. Dentelli, P., et al., *C-KIT, by interacting with the membrane-bound ligand, recruits endothelial progenitor cells to inflamed endothelium.* Blood, 2007. **109**(10): p. 4264-4271.

134. Du, F., et al., *Endothelial progenitor cells in atherosclerosis.* Frontiers in bioscience: a journal and virtual library, 2012. **17**: p. 2327.

135. Ge, Q., et al., *VEGF Secreted by Mesenchymal Stem Cells Mediates the Differentiation of Endothelial Progenitor Cells Into Endothelial Cells via Paracrine Mechanisms.* Molecular Medicine Reports, 2017.

136. Iruela-Arispe, M.L. and G.E. Davis, *Cellular and molecular mechanisms of vascular lumen formation.* Developmental cell, 2009. **16**(2): p. 222-231.

137. Yao, G., *Modelling mammalian cellular quiescence.* Interface focus, 2014. **4**(3): p. 20130074.

138. Holderfield, M.T. and C.C. Hughes, *Crosstalk between vascular endothelial growth factor, notch, and transforming growth factor-β in vascular morphogenesis.* Circulation research, 2008. **102**(6): p. 637-652.

139. Sartsoongnoen, N., *Neuroendocrinology of the reproductive cycle in the female native thai chicken: roles of dopamine and gonadotropin releasing hormone*. 2007, School of Biology, Institute of Science, Suranaree University of Technology.

140. Naor, Z., *Signaling by G-protein-coupled receptor (GPCR): studies on the GnRH receptor.* Frontiers in neuroendocrinology, 2009. **30**(1): p. 10-29.

141. Seeburg, P.H., et al., *The Mammalian GnRH Gene and Its Pivotal Role in Reproduction.* 1987.

142. Radovick, S., et al., *Isolation and Characterization of the Human Gonadotropin-Releasing Hormone Gene in the Hypothalamus and Placenta.* Molecular Endocrinology, 1990.

143. Limonta, P. and M. Manea, *Gonadotropin-releasing hormone receptors as molecular therapeutic targets in*

prostate cancer: Current options and emerging strategies. Cancer treatment reviews, 2013. **39**(6): p. 647-663.

144. Naor, Z., O. Benard, and R. Seger, *Activation of MAPK cascades by G-protein-coupled receptors: the case of gonadotropin-releasing hormone receptor*. Trends in Endocrinology & Metabolism, 2000. **11**(3): p. 91-99.

145. Bullock, W.H., et al., *Prospects for kinase activity modulators in the treatment of diabetes and diabetic complications.* Current Topics in Medicinal Chemistry, 2002. **2**(9): p. 915-938.

146. Kraus, S., Z. Naor, and R. Seger, *Intracellular signaling pathways mediated by the gonadotropin-releasing hormone (GnRH) receptor.* Archives of medical research, 2001. **32**(6): p. 499-509.

147. Suo, L., et al., *The anti-proliferative activity of GnRH through downregulation of the Akt/ERK pathways in pancreatic cancer.* Frontiers in endocrinology, 2019. **10**: p. 370.

148. Kaiser, U.B., *Gonadotropin hormones*, in *The pituitary*. 2011, Elsevier. p. 205-260.

149. Rispoli, L. and T. Nett, *Pituitary gonadotropin-releasing hormone (GnRH) receptor: structure, distribution and regulation of expression.* Animal reproduction science, 2005. **88**(1-2): p. 57-74.

150. Counis, R., et al., *Gonadotropin-releasing hormone and the control of gonadotrope function.* Reproduction Nutrition Development, 2005. **45**(3): p. 243-254.

151. Rasmussen, H., et al., *Diacylglycerol production, Ca2+ influx, and protein kinase C activation in sustained cellular responses.* Endocrine reviews, 1995. **16**(5): p. 649-681.

152. Gutiérrez, A., et al., *Role of phosphatidylinositol 3-kinase (PI3K), mitogen-activated protein kinase (MAPK), and protein kinase C (PKC) in calcium signaling pathways linked to the α1-adrenoceptor in resistance arteries.* Frontiers in physiology, 2019. **10**: p. 55.

153. Strauss III, J.F. and G.A. FitzGerald, *Steroid hormones and other lipid molecules involved in human reproduction*, in *Yen and Jaffe's Reproductive Endocrinology*. 2019, Elsevier. p. 75-114. e7.

154. Ranđelović, I., et al., *Improved in vivo anti-tumor and anti-metastatic effect of GnRH-III-daunorubicin analogs on colorectal and breast carcinoma bearing mice.* International journal of molecular sciences, 2019. **20**(19): p. 4763.

155. Krsmanovic, L.Z., et al., *An agonist-induced switch in G protein coupling of the gonadotropin-releasing hormone receptor regulates pulsatile neuropeptide secretion.* Proceedings of the National Academy of Sciences, 2003. **100**(5): p. 2969-2974.

156. Kim, S.-Y., et al., *Inhibition of γ ray-induced apoptosis by stimulatory heterotrimeric GTP binding protein involves Bcl-xL down-regulation in SH-SY5Y human neuroblastoma cells.* Experimental & Molecular Medicine, 2007. **39**(5): p. 583-593.

157. Steinhart, Z. and S. Angers, *Wnt signaling in development and tissue homeostasis.* Development, 2018. **145**(11): p. dev146589.

158. Willert, K. and R. Nusse, *Wnt proteins.* Cold Spring Harbor perspectives in biology, 2012. **4**(9): p. a007864.

159. Bejsovec, A., *Wingless/Wnt signaling in Drosophila: the pattern and the pathway.* Molecular reproduction and development, 2013. **80**(11): p. 882-894.

160. Meyers, S.L., *Analysis of the proto-oncogenes Wnt-1, int-2, c-myc andneu in primary human mammary carcinomas*. 1992: The University of Texas at Austin.

161. Saito-Diaz, K., et al., *The way Wnt works: components and mechanism.* Growth factors, 2013. **31**(1): p. 1-31.

162. Liu, Y., A. Neogi, and A. Mani, *The role of Wnt signaling in development of coronary artery disease and its risk factors.* Open Biology, 2020. **10**(10): p. 200128.

163. Amit, S., et al., *Axin-mediated CKI phosphorylation of β-catenin at Ser 45: a molecular switch for the Wnt pathway.* Genes & development, 2002. **16**(9): p. 1066-1076.

164. Chodaparambil, J.V., et al., *Molecular functions of the TLE tetramerization domain in W nt target gene repression.* The EMBO Journal, 2014. **33**(7): p. 719-731.

165. Warzecha, C.C., et al., *An ESRP-regulated splicing programme is abrogated during the epithelial–mesenchymal transition.* The EMBO journal, 2010. **29**(19): p. 3286-3300.

166. Saura, C.A. and J. Valero, *The role of CREB signaling in Alzheimer's disease and other cognitive disorders.* 2011.

167. Hecht, A., et al., *The p300/CBP acetyltransferases function as transcriptional coactivators of β-catenin in vertebrates.* The EMBO journal, 2000. **19**(8): p. 1839-1850.

168. Rockich, B.E., et al., *Sox9 plays multiple roles in the lung epithelium during branching morphogenesis.* Proceedings of the National Academy of Sciences, 2013. **110**(47): p. E4456-E4464.

169. Mann, Z., et al., *Hematopoietic stem cell factors: their functional role in self-renewal and clinical aspects.* Frontiers in Cell and Developmental Biology, 2022. **10**: p. 664261.

170. Nguyen, D.X., P.D. Bos, and J. Massagué, *Metastasis: from dissemination to organ-specific colonization.* Nature Reviews Cancer, 2009. **9**(4): p. 274.

171. Li, J. and B.P. Zhou, *Activation of β-catenin and Akt pathways by Twist are critical for the maintenance of EMT associated cancer stem cell-like characters.* BMC cancer, 2011. **11**: p. 1-11.

172. Wu, Z.-Q., et al., *Canonical Wnt signaling regulates Slug activity and links epithelial–mesenchymal transition with epigenetic Breast Cancer 1, Early Onset (BRCA1) repression.* Proceedings of the National Academy of Sciences, 2012. **109**(41): p. 16654-16659.

173. Katz, M., I. Amit, and Y. Yarden, *Regulation of MAPKs by growth factors and receptor tyrosine kinases.* Biochimica et Biophysica Acta (BBA)-Molecular Cell Research, 2007. **1773**(8): p. 1161-1176.

174. Wee, P. and Z. Wang, *Epidermal growth factor receptor cell proliferation signaling pathways.* Cancers, 2017. **9**(5): p. 52.

175. Wang, Z., *ErbB receptors and cancer.* ErbB receptor signaling: methods and protocols, 2017: p. 3-35.

176. Joshi, S., et al., *ERBB2/HER2 Mutations Are Transforming and Therapeutically Targetable in Leukemia.* Leukemia, 2020.

177. Xu, Q., et al., *BBS4 and BBS5 show functional redundancy in the BBSome to regulate the degradative sorting of ciliary sensory receptors.* Scientific reports, 2015. **5**(1): p. 11855.

178. Sierke, S.L., et al., *Biochemical Characterization of the Protein Tyrosine Kinase Homology Domain of the ErbB3 (HER3) Receptor Protein.* Biochemical Journal, 1997.

179. Sethi, S., et al., *Molecular markers of epithelial-to-mesenchymal transition are associated with tumor aggressiveness in breast carcinoma.* Translational oncology, 2011. **4**(4): p. 222-226.

180. Ranganathan, K. and K. Loganathan, *Biomarkers in Oral Submucous Fibrosis*, in *Oral Submucous Fibrosis: A Guide to Diagnosis and Management*. 2023, Springer. p. 227-260.

181. Nagao, T. and A.R. Kerr, *Noninvasive Diagnostic.* Oral Submucous Fibrosis: A Guide to Diagnosis and Management, 2023. **13**: p. 197.

182. Cordone, V., et al., *The constitutive activation of TLR4-IRAK1-NFκB axis is involved in the early NLRP3 inflammasome response in peripheral blood mononuclear cells of Rett syndrome patients.* Free Radical Biology and Medicine, 2022. **181**: p. 1-13.

183. Checa, J. and J.M. Aran, *Reactive oxygen species: drivers of physiological and pathological processes.* Journal of Inflammation research, 2020: p. 1057-1073.

184. Murphy, L.O. and J. Blenis, *MAPK signal specificity: the right place at the right time.* Trends in biochemical

sciences, 2006. **31**(5): p. 268-275.

185. Sarmiento-Salinas, F.L., et al., *Reactive oxygen species: Role in carcinogenesis, cancer cell signaling and tumor progression.* Life Sciences, 2021. **284**: p. 119942.

186. Zheng, K., et al., *Selective autophagy regulates cell cycle in cancer therapy.* Theranostics, 2019. **9**(1): p. 104.

187. Basak, D., M.N. Uddin, and J. Hancock, *The role of oxidative stress and its counteractive utility in colorectal cancer (CRC).* Cancers, 2020. **12**(11): p. 3336.

188. Tyavambiza, C., et al., *The Antimicrobial and Anti-Inflammatory Effects of Silver Nanoparticles Synthesised From Cotyledon Orbiculata Aqueous Extract.* Nanomaterials, 2021.

189. Tyavambiza, C., et al., *The Cytotoxicity of Cotyledon Orbiculata Aqueous Extract and the Biogenic Silver Nanoparticles Derived From the Extract.* Current Issues in Molecular Biology, 2023.

190. Tyavambiza, C., et al., *The Antioxidant and in Vitro Wound Healing Activity of Cotyledon Orbiculata Aqueous Extract and the Synthesized Biogenic Silver Nanoparticles.* International Journal of Molecular Sciences, 2022.

191. Van Wyk, B.-E. and N. Gericke, *People's plants: A guide to useful plants of Southern Africa*. 2000: Briza Publications.

192. Van Wyk, B.-E., B.v. Oudtshoorn, and N. Gericke, *Medicinal Plants of South Africa*. 1997: Briza.

193. Vahrmeijer, J., *Poisonous plants of southern Africa that cause stock losses*. 1981: Tafelberg Publishers, Limited.

194. Dlamini, Z. and D. Bates, *Medicinal plants show anticancer splicing activity of apoptotic genes*. 2015, AACR.

195. Dyson, A., *Discovering indigenous healing plants of the herb and fragrance gardens at kirstenbosch national botanical garden*. 1998: National Botanical Institute.

196. Kubec, R., J. Velisek, and R.A. Musah, *The amino acid precursors and odor formation in society garlic (Tulbaghia violacea Harv.).* Phytochemistry, 2002. **60**(1): p. 21-5.

197. Kubitzki, K., *The families and genera of vascular plants. 4. Flowering plants-Monocotyledons. Alismatanae and Commelinanae (except Gramineae).* Berlin, etc.: Springer-Verlag, 1998: p. 1-4.

198. Davison, C., R. Levendal, and C. Frost, *Cardiovascular benefits of an organic extract of Tulbaghia violacea: Its anticoagulant and anti-platelet properties.* Journal of Medicinal Plants Research, 2012. **6**(33): p. 4815-4824.

199. Aremu, A.O. and J. Van Staden, *The genus Tulbaghia (Alliaceae)—A review of its ethnobotany, pharmacology, phytochemistry and conservation needs.* Journal of ethnopharmacology, 2013. **149**(2): p. 387-400.

200. Burton, S.G., *A chemical investigation of Tulbaghia violacea.* 1990.

201. Madike, L.N., et al., *Genotoxicity of Aqueous Extracts of Tulbaghia Violacea as Determined Through an Allium Cepa Assay.* South African Journal of Science, 2019.

202. Lyantagaye, S.L., *Methyl-D-glucopyranoside from Tulbaghia violacea extract induces apoptosis in vitro in cancer cells.* Bangladesh Journal of Pharmacology, 2013. **8**(2): p. 93-101.

203. Lyantagaye, S.L., *Characterization of the Biochemical Pathway of Apoptosis Induced by D-Glucopyranoside Derivatives From Tulbaghia Violacea.* Annual Research & Review in Biology, 2014.

204. Bungu, L., et al., *Tulbaghia violacea inhibits growth and induces apoptosis in cancer cells in vitro.* African Journal of Biotechnology, 2006. **5**(20): p. 1936-1943.

205. Bungu, L., M.v.d. Venter, and C. Fros, *Evidence for an in vitro anticoagulant and antithrombotic activity in Tulbaghia violacea* African Journal of Biotechnology, 2008. **7**(5): p. 681-688.

206. Kubec, R., et al., *Flavor precursors and sensory-active sulfur compounds in alliaceae species native to South*

Africa and South America. Journal of agricultural and food chemistry, 2013. **61**(6): p. 1335-1342.

207. Uddin, M.J., et al., *Selective Visualization of Cyclooxygenase-2 in Inflammation and Cancer by Targeted Fluorescent Imaging Agents.* Cancer Research, 2010. **70**(9): p. 3618-3627.

208. Osmaniye, D., et al., *Design, Synthesis and Biological Evaluation of New <i>N</I>-Acyl Hydrazones With a Methyl Sulfonyl Moiety as Selective COX-2 Inhibitors.* Chemistry & Biodiversity, 2021. **18**(11).

209. Coy-Barrera, E., *Discrimination of Naturally-Occurring 2-Arylbenzofurans as Cyclooxygenase-2 Inhibitors: Insights Into the Binding Mode and Enzymatic Inhibitory Activity.* Biomolecules, 2020. **10**(2): p. 176.

210. Pavase, L.S., D.V. Mane, and K.G. Baheti, *Anti-inflammatory Exploration of Sulfonamide Containing Diaryl Pyrazoles With Promising COX-2 Selectivity and Enhanced Gastric Safety Profile.* Journal of Heterocyclic Chemistry, 2018. **55**(4): p. 913-922.

211. Vishwakarma, R.K., D.S. Negi, and A. Negi, *Abortitristoside a and Desrhamnosylverbanscoside: The Potential COX-2 Inhibitor From the Leaves of Nyctanthes Arbor-Tristis as Anti-Inflammatory Agents Based on the in Vitro Assay, Molecular Docking and ADMET Prediction.* Chemical Papers, 2023. **77**(6): p. 3035-3049.

212. M, R.K. and V.V. Dhayabaran, *Synthesis and Molecular Drug Efficacy of Indoline-based Dihydroxy-thiocarbamides: Inflammation Regulatory Property Unveiled Over COX-2 Inhibition, Molecular Docking, and Cytotoxicity Prospects.* Journal of Heterocyclic Chemistry, 2018. **55**(7): p. 1658-1668.

213. Guo, P. and Y.-Y. Feng, *Anti-Inflammatory Effects of Kaempferol, Myricetin, Fisetin and Ibuprofen in Neonatal Rats.* Tropical Journal of Pharmaceutical Research, 2017. **16**(8): p. 1819.

214. Hussen, N.H., *Synthesis, Characterization, Molecular Docking, ADMET Prediction, and Anti-Inflammatory Activity of Some Schiff Bases Derived From Salicylaldehyde as a Potential Cyclooxygenase Inhibitor*. Baghdad Science Journal, 2023.

215. Theoduloz, C., et al., *Inhibition of Key Enzymes in the Inflammatory Pathway by Hybrid Molecules of Terpenes and Synthetic Drugs: In Vitro and in Silico Studies.* Chemical Biology & Drug Design, 2018. **93**(3): p. 290-299.

216. Hakim, R., Y.R. Bintari, and D.S. Damayanti, *Studi Insilico Potensi Minyak Astiri Dan Ekstrak Etanol Daun Annona Muricata Sebagai Calon Herbal Terstandart Untuk Analgesik Dan Antiinflamasi.* Jurnal Kesehatan Islam Islamic Health Journal, 2018. **7**(01).

217. Allawi, M.M., M.F. Mahdi, and A.M.R. Raauf, *Synthesis, Anti-Inflammatory, Molecular Docking and ADME Studies of New Derivatives of Ketoprofen as Cyclooxygenases Inhibitor.* Al Mustansiriyah Journal of Pharmaceutical Sciences, 2019: p. 125-139.

218. Panyawong, S. and S. Devahastin, *Determination of Deformation of a Food Product Undergoing Different Drying Methods and Conditions via Evolution of a Shape Factor.* Journal of Food Engineering, 2007.

219. Guellec, S.L., et al., *ETV4 Is a Useful Marker for the Diagnosis of CIC-rearranged Undifferentiated Round-Cell Sarcomas: A Study of 127 Cases Including Mimicking Lesions.* Modern Pathology, 2016.

220. Farooqui, A.A., *Neurochemical aspects of neurotraumatic and neurodegenerative diseases*. 2010: Springer Science & Business Media.

221. De Coster, T., et al., *Parental genomes segregate into distinct blastomeres during multipolar zygotic divisions leading to mixoploid and chimeric blastocysts.* Genome Biology, 2022. **23**(1): p. 201.

222. Lobo, J., et al., *An Insight Into Morphometric Descriptors of Cell Shape That Pertain to Regenerative Medicine.* Journal of Tissue Engineering and Regenerative Medicine, 2015.

223. Hayes, P., et al., *Queuine Micronutrient Deficiency Promotes Warburg Metabolism and Reversal of the Mitochondrial ATP Synthase in Hela Cells.* Nutrients, 2020.

224. Blois, M.S., *Antioxidant determinations by the use of a stable free radical.* Nature, 1958. **181**(4617): p. 1199.

225. Schalley, C.A., *Mass Spectrometry—Principles and Applications.* International Journal of Mass Spectrometry,

2002.

226. Delmas, D., E. Solary, and N. Latruffe, *Resveratrol, a phytochemical inducer of multiple cell death pathways: apoptosis, autophagy and mitotic catastrophe.* Current medicinal chemistry, 2011. **18**(8): p. 1100-1121.

227. Li, Y., et al., *Regulation of apoptosis by ubiquitination in liver cancer.* American Journal of Cancer Research, 2023. **13**(10): p. 4832-4871.

228. Zhang, L., et al., *Effects of glabridin combined with 5-fluorouracil on the proliferation and apoptosis of gastric cancer cells.* Oncology letters, 2018. **15**(5): p. 7037-7045.

229. Sun, Y., et al., *The influence of cell cycle regulation on chemotherapy.* International journal of molecular sciences, 2021. **22**(13): p. 6923.

230. Meng, X., H. Liang, and L. Luo, *Antitumor polysaccharides from mushrooms: a review on the structural characteristics, antitumor mechanisms and immunomodulating activities.* Carbohydrate research, 2016. **424**: p. 30-41.

231. Häcker, G., *The morphology of apoptosis.* Cell and tissue research, 2000. **301**: p. 5-17.

232. Blachly, J.S. and J.C. Byrd, *Emerging drug profile: cyclin-dependent kinase inhibitors.* Leukemia & lymphoma, 2013. **54**(10): p. 2133-2143.

233. Kerr, J., A.H. Wyllie, and A.R. Currie, *Apoptosis: A Basic Biological Phenomenon With Wideranging Implications in Tissue Kinetics.* British Journal of Cancer, 1972.

234. Lopes, M., M. Foiani, and J.M. Sogo, *Multiple Mechanisms Control Chromosome Integrity After Replication Fork Uncoupling and Restart at Irreparable UV Lesions.* Molecular Cell, 2006.

235. Liu, Y., et al., *The intra-S phase checkpoint directly regulates replication elongation to preserve the integrity of stalled replisomes.* Proceedings of the National Academy of Sciences, 2021. **118**(24): p. e2019183118.

236. Sarkar, S., et al., *Tenascin-C stimulates glioma cell invasion through matrix metalloproteinase-12.* Cancer research, 2006. **66**(24): p. 11771-11780.

237. Olivares, I., *An investigation into the mechanisms of angiogenesis and breast cancer metastasis.* 2023.

238. Yamazaki, D., S. Kurisu, and T. Takenawa, *Involvement of Rac and Rho Signaling in Cancer Cell Motility in 3D Substrates.* Oncogene, 2009.

239. Alexandrova, A.Y., *Plasticity of Tumor Cell Migration: Acquisition of New Properties or Return to the Past?* Biochemistry (Moscow), 2014.

240. Lin, W.-J. and A. Pathak, *Transitions in Density, Pressure, and Effective Temperature Drive Collective Cell Migration Into Confining Environments.* 2023.

241. Ibo, M., et al., *Cell Blebbing in Confined Microfluidic Environments.* Plos One, 2016.

242. Gabbireddy, S.R., A.J. Chung, and J.S. Logue, *Melanoma Cells Adopt Features of Both Mesenchymal and Amoeboid Migration Within Confining Channels.* 2021.

243. Bergert, M., et al., *Cell Mechanics Control Rapid Transitions Between Blebs and Lamellipodia During Migration.* Proceedings of the National Academy of Sciences, 2012.

244. Jonkman, J., et al., *An Introduction to the Wound Healing Assay Using Live-Cell Microscopy.* Cell Adhesion & Migration, 2014.

245. Gilkes, D.M., G.L. Semenza, and D. Wirtz, *Hypoxia and the Extracellular Matrix: Drivers of Tumour Metastasis.* Nature Reviews Cancer, 2014.

246. Luan, M., et al., *Visualizing Breast Cancer Cell Proliferation and Invasion for Assessing Drug Efficacy With a Fluorescent Nanoprobe.* Analytical Chemistry, 2017.

247. Sh, Z., *Ability of Polymorphonuclear Leukocytes to Orient in Gradients of Chemotactic Factors.* The Journal of Cell Biology, 1977.

248. Gumbiner, B.M., *Cell Adhesion: The Molecular Basis of Tissue Architecture and Morphogenesis.* Cell, 1996.

249. Maruthamuthu, V., Y. Aratyn-Schaus, and M.L. Gardel, *Conserved F-Actin Dynamics and Force Transmission at Cell Adhesions.* Current Opinion in Cell Biology, 2010.

250. Aiyegoro, O.A. and A.I. Okoh, *Preliminary Phytochemical Screening and in Vitro Antioxidant Activities of the Aqueous Extract of Helichrysum Longifolium DC.* BMC Complementary and Alternative Medicine, 2010.

251. Park, Y.K., S.M.d. Alencar, and C.L.d. Aguiar, *Botanical Origin and Chemical Composition of Brazilian Propolis.* Journal of Agricultural and Food Chemistry, 2002.

252. Krishnamoorthy, K. and S. Paulsamy, *Phytochemical Profiling of Leaf, Stem, and Tuber Parts Of Solena Amplexicaulis (Lam.) Gandhi Using GC-MS.* International Scholarly Research Notices, 2014.

253. Onohuean, H., I.E. Bright, and I.A. Alagbonsi, *GC-MS Biocomponents Characterization and Antibacterial Potency of Ethanolic Crude Extracts of Camellia Sinensis.* Sage Open Medicine, 2022.

254. Ertürk, Ö., et al., *Gas Chromatography-Mass Spectrometry Analysis and Antimicrobial and Antioxidant Activities of Some Orchid (Orchidaceae) Species Growing in Turkey.* Brazilian Archives of Biology and Technology, 2023.

255. Berkov, S., et al., *Analysis of Galanthamine-type Alkaloids by Capillary Gas Chromatography–mass Spectrometry in Plants.* Phytochemical Analysis, 2008.

256. Bando, K., et al., *GC-MS-based Metabolomics Reveals Mechanism of Action for Hydrazine Induced Hepatotoxicity in Rats.* Journal of Applied Toxicology, 2010.

257. Hwang, S.-J. and J.-H. Lee, *Comparison of Antioxidant Activities Expressed as Equivalents of Standard Antioxidant.* Food Science and Technology, 2023.

258. Koerner, L., et al., *NEMO- And RelA-dependent NF-κB Signaling Promotes Small Cell Lung Cancer.* Cell Death and Differentiation, 2023.

259. Li, G., et al., *Ginsenoside Rg1 Exerts Anti-apoptotic Effects on Non-alcoholic Fatty Liver Cells by Downregulating the Expression of SGPL1*. Molecular Medicine Reports, 2022.

260. Kumar, J.S.D., et al., *Synthesis and Evaluation of Arylpiperazines Derivatives of 3,5-Dioxo-(2 H ,4 H)-1,2,4-Triazine as 5-Ht 1A R Ligands.* Bioorganic & Medicinal Chemistry Letters, 2014.

261. Berkowitz, P.T., et al., *Synthesis and Antimicrobial Activity of Certain 6h-1,2,4-Oxadiazin-3(2h)-Ones.* Journal of Medicinal Chemistry, 1977.

262. Adekoya, I., et al., *Manno-Heptose 1-Phosphate and Glycero-B-Manno-Heptose 1,7-Biphosphate Are Both Innate Immune Agonists.* The Journal of Immunology, 2018.

263. Malaisse, W., et al., *Pancreatic Fate Of 14 C-labelled Hexoses.* Cell Biochemistry and Function, 2000.

264. Cabanes, J., S. Chazarra, and F. García-Carmona, *Kojic Acid, a Cosmetic Skin Whitening Agent, Is a Slow-Binding Inhibitor of Catecholase Activity of Tyrosinase.* Journal of Pharmacy and Pharmacology, 1994.

265. Kubo, I. and I. Kinst-Hori, *Tyrosinase Inhibitors From Cumin.* Journal of Agricultural and Food Chemistry, 1998.

266. Lee, H.-S., *Tyrosinase Inhibitors of Pulsatilla Cernua Root-Derived Materials.* Journal of Agricultural and Food Chemistry, 2002.

267. Durant, S.T. and P. Karran, *Vanillins--a Novel Family of DNA-PK Inhibitors.* Nucleic Acids Research, 2003.

268. Yan, Y., et al., *Vanillin Derivative 6-Bromine-5-Hydroxy-4-Methoxybenzaldehyde-Elicited Apoptosis and*

G2/M Arrest of Jurkat Cells Proceeds Concurrently With DNA-PKcs Cleavage and Akt Inactivation. International Journal of Oncology, 2006.

269. Saad, H.B., et al., *Altered Hepatic mRNA Expression of Immune Response-Associated DNA Damage in Mice Liver Induced by Potassium Bromate: Protective Role of Vanillin.* Environmental Toxicology, 2015.

270. Park, E.-J., et al., *Vanillin Suppresses Cell Motility by Inhibiting STAT3-Mediated HIF-1α mRNA Expression in Malignant Melanoma Cells.* International Journal of Molecular Sciences, 2017.

271. Oladimeji, O.H., *A Cycloalkanol From Derivatization Studies on Vanillin: Evaluation of Antioxidant Activity of Obtained Derivatives.* 2022.

272. Ho, K.L., et al., *Vanillin Differentially Affects Azoxymethane-Injected Rat Colon Carcinogenesis and Gene Expression.* Journal of Medicinal Food, 2012.

273. Heger, M., et al., *The Molecular Basis for the Pharmacokinetics and Pharmacodynamics of Curcumin and Its Metabolites in Relation to Cancer.* Pharmacological Reviews, 2013.

274. Harini, S.T., et al., *Synthesis, Antioxidant and Antimicrobial Activity of Novel Vanillin Derived Piperidin-4-One Oxime Esters: Preponderant Role of the Phenyl Ester Substituents on the Piperidin-4-One Oxime Core.* Bioorganic & Medicinal Chemistry Letters, 2012.

275. Chakravarti, B., et al., *Thioaryl Naphthylmethanone Oxime Ether Analogs as Novel Anticancer Agents.* Journal of Medicinal Chemistry, 2014.

276. Basha, N.J., S.M. Basavarajaiah, and K. Shyamsunder, *Therapeutic Potential of Pyrrole and Pyrrolidine Analogs: An Update.* Molecular Diversity, 2022.

277. Petri, G.L., et al., *Bioactive Pyrrole-Based Compounds With Target Selectivity.* European Journal of Medicinal Chemistry, 2020.

278. Zhao, Y., et al., *A-Pinene Inhibits Human Prostate Cancer Growth in a Mouse Xenograft Model.* Chemotherapy, 2017.

279. Zhang, X., et al., *Schisandrin B Inhibits the Proliferation of Airway Smooth Muscle Cells via microRNA-135a Suppressing the Expression of Transient Receptor Potential Channel 1.* Cell Biology International, 2016.

280. Ran, J., et al., *Schisandrin B Ameliorated Chondrocytes Inflammation and Osteoarthritis via Suppression of NF-kappa B and MAPK Signal Pathways.* Drug Design Development and Therapy, 2018.

281. Song, S., et al., *Discoidin Domain Receptor 1.* American Journal of Pathology, 2011.

282. Lam, P.Y. and K.M. Ko, *Schisandrin B as a Hormetic Agent for Preventing Age-Related Neurodegenerative Diseases.* Oxidative Medicine and Cellular Longevity, 2012.

283. Zhang, Z., et al., *Schisandrin B Alleviates Diabetic Cardiac Autonomic Neuropathy Induced by P2X7 Receptor in Superior Cervical Ganglion via NLRP3.* Disease Markers, 2023.

284. Wang, J., et al., *Schisandrin B Inhibits Osteoclastogenesis and Protects Against Ovariectomy-Induced Bone Loss.* Frontiers in Pharmacology, 2020.

285. Xin, D., et al., *Schisandrin B Attenuates the Inflammatory Response, Oxidative Stress and Apoptosis Induced by Traumatic Spinal Cord Injury via Inhibition of P53 Signaling in Adult Rats.* Molecular Medicine Reports, 2017.

286. Wang, S., et al., *Inhibitory Effect of Schisandrin on the Pharmacokinetics of Poziotinib in Vivo and in Vitro by UPLC-MS/MS* Thoracic Cancer, 2023.

287. Zeng, L., et al., *Reduction of Aβ Generation by Schisandrin B Through Restraining Beta-Secretase 1 Transcription and Translation.* Medical Science Monitor, 2018.

288. Li, S., et al., *Schisandrin B Inhibits Epithelial-mesenchymal Transition and Stemness of Large-cell Lung Cancer Cells and Tumorigenesis in Xenografts via Inhibiting the NF-κB and P38 MAPK Signaling Pathways.* Oncology

Reports, 2021.

289. Park, C., et al., *Induction of G1 Arrest and Apoptosis by Schisandrin C Isolated From Schizandra Chinensis Baill in Human Leukemia U937 Cells.* International Journal of Molecular Medicine, 2009.

290. Walters, D.K., et al., *Taurolidine: A Novel Anti-Neoplastic Agent Induces Apoptosis of Osteosarcoma Cell Lines.* Investigational New Drugs, 2007.

291. Stendel, R., et al., *The Antibacterial Substance Taurolidine Exhibits Anti-Neoplastic Action Based on a Mixed Type of Programmed Cell Death.* Autophagy, 2009.

292. Möhler, H., R.W. Pfirrmann, and K. Frei, *Redox-Directed Cancer Therapeutics: Taurolidine and Piperlongumine as Broadly Effective Antineoplastic Agents (Review).* International Journal of Oncology, 2014.

293. Jo, H., et al., *A-Pinene Enhances the Anticancer Activity of Natural Killer Cells via ERK/AKT Pathway.* International Journal of Molecular Sciences, 2021.

294. Kusuhara, M., et al., *Fragrant Environment With A-Pinene Decreases Tumor Growth in Mice.* Biomedical Research, 2012.

295. Basholli-Salihu, M., et al., *Phytochemical Composition, Anti-Inflammatory Activity and Cytotoxic Effects of Essential Oils From Three Pinus Spp.* Pharmaceutical Biology, 2017.

296. Miller, J. and A.O. John, *The Malaria Metabolite HMBPP Does Not Trigger Erythrocyte Terpene Release.* Acs Infectious Diseases, 2020.

297. Rahmani, H., et al., *Alpha-Pinene Alleviates Motor Activity in Animal Model of Huntington's Disease via Enhancing Antioxidant Capacity.* Neurochemical Research, 2023.

298. Ibrahim, D., et al., *Thymol Nanoemulsion Promoted Broiler Chicken's Growth, Gastrointestinal Barrier and Bacterial Community and Conferred Protection Against Salmonella Typhimurium.* Scientific Reports, 2021.

299. Yu, Y., et al., *Thymol Reduces Oxidative Stress, Aortic Intimal Thickening, and Inflammation-Related Gene Expression in Hyperlipidemic Rabbits.* Journal of Food and Drug Analysis, 2016.

300. Satooka, H. and I. Kubo, *Effects of Thymol on B16-F10 Melanoma Cells.* Journal of Agricultural and Food Chemistry, 2012.

301. Hikiba, H., et al., *Ability of Fourteen Chemical Agents Used in Dental Practice to Induce Chromosome Aberrations in Syrian Hamster Embryo Cells.* Journal of Pharmacological Sciences, 2005.

302. Stawoska, I., et al., *Spectral Characteristic and Preliminary Anticancer Activity in Vitro of Selected Rhodanine-3-carboxylic Acids Derivatives.* Journal of Heterocyclic Chemistry, 2017.

303. Kryshchyshyn-Dylevych, A., *5-Ene-Rhodanine-3-Carboxylic Acids as Potential Antimicrobial and Antiparasitic Agents.* Biopolymers and Cell, 2020.

304. Kaminskyy, D., A. Kryshchyshyn, and R. Lesyk, *Recent Developments With Rhodanine as a Scaffold for Drug Discovery.* Expert Opinion on Drug Discovery, 2017.

305. Talele, T.T., et al., *Structure-Based Virtual Screening, Synthesis and SAR of Novel Inhibitors of Hepatitis C Virus NS5B Polymerase.* Bioorganic & Medicinal Chemistry, 2010.

306. Yagi, K., et al., *Agricultural Soil Fumigation as a Source of Atmospheric Methyl Bromide.* Proceedings of the National Academy of Sciences, 1993.

307. Ren, Y. and D. Mahon, *Fumigation Trials on the Application of Ethyl Formate to Wheat, Split Faba Beans and Sorghum in Small Metal Bins.* Journal of Stored Products Research, 2006.

308. Seo, S.-M., et al., *Development of Cellulose Nanocrystal-Stabilized Pickering Emulsions of Massoia and Nutmeg Essential Oils for the Control of Aedes Albopictus.* Scientific Reports, 2021.

309. El-Sayed, W.M.M., et al., *Antimicrobial Agents From Sea Urchin (Diadema Setosum) Collected From the Red Sea, Egypt.* Egyptian Journal of Aquatic Biology and Fisheries, 2020.

310. Wang, X., et al., *miR-30a Inhibits Epithelial-mesenchymal Transition and Metastasis in Triple-negative Breast Cancer by Targeting ROR1.* Oncology Reports, 2018.

311. Youssef, A.M.M., D.A.M. Maaty, and Y.M. Al-saraireh, *Phytochemistry and Anticancer Effects of Mangrove (Rhizophora Mucronata Lam.) Leaves and Stems Extract Against Different Cancer Cell Lines.* Pharmaceuticals, 2022.

312. Aluko, E.O., et al., *Anti-Lipidemic Effect of Fractions of Peristrophe Bivalvis Leaf in NG-nitro-L-arginine Methyl Ester (L-Name) Treated Rats.* Drug Research, 2020.

313. Eze, I.S., et al., *The Hepatoprotective Activity of the Methanol Leaf Extract of Lasimorpha Senegalensis Against Liver Injury Induced by Paracetamol (Acetaminophen) in Albino Wistar Rats.* Proceedings of the Nigerian Academy of Science, 2021.

314. Na, C. and T.M. Olson, *Stability of Cyanogen Chloride in the Presence of Free Chlorine and Monochloramine.* Environmental Science & Technology, 2004.

315. Abu-Soûd, H.M., et al., *The Reaction of HOCl and Cyanocobalamin: Corrin Destruction and the Liberation of Cyanogen Chloride.* Free Radical Biology and Medicine, 2012.

316. Maitra, D., et al., *Kinetic Studies on the Reaction Between Dicyanocobinamide and Hypochlorous Acid.* Plos One, 2014.

317. Yang, X., et al., *Fabrication of Hierarchically Porous CuBTC@PA-PEI Composite for High-Efficiency Elimination of Cyanogen Chloride.* Molecules, 2023.

318. Lee, K.H., et al., *Edible Algae (Ecklonia Cava) Bioprocessed With Mycelia of Shiitake (Lentinula Edodes) Mushrooms in Liquid Culture and Its Isolated Fractions Protect Mice Against Allergic Asthma.* BMC Complementary Medicine and Therapies, 2022.

319. Bennett, L., et al., *The Colonoscopy Cookbook: Analysis of Effect of a Recipe Resource on Quality and Experience of Bowel Preparation in Colonoscopy.* Endoscopy International Open, 2023.

320. Nipun, T.S., et al., *Preliminary Phytochemical Screening, in Vitro Antidiabetic, Antioxidant Activities, and Toxicity of Leaf Extracts of Psychotria Malayana Jack.* Plants, 2021.

321. Jiang, Y., et al., *Synthesis of a Copper 1,3,5-Triamino-2,4,6-Benzenetriol Metal–Organic Framework.* Journal of the American Chemical Society, 2020.

322. Bengiat, R., et al., *Selective Binding and Precipitation of Cesium Ions From Aqueous Solutions: A Size-Driven Supramolecular Reaction.* Chemistry - A European Journal, 2018.

323. Rydevik, A., U. Bondesson, and M. Hedeland, *Structural Elucidation of Phase I and II Metabolites of Bupivacaine in Horse Urine and Fungi of the Cunninghamella Species Using Liquid Chromatography/Multi-stage Mass Spectrometry.* Rapid Communications in Mass Spectrometry, 2012.

324. Panda, J., P.R. Virkler, and M.R. Detty, *A Comparison of Linear Optical Properties and Redox Properties in Chalcogenopyrylium Dyes Bearing Ortho-Substituted Aryl Substituents and tert-Butyl Substituents.* The Journal of Organic Chemistry, 2003.

325. Lambrechts, M.G. and I.S. Pretorius, *Yeast and Its Importance to Wine Aroma - A Review.* South African Journal of Enology and Viticulture, 2019.

326. Trinh, T.-T.-T., et al., *Effect of L-Isoleucine and L-Phenylalanine Addition on Aroma Compound Formation During Longan Juice Fermentation by a Co-Culture of Saccharomyces Cerevisiae and Williopsis Saturnus.* South African Journal of Enology and Viticulture, 2016.

327. Verstrepen, K.J., et al., *Expression Levels of the Yeast Alcohol Acetyltransferase Genes ATF1, Lg-Atf1, And ATF2 Control the Formation of a Broad Range of Volatile Esters.* Applied and Environmental Microbiology, 2003.

328. Ćorović, M., et al., *Immobilization of Candida Antarctica Lipase B Onto Purolite® MN102 and Its Application in Solvent-Free and Organic Media Esterification.* Bioprocess and Biosystems Engineering, 2016.

329. Lattanzi, R., et al., *Synthesis and Biological Evaluation of 14-Alkoxymorphinans. 22. Influence of the 14-Alkoxy Group and the Substitution in Position 5 in 14-Alkoxymorphinan-6-Ones on in Vitro and in Vivo Activities.* Journal of Medicinal Chemistry, 2005.

330. Dumitrascuta, M., et al., *Synthesis, Pharmacology, and Molecular Docking Studies on 6-Desoxo-<i>N</I>-Methylmorphinans as Potent M-Opioid Receptor Agonists.* Journal of Medicinal Chemistry, 2017.

331. Pagare, P.P., et al., *Design, Synthesis, and Biological Evaluation of NAP Isosteres: A Switch From Peripheral to Central Nervous System Acting Mu-Opioid Receptor Antagonists.* Journal of Medicinal Chemistry, 2022.

332. Olaniyi, T.D. and A. Adetutu, *In Silico Anti-Quorum Sensing Activities of Phytocompounds of Psidium Guajava in Salmonella Enterica Serovar Typhi.* Journal of Umm Al-Qura University for Applied Sciences, 2023.

333. Serra, M.E.S., D. Murtinho, and A.M.d.A.R. Gonsalves, *A Comparative Study of Reactivity and Selectivity of Chiral Diamines and Structurally Analogous Amino Alcohol Ligands in Enantioselective Alkylations With Diethylzinc.* Applied Organometallic Chemistry, 2008.

334. Büttner, A., et al., *Effects of Introducing Methoxy Groups Into the Ancillary Ligands in Bis(diimine) Copper(I) Dyes for Dye-Sensitized Solar Cells.* Inorganics, 2018.

335. Domin, D., et al., *Synthesis and Characterization of New Chiral Palladium B-Diimine Complexes.* Journal of Organometallic Chemistry, 2007.

336. Zheng, A., et al., *Control of Π–π Stacking of Dithienopyrrole-Based, Hole-Transporting Materials via Lateral Substituents for High-Efficiency Perovskite Solar Cells.* Acs Photonics, 2018.

337. Tu, C., et al., *Schisandrin a Inhibits the IL-1β-Induced Inflammation and Cartilage Degradation via Suppression of MAPK and NF-κB Signal Pathways in Rat Chondrocytes.* Frontiers in Pharmacology, 2019.

338. Piao, Z., et al., *Schisandrin Restores the Amyloid B-Induced Impairments on Mitochondrial Function, Energy Metabolism, Biogenesis, and Dynamics in Rat Primary Hippocampal Neurons.* Pharmacology, 2021.

339. Xu, L., et al., *From the Traditional Chinese Medicine Plant Schisandra Chinensis New Scaffolds Effective on HIV-1 Reverse Transcriptase Resistant to Non-Nucleoside Inhibitors.* The Journal of Microbiology, 2015.

340. Maia, M.d.S., et al., *Identification of New Targets and the Virtual Screening of Lignans Against Alzheimer's Disease.* Oxidative Medicine and Cellular Longevity, 2020.

341. Jiang, Y., et al., *Phenolic Profiling of Berries Waste and Determination of Their Antioxidant Potential.* Journal of Food Quality, 2022.

342. Olmo, A.d., J. Calzada, and M. Núñez, *Benzoic Acid and Its Derivatives as Naturally Occurring Compounds in Foods and as Additives: Uses, Exposure, and Controversy.* Critical Reviews in Food Science and Nutrition, 2015.

343. Lubbers, R.J.M., et al., *Discovery of Novel p-Hydroxybenzoate-m-Hydroxylase, Protocatechuate 3,4 Ring-Cleavage Dioxygenase, and Hydroxyquinol 1,2 Ring-Cleavage Dioxygenase From the Filamentous Fungus Aspergillus Niger.* Acs Sustainable Chemistry & Engineering, 2019.

344. Zuo, Y., C. Wang, and J. Zhan, *Separation, Characterization, and Quantitation of Benzoic and Phenolic Antioxidants in American Cranberry Fruit by GC−MS.* Journal of Agricultural and Food Chemistry, 2002.

345. Xiang, W., et al., *Complete Genome Sequence and Biodegradation Characteristics of Benzoic Acid-Degrading Bacterium Pseudomonas Sp. SCB32.* Biomed Research International, 2020.

346. Yalpani, N., et al., *Pathway of Salicylic Acid Biosynthesis in Healthy and Virus-Inoculated Tobacco.* Plant Physiology, 1993.

347. Zhang, K. and Y. Zuo, *GC-MS Determination of Flavonoids and Phenolic and Benzoic Acids in Human Plasma After Consumption of Cranberry Juice.* Journal of Agricultural and Food Chemistry, 2004.

348. Bridges, J.W., et al., *The Fate of Benzoic Acid in Various Species.* Biochemical Journal, 1970. **118**(1): p. 47-51.

349. Bacher, A., et al., *Biosynthesis of Vitamin B2 (Riboflavin).* Annual Review of Nutrition, 2000.

350. Köse, M., et al., *An Agonist Radioligand for the Proinflammatory Lipid-Activated G Protein-Coupled Receptor GPR84 Providing Structural Insights.* Journal of Medicinal Chemistry, 2019.

351. Fischer, M., et al., *Structures and Reaction Mechanisms of Riboflavin Synthases of Eubacterial and Archaeal Origin.* Biochemical Society Transactions, 2005.

352. Graupner, M., H. Xu, and R.H. White, *The Pyrimidine Nucleotide Reductase Step in Riboflavin and F 420 Biosynthesis In Archaea Proceeds by the Eukaryotic Route to Riboflavin.* Journal of Bacteriology, 2002.

353. Burnett, C.L., et al., *Safety Assessment of Plant-Derived Fatty Acid Oils.* International Journal of Toxicology, 2017.

354. Lee, J.Y., et al., *Comparative Volatile Profiles in Soy Sauce According to Inoculated Microorganisms.* Bioscience Biotechnology and Biochemistry, 2013.

355. DebMandal, M. and S. Mandal, *Coconut (Cocos Nucifera L.: Arecaceae): In Health Promotion and Disease Prevention.* Asian Pacific Journal of Tropical Medicine, 2011.

356. Vigentini, I., et al., *Indigenous Georgian Wine-Associated Yeasts and Grape Cultivars to Edit the Wine Quality in a Precision Oenology Perspective.* Frontiers in Microbiology, 2016.

357. Burnett, C.L., et al., *Final Report on the Safety Assessment of Cocos Nucifera (Coconut) Oil and Related Ingredients.* International Journal of Toxicology, 2011.

358. Ondo, D.A., F. Loyer, and N.D. Boscher, *Influence of Double Bonds and Cyclic Structure on the AP-PECVD of Low-korganosilicon Insulating Layers.* Plasma Processes and Polymers, 2021.

359. Wang, G., et al., *Adsorption and Aggregation Behaviors of Tetrasiloxane-Tailed Gemini Surfactants With (EO) m Spacers.* The Journal of Physical Chemistry B, 2013.

360. Abe, Y., K.I. Suyama, and T. Gunji, *Synthesis and Structure Of cis-transcis-1,3,5,7-Tetraisocyanato-1,3,5,7-Tetramethylcyclotetrasiloxane.* Chemistry Letters, 2006.

361. Mtemeli, F., et al., *Advances in schistosomiasis drug discovery based on natural products.* All Life, 2022. **15**(1): p. 608-623.

362. Nayak, S.S., et al., *Prospects of Novel and Repurposed Immunomodulatory Drugs against Acute Respiratory Distress Syndrome (ARDS) Associated with COVID-19 Disease.* Journal of Personalized Medicine, 2023. **13**(4): p. 664.

363. Saikia, S. and M. Bordoloi, *Molecular docking: challenges, advances and its use in drug discovery perspective.* Current drug targets, 2019. **20**(5): p. 501-521.

364. Allison, R.L., *Astrocyte-Targeted Therapeutics to Correct Glial Inflammatory Signaling and Neuron Loss in SMA and ALS*. 2023, The Medical College of Wisconsin.

365. Rowlinson, S.W., et al., *A Novel Mechanism of Cyclooxygenase-2 Inhibition Involving Interactions With Ser-530 and Tyr-385.* Journal of Biological Chemistry, 2003.

366. Manning, B.D. and L.C. Cantley, *AKT/PKB Signaling: Navigating Downstream.* Cell, 2007.

367. Jaiswal, N., et al., *The Role of Skeletal Muscle Akt in the Regulation of Muscle Mass and Glucose Homeostasis.* Molecular Metabolism, 2019.

368. Guo, Y., et al., *ERK/MAPK Signaling Pathway and Tumorigenesis (Review).* Experimental and Therapeutic Medicine, 2020.

369. Kholodenko, B.N., *Negative Feedback and Ultrasensitivity Can Bring About Oscillations in the Mitogen-*

activated Protein Kinase Cascades. European Journal of Biochemistry, 2000.

370. Shahrokhi, S.Z., et al., *Asthenozoospermia: Cellular and Molecular Contributing Factors and Treatment Strategies.* Andrologia, 2019.

371. Cheng, J., et al., *Synergistic Interaction of MEK Kinase 2, C-Jun N-Terminal Kinase (JNK) Kinase 2, and JNK1 Results in Efficient and Specific JNK1 Activation.* Molecular and Cellular Biology, 2000.

372. Elenjord, R., et al., *Collagen I Regulates Matrix Metalloproteinase-2 Activation in Osteosarcoma Cells Independent of S100A4.* Febs Journal, 2009.

373. Cario-André, M., *DDR1 and DDR2 in Skin.* Cell Adhesion & Migration, 2018.

374. Bauer, T., et al., *Identification of Axl as a Downstream Effector of TGF-β1 During Langerhans Cell Differentiation and Epidermal Homeostasis.* The Journal of Experimental Medicine, 2012.

375. Wium, M., et al., *The Role of the Receptor Tyrosine Kinase Axl in Carcinogenesis and Development of Therapeutic Resistance: An Overview of Molecular Mechanisms and Future Applications.* Cancers, 2021.

376. Mori, M., et al., *Gilteritinib, a FLT3/AXL Inhibitor, Shows Antileukemic Activity in Mouse Models of FLT3 Mutated Acute Myeloid Leukemia.* Investigational New Drugs, 2017.

377. Antony, J., et al., *The GAS6-AXL Signaling Network Is a Mesenchymal (Mes) Molecular Subtype–specific Therapeutic Target for Ovarian Cancer.* Science Signaling, 2016.

378. Barquilla, A. and E.B. Pasquale, *Eph Receptors and Ephrins: Therapeutic Opportunities.* The Annual Review of Pharmacology and Toxicology, 2015.

379. Yang, C., et al., *Transcriptome analysis reveals GA induced apoptosis in HCT116 human colon cancer cells through calcium and p53 signal pathways.* 2018. **8**(22): p. 12449-12458.

380. Pasquale, E.B., *Eph-Ephrin Bidirectional Signaling in Physiology and Disease.* Cell, 2008.

381. Xiang, Y.-P., et al., *Y772 Phosphorylation of EphA2 Is Responsible for EphA2-dependent NPC Nasopharyngeal Carcinoma Growth by Shp2/Erk-1/2 Signaling Pathway.* Cell Death and Disease, 2020.

382. Ieguchi, K. and Y. Maru, *Roles of EphA1/A2 and Ephrin-A1 in Cancer.* Cancer Science, 2019.

383. Miao, H., et al., *Activation of EphA2 Kinase Suppresses Integrin Function and Causes Focal-Adhesion-Kinase Dephosphorylation.* Nature Cell Biology, 1999.

384. Brantley, D.M., et al., *Soluble Eph a Receptors Inhibit Tumor Angiogenesis and Progression in Vivo.* Oncogene, 2002.

385. Al-Mathkour, M.M., et al., *The Hippo Effector YAP1/TEAD1 Regulates EPHA3 Expression to Control Cell Contact and Motility.* Scientific Reports, 2022.

386. Gallarda, B.W., et al., *Segregation of Axial Motor and Sensory Pathways via Heterotypic Trans-Axonal Signaling.* Science, 2008.

387. Mekki, Y.N., et al., *The Genetic Architecture of Language Functional Connectivity.* 2021.

388. Lamberto, I., et al., *Development and Structural Analysis of a Nanomolar Cyclic Peptide Antagonist for the EphA4 Receptor.* Acs Chemical Biology, 2014.

389. North, H.A., et al., *Promotion of Proliferation in the Developing Cerebral Cortex by EphA4 Forward Signaling.* Development, 2009.

390. Cruz-Orengo, L., et al., *Reduction of EphA4 Receptor Expression After Spinal Cord Injury Does Not Induce Axonal Regeneration or Return of tcMMEP Response.* Neuroscience Letters, 2007.

391. Masaoutis, C., et al., *Ephrin Receptors (Ephs) Expression in Thymic Epithelial Tumors: Prognostic*

Implications and Future Therapeutic Approaches. Diagnostics, 2021.

392. Raja, E., et al., *Tyrosine Kinase Eph Receptor A6 Sensitizes Glioma-initiating Cells Towards Bone Morphogenetic Protein-induced Apoptosis.* Cancer Science, 2019.

393. Liu, J., et al., *Loss of EphA7 Expression in Basal Cell Carcinoma by Hypermethylation of CpG Islands in the Promoter Region.* Analytical Cellular Pathology, 2022.

394. Zadeh, T., M. Lucero, and R.P. Kandpal, *Artesunate-Induced Cellular Effects Are Mediated by Specific EPH Receptors and Ephrin Ligands in Breast Carcinoma Cells.* Cancer Genomics & Proteomics, 2021.

395. Martiny-Baron, G., et al., *The Small Molecule Specific EphB4 Kinase Inhibitor NVP-BHG712 Inhibits VEGF Driven Angiogenesis.* Angiogenesis, 2010.

396. Shirkey, N.J., et al., *Dynamic Responses of Xenopus Retinal Ganglion Cell Axon Growth Cones to Netrin-1 as They Innervate Their in Vivo Target.* Developmental Neurobiology, 2012.

397. Larrivée, B., et al., *Activation of the UNC5B Receptor by Netrin-1 Inhibits Sprouting Angiogenesis.* Genes & Development, 2007.

398. Blasiak, A., D. Kilinc, and L. G, *Neuronal Cell Bodies Remotely Regulate Axonal Growth Response to Localized Netrin-1 Treatment via Second Messenger and DCC Dynamics.* Frontiers in Cellular Neuroscience, 2017.

399. Taylor, L., et al., *Netrin-1 Reduces Monocyte and Macrophage Chemotaxis Towards the Complement Component C5a.* Plos One, 2016.

400. Dravis, C., et al., *Bidirectional Signaling Mediated by Ephrin-B2 and EphB2 Controls Urorectal Development.* Developmental Biology, 2004.

401. Kwon, H.Y., et al., *Decreased Lymphangiogenic Activities and Genes Expression of Cord Blood Lymphatic Endothelial Progenitor Cells (VEGFR3+/Pod+/CD11b+ Cells) in Patient With Preeclampsia.* International Journal of Molecular Sciences, 2021.

402. Sen, A. and M. Ta, *Vitronectin Acts as a Key Regulator of Adhesion and Migration in Human Umbilical Cord-Derived MSCs Under Different Stress Conditions.* 2021.

403. Wu, Y., et al., *DNA Methylation Maintains the CLDN1-EPHB6-SLUG Axis to Enhance Chemotherapeutic Efficacy and Inhibit Lung Cancer Progression.* Theranostics, 2020.

404. Shiuan, E. and J. Chen, *Eph Receptor Tyrosine Kinases in Tumor Immunity.* Cancer Research, 2016.

405. Kjær, I.M., et al., *EGFR and EGFR Ligands in Serum in Healthy Women; Reference Intervals and Age Dependency.* Clinical Chemistry and Laboratory Medicine (Cclm), 2019.

406. Chakraborty, S., et al., *Constitutive and Ligand-Induced EGFR Signaling Triggers Distinct and Mutually Exclusive Downstream Signaling Networks.* Nature Communications, 2014.

407. Guo, G., et al., *Ligand-Independent EGFR Signaling.* Cancer Research, 2015.

408. Soto-Gamez, A., et al., *A Bispecific Inhibitor of the EGFR/ADAM17 Axis Decreases Cell Proliferation and Migration of EGFR-Dependent Cancer Cells.* Cancers, 2020.

409. Sanes, J.R. and J.W. Lichtman, *Development of the Vertebrate Neuromuscular Junction.* Annual Review of Neuroscience, 1999.

410. Lü, J., et al., *14-3-3ζ Cooperates With ErbB2 to Promote Ductal Carcinoma in Situ Progression to Invasive Breast Cancer by Inducing Epithelial-Mesenchymal Transition.* Cancer Cell, 2009.

411. Yen, L., et al., *Loss of Nrdp1 Enhances ErbB2/ErbB3–Dependent Breast Tumor Cell Growth.* Cancer Research, 2006.

412. Salt, M.B., S. Bandyopadhyay, and F. McCormick, *Epithelial-to-Mesenchymal Transition Rewires the*

Molecular Path to PI3K-Dependent Proliferation. Cancer Discovery, 2014.

413. Cheng, P., et al., *Effects of Notch Signaling on Regulation of Myeloid Cell Differentiation in Cancer.* Cancer Research, 2014.

414. Kaushansky, A., et al., *System-Wide Investigation of ErbB4 Reveals 19 Sites of Tyr Phosphorylation That Are Unusually Selective in Their Recruitment Properties.* Chemistry & Biology, 2008.

415. Neilson, K.M. and R. Friesel, *Ligand-Independent Activation of Fibroblast Growth Factor Receptors by Point Mutations in the Extracellular, Transmembrane, and Kinase Domains.* Journal of Biological Chemistry, 1996.

416. Farrell, B. and A.L. Breeze, *Structure, Activation and Dysregulation of Fibroblast Growth Factor Receptor Kinases: Perspectives for Clinical Targeting.* Biochemical Society Transactions, 2018.

417. Xie, H., et al., *Polymorphisms of FGFR1 in HBV-related Hepatocellular Carcinoma.* Tumor Biology, 2015. **36**(11): p. 8881-8886.

418. Crose, L.E.S., et al., *FGFR4 Blockade Exerts Distinct Antitumorigenic Effects in Human Embryonal Versus Alveolar Rhabdomyosarcoma*. Clinical Cancer Research, 2012.

419. French, D., et al., *Targeting FGFR4 Inhibits Hepatocellular Carcinoma in Preclinical Mouse Models.* Plos One, 2012.

420. Taylor, J.G., et al., *Identification of FGFR4-activating Mutations in Human Rhabdomyosarcomas That Promote Metastasis in Xenotransplanted Models.* Journal of Clinical Investigation, 2009.

421. Peláez-García, A., et al., *FGFR4 Role in Epithelial-Mesenchymal Transition and Its Therapeutic Value in Colorectal Cancer.* Plos One, 2013.

422. Loschi, M., et al., *FLT3 Tyrosine Kinase Inhibitors for the Treatment of Fit and Unfit Patients With FLT3-Mutated AML: A Systematic Review.* International Journal of Molecular Sciences, 2021.

423. Kazi, J.U. and L. Rönnstrand, *FMS-like Tyrosine Kinase 3/Flt3: From Basic Science to Clinical Implications.* Physiological Reviews, 2019.

424. Marensi, V., K. Keeshan, and D.J. MacEwan, *Pharmacological Impact of FLT3 Mutations on Receptor Activity and Responsiveness to Tyrosine Kinase Inhibitors.* Biochemical Pharmacology, 2021.

425. Adams, D.H., S. Pyne, and N.J. Pyne, *Sphingosine Kinases: Emerging Structure–Function Insights.* Trends in Biochemical Sciences, 2016.

426. Wu, X., et al., *P85α Regulates Osteoblast Differentiation by Cross-Talking With the MAPK Pathway.* Journal of Biological Chemistry, 2011.

427. Catellani, C., et al., *GH and IGF System: The Regulatory Role of miRNAs and lncRNAs in Cancer.* Frontiers in Endocrinology, 2021. **12**.

428. Hou, C.-F.D., et al., *MicroRNA Let-7i Induced Autophagy to Protect T Cell From Apoptosis by Targeting IGF1R.* Biochemical and Biophysical Research Communications, 2014. **453**(4): p. 728-734.

429. Mancarella, C., A. Morrione, and K. Scotlandi, *Unraveling the IGF System Interactome in Sarcomas Exploits Novel Therapeutic Options.* Cells, 2021. **10**(8): p. 2075.

430. Sipos, F., et al., *Survival of HT29 Cancer Cells Is Affected by IGF1R Inhibition via Modulation of Self-Dna-Triggered TLR9 Signaling and the Autophagy Response.* Pathology & Oncology Research, 2022. **28**.

431. Sperandio, S., et al., *Paraptosis: Mediation by MAP Kinases and Inhibition by AIP-1/Alix.* Cell Death and Differentiation, 2004. **11**(10): p. 1066-1075.

432. Yan, G., M. Elbadawi, and T. Efferth, *Multiple Cell Death Modalities and Their Key Features (Review).* World Academy of Sciences Journal, 2020.

433. Zhou, Y., et al., *Suppressor of Cytokine Signaling-2 Limits IGF1R-mediated Regulation of Epithelial–mesenchymal Transition in Lung Adenocarcinoma.* Cell Death and Disease, 2018. **9**(4).

434. Minchenko, O.H., et al., *Effect of Hypoxia on the Expression of Genes That Encode Some IGFBP and CCN Proteins in U87 Glioma Cells Depends on IRE1 Signaling.* The Ukrainian Biochemical Journal, 2015.

435. Molhoek, K.R., et al., *Comprehensive Analysis of Receptor Tyrosine Kinase Activation in Human Melanomas Reveals Autocrine Signaling Through IGF-1R.* Melanoma Research, 2011.

436. Hayashi, H., et al., *Down-regulation of the PI3-kinase/Akt Pathway by ERK MAP Kinase in Growth Factor Signaling.* Genes to Cells, 2008.

437. Lin, S., et al., *IGF-1 Promotes Angiogenesis in Endothelial Cells/Adipose-derived Stem Cells Co-culture System With Activation of PI3K/Akt Signal Pathway.* Cell Proliferation, 2017.

438. Grugan, K.D., et al., *Dual Regulation of Glucocorticoid-Induced Leucine Zipper (GILZ) by the Glucocorticoid Receptor and the PI3-kinase/AKT Pathways in Multiple Myeloma.* The Journal of Steroid Biochemistry and Molecular Biology, 2008.

439. Ekman, C.J., et al., *Plasma Concentrations of Gas6 and sAxl Correlate With Disease Activity in Systemic Lupus Erythematosus.* Rheumatology, 2011.

440. Kim, M.J. and E.J. Choi, *Pathological Roles of MAPK Signaling Pathways in Human Diseases.* Biochimica Et Biophysica Acta (Bba) - Molecular Basis of Disease, 2010.

441. Yue, X., et al., *Gain of Function Mutant P53 Protein Activates AKT Through the Rac1 Signaling to Promote Tumorigenesis.* Cell Cycle, 2020.

442. A-González, N., et al., *Apoptotic Cells Promote Their Own Clearance and Immune Tolerance Through Activation of the Nuclear Receptor LXR.* Immunity, 2009.

443. Rothlin, C.V., et al., *TAM Receptors Are Pleiotropic Inhibitors of the Innate Immune Response.* Cell, 2007.

444. Luiskandl, S., et al., *Endosomal Trafficking of the Receptor Tyrosine Kinase MuSK Proceeds via Clathrin-dependent Pathways, Arf6 and Actin.* Febs Journal, 2013.

445. Watty, A., et al., *The in Vitro And in Vivo Phosphotyrosine Map of Activated MuSK.* Proceedings of the National Academy of Sciences, 2000.

446. Fu, A.K.Y., et al., *Xenopus Muscle-specific Kinase: Molecular Cloning and Prominent Expression in Neural Tissues During Early Embryonic Development.* European Journal of Neuroscience, 1999.

447. Ding, Q., et al., *Impaired Signaling for Neuromuscular Synaptic Maintenance Is a Feature of Motor Neuron Disease.* Acta Neuropathologica Communications, 2022.

448. Donovan, J., *Platelet-Derived Growth Factor Signaling in Mesenchymal Cells.* Frontiers in Bioscience-Scholar, 2013.

449. Uezumi, A., et al., *Mesenchymal Progenitors Distinct From Satellite Cells Contribute to Ectopic Fat Cell Formation in Skeletal Muscle.* Nature Cell Biology, 2010.

450. Satir, P. and B.H. Satir, *The Conserved Ancestral Signaling Pathway From Cilium to Nucleus.* Journal of Cell Science, 2019.

451. Zhang, S., et al., *ROR1 Is Expressed in Human Breast Cancer and Associated With Enhanced Tumor-Cell Growth.* Plos One, 2012.

452. Cui, B., et al., *Targeting ROR1 Inhibits Epithelial–Mesenchymal Transition and Metastasis.* Cancer Research, 2013.

453. Nadanaka, S., J.i. Tamura, and H. Kitagawa, *Chondroitin Sulfates Control Invasiveness of the Basal-Like Breast Cancer Cell Line MDA-MB-231 Through ROR1.* Frontiers in Oncology, 2022.

454. Grumolato, L., et al., *Canonical and Noncanonical WNTS Use a Common Mechanism to Activate Completely Unrelated Coreceptors.* Genes & Development, 2010.

455. Lyu, J., V. Yamamoto, and W. Lu, *Cleavage of the WNT Receptor Ryk Regulates Neuronal Differentiation During Cortical Neurogenesis.* Developmental Cell, 2008.

456. Chang, W.-F., et al., *Smek1/2 Is a Nuclear Chaperone and Cofactor for Cleaved WNT Receptor Ryk, Regulating Cortical Neurogenesis.* Proceedings of the National Academy of Sciences, 2017.

457. Junco, P.T. and J.C. López-Gutiérrez, *Activity of a TIE2 Inhibitor (Rebastinib) in a Patient With a Life-threatening Cervicofacial Venous Malformation.* Pediatric Blood & Cancer, 2023. **70**(8).

458. Koch, P., et al., *Imaging of Tie2 With a Fluorescently Labeled Small Molecule Affinity Ligand.* Acs Chemical Biology, 2019. **15**(1): p. 151-157.

459. Limaye, N., et al., *Somatic Activating PIK3CA Mutations Cause Venous Malformation.* The American Journal of Human Genetics, 2015. **97**(6): p. 914-921.

460. Master, Z., et al., *Dok-R Plays a Pivotal Role in Angiopoietin-1-Dependent Cell Migration Through Recruitment and Activation of Pak.* The Embo Journal, 2001. **20**(21): p. 5919-5928.

461. Moore, J., M.A. Lemmon, and K.M. Ferguson, *Dimerization of Tie2 Mediated by Its Membrane-Proximal FNIII Domains.* Proceedings of the National Academy of Sciences, 2017. **114**(17): p. 4382-4387.

462. Seegar, T.C.M., et al., *Tie1-Tie2 Interactions Mediate Functional Differences Between Angiopoietin Ligands.* Molecular Cell, 2010. **37**(5): p. 643-655.

463. Singh, H., et al., *The Molecular Balance Between Receptor Tyrosine Kinases Tie1 and Tie2 Is Dynamically Controlled by VEGF and TNFα and Regulates Angiopoietin Signaling.* Plos One, 2012. **7**(1): p. e29319.

464. Wang, H., et al., *Transformation of Vascular Endothelial Cells by a Point Mutation in the Tie2 Gene From Human Intramuscular Haemangioma.* Oncogene, 2004. **23**(53): p. 8700-8704.

465. Witzenbichler, B., et al., *Chemotactic Properties of Angiopoietin-1 and -2, Ligands for the Endothelial-Specific Receptor Tyrosine Kinase Tie2.* Journal of Biological Chemistry, 1998. **273**(29): p. 18514-18521.

466. Yao, K., et al., *Ang1/Tie2 Induces Cell Proliferation and Migration in Human Papillary Thyroid Carcinoma via the PI3K/AKT Pathway.* Oncology Letters, 2017.

467. Yu, X., et al., *Structural Basis for Angiopoietin-1–mediated Signaling Initiation.* Proceedings of the National Academy of Sciences, 2013. **110**(18): p. 7205-7210.

468. Zwiers, P.J., et al., *Pattern of Tamoxifen-Induced Tie2 Deletion in Endothelial Cells in Mature Blood Vessels Using Endo SCL-Cre-ERT Transgenic Mice.* Plos One, 2022. **17**(6): p. e0268986.

469. Butkiewicz, D., et al., *Association of Genetic Variants in ANGPT/TEK and VEGF/VEGFR With Progression and Survival in Head and Neck Squamous Cell Carcinoma Treated With Radiotherapy or Radiochemotherapy.* Cancers, 2020. **12**(6): p. 1506.

470. Scholz, A., K.H. Plate, and Y. Reiss, *Angiopoietin-2: A Multifaceted Cytokine That Functions in Both Angiogenesis and Inflammation.* Annals of the New York Academy of Sciences, 2015. **1347**(1): p. 45-51.

471. Thomson, B.R., et al., *A Lymphatic Defect Causes Ocular Hypertension and Glaucoma in Mice.* Journal of Clinical Investigation, 2014. **124**(10): p. 4320-4324.

472. Siozopoulou, V., et al., *NTRK Fusions in Sarcomas: Diagnostic Challenges and Clinical Aspects.* Diagnostics, 2021.

473. Lei, L., et al., *The Zinc Finger Transcription Factor Klf7 Is Required for TrkA Gene Expression and Development of Nociceptive Sensory Neurons.* Genes & Development, 2005.

474. Nakagawara, A., et al., *Expression and Function of TRK-B and BDNF in Human Neuroblastomas.* Molecular

and Cellular Biology, 1994.

475. Ahmed, F., M. Paul, and K. Hristova, *The Biophysical Basis of Receptor Tyrosine Kinase Ligand Functional Selectivity: TRK-B Case Study*. Biochemical Journal, 2020.

476. Mizoguchi, Y., et al., *A Rapid Increase in the Total Number of Cell Surface Functional GABAA Receptors Induced by Brain-Derived Neurotrophic Factor in Rat Visual Cortex.* Journal of Biological Chemistry, 2003.

477. Uren, R.T. and A.M. Turnley, *Regulation of Neurotrophin Receptor (Trk) Signaling: Suppressor of Cytokine Signaling 2 (SOCS2) Is a New Player*. Frontiers in Molecular Neuroscience, 2014.

478. Skaper, S.D., *The Biology of Neurotrophins, Signaling Pathways, and Functional Peptide Mimetics of Neurotrophins and Their Receptors.* CNS & Neurological Disorders - Drug Targets, 2008.

479. Zhou, X., et al., *MiRNA-128-3p Restrains Malignant Melanoma Cell Malignancy by Targeting NTRK3*. Frontiers in Oncology, 2021.

480. Wang, H., et al., *DNA damage checkpoint recovery and cancer development.* Experimental cell research, 2015. **334**(2): p. 350-358.

481. Olsson, A.K., et al., *VEGF Receptor Signaling ? In Control of Vascular Function.* Nature Reviews Molecular Cell Biology, 2006.

482. Uemura, A., et al., *VEGFR1 Signaling in Retinal Angiogenesis and Microinflammation.* Progress in Retinal and Eye Research, 2021.

483. Byeon, S.H., et al., *Vascular Endothelial Growth Factor as an Autocrine Survival Factor for Retinal Pigment Epithelial Cells Under Oxidative Stress via the VEGF-R2/PI3K/Akt.* Investigative Opthalmology & Visual Science, 2010.

484. Yoo, J.M., et al., *Anti-angiogenic Effect of Mountain Ginseng in vitro and in vivo: Comparison With Farm-cultivated Ginseng.* Molecular Medicine Reports, 2021.

485. Cydzik, M., et al., *Slow Binding Kinetics of Secreted Protein, Acidic, Rich in Cysteine-Vegf Interaction Limit VEGF Activation of VEGF Receptor 2 and Attenuate Angiogenesis.* The Faseb Journal, 2015.

486. Koch, S. and L. Claesson-Welsh, *Signal Transduction by Vascular Endothelial Growth Factor Receptors.* Cold Spring Harbor Perspectives in Medicine, 2012.

487. Babaei, Z., et al., *VEGFR3 Suppression Through miR-1236 Inhibits Proliferation and Induces Apoptosis in Ovarian Cancer via ERK1/2 and AKT Signaling Pathways.* Journal of Cellular Biochemistry, 2023.

488. Vorlová, S., et al., *Induction of Antagonistic Soluble Decoy Receptor Tyrosine Kinases by Intronic PolyA Activation*. Molecular Cell, 2011.

489. Deng, Y., X. Zhang, and M. Simons, *Molecular Controls of Lymphatic VEGFR3 Signaling.* Arteriosclerosis Thrombosis and Vascular Biology, 2015.

490. Elmore, S.A., *Apoptosis: A Review of Programmed Cell Death.* Toxicologic Pathology, 2007.

491. Yap, T.A., et al., *Targeting cell cycle kinases and kinesins in anticancer drug development.* Expert Opinion on Drug Discovery, 2007. **2**(4): p. 539-560.

492. Hua, M.J., *Staging Efficacy: Cancer Treatment in Contemporary China*. 2020, The University of Chicago.

493. Yan, Q. and S.S. Fong, *Challenges and Advances for Genetic Engineering of Non-Model Bacteria and Uses in Consolidated Bioprocessing.* Frontiers in Microbiology, 2017.

494. Michels, D.C., *Endothelial Cell-specific Loss of Breast Cancer Susceptibility Gene 2 Exacerbates Atherosclerosis*. 2021, The University of Western Ontario (Canada).

495. Shackelford, R.E., W.K. Kaufmann, and R.S. Paules, *Cell cycle control, checkpoint mechanisms, and genotoxic stress.* Environmental health perspectives, 1999. **107**(suppl 1): p. 5-24.

496. Slotkin, E.K., M.V. Ortiz, and J.G. Bender, *Pediatric DDR Inhibitor Combinations: Are WEE1 There Yet?* Cancer, 2023.

497. King, K.A. and J.A. Cidlowski, *Cell Cycle Regulation and Apoptosis.* Annual Review of Physiology, 1998.

498. McDonald, E. and W.S. El-Deiry, *Cell cycle control as a basis for cancer drug development.* International journal of oncology, 2000. **16**(5): p. 871-957.

499. Gupta, S.C., et al., *Regulation of survival, proliferation, invasion, angiogenesis, and metastasis of tumor cells through modulation of inflammatory pathways by nutraceuticals.* Cancer and Metastasis Reviews, 2010. **29**: p. 405-434.

500. Urbano, A.M., et al., *DNA damage, repair and misrepair in cancer and in cancer therapy*. 2011: INTECH Open Access Publisher.

501. Eymin, B. and S. Gazzeri, *Role of cell cycle regulators in lung carcinogenesis.* Cell adhesion & migration, 2010. **4**(1): p. 114-123.

502. Giannattasio, M. and D. Branzei, *S-phase checkpoint regulations that preserve replication and chromosome integrity upon dNTP depletion.* Cellular and Molecular Life Sciences, 2017. **74**(13): p. 2361-2380.

503. Bernal, F., et al., *Reactivation of the P53 Tumor Suppressor Pathway by a Stapled P53 Peptide.* Journal of the American Chemical Society, 2007. **129**(9): p. 2456-2457.

504. Huang, J. and M.J. Thayer, *Interactions between the cell cycle and the myogenic program.* 2002.

505. Saxena, S. and L. Zou, *Hallmarks of DNA replication stress.* Molecular cell, 2022. **82**(12): p. 2298-2314.

506. Bhowmick, R., I.D. Hickson, and Y. Liu, *Completing genome replication outside of S phase.* Molecular Cell, 2023.

507. Constantinou, S., *Mechanisms of human RAD51 regulation by RAD52 and BRCA2*. 2020.

508. Karri, K. and D.J. Waxman, *Widespread dysregulation of long noncoding genes associated with fatty acid metabolism, cell division, and immune response gene networks in xenobiotic-exposed rat liver.* Toxicological Sciences, 2020. **174**(2): p. 291-310.

509. Zhang, L., et al., *Recent progress in the development of nanomaterials targeting multiple cancer metabolic pathways: a review of mechanistic approaches for cancer treatment.* Drug Delivery, 2023. **30**(1): p. 1-18.

510. Nieszporek, A., et al., *Molecular mechanisms of epithelial to mesenchymal transition in tumor metastasis.* Acta Biochimica Polonica, 2019. **66**(4).

511. Lee, H.-M., K.-A. Hwang, and K.-C. Choi, *Diverse pathways of epithelial mesenchymal transition related with cancer progression and metastasis and potential effects of endocrine disrupting chemicals on epithelial mesenchymal transition process.* Molecular and cellular endocrinology, 2017. **457**: p. 103-113.

512. Khotimchenko, Y.S., D.N. Silachev, and V.L. Katanaev, *Marine natural products from the Russian Pacific as sources of drugs for neurodegenerative diseases.* Marine Drugs, 2022. **20**(11): p. 708.

513. Majidpoor, J. and K. Mortezaee, *Steps in metastasis: an updated review.* Medical Oncology, 2021. **38**: p. 1-17.

514. Yap, S.H., *Identification and characterization of micrornas involved in the invasion and migration properties of lung, prostate and breast cancer cells/Yap Seow Hui*. 2012, University Malaya.

515. Zaccolo, M., A. Zerio, and M.J. Lobo, *Subcellular organization of the cAMP signaling pathway.* Pharmacological reviews, 2021. **73**(1): p. 278-309.

516. Sapio, L., et al., *Targeting protein kinase A in cancer therapy: an update.* EXCLI journal, 2014. **13**: p. 843.

517. Li, C., et al., *The potential of Plant Extracts in Cell Therapy.* Stem Cell Research & Therapy, 2022.

518. Kraemer, R., *Regulation of Cell Migration in Atherosclerosis.* Current Atherosclerosis Reports, 2000.

519. Pisoschi, A.M. and A. Pop, *The role of antioxidants in the chemistry of oxidative stress: A review.* European journal of medicinal chemistry, 2015. **97**: p. 55-74.

520. Pisoschi, A.M., et al., *Oxidative stress mitigation by antioxidants-an overview on their chemistry and influences on health status.* European Journal of Medicinal Chemistry, 2021. **209**: p. 112891.

521. Su, L.-J., et al., *Reactive oxygen species-induced lipid peroxidation in apoptosis, autophagy, and ferroptosis.* Oxidative medicine and cellular longevity, 2019. **2019**.

522. Hockenbery, D.M., et al., *Bcl-2 functions in an antioxidant pathway to prevent apoptosis.* Cell, 1993. **75**(2): p. 241-251.

523. Jang, J.-H. and Y.-J. Surh, *Potentiation of cellular antioxidant capacity by Bcl-2: implications for its antiapoptotic function.* Biochemical pharmacology, 2003. **66**(8): p. 1371-1379.

524. Christodoulou, M.-I., et al., *Nature promises new anticancer agents: Interplay with the apoptosis-related BCL2 gene family.* Anti-Cancer Agents in Medicinal Chemistry (Formerly Current Medicinal Chemistry-Anti-Cancer Agents), 2014. **14**(3): p. 375-399.

525. de Graaf, A.O., *Apoptosis in Haematological Cancer. Regulation by mitochondria, the Bcl-2 family and IAPs*. 2006: [Sl]:[Sn].

526. Kannan, K. and S.K. Jain, *Oxidative stress and apoptosis.* Pathophysiology, 2000. **7**(3): p. 153-163.

527. Matés, J.M., et al., *Oxidative stress in apoptosis and cancer: an update.* Archives of toxicology, 2012. **86**: p. 1649-1665.

528. Kaurinovic, B. and D. Vastag, *Flavonoids and phenolic acids as potential natural antioxidants*. 2019: IntechOpen London, UK.

529. Batty, M., M.R. Bennett, and E. Yu, *The role of oxidative stress in atherosclerosis.* Cells, 2022. **11**(23): p. 3843.

530. Graßmann, J., *Terpenoids as plant antioxidants.* Vitamins & Hormones, 2005. **72**: p. 505-535.

531. Hossain, M. and M. Hossain, *Selected reaction monitoring mass spectrometry.* Selected Reaction Monitoring Mass Spectrometry (SRM-MS) in Proteomics: A Comprehensive View, 2020: p. 53-88.

532. Sengar, G. and H.K. Sharma, *Food Caramels: A Review*. Journal of Food Science and Technology, 2012. **51**(9): p. 1686-1696.

533. He, Q., et al., *IGF-IR Promotes Clonal Cell Proliferation in Myelodysplastic Syndromes via Inhibition of the MAPK Pathway.* Oncology Reports, 2020.

534. Wahab, S., et al., *Glycyrrhiza glabra (Licorice): A comprehensive review on its phytochemistry, biological activities, clinical evidence and toxicology.* Plants, 2021. **10**(12): p. 2751.

535. Rahmani, A.H., et al., *The potential role of apigenin in cancer prevention and treatment.* Molecules, 2022. **27**(18): p. 6051.

536. Zinatizadeh, M.R., et al., *The Nuclear Factor Kappa B (NF-kB) Signaling in Cancer Development and Immune Diseases.* Genes & Diseases, 2021.

537. Bakshi, H.A., et al., *Crocin Inhibits Angiogenesis and Metastasis in Colon Cancer via TNF-α/NF-kB/VEGF Pathways.* Cells, 2022.

538. Rayet, B. and C. Gélinas, *Aberrant Rel/NFKB Genes and Activity in Human Cancer.* Oncogene, 1999.

539. Saha, S., et al., *Long Noncoding RNA DRAIC Inhibits Prostate Cancer Progression by Interacting With IKK to Inhibit NF-κB Activation.* Cancer Research, 2020.

540. Ibrahim, O.H.M., et al., *Azadirachta Indica A. Juss Fruit Mesocarp and Epicarp Extracts Induce Antimicrobial*

and Antiproliferative Effects Against Prostate (PC-3), Breast (MCF-7), and Colorectal Adenocarcinoma (Caco-2) Cancer Cell Lines Through Upregulation of Proapoptotic Genes. Plants, 2022.

541. Lin, L., C. Wu, and K. Hu, *Tissue Plasminogen Activator Activates NF-κB Through a Pathway Involving Annexin A2/CD11b and Integrin-Linked Kinase.* Journal of the American Society of Nephrology, 2012.

542. Hin, N., et al., *6-Hydroxy-1,2,4-Triazine-3,5(2H,4H)-Dione Derivatives as Novel-Amino Acid Oxidase Inhibitors.* Journal of Medicinal Chemistry, 2015.

543. Avery, T.L. and D. Roberts, *Combination chemotherapy with cytosine arabinoside, L-asparaginase, and 6-azauridine for transplantable murine leukemias.* Cancer Research, 1973. **33**(4): p. 791-799.

544. Harris, A.L., et al., *Cytosine Arabinoside Deamination in Human Leukaemic Myeloblasts and Resistance to Cytosine Arabinoside Therapy.* Clinical Science, 1981.

545. Boer, N.K.H.d., et al., *Drug Insight: Pharmacology and Toxicity of Thiopurine Therapy in Patients With IBD.* Nature Clinical Practice Gastroenterology Hepatology, 2007.

546. Krynetski, E.Y., et al., *A Single Point Mutation Leading to Loss of Catalytic Activity in Human Thiopurine S-Methyltransferase.* Proceedings of the National Academy of Sciences, 1995.

547. Palmer, J.M., et al., *Loss of CclA, Required for Histone 3 Lysine 4 Methylation, Decreases Growth but Increases Secondary Metabolite Production In Aspergillus Fumigatus.* Peerj, 2013.

548. Conlon, K.C., M.D. Miljković, and T.A. Waldmann, *Cytokines in the Treatment of Cancer*. Journal of Interferon & Cytokine Research, 2019.

549. Lim, J.S., et al., *Intratumoural Heterogeneity Generated by Notch Signaling Promotes Small-Cell Lung Cancer.* Nature, 2017.

550. He, S., et al., *Potent Activity of the Hsp90 Inhibitor Ganetespib in Prostate Cancer Cells Irrespective of Androgen Receptor Status or Variant Receptor Expression.* International Journal of Oncology, 2012.

551. Afsah, E.M., A.M. Arab, and E. Abdel-Galil, *Synthesis and Biological Evaluation of Novel Tetrahydro-1,2,4-triazines Incorporating Triazene and Tetraazene Moieties.* Chemistryselect, 2019.

552. John, V., et al., *Developments on 1,2,4-Triazine Scaffold Substitutions for Possible Anticancer Agents.* Caribbean Journal of Science and Technology, 2020.

553. Zhang, Y., et al., *An Update Mini-Review on the Progress of Azanucleoside Analogues.* Chemical and Pharmaceutical Bulletin, 2022.

554. Hernández, D. and A. Boto, *Nucleoside Analogues: Synthesis and Biological Properties of Azanucleoside Derivatives.* European Journal of Organic Chemistry, 2014.

555. Abdelnabi, R., *Antiviral Strategies Against Arthritogenic Alphaviruses.* Microorganisms, 2020.

556. Riles, L., et al., *Large-scale Screening of Yeast Mutants for Sensitivity to the IMP Dehydrogenase Inhibitor 6-azauracil.* Yeast, 2004.

557. Shaw, R.J. and D. Reines, *Saccharomyces Cerevisiae Transcription Elongation Mutants Are Defective in PUR5 Induction in Response to Nucleotide Depletion.* Molecular and Cellular Biology, 2000.

558. Choi, Y., M. Lee, and K.S. Shin, *The Lysine Demethylases KdmA and KdmB Differently Regulate Asexual Development, Stress Response, and Virulence in Aspergillus Fumigatus.* Journal of Fungi, 2022.

559. Amit, I., et al., *704 The Computationally Designed Human Antibody, AU-007, Mediates Human Immune Activation by Endogenous IL-2, While Uniquely Breaking the IL-2 Auto-Inhibitory Loop and Preventing Treg Expansion.* Journal for Immunotherapy of Cancer, 2021.

560. Azam, S.S., R. Uddin, and Z. Ul-Haq, *Molecular Docking Studies of Potent Inhibitors of Tyrosinase and A-Glucosidase.* Medicinal Chemistry Research, 2011.

561. Tsai, K.-D., et al., *Cuminaldehyde From Cinnamomum Verum Induces Cell Death Through Targeting Topoisomerase 1 and 2 in Human Colorectal Adenocarcinoma COLO 205 Cells.* Nutrients, 2016.

562. Sarkar, D., *A Review of the Seeds Comprising Panch Phoron, a Spice Used in Indian Cuisine.* International Journal of Pharmaceutical Investigation, 2019.

563. Li, P., et al., *Cytochrome C and dATP-Dependent Formation of Apaf-1/Caspase-9 Complex Initiates an Apoptotic Protease Cascade.* Cell, 1997.

564. Yuan, S., et al., *Structure of an Apoptosome-Procaspase-9 CARD Complex.* Structure, 2010.

565. Ahmed, W., et al., *Transcription Facilitated Genome-Wide Recruitment of Topoisomerase I and DNA Gyrase.* Plos Genetics, 2017.

566. McKinnon, P.J., *Topoisomerases and the Regulation of Neural Function.* Nature Reviews Neuroscience, 2016.

567. Ishida, R., et al., *Threonine 1342 in Human Topoisomerase IIα Is Phosphorylated Throughout the Cell Cycle.* Journal of Biological Chemistry, 1996.

568. Marchion, D.C., et al., *Synergistic Interaction Between Histone Deacetylase and Topoisomerase II Inhibitors Is Mediated Through Topoisomerase IIβ.* Clinical Cancer Research, 2005.

569. Leppard, J.B. and J.J. Champoux, *Human DNA Topoisomerase I: Relaxation, Roles, and Damage Control.* Chromosoma, 2005.

570. Suyama, K., et al., *An Akt3 Splice Variant Lacking the Serine 472 Phosphorylation Site Promotes Apoptosis and Suppresses Mammary Tumorigenesis.* Cancer Research, 2018.

571. Markowitz, S.D. and M.M. Bertagnolli, *Molecular Basis of Colorectal Cancer.* New England Journal of Medicine, 2009.

572. Gilbert, D.C., A.J. Chalmers, and S.F. El-Khamisy, *Topoisomerase I Inhibition in Colorectal Cancer: Biomarkers and Therapeutic Targets.* British Journal of Cancer, 2011.

573. Jeon, K.-H., et al., *Anticancer Activity of Indeno[1,2-B]-Pyridinol Derivative as a New DNA Minor Groove Binding Catalytic Inhibitor of Topoisomerase IIα.* Biomolecules & Therapeutics, 2021.

574. Carvalho, I., et al., *Overexpression of Platelet-Derived Growth Factor Receptor A in Breast Cancer Is Associated With Tumour Progression.* Breast Cancer Research, 2005.

575. Maurya, V., et al., *Unraveling Topoisomerase IA Gate Dynamics in Presence of PPEF and Its Preclinical Evaluation Against Multidrug-Resistant Pathogens.* Communications Biology, 2023.

576. Bezerra, D.P., A.K.N. Soares, and D.P.d. Sousa, *Overview of the Role of Vanillin on Redox Status and Cancer Development.* Oxidative Medicine and Cellular Longevity, 2016.

577. Douglas, P., et al., *Identification of in Vitro and in Vivo Phosphorylation Sites in the Catalytic Subunit of the DNA-dependent Protein Kinase.* Biochemical Journal, 2002.

578. Liang, J.A., et al., *Vanillin Inhibits Matrix Metalloproteinase-9 Expression Through Down-Regulation of Nuclear Factor-KB Signaling Pathway in Human Hepatocellular Carcinoma Cells.* Molecular Pharmacology, 2008.

579. Abraham, D.J., et al., *Vanillin, a Potential Agent for the Treatment of Sickle Cell Anemia.* Blood, 1991.

580. Dai, C., et al., *RNA Interferences Targeting the Fanconi Anemia/Brca Pathway Upstream Genes Reverse Cisplatin Resistance in Drug-Resistant Lung Cancer Cells.* Journal of Biomedical Science, 2015.

581. Zhu, L.J., et al., *Glycopolymer Engineering of the Cell Surface Changes the Single Cell Migratory Direction and Inhibits the Collective Migration of Cancer Cells.* Acs Applied Materials & Interfaces, 2022.

582. Zhao, Y., et al., *MiR-450a-5p Inhibits Gastric Cancer Cell Proliferation, Migration, and Invasion and Promotes Apoptosis via Targeting CREB1 and Inhibiting AKT/GSK-3β Signaling Pathway.* Frontiers in Oncology, 2021.

583. Li, Z., et al., *Hsa-miR-15a-5p Inhibits Colon Cell carcinoma via Targeting CCND1*. Molecular Medicine Reports, 2021.

584. Zhong, Y., F. Zhu, and Y. Ding, *Differential microRNA Expression Profile in the Plasma of Preeclampsia and Normal Pregnancies.* Experimental and Therapeutic Medicine, 2019.

585. Gallage, N.J., et al., *Vanillin Formation From Ferulic Acid in Vanilla Planifolia Is Catalysed by a Single Enzyme.* Nature Communications, 2014.

586. Alshehri, E., et al., *COVID-19 Diagnosis From Medical Images Using Transfer Learning.* Saudi Journal of Health Systems Research, 2022.

587. Wong, R.S.Y., *Role of Nonsteroidal Anti-Inflammatory Drugs (NSAIDs) in Cancer Prevention and Cancer Promotion.* Advances in Pharmacological Sciences, 2019.

588. Dhillon, P.K., et al., *Aspirin Use After a Prostate Cancer Diagnosis and Cancer Survival in a Prospective Cohort.* Cancer Prevention Research, 2012.

589. Shi, C., et al., *Aspirin Inhibits IKK-β-mediated Prostate Cancer Cell Invasion by Targeting Matrix Metalloproteinase-9 and Urokinase-Type Plasminogen Activator.* Cellular Physiology and Biochemistry, 2017.

590. Pathi, S.S., et al., *Aspirin Inhibits Colon Cancer Cell and Tumor Growth and Downregulates Specificity Protein (Sp) Transcription Factors.* Plos One, 2012.

591. Marton, A., et al., *Vanillin Analogues O-Vanillin and 2,4,6-Trihydroxybenzaldehyde Inhibit NFκB Activation and Suppress Growth of A375 Human Melanoma.* Anticancer Research, 2016.

592. Yousuf, M., et al., *Targeting Cyclin-dependent Kinase 6 by Vanillin Inhibits Proliferation of Breast and Lung Cancer Cells: Combined Computational and Biochemical Studies.* Journal of Cellular Biochemistry, 2021.

593. Vaseghi, G., et al., *The Inhibitory Effects of Vanillin on the Growth of Melanoma by Reducing Nuclear Factor-KB Activation.* Advanced Biomedical Research, 2022.

594. Wu, S.-L., et al., *Vanillin Improves and Prevents Trinitrobenzene Sulfonic Acid-Induced Colitis in Mice.* Journal of Pharmacology and Experimental Therapeutics, 2009.

595. Hennings, H., et al., *Malignant Conversion of Mouse Skin Tumours Is Increased by Tumour Initiators and Unaffected by Tumour Promoters.* Nature, 1983.

596. Konarzewska, Z., et al., *Assessment of the Allelochemical Activity and Biochemical Profile of Different Phenotypes of Picocyanobacteria From the Genus Synechococcus.* Marine Drugs, 2020.

597. Sun, J., et al., *Cell Cycle Arrest and Autophagy Induced by Compound Kushen Injection in Sw620 and Sw480 Colorectal Cancer Cells With P53 Mutation.* 2019.

598. Haupt, Y., et al., *Mdm2 Promotes the Rapid Degradation of P53.* Nature, 1997.

599. Crighton, D., et al., *DRAM, a P53-Induced Modulator of Autophagy, Is Critical for Apoptosis.* Cell, 2006.

600. Hougardy, B.M.T., et al., *Proteasome Inhibitor MG132 Sensitizes HPV-positive Human Cervical Cancer Cells to rhTRAIL-induced Apoptosis.* International Journal of Cancer, 2005.

601. Makgoo, L., S. Mosebi, and Z. Mbita, *Molecular Mechanisms of HIV Protease Inhibitors Against HPV-Associated Cervical Cancer: Restoration of TP53 Tumour Suppressor Activities.* Frontiers in Molecular Biosciences, 2022.

602. Lewandowski, M. and K. Gwoździński, *Nitroxides as Antioxidants and Anticancer Drugs.* International Journal of Molecular Sciences, 2017.

603. Petri, G.L., et al., *Pyrrolidine in Drug Discovery: A Versatile Scaffold for Novel Biologically Active Compounds.* Topics in Current Chemistry, 2021.

604. Ji, J., et al., *Synthesis and Biological Evaluation of Substituted Pyrrolidines and Pyrroles as Potential Anticancer Agents.* Archiv Der Pharmazie, 2020.

605. Bello, C., et al., *Induction of Cell Killing and Autophagy by Amphiphilic Pyrrolidine Derivatives on Human Pancreatic Cancer Cells.* European Journal of Medicinal Chemistry, 2018.

606. Nosálová, N., et al., *Oxidative Stress Mediated by Pyrrolidine SS13 Is Involved in Autophagic Cell Death Induction in Colorectal Cancer Cells.* 2023.

607. Panossian, A. and G. Wikman, *Pharmacology of Schisandra Chinensis Bail.: An Overview of Russian Research and Uses in Medicine.* Journal of Ethnopharmacology, 2008.

608. Kelly, M.M., B. Hoel, and C. Voelkel-Johnson, *Doxorubicin Pretreatment Sensitizes Prostate Cancer Cell Lines to TRAIL Induced Apoptosis Which Correlates With the Loss of C-Flip Expression.* Cancer Biology & Therapy, 2002.

609. Hammond, E.M., et al., *Hypoxia Links ATR and P53 Through Replication Arrest.* Molecular and Cellular Biology, 2002.

610. Zhang, X., et al., *Schizandrin Protects H9c2 Cells Against Lipopolysaccharide-induced Injury by Downregulating Smad3.* Journal of Biochemical and Molecular Toxicology, 2019.

611. Wang, J., S.-J. Hwang, and C.G. Son, *Comparative Analysis of the Antioxidative and Hepatoprotective Activities of Dimethyl Diphenyl Bicarboxylate in Four Animal Models of Hepatic Injury.* Antioxidants, 2021.

612. Lin, X., et al., *Regulation of Cell Signaling Pathways by Schisandrin in Different Cancers: Opting for "Swiss Army Knife" Instead of "Blunderbuss".* Cellular and Molecular Biology, 2021.

613. Jiang, Y., et al., *Schisandrin B Suppresses Glioma Cell Metastasis Mediated by Inhibition of mTOR/MMP-9 Signal Pathway.* Biomedicine & Pharmacotherapy, 2015.

614. Guo, J., et al., *Effects of Karanjin on Cell Cycle Arrest and Apoptosis in Human A549, HepG2 and HL-60 Cancer Cells.* Biological Research, 2015.

615. Zhuang, W., et al., *Schisandrin B Inhibits TGF-β1-induced Epithelial-Mesenchymal Transition in Human A549 Cells Through Epigenetic Silencing of ZEB1.* Experimental Lung Research, 2019.

616. Lee, M.-S., et al., *Schizandrin Protects Primary Rat Cortical Cell Cultures From Glutamate-Induced Apoptosis by Inhibiting Activation of the MAPK Family and the Mitochondria Dependent Pathway.* Molecules, 2012.

617. Gong, R.-H., et al., *Cell Death Mechanisms Induced by Synergistic Effects of Halofuginone and Artemisinin in Colorectal Cancer Cells.* International Journal of Medical Sciences, 2022.

618. Miao, G., et al., *Bax Targeted by miR-29a Regulates Chondrocyte Apoptosis in Osteoarthritis.* Biomed Research International, 2019.

619. Fang, J., et al., *Intervention of Electroacupuncture on Spinal P38 MAPK/ATF-2/VR-1 Pathway in Treating Inflammatory Pain Induced by CFA in Rats.* Molecular Pain, 2013.

620. Zhang, H., et al., *Transforming Growth Factor-B1-Induced Epithelial-Mesenchymal Transition in Human Esophageal Squamous Cell Carcinoma via the PTEN/PI3K Signaling Pathway.* Oncology Reports, 2014.

621. Hu, Y., et al., *Protective Effects of Schisandrin B Against D-GalN-Induced Cell Apoptosis in Human Hepatocyte (L02) Cells via Modulating BCL-2 and Bax.* Bioengineered, 2021.

622. Singh, S.V., et al., *Sulforaphane-Induced G2/M Phase Cell Cycle Arrest Involves Checkpoint Kinase 2-Mediated Phosphorylation of Cell Division Cycle 25C.* Journal of Biological Chemistry, 2004.

623. Sarin, N., et al., *Cisplatin Resistance in Non-Small Cell Lung Cancer Cells Is Associated With an Abrogation of Cisplatin-Induced G2/M Cell Cycle Arrest.* Plos One, 2017.

624. Fu, M., et al., *Minireview: Cyclin D1: Normal and Abnormal Functions.* Endocrinology, 2004.

625. Cheng, T., et al., *Stem Cell Repopulation Efficiency but Not Pool Size Is Governed by P27kip1*. Nature Medicine, 2000.

626. Abbas, T. and A. Dutta, *P21 in Cancer: Intricate Networks and Multiple Activities.* Nature Reviews Cancer, 2009.

627. Pu, Z., et al., *Schisandrin B Attenuates Colitis-Associated Colorectal Cancer Through SIRT1 Linked SMURF2 Signaling.* The American Journal of Chinese Medicine, 2021.

628. Torres-Viera, C., et al., *Activities of Taurolidine in Vitro and in Experimental Enterococcal Endocarditis.* Antimicrobial Agents and Chemotherapy, 2000. **44**(6): p. 1720-1724.

629. McCourt, M., et al., *Taurolidine Inhibits Tumor Cell Growth in Vitro and in Vivo.* Annals of Surgical Oncology, 2000.

630. Nici, L., B. Monfils, and P. Calabresi, *The Effects of Taurolidine, a Novel Antineoplastic Agent, on Human Malignant Mesothelioma.* Clinical Cancer Research, 2004.

631. Marley, K., et al., *The Effects of Taurolidine Alone and in Combination With Doxorubicin or Carboplatin in Canine Osteosarcoma in Vitro.* BMC Veterinary Research, 2013.

632. Jacobi, C.A., C. Menenakos, and C. Braumann, *Taurolidine–a New Drug With Anti-Tumor and Anti-Angiogenic Effects.* Anti-Cancer Drugs, 2005.

633. Wouters, Y., et al., *The Antiseptic and Antineoplastic Agent Taurolidine Modulates Key Leukocyte Functions.* In Vivo, 2022.

634. Ogura, T., et al., *Docetaxel Induces BCL-2- And Pro-Apoptotic Caspase-Independent Death of Human Prostate Cancer DU145 Cells.* International Journal of Oncology, 2016.

635. Darnowski, J.W., et al., *Mechanistic and Antineoplastic Evaluation of Taurolidine in the DU145 Model of Human Prostate Cancer.* Cancer Chemotherapy and Pharmacology, 2004.

636. Singh, S.V., et al., *Sulforaphane-Induced Cell Death in Human Prostate Cancer Cells Is Initiated by Reactive Oxygen Species.* Journal of Biological Chemistry, 2005.

637. Hu, J., et al., *Effect of Combination of All-Trans Retinoic Acid and Arsenic Trioxide on Apoptosis of Acute Promyelocytic Leukemia Cells.* Cellular and Molecular Biology, 2019.

638. Chromik, A.M., et al., *Oral Administration of the Anti-Proliferative Substance Taurolidine Has No Impact on Dextran Sulfate Sodium-Induced Colitis-Associated Carcinogenesis in Mice.* Journal of Carcinogenesis, 2010.

639. Hotchkiss, R.S., et al., *Cell Death.* New England Journal of Medicine, 2009.

640. Hopkins-Donaldson, S., et al., *P53-Induced Apoptosis Occurs in the Absence of P14ARF in Malignant Pleural Mesothelioma.* Neoplasia, 2006.

641. Williams, M.M., et al., *Key Survival Factor, McL-1, Correlates With Sensitivity to Combined BCL-2/BCL-xL Blockade.* Molecular Cancer Research, 2017.

642. Campbell, K.J., et al., *Breast Cancer Dependence on McL-1 Is Due to Its Canonical Anti-Apoptotic Function.* Cell Death and Differentiation, 2021.

643. Bae, I.H., et al., *BCL-W Promotes Gastric Cancer Cell Invasion by Inducing Matrix Metalloproteinase-2 Expression via Phosphoinositide 3-Kinase, Akt, and Sp1.* Cancer Research, 2006.

644. Schneider, L., et al., *PDGFRαα Signaling Is Regulated Through the Primary Cilium in Fibroblasts.* Current Biology, 2005.

645. Opitz, I., et al., *Instillation of Taurolidine/Heparin After Laparotomy Reduces Intraperitoneal Tumour Growth in a Colon Cancer Rat Model.* European Surgical Research, 2007.

646. Redmond, H.P., et al., *RandomiSed Clinical Trial Assessing Use of an Anti-inflammatoRy aGent in attenUating Peri-operatiVe inflAmmatioN in Non-meTastatic Colon Cancer – The S.U.R.G.U.V.A.N.T. Trial.* BMC Cancer, 2018.

647. Sun, B.S., et al., *Taurolidine Induces Apoptosis of Murine Melanoma Cells in Vitro and in Vivo by Modulation of the Bcl-2 Family Proteins.* Journal of Surgical Oncology, 2007.

648. Anh, P. and C.H. Lee, *The Role of CDK5 in Tumours and Tumour Microenvironments.* Cancers, 2020.

649. Ciccia, A. and S.J. Elledge, *The DNA Damage Response: Making It Safe to Play With Knives.* Molecular Cell, 2010.

650. Aydın, E., H. Türkez, and F. Geyikoğlu, *Antioxidative, Anticancer and Genotoxic Properties of A-Pinene on N2a Neuroblastoma Cells.* Biologia, 2013.

651. Salehi, B., et al., *Therapeutic Potential of A- And B-Pinene: A Miracle Gift of Nature.* Biomolecules, 2019.

652. Matsuda, T., et al., *Tumor Necrosis Factor-Alpha-Nuclear Factor-Kappa B-Signaling Enhances St2b2 Expression During 12-O-Tetradecanoylphorbol-13-Acetate-Induced Epidermal Hyperplasia.* Biological and Pharmaceutical Bulletin, 2011.

653. Neves, A.S.C., et al., *Screening of Five Essential Oils for Identification of Potential Inhibitors of IL-1-induced Nf-κB Activation and NO Production in Human Chondrocytes: Characterization of the Inhibitory Activity Of α-Pinene.* Planta Medica, 2009.

654. Hou, J., et al., *A-Pinene Induces Apoptotic Cell Death via Caspase Activation in Human Ovarian Cancer Cells.* Medical Science Monitor, 2019.

655. Zhu, Z., et al., *FMS-Related Tyrosine Kinase 3 Ligand Promotes Radioresistance in Esophageal Squamous Cell Carcinoma.* Frontiers in Pharmacology, 2021.

656. Yang, O.C.Y., P.H. Maxwell, and P.J. Pollard, *Renal Cell Carcinoma: Translational Aspects of Metabolism and Therapeutic Consequences.* Kidney International, 2013.

657. Zhao, Q., et al., *Brevilin A, a Natural Sesquiterpene Lactone Inhibited the Growth of Triple-Negative Breast Cancer Cells via Akt/mTOR and STAT3 Signaling Pathways.* Oncotargets and Therapy, 2020.

658. Tang, Y., et al., *Tip60-Dependent Acetylation of P53 Modulates the Decision Between Cell-Cycle Arrest and Apoptosis.* Molecular Cell, 2006.

659. Brunet, A., et al., *Akt Promotes Cell Survival by Phosphorylating and Inhibiting a Forkhead Transcription Factor.* Cell, 1999.

660. Pasquale, E.B., *Eph Receptors and Ephrins in Cancer: Bidirectional Signaling and Beyond.* Nature Reviews Cancer, 2010.

661. Hafner, C., et al., *Expression Profile of Eph Receptors and Ephrin Ligands in Human Skin and Downregulation of EphA1 in Nonmelanoma Skin Cancer.* Modern Pathology, 2006.

662. Mosch, B., D. Pietzsch, and J. Pietzsch, *Irradiation Affects Cellular Properties and Eph Receptor Expression in Human Melanoma Cells.* Cell Adhesion & Migration, 2012.

663. Nikas, I.P., et al., *EPHA2, EPHA4, and EPHA7 Expression in Triple-Negative Breast Cancer.* Diagnostics, 2022.

664. Santolla, M.F. and M. Maggiolini, *The FGF/FGFR System in Breast Cancer: Oncogenic Features and Therapeutic Perspectives.* Cancers, 2020.

665. Harrasser, M., et al., *Inducible Localized Delivery of an Anti-Pd-1 scFv Enhances Anti-Tumor Activity of ROR1 CAR-T Cells in TNBC.* Breast Cancer Research, 2022.

666. McKenzie, M.G., et al., *Non-Canonical WNT Signaling Through Ryk Regulates the Generation of Somatostatin- And Parvalbumin-Expressing Cortical Interneurons.* Neuron, 2019.

667. Gupta, V.K., et al., *TrkB Receptor Signaling: Implications in Neurodegenerative, Psychiatric and Proliferative Disorders.* International Journal of Molecular Sciences, 2013.

. Lemmon, M.A. and J. Schlessinger, *Cell Signaling by Receptor Tyrosine Kinases.* Cell, 2010.

. Chen, J. and A. Stinnett, *Disruption of Ang-1/Tie-2 Signaling Contributes to the Impaired Myocardial Vascular Maturation and Angiogenesis in Type II Diabetic Mice.* Arteriosclerosis Thrombosis and Vascular Biology, 2008.

670. Takahashi, H. and M. Shibuya, *The Vascular Endothelial Growth Factor (VEGF)/VEGF Receptor System and Its Role Under Physiological and Pathological Conditions.* Clinical Science, 2005.